The Atmospheric Parameters of Main Sequence A and F Stars

by

Barry Smalley

Thesis submitted for the degree of Doctor of Philosophy
in the Faculty of Science of the University of London.

Department of Physics & Astronomy
University College London

April 1992

ProQuest LLC.
789 East Eisenhower Parkway
P.O. Box 1346
Ann Arbor, MI 48106 – 1346

To

Mum, Dad, John

and

Carol

Abstract

The problem of the fundamental atmospheric parameters of main-sequence A and F stars has been investigated using several different techniques. This work was motivated by the fact that recent analyses based on fitting optical and ultraviolet energy distributions have yielded systematically lower effective temperatures and surface gravities for metallic-lined (Am) stars than have previously been obtained using photometric methods. Abundance analyses using these lower values implied that the atmospheric composition of Am stars is roughly solar, compared to the usually expected enhancement.

The use of photometry and spectrophotometry in the determination of effective temperatures and surface gravities has been critically evaluated. It is found that all the calibrations and methods yield broadly the same values, but only provided that metal abundance is known or explicitly allowed for in the determinations. Some methods are highly sensitive to metal abundance.

The hydrogen Balmer lines have been studied extensively and used to confirm that the effective temperatures of Am stars are consistent with those determined from photometry. It has been found that photometry is not adversely affected by an flux excess around 4785Å, as had previously been suggested. This flux excess is not apparent in high-quality spectra and appears to have originated due to deficiencies in the model atmosphere fluxes around that wavelength.

A differential abundance analysis has confirmed that Am stars are metal-rich. The atmospheric abundances are enhanced by up to a factor of about five, which is consistent with the current models for the origin of such anomalies. The atmospheric parameters of Am stars indicate that their masses, luminosities and radii are not significantly different from those of normal A and F stars of the same age. The abundance anomalies are most definitely real and presumably caused by atmospheric processes, such as radiative diffusion and gravitational settling.

Contents

List of Tables

List of Figures

Chapter 1

Introduction

It has long been thought that metallic-line (Am) stars are metal rich objects with similar T_{eff} and $\log g$ to normal A and F stars. However, the work of Lane & Lester (1984, 1987) has thrown this notion into confusion. They found, from spectrophotometric flux fitting, systematically lower T_{eff} and $\log g$ for Am stars than had previously been obtained using photometric methods. In a detailed abundance analysis they obtained iron-group abundances that were roughly solar, compared to the usually obtained enhancements.

Lester (1987) suggested that Am stars have a flux excess around 4785 Å, which adversely affects the Strömgren *b*-filter. This would make photometric measures involving the *b*-magnitude erroneous.

1.1 The atmospheric parameters of stars

The stellar atmospheric parameters of effective temperature (T_{eff}), surface gravity (usually expressed in terms of $\log g$; g in cgs units) and chemical composition are of fundamental astrophysical importance. As well as defining the physical conditions in the stellar atmospheres, they are directly related to the physical properties of stars; mass (M), radius (R) and luminosity (L):

$$\sigma \, T_{eff}^4 \equiv \int_0^\infty F_\nu \, d\nu = \frac{L}{4\pi R^2} \tag{1.1}$$

$$\log g \; = \log \left(\frac{GM}{R^2} \right) \tag{1.2}$$

Chemical composition is also of importance. Hydrogen and helium are the dominant constituents of stars with typical mass fractions of $X = 0.73$ and $Y = 0.25$

respectively. All the other elements contribute a mass fraction of only $Z = 0.017$, but their effects on the emergent flux from the stellar surface can be very significant, especially for the cooler stars such as we are considering in the present work.

In stellar abundance determinations the abundance of an element is usually given as the logarithmic number fraction with respect to hydrogen:

$$\log_{10}\epsilon = \log_{10}\left(\frac{N_{EL}}{N_H}\right) \quad \text{or} \quad \log_{10}A = \log_{10}\left(\frac{N_{EL}}{N_H}\right) + 12 \tag{1.3}$$

where the constant 12 is often added to give the abundance of hydrogen as 12.00 and to prevent the other abundances being negative. In the present work two further metal abundance definitions will be used:

- The iron abundance relative to the solar iron abundance:

$$[\text{Fe/H}] = \log_{10}\left(\frac{N_{FE}}{N_H}\right)_\star - \log_{10}\left(\frac{N_{FE}}{N_H}\right)_\odot \tag{1.4}$$

- The logarithmic scaling factor of all elements, except H and He, relative to the solar values; [M/H] is used as a parameter in model atmosphere calculations (see Kurucz, 1970). For example, [M/H] = 0.0 indicates solar abundances, while [M/H] = +1.0 indicates that all elements are 10 times the solar values. The global shift, given by [M/H], is not the case in real stars. However, most of the blanketing in A and F stars is caused by iron-group transition elements, so [M/H] is strongly correlated with [Fe/H].

Model atmospheres are the analytical link between the physical properties of the star (M, R and L) and the observable spectral features of flux distribution and absorption line profiles. Hence, the understanding of stellar atmospheres is vital to the understanding of stellar structure. Observations can be related, via model atmosphere analyses, to the fundamental stellar parameters, assuming of course that the models are adequate. The values of $T_{\rm eff}$ and $\log g$ must necessarily be consistent with the actual values of M, R and L. Unfortunately, the physical properties of the star are not generally readily ascertainable except in the cases of certain binary stars and we have to rely on model atmosphere analysis of spectra to deduce them.

1.2 The main sequence A and F stars

Hydrogen lines dominate the spectra of the A-type stars, reaching their maximum strength around A0V. The strength of the hydrogen lines falls rapidly through the

Table 1.1: *Typical parameters of main-sequence A and F stars.*

Sp.	M_V	$M/M_\odot$	$R/R_\odot$	$L/L_\odot$	$\overline{v \sin i}$	T_{eff}	$\log g$	M_{bol}
A0	+0.7	3.2	2.5	80	150	9900	4.1	+0.1
A5	+2.0	2.1	1.7	20	115	8500	4.2	+1.7
F0	+2.6	1.7	1.3	6	78	7400	4.3	+2.6
F5	+3.4	1.3	1.2	3	22	6580	4.3	+3.4

Adapted from Allen (1973)

F-type stars. The strength of metal lines increases markedly from A0 to F9. For A-type stars the singly ionized metals dominate, reaching a peak around A5. The neutral metals appear stronger in the later type stars and gain over ionized metals by late F-type. In A-type spectra the elements Fe, Cr and Ti contribute over half of the visible lines. Their increase in line-strength, with decreasing T_{eff}, means that more and more of the individual absorption lines become blended together, making the location of the continuum level difficult. As will be demonstrated in the present work, line-blanketing can have a significant effect on the determination of T_{eff}, $\log g$ and [M/H] for late-A and F stars.

In contrast to most other parts of the HR diagram, the A-type stars form a much less heterogeneous group of objects; abnormalities appear to be the norm rather than the exception. Even at standard classification dispersions, one in five stars have conspicuous spectral anomalies (Cowley *et al.*, 1969). At higher resolutions more stars appear anomalous. The relatively high rotational velocities of normal A stars (Table 1.1) make detailed spectral analyses difficult, hence generally only the stars with low $v \sin i$ are studied in depth; these tend to be abnormal. In fact, Abt & Moyd (1973) concluded that there is probably no slowly rotating late-A star that could be reasonably classified as normal. The pronounced line-strength anomalies makes the MK (Morgan & Keenan, 1973) spectral classification scheme an efficient means of identifying peculiar stars. The F-type stars, however, contain relatively few peculiar objects. Those few that do appear can be regarded as late peculiar A-type stars (Jaschek & Jaschek, 1987).

The use of photometry provides an alternative method of characterizing A and F stars. The Strömgren-Crawford *uvbyβ* system is particularly useful since it provides a measure of temperature and luminosity, as well as giving an estimate of metal abundance. Model atmosphere flux calculations have been used to calibrate

photometric indices and provide quantitative estimates of T_{eff} and $\log g$. However, the present generation of models are unable to adequately reproduce the observed colours of late-A and F stars (Relyea & Kurucz, 1978).

The binary nature of normal A-type stars was extensively studied by Abt (1965), who found that, for stars in the spectral range A4 – F2, nearly 30% were spectroscopic binaries. All the orbital periods obtained were longer than 100 days; whereas the majority of known Am star binaries have periods shorter than 100 days (Abt, 1961). The A-type binaries with very short orbital periods (< 2.5 days) have generally normal spectra (Abt & Bidelman, 1969). A survey of F-type stars indicated that about 50% are binaries (Abt & Levy, 1976). The binary nature of A and F stars is of considerably importance in the determination of atmospheric parameters. The presence of a cool companion can distort the observed flux distribution and influence the methods of obtaining T_{eff} and $\log g$.

Relatively few detailed abundance analyses of normal A-type stars have been performed. This is mostly because there are very few normal stars with sharp-enough lines to permit such analyses. The available results show a larger than expected scatter in the abundances (Dreiling & Bell, 1980; Sadakane, 1981). Cowley *et al.* (1982) found evidence for a group of metal-deficient stars near A0. Even Vega, the primary photometric standard, has been shown to be metal-poor by ~0.6 dex (Gigas, 1986; Adelman & Gulliver, 1990). This has implications for its use in the calibration of photometric systems (Kurucz, 1991b).

In analyses of normal early A-type stars, Holweger, Gigas & Steffen (1986) and Holweger, Steffen & Gigas (1986) found significant abundance variations from star-to-star. They found that variations in iron-group abundances were correlated with Mg and Ba, while C varies considerably but independent of Fe. Additionally, they found that Sirius fitted surprising well into the sample of normal stars, even though it has been considered an Am star (Kohl, 1964; Lane & Lester, 1984).

Among the late-A and F stars abundance analyses become complicated by the extensive metal line-blanketing prevalent in these objects. Nevertheless, high-resolution observations of these stars has revealed that the abundances are generally consistent with solar values (Steffen, 1985; Lane & Lester, 1987; Adelman, 1987a; Adelman *et al.*, 1991). However, most of the slowing rotating stars in this temperature range tend to be metallic-lined.

1.3 The Am stars

The metallic-line (Am) stars are a spectroscopic class of A-type stars in which the Ca II K-line is considerably weaker than would be expected for the average metallic line type (Titus & Morgan, 1940; Roman, Morgan & Eggen, 1948). Often a more restrictive definition is used in which the metallic and K-line types must differ by more than five spectral subclasses.

However, based on a survey of A-type stars at high-resolution, Conti (1970) proposed an alternative definition for the Am class:

> ...The Am phenomenon is present in stars that have an apparent surface underabundance of Ca (and/or Sc) and/or an apparent overabundance of the Fe group and heavier elements.

This definition presupposes an identity between line-strength anomalies and abundance anomalies. The evidence favours this, but it is a point that must be proved, not simply assumed (Wolff, 1983).

The spectroscopic notation for Am stars is an extension of the standard MK system. Three spectral types are generally given based on the appearance of the Ca II K-line, the hydrogen lines and the metal lines. Thus a typical spectral notation of an Am star is kA2hA8mF1, where the prefixes indicate the spectral type based on the Ca II K-line, hydrogen lines and metal lines respectively. Throughout the present work this type of notation will be used to describe Am stars. Additionally, several stars are given with the suffix m, this indicates that the star is an Am, but a full classification has not been determined.

The incidence of Am stars varies along the A-type spectral range, reaching a maximum of ~50% around A7 (Smith, 1973). In fact, there are very few normal A7 and A8 stars (Jaschek & Jaschek, 1987). There is a rather abrupt cut-off around F2, which has been linked to the onset of sub-surface convection (Conti, 1970). Among the early A-type stars, however, anomalies are difficult to detect at classification dispersions due to the extensive hydrogen lines and weak metal lines. Nevertheless, detailed analyses have shown that a number of well-known normal early A-type stars exhibit abundance anomalies characteristic of Am stars (Conti, Wallerstein & Wing, 1965). The overall temperature range in which Am stars are found is 7400 to 10200 K (Wolff, 1983), although Lane & Lester (1987) claimed to have extended the lower-limit to 6600 K.

The rotation and binary characteristics of Am stars are markedly different from those of normal A-type stars. Virtually all Am stars have rotational velocities less than 100 km/s (Abt & Moyd, 1973), and nearly all late-A stars with $v \sin i < 40$ km/s tend to be metallic-lined. Abt (1961) found that practically all the Am stars he studied were spectroscopic binaries and two-thirds of them had periods of less than 100 days. In contrast, the normal A-type binaries have periods longer than 100 days. The fact that most Am stars occur in short-period binary systems probably accounts for the low rotational velocities. The tidal interactions occurring in a close-binary system will tend to synchronize the rotational and orbital periods.

The pioneering work by Greenstein (1948, 1949) showed that the anomalies found in τ UMa could not be caused a composite spectrum of two stars. Since then, there have been numerous abundance analyses of Am stars. The work of Smith (1971) is a particularly good example. The elemental abundances were determined for 16 Am stars and the following general abundance patterns were established:

- Calcium and scandium are underabundant by up to 1.0 dex.
- There are also marked deficiencies of other light elements, especially carbon.
- The iron-group elements are overabundant by up to 0.7 dex.
- An overabundance of the heavy elements (rare-earths) by 1.0 dex or more.

Nevertheless, there is considerable variation in abundances from star-to-star. Modern analyses, using higher-quality data, better atomic data and fully line-blanketed model atmospheres, have confirmed the general abundance patterns (Burkhart & Coupry, 1989; Cayrel, Burkhart & Van't Veer, 1991). However, the work of Lane & Lester (1987) gave iron-group abundances that were roughly solar compared to the generally expected enhancements.

Many explanations of the Am phenomenon have been proposed (Wolff, 1983). The generally adopted possibility is that of the diffusion process (Michaud, 1970; 1976). The diffusion process postulates that the deficiencies of the light elements (*e.g.* C, Ca, Sc) are caused by gravitational settling, while the overabundances of the heavy elements are caused by excess radiation pressure forcing the elements upwards in the atmosphere. Charbonneau & Michaud (1988) investigated the effects of meridional circulation on the diffusion process. They determined that the limiting equatorial rotational velocity for an Am star should be $\sim$100 km/s, this agrees

well with the observed rotational velocities. The diffusion process has gone a long way to explaining the observed abundance anomalies of Am stars (Michaud, 1991). Unfortunately, the results of Lane & Lester (1894, 1987) are at odds with these current theories and need to be investigated fully. An investigation into the methods employed by Lane & Lester forms the main body of the present work.

1.4 Summary

The determination of the stellar atmospheric parameters, T_{eff}, $\log g$ and [M/H] are the necessary prerequisites for detailed analyses of stellar structure. Their values must be accurately estimated prior to any detailed analysis. The values of M, L and R can be obtained and compared to theoretical stellar structure calculations.

This work is an investigation into the determination of the atmospheric parameters of main-sequence A and F stars. The generally used techniques of photometry and spectrophotometric flux fitting are reviewed. Particularly, the results of Moon & Dworetsky (1985) and Lane & Lester (1984) are considered in detail. The systematic differences in the T_{eff} and $\log g$ values given by the two methods were discussed by Dworetsky & Moon (1986) and Lester (1987). Dworetsky & Moon found that the systematic differences were due to metallicity effects; Lester found that a flux excess at 4785Å was responsible. This flux excess detrimentally affects the atmospheric parameters given by photometry. The two conflicting explanations are analysed and an attempt made to resolve the controversy.

Medium-resolution spectra of many A and F stars, including several Am stars, have been obtained. These stars will be referred to as the JKT programme stars throughout the present work. The spectra of the Hβ and Hγ lines are analysed and used to derive T_{eff} values. The results are compared to those obtained from photometry and spectrophotometry. Observations of the region around the flux excess were also obtained and used in a detailed investigation of the flux excess. The cause of the flux excess has been identified and its effects evaluated.

The effects of metal abundance and secondary companion stars on the determination of the atmospheric parameters are investigated. Modifications to the standard techniques are presented which allow for the relative effects of cool companion stars in binary systems. A critical evaluation of the T_{eff}, $\log g$ and [M/H] of the JKT programme stars is given.

Chapter 2

Atmospheric parameters from photometry

2.1 Introduction

The intensity of stellar flux varies as a function of wavelength and these variations are linked to temperature, surface gravity and chemical composition. A measurement of stellar flux at several wavelengths can be used to determine such parameters. Ideally, continuous spectrophotometric wavelength coverage through a narrow bandpass would be the preferred observations, but this is time consuming and generally only possible for relatively bright stars (see Chapter 3).

Wide and intermediate band photometric systems have been developed to describe the shape of stellar flux distributions via magnitude (colour) differences. Since they use wide bandpasses the observations can be obtained in a fraction of the time required by spectrophotometry and can be extended to much fainter magnitudes. The use of standardized filters allows for the quantitative analysis of stars over a wide magnitude range.

By carefully designing the filter bandpasses that define a photometric system, colour indices can be obtained that are particularly sensitive to one or more of the stellar parameters. Indeed, photometric surveys of faint stars are used to identify anomalous stars which warrant much closer spectroscopic investigation.

Many photometric systems have been developed, each with its own particular set of standard filters and specific uses. Three widely used systems will be discussed:

- The Johnson & Morgan UBV system

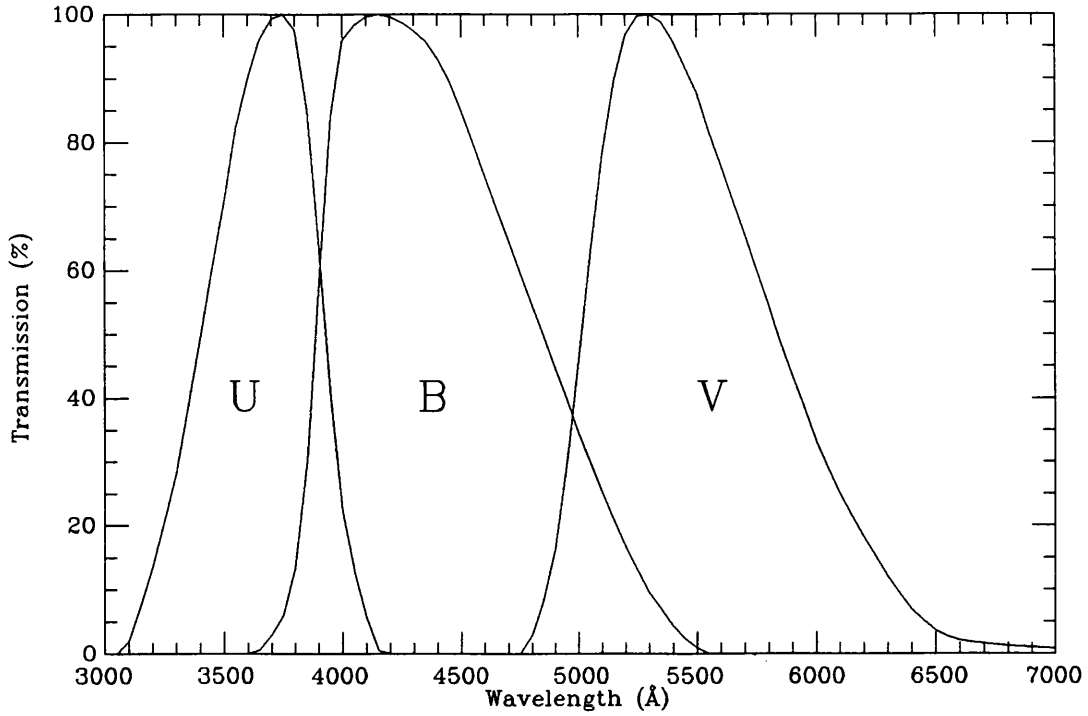

Figure 2.1: *The UBV passbands. From Buser & Kurucz (1978)*

- The Strömgren-Crawford $uvby\beta$ system
- The Geneva Observatory $UBVB_1B_2V_1G$ system

Particular emphasis will be placed on the $uvby\beta$ system, since it is the most widely used system in A and F star work. Also, the present work will be mainly concerned with calibrations for stars later than A3 ($T_{eff} \leq 8500$ K).

2.2 *UBV* photometry

The *UBV* photometric system, developed by Johnson & Morgan (1953), makes use of three broad bandpasses, approximately 1000Å wide, centred around 3500Å, 4300Å and 5500Å (Figure 2.1). This system was established for the photometric study of stars which are classified in the MK system. The choice of the bandpasses was dictated by the need to limit the system to a small number of broad filters so that measurements of faint stars could be readily obtained, coupled with a desire to match, approximately, existing systems based on the sensitivity of the eye (V) and photographic plates (B). The addition of a third ultraviolet filter (U) allows for treatment of reddening and improves sensitivity of the system to the temperatures

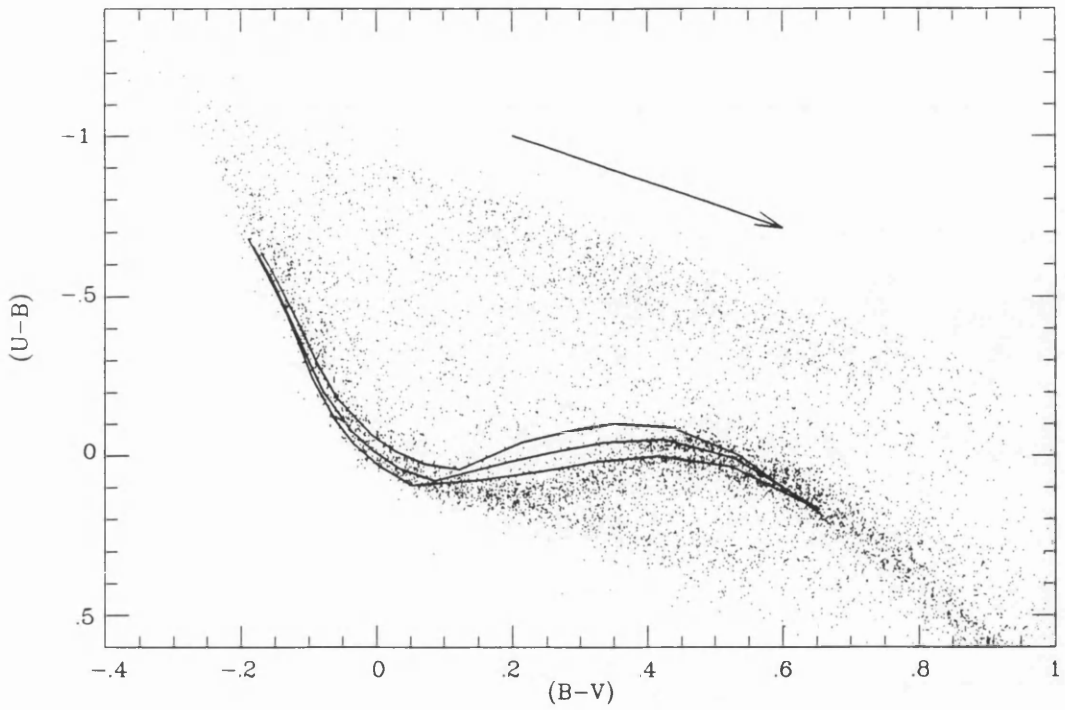

Figure 2.2: *Comparison of model UBV colours with observations. The dots are individual measurements taken from Nicolet (1978). The Buser & Kurucz (1978) calibration lines are, from top to bottom, for* $\log g$ *= 3.5, 4.0 and 4.5. The models fit the early-type stars well, but for cooler stars there are some major discrepancies. The arrow shows the direction of interstellar reddening.*

of hot stars and to chemical composition.

While the UBV colours do correlate well with spectral type for stars of similar composition, they do not provide a separation of luminosity classes and are strongly affected by interstellar reddening (Johnson, 1958). Because the U filter includes the Balmer Jump at 3646Å, it is very difficult to relate observed colours to those calculated from models, particularly for A-type stars.

Buser & Kurucz (1978) presented theoretical UBV colours based on the solar-composition Kurucz (1979a) model atmospheres. The model fluxes were integrated through the filter response function which they also presented. The UBV colours agree very well with the observed colours for early-type stars, but the $(U-B)$ colours of the models for A to G stars are discrepant with the observations (Figure 2.2). Various explanations for the discrepancies were discussed by Relyea & Kurucz (1978) and their discussion is given in Section 2.3.1.

2.3 *uvbyβ* photometry

It was in part to remedy the deficiencies in the UBV system that Strömgren (1963a) devised a four-colour, filter-defined system, using the following filters:

Band	Wavelength (Å)	Half-width (Å)
u	3500	300
v	4110	190
b	4670	180
y	5470	230

Very often the four-colour photometry is supplemented by narrow (~30Å) and broad (~150Å) filters centred on Hβ at 4861Å. The four colours plus Hβ, known as the Strömgren-Crawford *uvbyβ* system, allow discrimination of both temperature and luminosity classes, even in reddened stars (Strömgren, 1966). The indices and colours are as follows:

$(b-y)$: colour index analogous to the $(B-V)$ of the UBV system, that is relatively insensitive to chemical composition effects, but is sensitive to temperature, and cannot be used directly in reddened stars.

$m_1 = (v-b)-(b-y)$: colour difference that is a measure of the total intensity in later-type stars of metal lines around 4100Å, and provides a measure of composition. In earlier-type stars it provides a measure of the strength of Hδ.

$c_1 = (u-v)-(v-b)$: colour difference that is a measure of the size of the Balmer Jump at 3646Å.

$\beta = \beta_{\text{narrow}} - \beta_{\text{wide}}$: provides a measure of the strength of the Hβ Balmer line at 4861Å. It is virtually unaffected by metal line-blanketing and reddening.

$(u-b)$: colour index analogous to the $(U-B)$ colour index in the UBV system, but without the problems caused by the inclusion of the Balmer Jump and confluence.

For stars later than about A3, the hydrogen line index β is an excellent measure of spectral type or temperature and the index c_1 depends primarily on surface gravity. Earlier than A0, these roles are reversed. There is an intermediate region from A0 to A3, at the hydrogen absorption maximum, where neither c_1 nor β can be used alone to yield accurate values of temperature and surface gravity. In this region linear

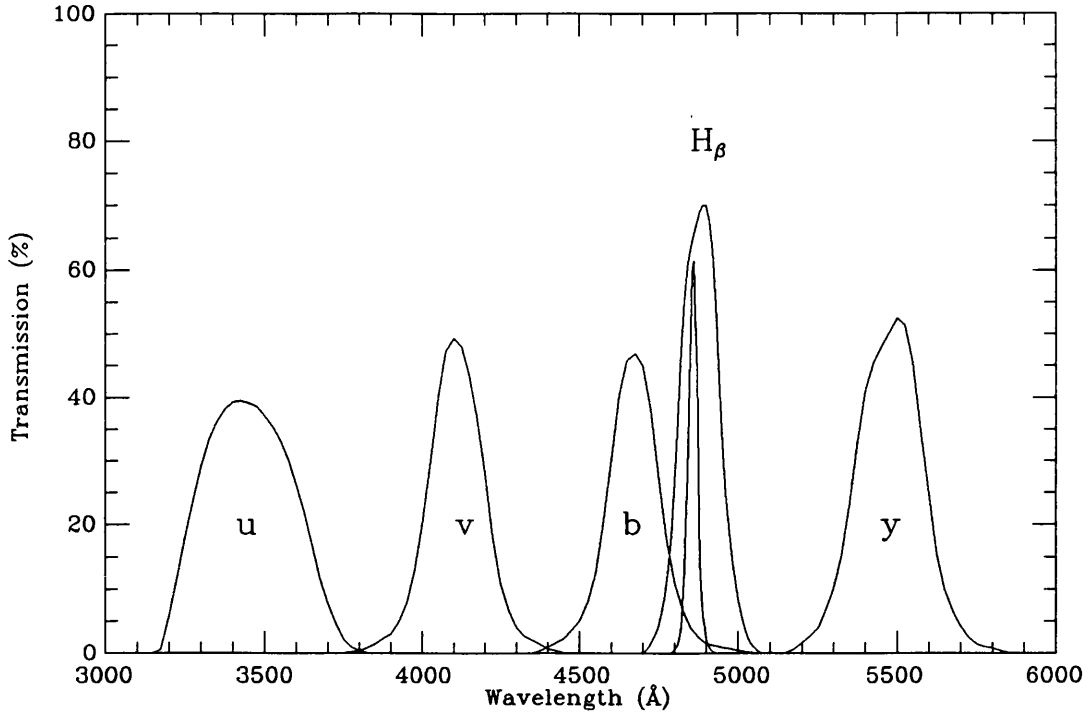

Figure 2.3: *The uvbyβ passbands. From Matsushima (1969), with the Hβ responses taken from Crawford & Mander (1966).*

combinations of the various indices are used to allow two-dimensional classification for normal stars (Strömgren, 1966; Moon & Dworetsky, 1985):

$$a_0 = 1.36(b-y)_0 + 0.36m_0 + 0.18c_0 - 0.2448 \tag{2.1}$$

$$r^* = 0.35c_0 - 0.07(b-y)_0 - \beta + 2.565. \tag{2.2}$$

The observed photometric indices must be corrected for the effects of interstellar reddening prior to their use in the determination of atmospheric parameters. Crawford (1975, 1979) and Hilditch, Hill & Barnes (1983) obtained standard relationships between the photometric indices, the position of the zero-age main-sequence (ZAMS) and the absolute visual magnitude (M_V). Using these relationships, the dereddened colours can be readily obtained. Moon (1985) presented a program, UVBYBETA, to obtain dereddened colours and this code will be used in the present work. However, for the majority of the A and F stars considered the effects of reddening are negligible.

Note that it is conventional to denote m_1, c_1 and $(b-y)_1$ as observed colours and m_0, c_0 and $(b-y)_0$ as dereddened colours.

Before discussing the model calibrations, the m_0 and c_0 colour indices will be outlined, as they are important in the present study of A and F stars.

The m_0 index can be used to provide a measure of metallicity via the δm_0 index, which is defined as follows:

$$\delta m_0 = m_{0\ (\mathrm{ZAMS})} - m_{0\ (\mathrm{STAR})} \tag{2.3}$$

Strömgren (1963b) defined δm_0 in terms of $(b-y)$ as the independent parameter, whereas Crawford (1975) used β as the independent parameter. It is Crawford's definition that will be used here. Moon (1985) used this definition in his programs and stars can be approximately categorized, according to their δm_0, as follows:

Range of δm_0	Category
$\delta m_0 < -0.010$	Am and Ap stars
$-0.010 < \delta m_0 < 0.025$	Normal population I stars
$0.025 < \delta m_0 < 0.045$	Older population I and old disk stars
$0.045 < \delta m_0 < 0.090$	Intermediate population II stars
$0.090 < \delta m_0$	Extreme population II stars

The use of δm_0 in the estimation of metal abundance will be discussed fully in Chapter 6.

The c_0 index can be used to provide a measure of stellar age or evolution from the main sequence via the δc_0 index, which is defined as follows:

$$\delta c_0 = c_{0\ (\mathrm{STAR})} - c_{0\ (\mathrm{ZAMS})} \tag{2.4}$$

The value of δc_0 increases as a star evolves off the ZAMS and is correlated with $\log g$. However, c_0 is not entirely independent of metallicity, so a δm_0 correction should be applied either to $\log g$ (Dworetsky & Moon, 1986) or to c_0 itself, along with a small adjustment for the effects of rotation (Guthrie, 1987):

$$\delta' c_0 = \delta c_0 - 1.2\,\delta m_0 - 1.1 \times 10^{-6} (v \sin i)^2 \tag{2.5}$$

The effect of stellar rotation on δc_0 was also discussed by Gray & Garrison (1989) who found a linear relationship between δc_0 and $v \sin i$ for early F-type cluster dwarfs:

$$\delta c_0 = \delta c_0 - 0.037 \left(\frac{v \sin i}{100} \right) \tag{2.6}$$

This relationship shows that δc_0 is more sensitive to rotational effects than the Guthrie relationship. However, this relationship is strictly an empirical one and valid only for early F-type stars.

2.3.1 Calibration in terms of T_{eff}, log g and [M/H]

By the comparison with colours calculated using model atmosphere flux distributions, the atmospheric parameters of a star can be determined. Ever since the development of the *uvby* system, model atmosphere fluxes have been used to calculate theoretical colours (Strömgren, 1966).

The early calibrations, such as Matsushima (1969) and Olson (1974) suffered from the lack of adequate metal line-blanketing in the model atmosphere calculations. Hence, the colours for the late-type stars were inadequate. With the advent of the Kurucz (1979a) fully line-blanketed model atmosphere calculations, considerably more-reliable colours could be obtained. Several of the important calibrations will now be discussed.

Relyea & Kurucz (1978)

The Relyea & Kurucz (1978) *uvby* calibration was the first using the fully line-blanketed model atmospheres of Kurucz (1979a). They integrated the model fluxes through the filter response functions given by Matsushima (1969). The model *uvby* colours were placed on the standard system by a zero-point shift to align the model colours with the observed values for Vega. The adopted model for this alignment was T_{eff} = 9400 K, log g = 3.95 (Kurucz, 1979a). This zero-point correction was the only shift made to the theoretical colours.

They investigated the accuracy of their calibration and found significant discrepancies for stars cooler than 8500 K (Figure 2.4). The major discrepancy was that the model m_1 colours did not fit the observed main-sequence values. They investigated various causes of the discrepancies, including the inadequate treatment of convection, changes in abundances and microturbulence, missing line opacity, and inaccuracies in the model for Vega. They concluded that there was probably no single cause for the discrepancies, suggesting that convection was probably a major source of error, with contributions from missing opacity and changes in microturbulence.

Philip & Relyea (1979) applied a small correction to the colours of Relyea & Kurucz (1978). They moved the $(b-y), c_1$ grid so that the ZAMS of Crawford (1975) fell on the log g = 4.3 grid line. This shift corrected a small discrepancy in the log g values calculated for F-type stars noted by Relyea & Kurucz.

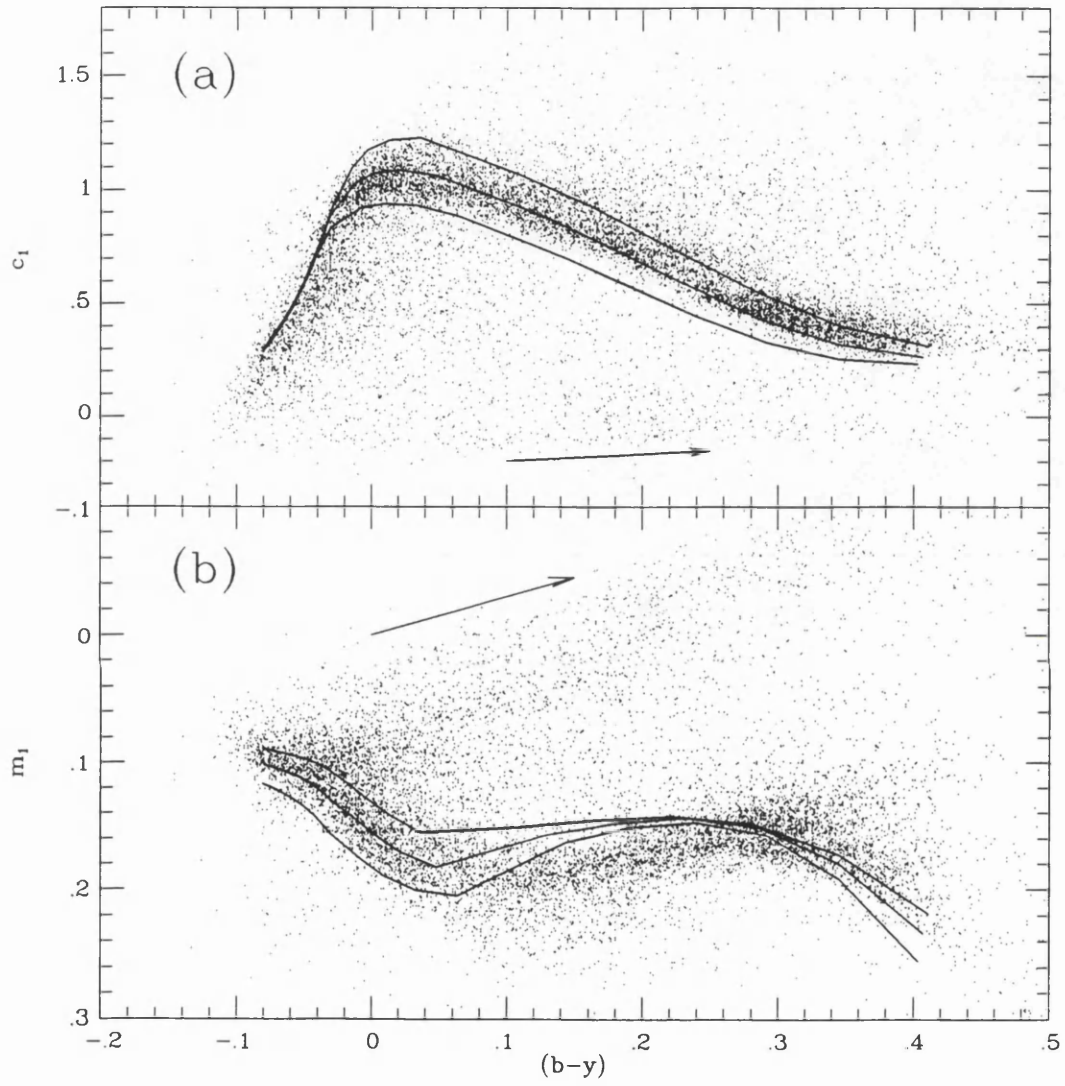

Figure 2.4: *Comparisons of Relyea & Kurucz (1978) indices with observations. The dots are observations from Hauck & Mermilliod (1980). The various lines are, from top to bottom, for* $\log g = 3.5$, *4.0 and 4.5. The direction of interstellar reddening is indicated by the arrow.*

Schmidt (1979)

Schmidt & Taylor (1979) obtained scanner observations of a selection of stars from the list of Crawford & Mander (1966). They calculated values of β from the spectra using:

$$\beta_{\rm calc} = -2.5 \log \left(\frac{\int T_N(\lambda) E(\lambda) d\lambda}{\int T_W(\lambda) E(\lambda) d\lambda} \right) \tag{2.7}$$

where $T_N(\lambda)$ and $T_W(\lambda)$ are the transmission functions of the narrow and wide Hβ filters, respectively, and $E(\lambda)$ is the measured flux of the star. The transmission functions were assumed to be Gaussians centred at 4861Å, with widths of 25Å and 150Å for the narrow and wide filters, respectively. The peak transmissions of the filters were taken to be the same and integrations were truncated where the responses reached 10% of the peak transmission. A comparison with the standard photometric values of β for the stars observed enabled a transformation between the calculated and standard systems to be obtained:

$$\beta_{\rm Std} = 0.993 \beta_{\rm Calc} + 0.559. \tag{2.8}$$

Schmidt (1979) used the above procedure to obtain β indices for the Kurucz (1979a) models. The model Hβ profiles were integrated through the same Gaussian filters and then transformed onto the standard system using the above transformation. Although the models are line-blanketed, the hydrogen line profiles were not. Hence, for the cooler stars, where line-blanketing becomes significant, the indices will not be reliable. Schmidt's β values are, also, too large for stars around A3.

Moon & Dworetsky (1985)

It was because of the above deficiencies that Moon & Dworetsky (1985) undertook to produce empirically calibrated *uvbyβ* grids for the determination of the effective temperature and surface gravity of B, A and F stars. They adjusted the Relyea & Kurucz *uvby* colours and Schmidt Hβ indices to agree with several fundamental $T_{\rm eff}$ stars from Code *et al.* (1976) and carefully selected double-lined detached eclipsing binaries whose surface gravities were well established, mainly from Popper (1980). The fundamental stars are given in Table 2.1. Moon & Dworetsky compared the observed β indices with those interpolated in the grid given by Schmidt. A linear transformation was obtained:

$$\Delta\beta = \beta_{\rm Schmidt} - \beta_{\rm Obs} = 0.1467 \beta_{\rm Schmidt} - 0.3881 \pm 0.011 \tag{2.9}$$

Table 2.1: *Fundamental stars used by Moon & Dworetsky (1985)*

Name	HD	$(b-y)_0$	m_0	c_0	β	T_{eff}	$\log g$
V539 Ara	161783	−0.085	0.106	0.267	2.668	18000	4.01
β Aur	40183	0.017	0.174	1.091	2.888	9200	4.01
AR Aur	34364	−0.035	0.156	0.872	2.862	11000	4.30
α CMa	48915	−0.004	0.158	0.982	2.906	9900	4.32
α CMi	61421	0.272	0.167	0.532	2.674	6500	4.06
RS Cha	75747	0.134	0.191	0.857	2.792	7600	3.99
RZ Cha	93486	0.304	0.165	0.486		6400	3.91
V1143 Cyg	185912	0.290	0.166	0.450	2.663	6500	4.32
δ Equ	202275	0.331	0.158	0.421	2.629	6300	4.35
HS Hya	90242	0.287	0.160	0.397	2.652	6500	4.34
α Lyr	172167	0.004	0.157	1.089	2.903	9500	3.90
U Oph	156247	−0.077	0.101	0.373	2.694	16000	4.12
12 Per	16739	0.341	0.207	0.395	2.633	6200	4.26
PV Pup	62863	0.201	0.165	0.634	2.733	7100	4.27
VV Pyx	71581	0.001	0.161	1.025	2.890	9500	4.09
V760 Sco	147683				2.703	15500	4.21
CD Tau	34335	0.317	0.163	0.456		6400	4.12
γ Vir	110379	0.236	0.156	0.520	2.692	6900	4.21
DM Vir	123423	0.300	0.177	0.477	2.655	6500	4.11

There was no evidence for bifurcation. They also found that the c_0 colours of Relyea & Kurucz for $T_{eff} \geq 8500$ K and Philip & Relyea for $T_{eff} < 8500$ K were free from scaling errors, but were on average 0.008 mag lower than observed values. A zero-point shift was thus applied to the c_0 values. No significant difference was found between the observed and synthetic $(b-y)_0$ values and for $T_{eff} \geq 8500$ K the observed m_0 values agreed with Relyea & Kurucz. Moon & Dworetsky used the corrected synthetic β indices and c_0 colours to construct two grids; one for T_{eff} <8500 K (Figure 2.5), the other for T_{eff} >8500 K. However, the (β, c_0) grids cannot be used for unambiguous determination of T_{eff} and $\log g$ in the region of $8500 < T_{eff} < 11000$ K and $3.5 < \log g < 4.5$. For stars within this range a (a_0, r^*) grid was constructed.

Comparing the grids with the fundamental values, suggests that they should be able to reproduce the T_{eff} and $\log g$ of a star to ±250 K and ±0.10 dex respectively. Moon & Dworetsky performed an analysis of three Am binaries whose components were sufficiently similar for a mean value of $\log g$ to be calculated. They found good agreement between the grid values of $\log g$, and the $\log g$ determined from mass and radius. This agreement coupled with the apparent insensitivity of the synthetic β indices to metal abundances (Schmidt, 1979), suggested that the grids are applicable to the calculation of T_{eff} and $\log g$ for Am stars.

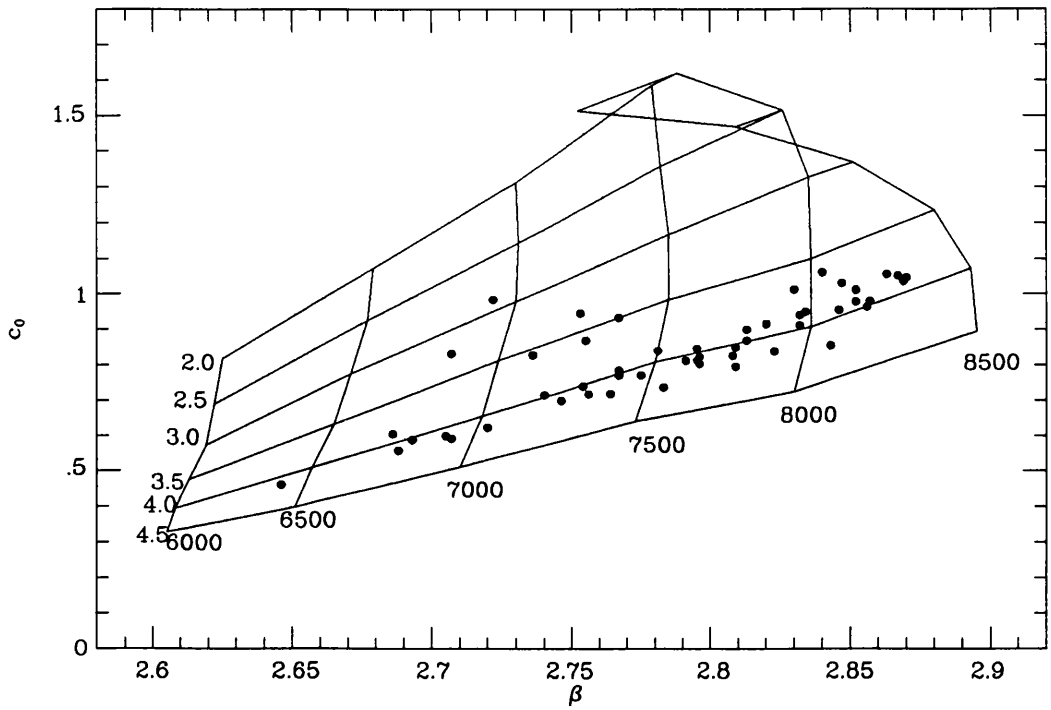

Figure 2.5: *The Moon & Dworetsky (1985) (β, c_0) grid. The dots are the photometry points for the JKT programme stars.*

Dworetsky & Moon (1986) studied the surface gravities of the stars in five open clusters. They plotted the difference between the photometric $\log g$ of each star and a mean 'cluster' $\log g$ as a function of δm_0, for both 48 normal and 34 Am stars in the clusters; there was no significant difference between the normal and Am relationships. From a least-squares fit they obtained a correction which must be applied to the value of $\log g$ obtained from their grids:

$$\log g \ = \log g_{(\mathrm{grid})} + 3.442 \, \delta m_0 \qquad (2.10)$$

Except for this, they concluded that the grids seemed very insensitive to line blanketing effects. There was no T_{eff} correction because the β index was not apparently sensitive to δm_0 and because of a lack of fundamental T_{eff} values for Am stars.

Lester, Gray & Kurucz (1986)

Lester, Gray & Kurucz (1986) calculated theoretical *uvbyβ* indices based on the Kurucz (1979a) model fluxes. The *uvby* colours were obtained using the methods employed by Relyea & Kurucz (1978). The β indices were obtained by integrat-

ing model fluxes through the transmission functions given by Crawford & Mander (1966).

Their transformation procedure was, however, different from that of Relyea & Kurucz (1978). They took spectrophotometry from the secondary standard stars of Taylor (1984) and additionally included α CMi for the cool T_{eff} region. They used ultraviolet fluxes from various sources and obtained the T_{eff} and $\log g$ for these stars using the flux fitting technique employed by Lane & Lester (1984) (See Chapter 3 for details). The adopted parameters for their standard stars are given in Table 2.2. They found that their values for T_{eff} agreed well with those of Code *et al.* (1976), being on average 170K cooler, but still within the error bars. The values of $\log g$ agreed with those obtained by Code (1975) using the mass-luminosity relationship. The *uvbyβ* indices for the five stars were then obtained from the uncalibrated grids. Note that *uvbyβ* indices are the raw model values and needed to be transformed onto the standard system.

Table 2.2: *Standard stars used by Lester, Gray & Kurucz (1986)*

parameter	γ Gem (HR 2421)	α CMi (HR 2943)	β Leo (HR 4534)	η UMa (HR 5191)	α Lyr (HR 7001)
spectral type	A0 IV	F5 IV-V	A3 V	B3 V	A0 Va
T_{eff}	9000	6500	8600	17000	9500
$\log g$	3.65	3.95	4.20	3.90	3.95
$(b-y)$	0.007	0.272	0.044	−0.080	0.004
m_1	0.149	0.167	0.210	0.106	0.157
c_1	1.186	0.532	0.975	0.296	1.089
β	2.869	2.674	2.900	2.694	2.903

The transformation from the models to the standard system was performed by a least squares fit to the relations of Crawford & Barnes (1970) and Crawford & Mander (1966):

$$(b-y)_{\rm std} = C + D \times (b-y)_{\rm nat} \quad (2.11)$$

$$(c_1)_{\rm std} = G + H \times (c_1)_{\rm nat} + I \times (b-y) \quad (2.12)$$

$$(m_1)_{\rm std} = E + F \times (m_1)_{\rm nat} + J \times (b-y) \quad (2.13)$$

$$\beta_{\rm std} = A_0 + A_1 \times \beta_{\rm nat} \quad (2.14)$$

The coefficients thus obtained were used to transform the whole model grid onto the standard system. They did not give the coefficients but stated that they compared their values with those given by Crawford & Mander and Crawford & Barnes. They

found that their values were consistent except that they did not get $I \simeq -2J$ and the zero-point adjustment for the β fit was larger than any of Crawford & Mander's examples.

This procedure, they argued, should be preferred to the Relyea & Kurucz (1978) zero-point shift, since it is more like the method employed in the transformation of photometric observations onto the standard *uvbyβ* system. However, any inherent deficiencies in the model colours may be masked by the transformation. Also, using only 5 stars for the transformation means that the coefficients are not that reliable. Especially important here is that the cool values rely on the adopted T_{eff} and $\log g$ of α CMi, where metallicity (blanketing) effects can be significant. Also, they assumed that all the stars have solar abundances, which is not necessarily the case. Ideally, more standard stars are needed when employing this transformation.

The Lester, Gray & Kurucz grids based on the Kurucz (1979a) models are denoted LGK_a. They also presented a second set of grids based on the modified convection models of Lester, Lane & Kurucz (1982), these are denoted LGK_b.

Kurucz (1991)

After completion of the majority of the present work preprints were received from Kurucz (1991a,b) in which he outlined his new opacity calculations and new model calculations. He also gave preliminary *UBV* and *uvby* colours obtained using the procedures of Buser & Kurucz (1978) and Relyea & Kurucz (1978). These new models, not yet published, are a considerable improvement on the previous Kurucz (1979a) standard.

2.3.2 Conclusion

The various *uvbyβ* calibrations were compared to the observed main sequence relationships of Philip & Egret (1980) (see Figure 2.6). All the calibrations fit the c_0 reference line very well. None of the calibrations fit the observed m_0 reference line for $(b-y) > 0.1$, due to the inadequacies of the Kurucz (1979a) models. The new Kurucz (1991b) colours reproduces the shape of the observed main-sequence m_0 curve well, but appears to be displaced. This displacement could well be due to the zero-point shift used by Kurucz.

North & Kobi (1991) compared the Moon & Dworetsky and Lester, Gray &

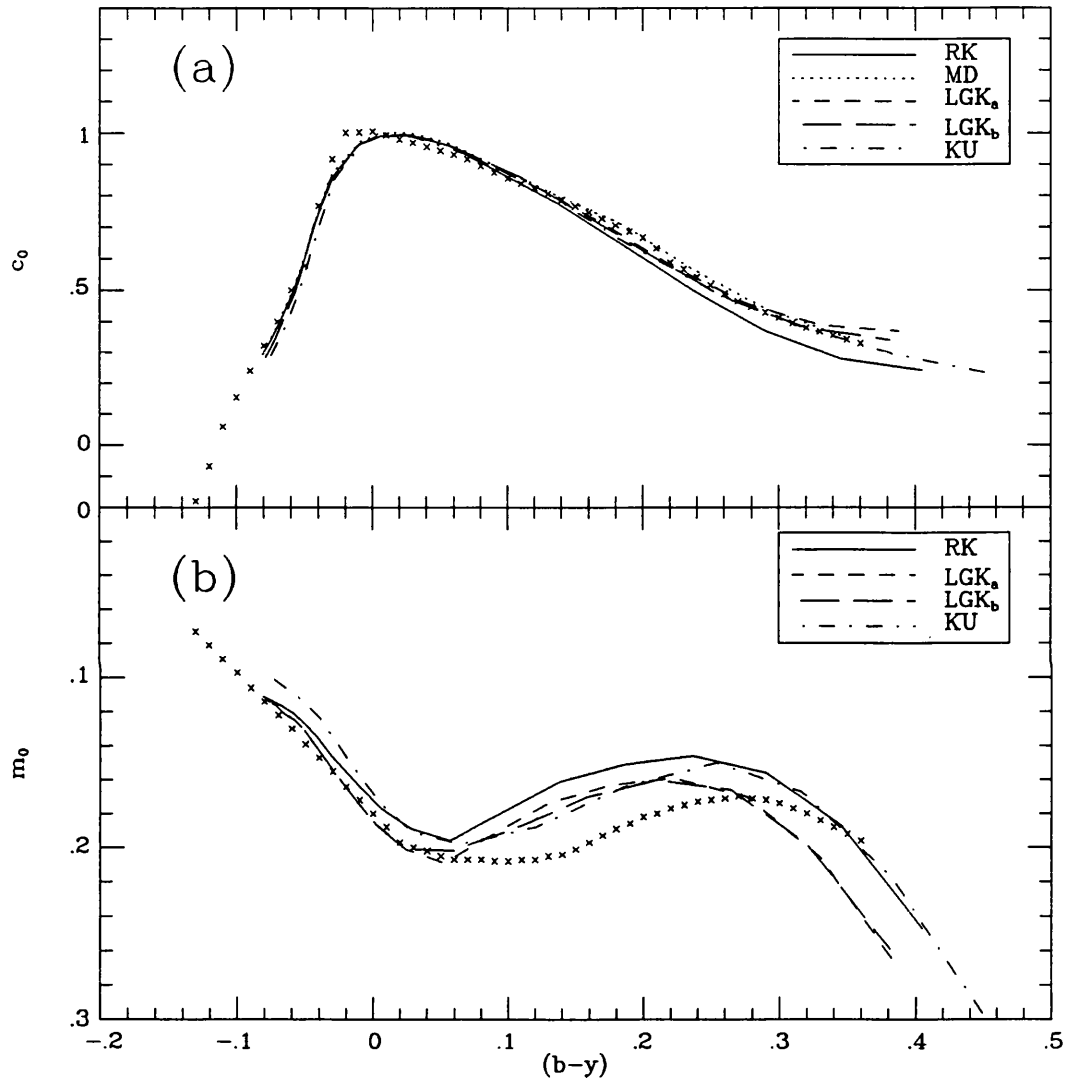

Figure 2.6: *Comparison of the various uvbyβ calibrations. The various calibrations are presented for* $\log g = 4.3$. *The crosses indicate the position of the main sequence as given by Philip & Egret (1980). All the model calibrations fit the observed* c_0 *line (a), but the fit to the* m_0 *line (b) is not so good.*

Kurucz grids. They found good agreement in the range $7500 < T_{eff} < 12000$ K and $3.5 < \log g < 4.5$. They stated that the Moon & Dworetsky calibration appeared more reliable due to the larger number of fundamental stars. Both grids tended to overestimate $\log g$ for $T_{eff} < 6500$ K and underestimate it for $T_{eff} > 12000$ K, but the MD grid is better in the latter range. They suggested that it would be possible to improve the $\log g$ calibration using cluster members as standard stars.

Napiwotzki, Schönberner & Wenske (1991) compared the MD and LGK_a $uvby\beta$ calibrations and found that the MD grid was in better agreement with their results. They recommended that the MD calibration be used to determine the T_{eff} and $\log g$ of main-sequence stars.

2.4 Geneva photometry

An intermediate and wide-passband type of photometry has been used since 1960 at the Geneva Observatory. This seven colour system has the following passbands:

Band	Wavelength (Å)	Half-width (Å)
U	3458	170
B	4248	283
V	5508	298
B_1	4022	171
B_2	4480	164
V_1	5408	202
G	5814	206

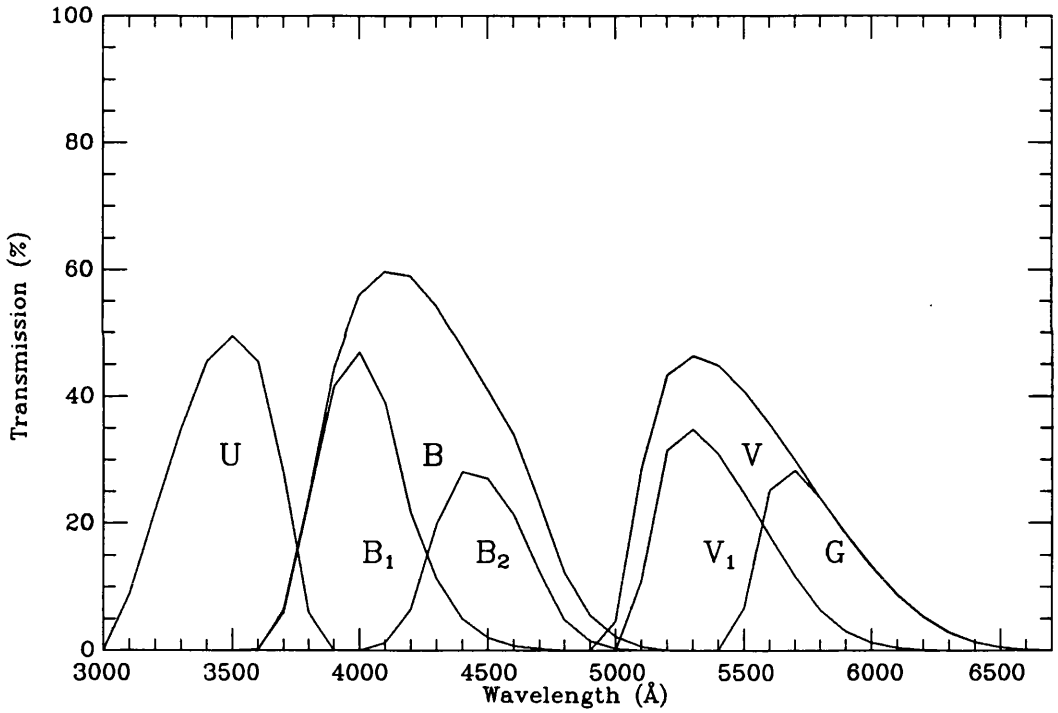

Figure 2.7: *The $UBVB_1B_2V_1G$ passbands. From Rufener & Maeder (1971)*

The parameters adopted by Golay (1972) which summarize the main characteristics of the system are the following:

$$d = (U - B_1) - 1.430\,(B_1 - B_2) \tag{2.15}$$

$$\Delta = (U - B_2) - 0.832\,(B_2 - G) \tag{2.16}$$

$$g = (B_1 - B_2) - 1.357\,(V_1 - G) \tag{2.17}$$

The basic colour index of this photometric system is $(B_2 - V_1)$. The g parameter is very sensitive to the Balmer line strengths and thus can be used as a luminosity

parameter for hot stars. It is also very sensitive to differential blanketing by metal lines between B_1 and B_2 and can be used to separate Am stars from normal stars. The d parameter is a measure of the Balmer discontinuity and is sensitive to chemical composition for Am stars. The Δ parameter is also a measure of the Balmer discontinuity and is very sensitive to chemical composition for A and F stars. Other parameters have been discussed by Hauck (1968), specifically the m_2 index which has almost the same properties as g and is defined as follows:

$$m_2 = (B_1 - B_2) - 0.457\,(B_2 - V_1) \tag{2.18}$$

Hauck (1973, 1975) discussed a three-dimensional representation for stars in the spectral range A0 to G5. This representation used $(B_2 - V_1)$ as the temperature parameter, d as the luminosity parameter and m_2 as a blanketing parameter. He reported that for the Am stars the absolute magnitude obtained was no different from that of normal stars. Also, as Hauck & Van't Veer (1970) found, the effect of blanketing on $(B_2 - V_1)$ in Am stars was negligible.

In a similar manner to the Strömgren δm_0 index the m_2 index can be used to provide a measure of metallicity. The colour difference, Δm_2 is defined as follows:

$$\Delta m_2 \; = m_{2\ (\mathrm{STAR})} - m_{2\ (\mathrm{HYADES})} \tag{2.19}$$

The Hyades reference sequence used in the present work is that given by Hauck (1973). The independent variable used is the $(B_2 - V_1)$ index. This parameter will be used in Chapter 6 to determine stellar metal abundances.

North & Hauck (1979) presented a calibration of Geneva parameters for the Kurucz (1979a) models. They compared their calibration with the T_{eff} values given by Code *et al.* (1976). The T_{eff} vs $(B_2 - V_1)$ diagram gave excellent agreement between the models and the observations. But again, there is a large discrepancy between the observed and model d and m_2 colours for A and F stars.

Kobi & North (1990) presented a semi-empirical calibration of Geneva Photometry in terms of T_{eff}, $\log g$ and [M/H] for main sequence A4 to G5 stars, using the three dimensional representation outlined by Hauck (1973, 1975). The calibration based on Kurucz (1979a) model atmospheres and corrected by means of fundamental stars, is valid for stars whose interstellar reddening is either negligible or well known. Indeed, in this T_{eff} range, Geneva photometry is unable to discriminate between reddening and temperature effects (Nicolet, 1981).

Kobi & North used three sets of standard stars to empirically calibrate model $(B_2 - V_1)$, d and m_2 indices in terms of T_{eff}, $\log g$ and [M/H]. They used a large number of stars to make the calibration less sensitive to error caused by only using a few well-known fundamental stars. The surface gravity standards were augmented by members of the Pleiades. For the Pleiades stars the $\log g$ was obtained from the age of the cluster and the evolutionary tracks of Maeder & Meynet (1988). The final calibration was able to recover the parameters of the standard stars to ± 76 K and ± 0.19 dex in T_{eff} and $\log g$ respectively.

Due to the shortcomings of the Kurucz (1979a,b) models, the Kobi & North calibration does not fit with the observations of Am stars. The [M/H] = +1.0 models give m_2 values that are lower than those calculated using [M/H] = +0.5 models. Many Am stars are observed to have m_2 values which are larger than any of the model values. The Kurucz model opacities clearly cannot adequately represent the fluxes of Am stars.

2.5 Results and conclusion

Various published calibrations of photometry in terms of T_{eff} and $\log g$ have been discussed. The current work, however, will concentrate on the $uvby\beta$ system. The main calibrations used in the present work will be those of Moon & Dworetsky and Lester, Gray & Kurucz. Both of these calibrations were based on the Kurucz (1979a) models. The results for the JKT programme stars are given in the tables at the end of the chapter.

The UBV results give values of $\log g$ which are clearly too low. This is because the model $(U - B)$ colours are not adequately represented, due to the difficulty of reproducing the U-band magnitude (Buser & Kurucz, 1978).

Figure 2.8 shows a comparison of the results obtained from the various $uvby\beta$ calibrations. The results from the (β, c_0) grid of MD are systematically hotter than those obtained from the LGK_a grid by $\sim$100 K. The LGK_b grid, based on the modified convection models, gives values of T_{eff} which are even lower, but still only $\sim$200 K. The discrepancies are larger when the $((b-y), c_0)$ grids are used to obtain T_{eff}.

The behaviour of the Kurucz (1991b) grid is different from the others. This change is due to the improvement in the opacity distributions used in the model

calculations. Even so, the changes amount to only ~200 K at most. Between 7000 ~ 7500 K the new grid give practically the same results as the Moon & Dworetsky $((b-y), c_0)$ grid.

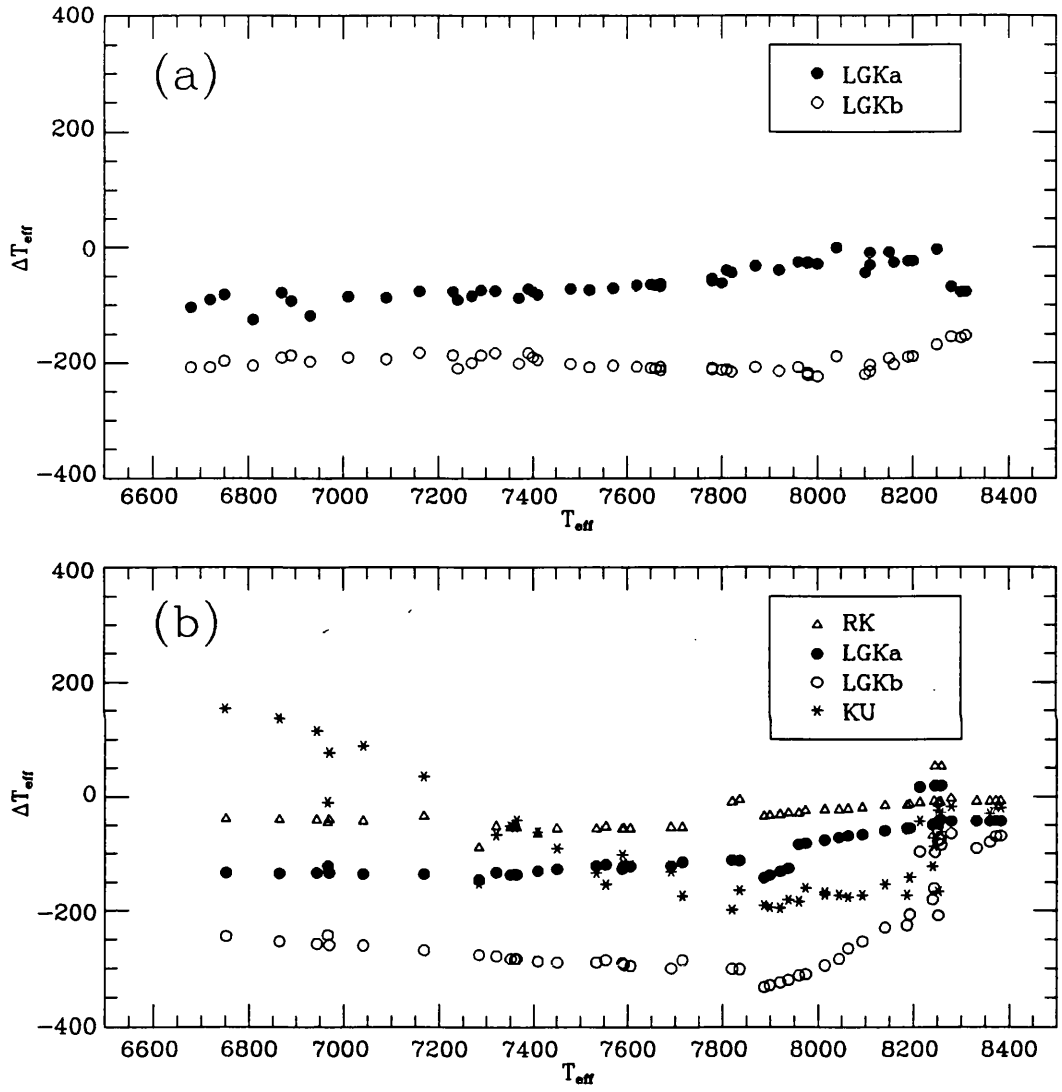

Figure 2.8: *Comparison of the $T_{\rm eff}$ values obtained from the various uvbyβ grids. The differences are given relative to the $T_{\rm eff}$ obtained from the Moon & Dworetsky grids, $\Delta T_{\rm eff} = T_{\rm eff}(grid) - T_{\rm eff}(MD)$. The two plots show the differences for (a) the (β, c_0) and (b) the $((b-y), c_0)$ grids respectively.*

The Geneva photometry results are in good agreement with the *uvbyβ* calibrations. They give slightly cooler temperatures than the MD grid for late-A and F stars, but by only ~200 K.

In conclusion, the various photometric calibrations all give generally the same

T_{eff} and $\log g$ for A and F stars to within ± 200 K and ± 0.2 dex. However, the model m_0 and m_2 colours do not adequately reproduce the observed values. This means that using such colours to obtain theoretical metal abundances is not practicable. Nevertheless, empirical calibration of [M/H] in terms of δm_0 or Δm_2 is possible and will be discussed in Chapter 6.

Table 2.3: *Results from UBV grids*

			BK		KU	
HR	$(B-V)$	$(U-B)$	T_{eff}	$\log g$	T_{eff}	$\log g$
63	0.06	0.04	8940	4.29	8970	4.27
114	0.24	0.09	7370	3.06	7460	3.58
269	0.13	0.15	7590	2.25	7820	3.09
972	−0.01	−0.01	9430	3.88	9420	3.88
984	0.23	0.09	7430	3.09	7530	3.65
1197	0.20	0.14	7390	2.50	7520	3.16
1254	0.37	0.00	6730	3.53	6890	3.54
1292	0.36	0.01	6780	3.50	6920	3.48
1331	0.28	0.08	7130	3.04	7280	3.50
1351	0.28	0.08	7130	3.04	7280	3.50
1354	0.37	0.02	6700	3.36	6860	3.41
1356	0.22	0.10	7450	2.99	7560	3.59
1368	0.32	0.10	6880	2.75	6970	3.15
1376	0.30	0.13	6930	2.46	7010	3.01
1380	0.15	0.12	7750	2.90	7920	3.58
1385	0.37	0.04	6680	3.18	6830	3.30
1387	0.13	0.13	7790	2.86	7970	3.44
1388	0.25	0.10	7280	2.91	7360	3.38
1389	0.05	0.08	8640	3.75	8650	3.69
1392	0.26	0.14	7090	2.39	7170	3.00
1394	0.25	0.14	7140	2.40	7250	3.03
1403	0.27	0.10	7140	2.85	7240	3.26
1408	0.32	0.06	6930	3.14	7030	3.28
1412	0.18	0.13	7540	2.67	7690	3.36
1414	0.23	0.12	7320	2.71	7420	3.27
1422	0.32	0.10	6880	2.75	6970	3.15
1427	0.17	0.13	7570	2.62	7750	3.40
1428	0.26	0.10	7200	2.87	7300	3.32
1430	0.26	0.10	7200	2.87	7300	3.32
1444	0.25	0.08	7330	3.15	7430	3.63
1458	0.18	0.11	7640	2.97	7790	3.64
1472	0.31	0.06	6990	3.16	7170	3.50
1473	0.12	0.13	7840	2.87	8020	3.43
1479	0.15	0.13	7700	2.75	7860	3.44
1480	0.26	0.13	7120	2.52	7220	3.07
1507	0.25	0.08	7330	3.15	7430	3.63
1519	0.19	0.14	7440	2.52	7570	3.18
1547	0.21	0.12	7430	2.75	7540	3.37
1620	0.16	0.15	7500	2.35	7680	3.06
1670	0.27	0.04	7300	3.50	7400	3.96
1672	0.24	0.16	7120	2.12	7220	2.86
1905	0.22	0.10	7450	2.99	7560	3.59
2085	0.33	0.01	6950	3.56	7070	3.56
2124	0.16	0.11	7750	3.09	7910	3.69
3569	0.19	0.07	7780	3.47	7910	4.04
3624	0.35	0.15	6660	2.16	6770	2.58
3775	0.46	0.02	6270	3.40	6490	3.52
3888	0.29	0.10	7030	2.80	7110	3.21
4031	0.31	0.20	6790	1.56	6830	2.17
4033	0.03	0.06	8800	3.66	8810	3.64
4295	−0.02	0.01	9000	3.08	8540	2.12
4300	0.05	0.05	8880	4.07	8910	4.05
4357	0.12	0.12	7900	3.02	8090	3.57
4359	−0.01	0.06	8510	2.59	8520	2.60
4399	0.41	0.07	6460	2.89	6630	3.00
4534	0.09	0.07	8570	4.20	8610	4.15
4554	0.00	0.02	9120	3.65	9130	3.66
4660	0.08	0.07	8640	4.19	8660	4.10
4689	0.02	0.06	8810	3.50	8780	3.44
4715	0.33	0.18	6710	1.81	6790	2.31
4963	−0.01	−0.01	9430	3.88	9420	3.88
7001	0.00	−0.01	9470	4.08	9460	4.06
7653	0.18	0.16	7380	2.25	7520	2.92
8410	0.23	0.15	7200	2.28	7320	2.99
8641	−0.01	−0.01	9430	3.88	9420	3.88

Colours taken from Hoffleit (1982). BK = Buser & Kurucz (1978), KU = Kurucz (1991b). The $\log g$ values are very unreliable due to calibration problems discussed in the text.

Table 2.4: *uvbyβ photometry for the JKT programme stars*

HR	$(b-y)_0$	m_0	c_0	β	$E(b-y)$	δm_0	δc_0	$\delta' c_0$
63	0.026	0.180	1.050	2.879	−0.001	0.000		
114	0.169	0.165	0.869	2.755	−0.004	0.023	0.179	0.151
269	0.067	0.194	1.056	2.863	0.001	0.008	0.160	0.145
972	−0.014	0.158	1.105	2.888	−0.007	−0.011		
984	0.138	0.190	0.846	2.795	−0.005	0.009	0.076	0.060
1197	0.103	0.196	0.941	2.832	0.011	0.008	0.107	0.072
1254	0.249	0.147	0.557	2.688	−0.002	0.023	0.067	0.038
1292	0.231	0.163	0.592	2.707	−0.002	0.010	0.040	0.028
1331	0.172	0.186	0.786	2.767	0.003	0.006	0.072	0.054
1351	0.172	0.193	0.771	2.767	−0.001	−0.001	0.057	0.045
1354	0.240	0.171	0.588	2.693	−0.009	−0.001	0.082	0.064
1356	0.127	0.205	0.870	2.813	0.002	−0.003	0.064	0.063
1368	0.192	0.205	0.718	2.756	0.004	−0.017	0.026	0.046
1376	0.176	0.238	0.737	2.783	0.004	−0.042	−0.009	0.041
1380	0.080	0.210	0.981	2.857	0.001	−0.007	0.097	0.102
1385	0.237	0.178	0.599	2.705	0.005	−0.005	0.054	0.043
1387	0.064	0.202	1.053	2.867	0.006	0.000	0.149	0.142
1388	0.149	0.193	0.840	2.781	−0.006	0.003	0.098	0.069
1389	0.020	0.193	1.046	2.889	−0.019	−0.017		
1392	0.165	0.175	0.947	2.753	−0.001	0.012	0.261	0.204
1394	0.150	0.188	0.934	2.767	−0.006	0.004	0.220	0.175
1403	0.165	0.212	0.771	2.775	−0.006	−0.017	0.041	0.053
1408	0.197	0.173	0.699	2.746	0.009	0.012	0.027	0.001
1412	0.097	0.203	1.013	2.830	0.002	0.001	0.183	0.175
1414	0.112	0.226	0.912	2.832	0.002	−0.022	0.078	0.093
1422	0.197	0.196	0.716	2.740	−0.006	−0.014	0.056	0.053
1427	0.085	0.218	0.964	2.856	0.003	−0.015	0.082	0.094
1428	0.141	0.234	0.796	2.809	−0.005	−0.032	−0.002	0.036
1430	0.147	0.203	0.813	2.795	0.007	−0.004	0.043	0.038
1444	0.144	0.205	0.823	2.796	−0.002	−0.005	0.051	0.042
1458	0.096	0.190	0.951	2.834	−0.004	0.014	0.113	0.095
1472	0.187	0.188	0.741	2.754	0.005	0.000	0.053	0.038
1473	0.062	0.199	1.047	2.870	0.005	0.003	0.137	0.127
1479	0.080	0.196	1.012	2.852	0.008	0.008	0.138	0.113
1480	0.142	0.230	0.827	2.808	0.003	−0.028	0.031	0.061
1507	0.150	0.195	0.813	2.791	0.000	0.003	0.051	0.039
1519	0.091	0.252	0.955	2.846	−0.011	−0.048	0.093	0.148
1547	0.122	0.207	0.900	2.813	−0.002	−0.005	0.094	0.078
1620	0.080	0.203	1.031	2.847	−0.002	0.001	0.167	0.148
1670	0.149	0.245	0.803	2.796	−0.009	−0.045	0.031	0.084
1672	0.133	0.247	0.839	2.823	0.005	−0.044	0.023	0.076
1905	0.132	0.203	0.850	2.809	0.001	−0.002	0.052	0.040
2085	0.218	0.160	0.622	2.720	−0.001	0.018	0.023	0.001
2124	0.083	0.203	0.979	2.852	0.010	0.002	0.105	0.102
3569	0.104	0.216	0.856	2.843	−0.002	−0.012	0.000	−0.011
3624	0.196	0.245	0.719	2.764	0.021	−0.054	0.011	0.075
3775	0.304	0.156	0.461	2.646	0.010	0.023	0.079	0.051
3888	0.192	0.163	0.829	2.736	0.004	0.017	0.181	0.147
4031	0.185	0.172	0.984	2.722	0.011	0.001	0.378	0.369
4033	0.003	0.164	1.137	2.873	0.017	−0.002		
4295	−0.005	0.157	1.088	2.880	0.000	−0.002		
4300	0.021	0.194	1.020	2.916	−0.007	−0.018		
4357	0.064	0.197	1.036	2.869	0.002	0.005	0.128	0.086
4359	−0.005	0.157	1.149	2.874	0.009	−0.002		
4399	0.257	0.175	0.605	2.686	0.010	−0.005	0.121	0.127
4534	0.044	0.210	0.975	2.900	−0.005	−0.020	0.005	0.013
4554	−0.005	0.157	1.111	2.885	0.011	−0.002		
4660	0.035	0.184	1.054	2.883	0.006	0.001		
4689	0.006	0.166	1.131	2.863	0.010	−0.001		
4715	0.223	0.179	0.832	2.707	0.003	−0.006	0.280	0.281
4963	−0.014	0.148	1.145	2.838	0.021	−0.001		
7001	−0.003	0.159	1.088	2.903	0.007	−0.002		
7653	0.084	0.205	1.062	2.840	0.014	−0.001	0.212	0.213
8410	0.117	0.251	0.917	2.820	−0.010	−0.048	0.097	0.154
8641	−0.010	0.153	1.107	2.857	0.005	−0.001		

uvbyβ photometry taken from Hauck & Mermilliod (1990) and dereddened using the code of Moon (1985).

Table 2.5: *Results from (β, c_0) grids*

					MD		LGK_a		LGK_b	
HR	c_0	β	a_0	r^*	T_{eff}	$\log g$	T_{eff}	$\log g$	T_{eff}	$\log g$
63			0.044	0.052	8970	3.97	8940	3.91	8940	3.91
114	0.869	2.755			7270	3.54	7180	3.49	7070	3.49
269	1.056	2.863			8250	3.81	8240	3.80	8080	3.82
972			−0.008	0.065	9750	3.88	9680	3.87	9680	3.87
984	0.846	2.795			7650	3.97	7580	3.91	7440	3.92
1197	0.941	2.832			7980	3.94	7950	3.89	7750	3.91
1254	0.557	2.688			6720	4.10	6620	3.98	6510	3.93
1292	0.592	2.707			6890	4.15	6790	4.00	6700	4.01
1331	0.786	2.767			7400	3.94	7320	3.88	7210	3.89
1351	0.771	2.767			7410	4.00	7320	3.93	7210	3.94
1354	0.588	2.693			6750	4.00	6660	3.89	6550	3.86
1356	0.870	2.813			7820	4.03	7770	3.96	7600	3.98
1368	0.718	2.756			7320	4.10	7240	4.02	7130	4.03
1376	0.737	2.783			7570	4.27	7490	4.17	7360	4.18
1380	0.981	2.857			8200	3.98	8170	3.95	8010	3.97
1385	0.599	2.705			6870	4.09	6790	3.98	6670	3.96
1387	1.053	2.867			8280	3.84	8210	3.84	8120	3.85
1388	0.840	2.781			7520	3.88	7440	3.82	7310	3.82
1389			0.040	0.041	9030	4.06	9000	3.99	9000	3.99
1392	0.947	2.753			7240	3.29	7140	3.22	7030	3.22
1394	0.934	2.767			7370	3.46	7280	3.39	7160	3.40
1403	0.771	2.775			7480	4.07	7400	4.00	7270	4.00
1408	0.699	2.746			7230	4.08	7150	4.00	7040	4.00
1412	1.013	2.830			7960	3.73	7930	3.67	7750	3.70
1414	0.912	2.832			7980	4.03	7950	3.97	7760	3.99
1422	0.716	2.740			7160	3.95	7080	3.88	6970	3.88
1427	0.964	2.856			8190	4.02	8160	3.99	8000	4.01
1428	0.796	2.809			7800	4.25	7730	4.17	7580	4.18
1430	0.813	2.795			7660	4.09	7590	4.02	7450	4.02
1444	0.823	2.796			7670	4.06	7600	3.99	7450	4.00
1458	0.951	2.834			8000	3.93	7970	3.87	7770	3.89
1472	0.741	2.754			7290	3.99	7210	3.92	7100	3.92
1473	1.047	2.870			8310	3.87	8230	3.87	8150	3.89
1479	1.012	2.852			8150	3.87	8140	3.83	7950	3.85
1480	0.827	2.808			7780	4.14	7720	4.07	7560	4.08
1507	0.813	2.791			7620	4.05	7550	3.98	7410	3.99
1519	0.955	2.846			8110	3.99	8080	3.95	7890	3.97
1547	0.900	2.813			7810	3.94	7770	3.87	7590	3.89
1620	1.031	2.847			8110	3.79	8100	3.74	7900	3.77
1670	0.803	2.796			7670	4.13	7600	4.05	7460	4.06
1672	0.839	2.823			7920	4.20	7880	4.12	7700	4.15
1905	0.850	2.809			7780	4.07	7720	4.00	7570	4.01
2085	0.622	2.720			7010	4.15	6920	4.05	6810	4.04
2124	0.979	2.852			8160	3.96	8130	3.92	7950	3.94
3569	0.856	2.843			8100	4.28	8050	4.21	7880	4.23
3624	0.719	2.764			7390	4.17	7310	4.09	7200	4.09
3775	0.461	2.646			6360	4.09	6130	3.91	6030	3.81
3888	0.829	2.736			7090	3.48	7000	3.43	6890	3.43
4031	0.984	2.722			6930	2.85	6810	2.72	6730	2.72
4033			0.023	0.090	9290	3.68	9230	3.69	9230	3.69
4295			0.001	0.066	9620	3.87	9540	3.85	9540	3.85
4300			0.037	0.005	9050	4.34	9030	4.23	9030	4.23
4357	1.036	2.869			8300	3.89	8220	3.90	8140	3.91
4359			0.012	0.093	9460	3.66	9390	3.68	9390	3.68
4399	0.605	2.686			6680	3.83	6570	3.73	6470	3.70
4534			0.066	0.003	8660	4.34	8600	4.26	8660	4.26
4554			0.005	0.069	9550	3.84	9480	3.83	9480	3.83
4660			0.059	0.048	8770	3.99	8700	3.94	8750	3.94
4689			0.027	0.097	9230	3.62	9180	3.64	9180	3.64
4715	0.832	2.707			6810	3.15	6680	3.05	6600	3.04
4963			−0.004	0.129	9710	3.49	9640	3.46	9640	3.46
7001			0.004	0.043	9550	4.06	9490	3.99	9490	3.99
7653	1.062	2.840			8040	3.67	8030	3.61	7850	3.65
8410	0.917	2.820			7870	3.94	7830	3.87	7660	3.89
8641			−0.004	0.096	9700	3.65	9630	3.67	9630	3.67

Colours taken from Hauck & Mermilliod (1990) and dereddened using relations of Crawford (1975, 1979). MD = Moon & Dworetsky (1985), LGK = Lester, Gray & Kurucz (1986) with the subscript referring to the Kurucz grid used (see text).

Table 2.6: *Results from $((b-y), c_0)$ grids*

			RK		MD		LGK_a		LGK_b		KU	
HR	$(b-y)_0$	c_0	T_{eff}	$\log g$	T_{eff}	$\log g$	T_{eff}	$\log g$	T_{eff}	$\log g$	T_{eff}	$\log g$
63	0.026	1.050	8940	4.12	8950	4.15	8880	4.12	8880	4.12	8940	4.10
114	0.169	0.869	7500	3.65	7550	3.86	7430	3.72	7260	3.69	7390	3.69
269	0.067	1.056	8320	3.89	8330	3.93	8280	3.90	8240	3.91	8290	3.89
972	−0.014	1.105	9950	3.50	9960	3.56	10050	2.74	10050	2.74	9990	3.46
984	0.138	0.846	7930	4.04	7960	4.14	7870	4.10	7640	4.08	7770	4.09
1197	0.103	0.941	8170	4.00	8190	4.06	8130	4.04	7980	4.06	8050	4.04
1254	0.249	0.557	6820	3.92	6860	4.20	6720	4.10	6610	4.04	7000	4.01
1292	0.231	0.592	6990	3.98	7040	4.25	6900	4.14	6770	4.10	7120	4.07
1331	0.172	0.786	7530	3.91	7590	4.13	7470	4.00	7290	3.97	7470	4.02
1351	0.172	0.771	7540	3.96	7600	4.18	7480	4.06	7300	4.03	7480	4.06
1354	0.240	0.588	6900	3.90	6940	4.17	6800	4.06	6680	4.00	7050	3.98
1356	0.127	0.870	8020	4.05	8040	4.13	7970	4.10	7760	4.10	7870	4.10
1368	0.192	0.718	7340	3.94	7400	4.20	7270	4.06	7120	4.01	7340	4.05
1376	0.176	0.737	7530	4.05	7580	4.27	7460	4.15	7290	4.13	7480	4.13
1380	0.080	0.981	8270	4.06	8270	4.10	8230	4.07	8210	4.09	8260	4.06
1385	0.237	0.599	6920	3.89	6960	4.16	6830	4.04	6700	3.99	7040	3.87
1387	0.064	1.053	8350	3.92	8360	3.96	8310	3.93	8280	3.94	8330	3.92
1388	0.149	0.840	7810	3.96	7820	4.10	7700	4.02	7510	4.00	7620	4.00
1389	0.020	1.046	9080	4.14	9090	4.17	9010	4.14	9010	4.14	9070	4.13
1392	0.165	0.947	7470	3.40	7530	3.63	7410	3.47	7240	3.44	7390	3.45
1394	0.150	0.934	7660	3.60	7710	3.79	7600	3.66	7420	3.65	7540	3.67
1403	0.165	0.771	7630	4.04	7690	4.23	7570	4.12	7390	4.10	7550	4.12
1408	0.197	0.699	7310	3.96	7360	4.22	7220	4.06	7080	4.04	7320	4.00
1412	0.097	1.013	8170	3.79	8180	3.86	8130	3.82	7960	3.85	8010	3.83
1414	0.112	0.912	8120	4.03	8140	4.10	8080	4.07	7910	4.09	7980	4.07
1422	0.197	0.716	7290	3.90	7350	4.16	7210	4.00	7060	3.97	7300	4.00
1427	0.085	0.964	8240	4.07	8250	4.12	8200	4.09	8170	4.11	8220	4.09
1428	0.141	0.796	7940	4.19	7970	4.28	7890	4.26	7660	4.24	7810	4.25
1430	0.147	0.813	7860	4.07	7890	4.19	7760	4.14	7570	4.12	7700	4.13
1444	0.144	0.823	7880	4.06	7920	4.18	7790	4.13	7590	4.11	7720	4.12
1458	0.096	0.951	8170	4.03	8240	4.08	8190	4.05	8050	4.08	8110	4.06
1472	0.187	0.741	7390	3.92	7450	4.16	7320	4.02	7160	3.98	7350	4.00
1473	0.062	1.047	8370	3.96	8380	4.00	8330	3.97	8310	3.98	8360	3.95
1479	0.080	1.012	8310	3.94	8250	3.99	8270	3.95	8170	3.98	8190	3.95
1480	0.142	0.827	7900	4.07	7930	4.18	7810	4.13	7610	4.12	7750	4.13
1507	0.150	0.813	7820	4.04	7830	4.19	7720	4.11	7530	4.09	7670	4.11
1519	0.091	0.955	8200	4.05	8210	4.11	8220	4.08	8110	4.10	8170	4.08
1547	0.122	0.900	8040	3.98	8060	4.07	7990	4.04	7790	4.05	7880	4.03
1620	0.080	1.031	8290	3.87	8240	3.93	8260	3.88	8140	3.92	8170	3.89
1670	0.149	0.803	7850	4.09	7880	4.21	7740	4.15	7550	4.14	7690	4.15
1672	0.133	0.839	7990	4.11	8010	4.20	7930	4.17	7710	4.16	7840	4.16
1905	0.132	0.850	7990	4.07	8010	4.17	7930	4.13	7710	4.13	7840	4.13
2085	0.218	0.622	7130	4.03	7160	4.27	7030	4.15	6890	4.12	7200	4.14
2124	0.083	0.979	8240	4.03	8250	4.09	8210	4.06	8180	4.07	8220	4.05
3569	0.104	0.856	8230	4.29	8240	4.34	8190	4.33	8080	4.35	8150	4.34
3624	0.196	0.719	7300	3.90	7360	4.16	7220	4.00	7070	3.97	7300	4.00
3775	0.304	0.461	6320	3.67	6350	4.06	6210	3.99	6130	3.93	6570	3.96
3888	0.192	0.829	7260	3.54	7320	3.79	7180	3.62	7040	3.59	7250	3.57
4031	0.185	0.984	7190	3.00	7280	3.31	7130	3.09	7000	3.08	7130	3.09
4033	0.003	1.137	9350	3.76	9360	3.79	9270	3.75	9270	3.75	9350	3.76
4295	−0.005	1.088	9640	3.88	9650	3.91	9550	3.87	9550	3.87	9670	3.87
4300	0.021	1.020	9090	4.23	9100	4.26	9020	4.23	9020	4.23	9100	4.22
4357	0.064	1.036	8360	3.98	8370	4.02	8330	3.99	8300	4.00	8350	3.98
4359	−0.005	1.149	9560	3.60	9900	2.50	9480	3.59	9480	3.59	9570	3.61
4399	0.257	0.605	6710	3.62	6750	3.90	6610	3.78	6500	3.74	6900	3.66
4534	0.044	0.975	8700	4.31	8710	4.34	8630	4.32	8680	4.31	8740	4.29
4554	−0.005	1.111	9620	3.77	9630	3.80	9940	2.38	9940	2.38	9630	3.77
4660	0.035	1.054	8670	4.11	8680	4.13	8620	4.11	8690	4.09	8740	4.07
4689	0.006	1.131	9280	3.80	9290	3.83	9200	3.79	9200	3.79	9280	3.80
4715	0.223	0.832	6920	3.14	6960	3.40	6840	3.25	6720	3.19	6950	3.22
4963	−0.014	1.145	9930	3.06	9970	3.00	9870	3.02	9870	3.02	9920	3.09
7001	−0.003	1.088	9580	3.90	9590	3.93	9490	3.90	9490	3.90	9610	3.89
7653	0.084	1.062	8240	3.73	8250	3.78	8200	3.74	8040	3.78	8080	3.76
8410	0.117	0.917	8070	3.97	8090	4.04	8020	4.01	7830	4.03	7920	4.01
8641	−0.010	1.107	9790	3.67	9800	3.71	10000	2.54	10000	2.54	9820	3.66

Colours taken from Hauck & Mermilliod (1990) and dereddened using relations of Crawford (1975, 1979).

RK = Relyea & Kurucz (1978), MD = Moon & Dworetsky (1985), LGK = Lester, Gray & Kurucz (1986) with the subscript referring to the Kurucz grid used (see text), KU = Kurucz (1991b).

Table 2.7: *Results from Geneva grids*

					NH		KN				NN	
HR	$B_2 - V_1$	d	m_2	Δm_2	T_{eff}	$\log g$	T_{eff}	$\log g$	X	Y	T_{eff}	$\log g$
63	−0.112	1.446	−0.521	−0.009	8730	3.97			1.633	−0.039	9200	4.09
114	0.070	1.256	−0.500	−0.031	7260	3.43	7290	3.55				
269	−0.048	1.415	−0.495	−0.029	8230	3.80	8170	3.78	1.651	−0.096	8300	4.00
972	−0.167	1.533	−0.558	−0.009	9570	3.89			1.674	0.045	9620	3.86
984	0.023	1.237	−0.485	−0.022	7820	3.96	7750	3.97				
1197												
1254	0.166	0.952	−0.506	−0.029	6630	3.61	6780	4.05				
1292	0.137	0.975	−0.481	−0.003	6860	3.86	6980	4.17				
1331	0.073	1.143	−0.474	−0.004	7340	3.84	7380	3.98				
1351	0.075	1.149	−0.479	−0.009	7310	3.80	7350	3.94				
1354	0.161	0.958	−0.478	−0.001	6670	3.64	6810	4.06				
1356	0.025	1.225	−0.470	−0.007	7810	3.98	7740	4.01				
1368	0.101	1.104	−0.463	0.013	7090	3.72	7160	3.92				
1376	0.078	1.108	−0.433	0.038	7320	3.93	7370	4.08				
1380	−0.030	1.340	−0.483	−0.021	8160	3.95	8110	3.93				
1385	0.161	0.980	−0.476	0.001	6640	3.50	6790	3.96				
1387	−0.053	1.434	−0.489	−0.021	8240	3.76	8200	3.75				
1388	0.048	1.212	−0.482	−0.016	7520	3.81	7530	3.90				
1389	−0.121	1.436	−0.507	0.012	8880	4.03			1.643	−0.058	8870	4.05
1392	0.051	1.330	−0.494	−0.028	7380	3.34	7370	3.42				
1394	0.041	1.288	−0.477	−0.012	7520	3.59	7510	3.66				
1403	0.066	1.157	−0.466	0.002	7390	3.85	7430	3.97				
1408	0.119	1.075	−0.489	−0.011	6950	3.64	7040	3.89				
1412	−0.015	1.355	−0.479	−0.018	8030	3.81	7940	3.79				
1414	0.003	1.266	−0.461	0.000	7980	4.00	7900	4.00				
1422	0.118	1.093	−0.477	0.001	6950	3.58	7040	3.83				
1427	−0.018	1.347	−0.486	−0.025	8060	3.85	7980	3.83				
1428	0.046	1.162	−0.452	0.013	7600	4.01	7600	4.10				
1430	0.055	1.172	−0.472	−0.005	7490	3.89	7510	4.00				
1444	0.045	1.204	−0.479	−0.014	7560	3.86	7570	3.95				
1458	−0.017	1.311	−0.492	−0.031	8090	3.97	8030	3.96				
1472	0.099	1.109	−0.475	0.001	7110	3.72	7170	3.92				
1473	−0.065	1.397	−0.480	−0.007	8300	3.94	8410	3.93				
1479	−0.038	1.371	−0.471	−0.008	8190	3.87	8140	3.87				
1480	0.037	1.168	−0.440	0.024	7690	4.07	7690	4.14				
1507	0.052	1.172	−0.477	−0.011	7520	3.92	7530	4.02				
1519	−0.023	1.301	−0.441	0.020	8150	4.04	8100	4.02				
1547	0.025	1.278	−0.482	−0.019	7700	3.77	7670	3.81				
1620	−0.036	1.388	−0.482	−0.019	8160	3.82	8100	3.80				
1670	0.081	1.125	−0.439	0.033	7270	3.83	7320	3.99				
1672	0.028	1.206	−0.436	0.027	7800	4.04	7740	4.06				
1905	0.023	1.214	−0.475	−0.012	7850	4.05	7780	4.06				
2085	0.134	1.022	−0.509	−0.031	6880	3.75	6970	4.00				
2124	−0.024	1.306	−0.480	−0.019	8150	4.03	8100	4.01				
3569	0.010	1.212	−0.478	−0.016	7970	4.15	7910	4.15				
3624	0.120	1.088	−0.430	0.048	6930	3.58	7030	3.83				
3775	0.250	0.846	−0.489	−0.029	6170	3.91	6310	3.89				
3888	0.100	1.220	−0.503	−0.027	7010	3.25	7070	3.46				
4031	0.105	1.345	−0.493	−0.016	6880	2.66	6930	2.89				
4033	−0.121	1.536	−0.531	−0.012	8660	3.76			1.735	0.006	8980	3.80
4295	−0.154	1.521	−0.559	−0.018	9330	3.91			1.660	0.038	9640	3.90
4300	−0.122	1.417	−0.507	0.013	8930	4.09	9090	4.15	1.618	−0.065	9060	4.15
4357	−0.051	1.428	−0.509	−0.042	8230	3.77	8190	3.76				
4359	−0.152	1.570	−0.555	−0.015	9170	3.71			1.738	0.046	9290	3.74
4399	0.192	0.974	−0.473	0.001	6430	3.18	6590	3.74				
4534	−0.072	1.367	−0.503	−0.024	8370	4.06	8550	4.06				
4554	−0.151	1.527	−0.548	−0.009	9250	3.87			1.683	0.034	9520	3.87
4660	−0.088	1.435	−0.515	−0.022	8440	3.93	8630	3.92				
4689	−0.126	1.551	−0.548	−0.025	8700	3.73			1.727	0.026	9220	3.80
4715	0.132	1.171	−0.469	0.009	6790	3.13	6870	3.38				
4963	−0.152	1.597	−0.566	−0.026	9120	3.63			1.749	0.074	9400	3.65
7001	−0.152	1.477	−0.541	−0.001	9380	4.05			1.646	−0.015	9370	4.04
7653	−0.006	1.436	−0.495	−0.034	7820	3.45	7740	3.44				
8410	0.017	1.298	−0.454	0.008	7790	3.78	7720	3.79				
8641	−0.164	1.556	−0.562	−0.015	9450	3.80			1.695	0.061	9610	3.77

Colours taken from Rufener (1981). NH = North & Hauck (1979), KN = Kobi & North (1990), NN = North & Nicolet (1990).

Chapter 3

Atmospheric parameters from spectrophotometry

3.1 Introduction

In contrast to the wide bandpasses used by photometric systems, spectrophotometry is the measurement of stellar flux through (generally) narrow bandpasses, usually over wider wavelength ranges. Only a restricted wavelength range can be observed from the ground; optical spectrophotometry generally covers 3300 $\sim$ 10000 Å. However, a lot can be determined from such spectrophotometry, since it contains the Balmer Jump and the Paschen continuum, as well as representing a large fraction of the total energy output of A and F stars (Malagnini *et al.*, 1986).

Satellite observations have been used to extend coverage into the ultraviolet and infra-red, giving virtually complete energy coverage for most for the JKT programme stars. Coupling the total observed flux with the observed stellar angular diameter enables the effective temperature of a star to be obtained directly (see Code *et al.*, 1976). Unfortunately, this can only be applied to stars with measurable angular diameters. Such fundamental values of T_{eff} are important in the calibration of photometric systems. Two other methods of using spectrophotometry can be readily applied to the stars under discussion in the present work:

- Spectrophotometric flux fitting
- The Infra-Red Flux method

3.2 Spectrophotometric flux fitting

The atmospheric parameters of a star can be obtained by fitting a model flux distribution to the observed spectrophotometry. This process, known as, spectrophotometric flux fitting has been used by many previous workers to obtain values of T_{eff} and $\log g$ for normal A and F stars, and also Am stars.

Lane & Lester (1980) performed visual spectrophotometry through bandpasses of 40 Å and 80 Å, using a scanning spectrometer on the 0.9 m telescope at Kitt Peak in October 1978, covering the range 3400 to 8090 Å. They converted the observed detector counts to magnitudes, m_ν, by comparing observations they made of ξ^2 Cet with the magnitudes tabulated by Breger (1976a), which were based on the Hayes & Latham (1975) calibration of Vega. Their observed magnitudes were then normalized to 0.00 at 5556 Å.

To extend their distributions into the ultraviolet, Lane & Lester (1984) made observations with the *IUE* satellite, during February 1980, in the range 1920 to 3187 Å. They integrated the observed fluxes over bandpasses between 25 – 50 Å and converted them to F_ν units. Finally they expressed the energy distributions in magnitude units using $-2.5 \log F_\nu$ + constant, where the constant was chosen to normalize the distributions to 0.00 at 5556 Å, as before. The normalization was based on the absolute flux for Vega at 5556 Å: $F_\nu = 3.50 \times 10^{-20}$ erg cm^{-2} s^{-1} Hz^{-1} (Hayes & Latham, 1975). The corresponding flux at 5556 Å for each of the program stars was scaled from this value by comparing the V magnitude of the stars, from Blanco *et al.* (1970), with that of Vega, which was assumed to be 0.00.

Lane & Lester (1984) determined the effective temperatures and surface gravities of several Am stars, by comparing their visual and ultraviolet energy distributions to the emergent fluxes predicted by a grid of model stellar atmospheres. The models used were those of Kurucz (1979a) for $T_{eff} > 8500$ K, and the models of Lester, Lane & Kurucz (1982) for cooler stars. Both sets of models represented atomic line-blanketing by the same opacity distribution functions. They used grids with the line-blanketing scaled from the solar value by factors of 0.3, 1, 3 and 10.

A weighted least-squares technique was used to fit the observed energy distributions to those calculated from the model atmospheres. In making their comparisons, they gave the energy distributions measured from the ground three times the weight of the satellite data. This was done because the ground-based observations were

more reliable, and because there were fewer data points in the visible. From their fitting technique, Lane & Lester obtained values of T_{eff} and $\log g$ with formal uncertainties of ± 50 K and ± 0.05 dex respectively. Observational errors will make the uncertainty larger than this, and they suggested errors of ± 100 K and ± 0.2 dex.

Lane & Lester (1984) found that the best fits to the observed spectrophotometry were given by solar-composition models, even for the strong Am stars (such as 63 Tau and τ UMa), which are thought to be metal-rich. Figure 3.1 shows their best fit for 63 Tau. The fit is certainly very good and the solar-composition model with $T_{eff} = 7000$ K and $\log g = 3.4$ does indeed give a very good formal least-squares fit. Further discussion of the Lane & Lester (1984) results is given in Section 3.5.

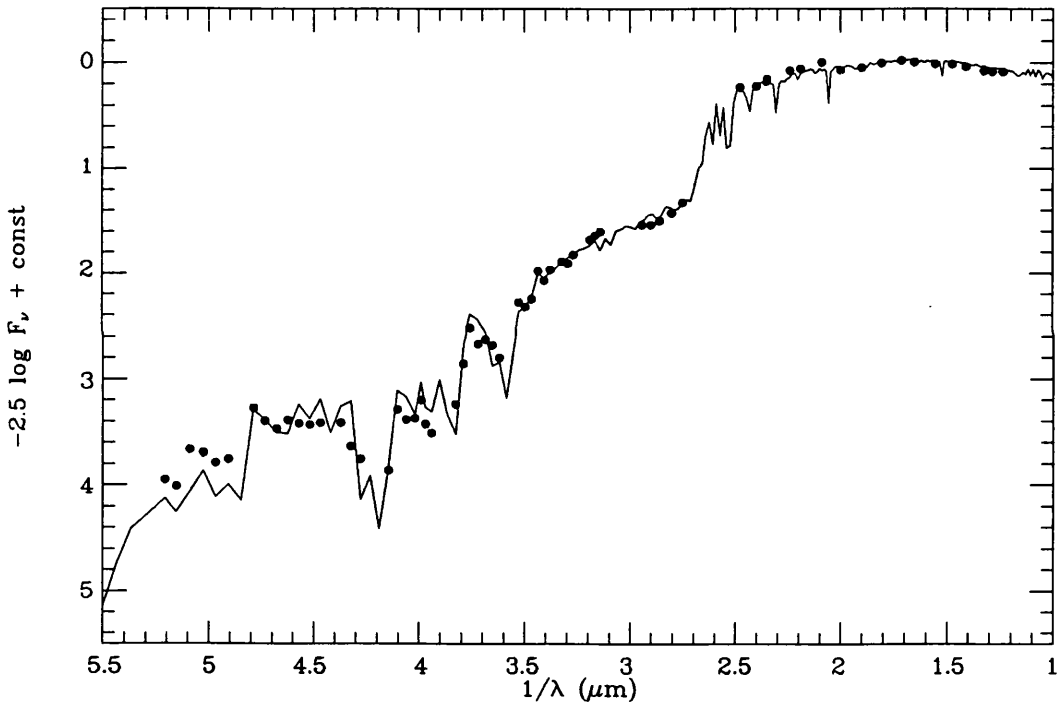

Figure 3.1: *The spectrophotometric fit to 63 Tau. A solar-composition fit by Lane & Lester (1984) gave* $T_{eff} = 7000$ *K and* $\log g = 3.4$.

Another study into the use of spectrophotometric flux fitting was undertaken by Malagnini *et al.* (1982). They compared the observed and computed ultraviolet flux distributions of over 100 normal A and F stars. The Jamar *et al.* (1976) ultraviolet fluxes and solar-composition Kurucz (1979a) models were used. They found that the models matched the observed fluxes fairly well and that the T_{eff} from the ultraviolet fluxes agreed with those obtained from *uvbyβ* photometry by Philip, Miller & Relyea (1976) to within ± 200 K.

Malagnini, Faraggiana & Morossi (1983) extended this study to late-B stars and used both optical and ultraviolet energy distributions. They pointed out that the value of $\log g$ obtained from spectrophotometry is not satisfactory, since the Breger (1976b) scans represent only continuum or near-continuum levels which are not sufficiently sensitive to $\log g$. Hence, they chose to fix $\log g$ based on luminosity class ($\log g = 3.5$ for class III, $\log g = 4.0$ for class IV to V) and then obtain T_{eff}. The effect of fixing $\log g$ on the T_{eff} obtained from the fit was not significant. However, for late-A and F stars, as considered here, $\log g$ will be more important.

Morossi & Malagnini (1985) applied the above procedures to the optical spectrophotometry of normal O9 – G8 stars given in the Breger (1976b) catalogue. They fixed $\log g$ according to spectral type and luminosity class (Table 3.1).

Table 3.1: *Adopted* $\log g$ *values for various luminosity classes. From Morossi & Malagnini (1985).*

Luminosity Class	Spectral Type Range B2.5 – A7	A8 – G0
V	4.0	4.5
IV – V	4.0	4.5
IV	4.0	4.0
III – IV	3.5	3.5
III	3.5	3.5

The general conclusion from this series of papers was that optical fits were the most reliable because of deficiencies in the ultraviolet opacity distribution functions used in the Kurucz (1979a) models. However, this study did not address the subject of Am stars and their T_{eff} and $\log g$ as determined from spectrophotometry.

3.2.1 Application of flux fitting to programme stars

Optical spectrophotometry for the JKT programme stars was taken primarily from Breger (1976a,b) and Lane & Lester (1980), with the corresponding *uvbyβ* photometry obtained from the Hauck & Mermilliod (1990) catalogue. Additional spectrophotometry was taken from Adelman (1978, 1980), Adelman & Pyper (1983), Ardeberg & Virdefors (1980), Oke & Gunn (1983) and Taylor (1984). Generally the spectrophotometry was given in magnitude units (m_ν) normalized to 5000Å; these were re-normalized to 5556Å for the present work.

The ultraviolet flux distributions were taken from the S2/68 database maintained by *Starlink*. Additional ultraviolet flux distributions were taken from Jamar *et al.* (1976) and Macau-Hercot *et al.* (1978), as well as from *IUE* fluxes given by Lane & Lester (1984), Heck *et al.* (1984) and from the image archive maintained by *Starlink* at RAL. The latter were extracted using the *Starlink* reduction package IUEDR (Giddings & Rees, 1989).

With the exception of Lane & Lester, the ultraviolet fluxes were given in wavelength flux units (erg cm^{-2} s^{-1} $Å^{-1}$). These were converted into frequency units using:

$$F_\nu = \frac{\lambda^2 F_\lambda}{3 \times 10^{18}} \tag{3.1}$$

and converted into magnitude units normalized to 5556Å to be compatible with the optical spectrophotometry:

$$m_\nu = -2.5 \log F_\nu + 2.5 \log F_\nu^{5556} \tag{3.2}$$

where

$$\log F_\nu^{5556} = -0.4V + 0.016(B-V) - 19.444 \tag{3.3}$$

on the Hayes & Latham (1975) absolute flux calibration (Gray, 1976, p.202), with the colour term re-determined by Keith Smith (priv. comm.).

A grid of Kurucz (1979a) solar-composition models was used, with the fluxes converted into magnitude units and normalized to 5556 Å. A second grid of Kurucz ATLAS6 models was calculated using the CRAY COS1M at ULCC. These models were calculated using the same code and input data as that used to generate the solar-composition models, except that [M/H] = +0.5 metal abundances were used. Models were calculated covering the range 5500 K $\leq$ T_{eff} $\leq$ 8500 K and 3.0 $\leq$ $\log g$ $\leq$ 4.5 in steps of 500 K and 0.5 dex respectively. All the models, except the 8500 K ones, were convective using a mixing length ratio of $l/H = 2$, to be consistent with the existing solar-composition grid. The grid was extended to higher temperatures by the use of models which had previously been calculated by Keith Smith. Thus, there was a complete grid of [M/H] = +0.5 models up to T_{eff} = 16000 K.

A least-squares grid search procedure was used to converge on the best fit to the observed spectrophotometry and hence obtain T_{eff} and $\log g$. The solution was that which minimized the sum of the squares of the differences between the observed

spectrophotometry $O(\lambda)$ and the model fluxes $M(T_{eff}, \log g, \lambda)$:

$$S = \sum_{\lambda=\lambda_1}^{\lambda_N} w_\lambda \{O(\lambda) - M(T_{eff}, \log g, \lambda)\}^2 \tag{3.4}$$

where w_λ is the weight given to the wavelength point λ. The optical fluxes were given 3 times the weight of the ultraviolet fluxes to be compatible with Lane & Lester (1984).

A value for S was obtained for each of the grid points. The point with the smallest value, S_{min}, was selected along with the 8 points surrounding it, to form a 3×3 box for the basis of the iterative convergence process. This box, adjusted to allow for the edges of the main grid if necessary, was used in conjunction with a 2-d interpolation routine (Press *et al.*, 1989) to obtain new values of S for various values of T_{eff} and $\log g$. After each iteration the size of the box was halved and re-centred upon the new value of S_{min}. The iteration was repeated until the size of the box was smaller than 1 K and 0.01 dex in T_{eff} and $\log g$ respectively. Convergence was then deemed to have occurred, with the value of S_{min} indicating the goodness of fit.

Table 3.2: *Comparison between present fits (BS) and those of Lane & Lester (LL).*

		BS		LL		BS − LL	
name	HR	T_{eff}	$\log g$	T_{eff}	$\log g$	ΔT_{eff}	$\Delta \log g$
60 Tau	1368	7010	3.6	6900	3.6	110	0.0
63 Tau	1376	7050	3.4	7000	3.4	50	0.0
68 Tau	† 1389	8710	4.5	8700	4.3	10	0.2
81 Tau	1428	7420	3.7	7300	3.8	80	−0.1
88 Tau	1458	7930	4.0	7800	4.0	130	0.0
η Lep	2085	7080	4.2	7000	4.1	80	0.1
μ Ori	† 2124	7900	3.9	8500	4.0	−600	−0.1
τ UMa	3624	6730	3.0	6600	3.1	130	−0.1
15 Vul	7653	7630	3.4	7500	3.5	130	−0.1

† see text

The values of T_{eff} and $\log g$ obtained using the [M/H] = 0.0 grid in the present work were compared to those obtained by Lane & Lester (1984). This comparison was performed using the same spectrophotometry as Lane & Lester, with the only difference being the models. Table 3.2 gives the respective values. The respective fits are also shown in Figure 3.2. With the exception of 68 Tau and μ Ori (see below) the present fits are 100 ±30 K hotter than those of Lane & Lester. This difference is caused by the differing treatments of convection employed in the two sets of models. In fact, Lane & Lester stated that the Kurucz (1979a) models, as used here, gave

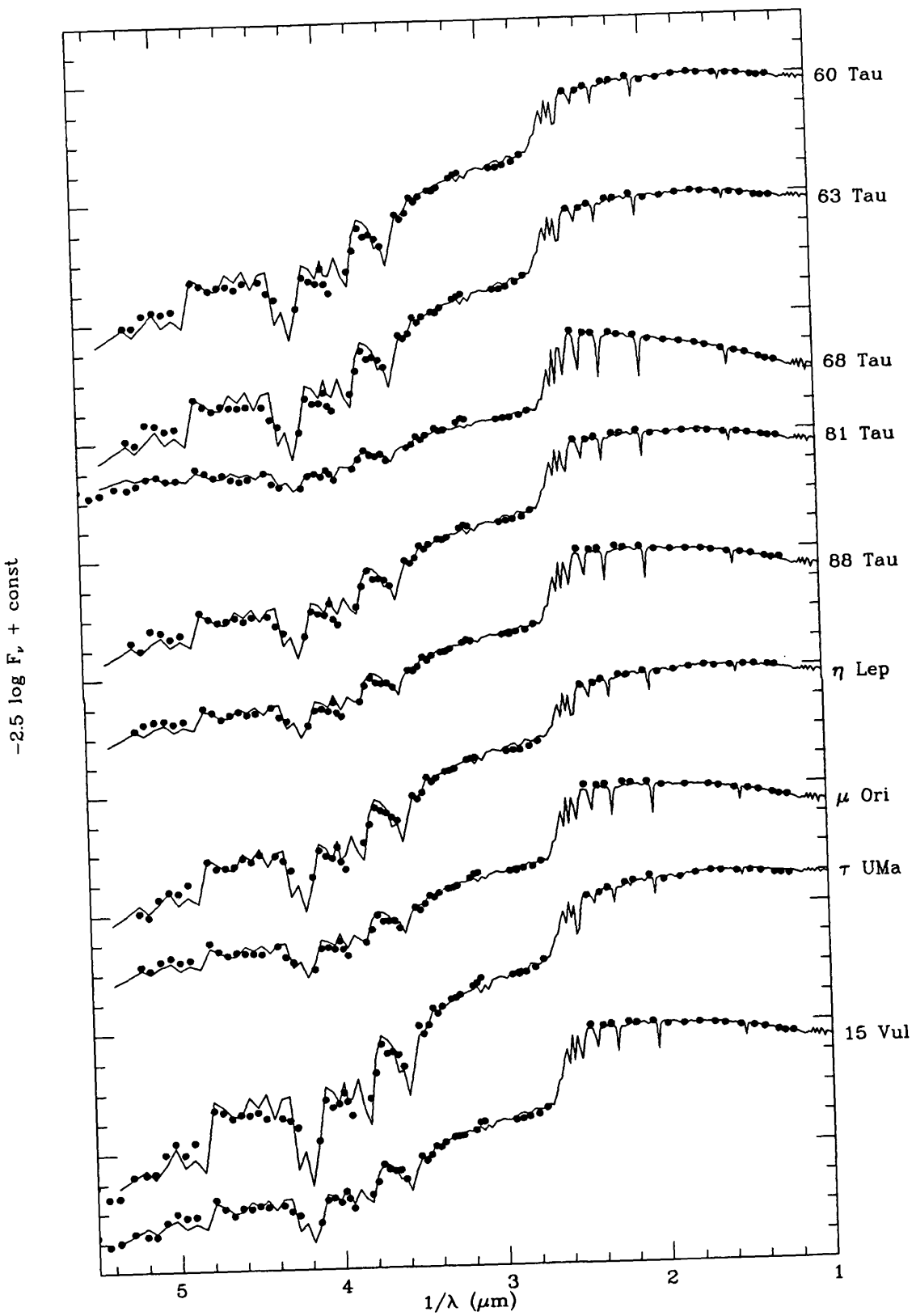

Figure 3.2: *Solar-composition fits to the Lane & Lester (1984) stars.*

temperatures that were 100 – 200 K hotter than those given by the models of Lester, Lane & Kurucz (1982).

68 Tau was excluded from the average because it falls above the region of convective models and hence was expected to be in agreement with Lane & Lester. The large difference for μ Ori was caused by the fact that Lane & Lester made allowances for the fluxes from the companion stars of this multiple system. The present fits do not make such allowances, but in the discussion in Chapter 8 allowances will be made for companions to all the JKT programme stars.

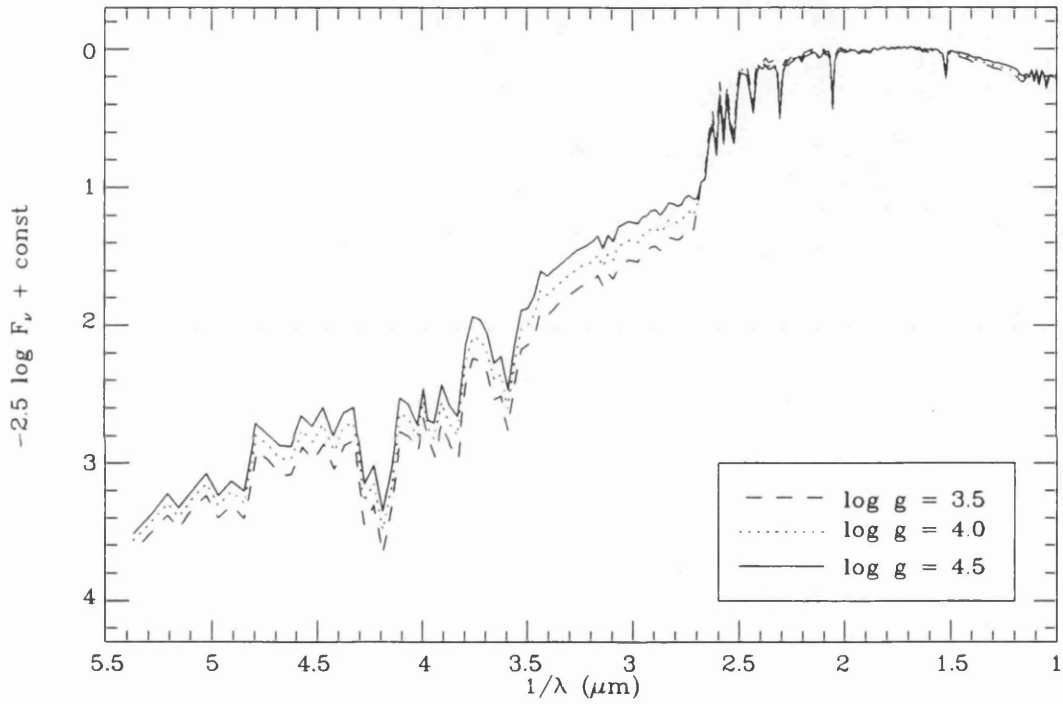

Figure 3.3: *The effect of* $\log g$ *on the flux distribution of a model with* $T_{\rm eff} = 7500$ *K and [M/H] = 0.0.*

For the stars under consideration in the present work the flux distributions are sensitive to surface gravity (Figure 3.3). The flux in the Paschen continuum is very insensitive to surface gravity variations. However, the flux below the Balmer Jump, in the Balmer continuum, is clearly sensitive to $\log g$ changes. This indicates that for late-A and F stars the value of $\log g$ ought to be relatively well-determined by spectrophotometric flux fits. Hence, $\log g$ was retained as a free parameter.

The amount of metal line-blanketing has an important effect on the emergent flux distribution. Increasing the metal abundance reduces the flux in the ultraviolet and the flux in the red is enhanced to compensate. Figure 3.4 shows the relative effects

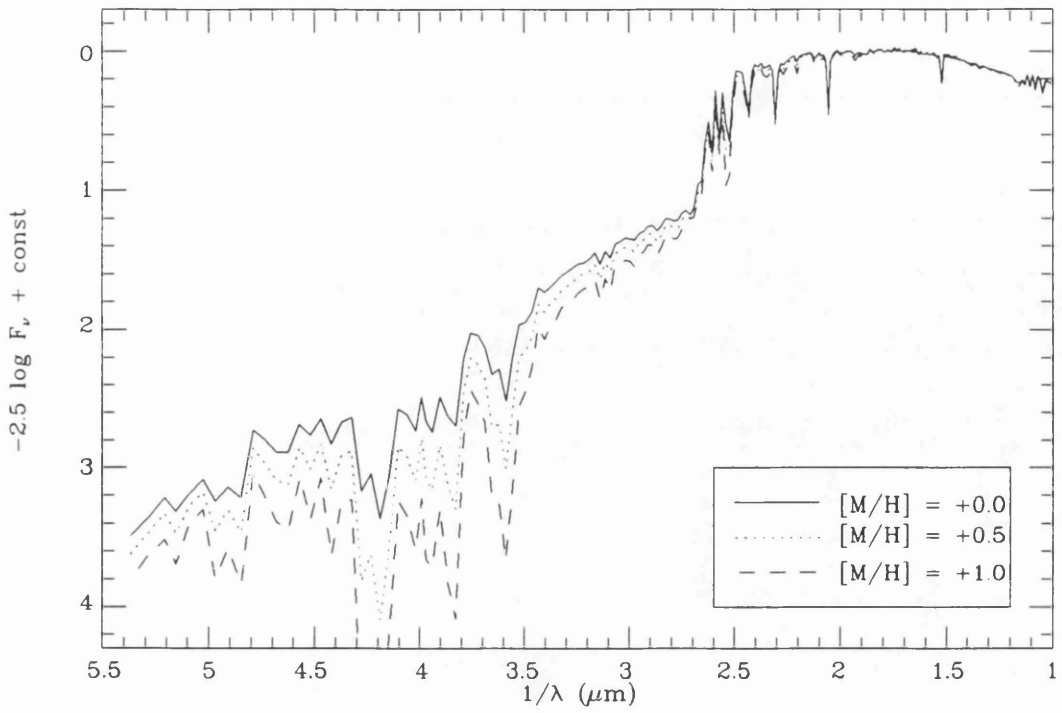

Figure 3.4: *The effect of [M/H] on the flux distribution of a model with* $T_{\rm eff}$ = *7500 K and* $\log g$ = *4.0.*

of increasing the model atmosphere metal content from [M/H] = 0.0 to [M/H] = +1.0. There is a clear and marked decrease in the ultraviolet flux, below the Balmer Jump.

The effects of metal abundance on the value of $T_{\rm eff}$ and $\log g$ obtained from spectrophotometric flux fitting were investigated using the model atmosphere grids already described. Synthetic spectrophotometric 'observations' were generated by binning the [M/H] = +0.5 model fluxes on the wavelength points typical of the S2/68 and Breger (1976b) fluxes. Solar-abundance spectrophotometric fits were performed to these 'observations'. Figure 3.5 shows that, for $T_{\rm eff} < 8500$ K, the solar-composition fits clearly underestimate the $T_{\rm eff}$ and $\log g$ of the metal-rich 'observations'. Above 8500 K there is no clear trend due to the relative insensitivity of the flux distributions to line-blanketing effects. Clearly, for cool stars, if a metal-rich star is fitted by a solar-composition model the $T_{\rm eff}$ and $\log g$ will be systematically underestimated.

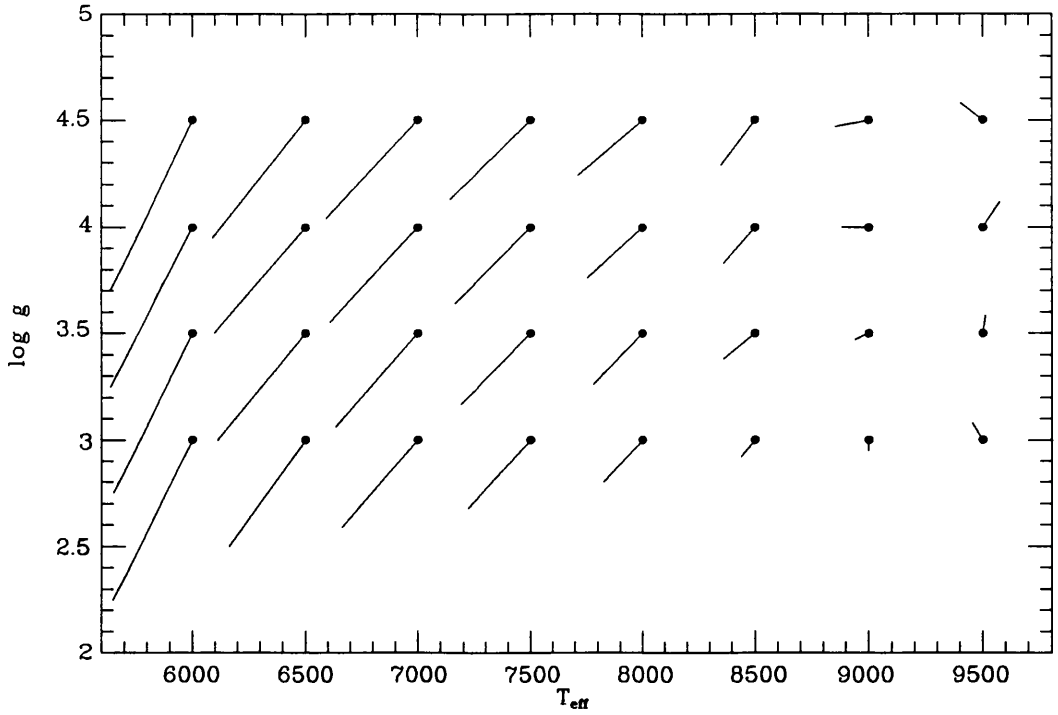

Figure 3.5: *The effect of increasing metal abundance on the fit. The dots represent the* $T_{\rm eff}$ *and* $\log g$ *of the [M/H] = +0.5 model 'observations'. The lines point to the* $T_{\rm eff}$ *and* $\log g$ *obtained from solar-composition fits to these 'observations'.*

3.3 Results

The results from spectrophotometric flux fitting are given in Table 3.3. The optical only fits gave the lowest value of $S_{\rm min}$, because the optical model and observational fluxes are very reliable. Owing to missing opacity, the model ultraviolet fluxes are not as reliable. The solar-composition fits to the combined S2/68 and optical fluxes are in very good agreement with the values obtained earlier for the Lane & Lester spectrophotometry (Table 3.2). The S2/68 fluxes were preferred because measurements were available for all of the JKT programme stars. The complete set of spectrophotometric fits is given in Appendix B.

Spectrophotometric fits using [M/H] = +0.5 models gave larger values of $S_{\rm min}$ than those from solar-abundance fits. The increase is due to a slightly poorer fit to the ultraviolet fluxes. This is due to the missing ultraviolet opacity in the models. It was this result that led Lane & Lester to conclude that solar-abundance fits gave the most reliable values of $T_{\rm eff}$ and $\log g$. However, for metal-rich stars enhanced-abundance models must be used, even though the formal fit is not as good.

Table 3.3: *Spectrophotometric fits to the JKT programme stars*

		Optical only			Optical & S2/68			Optical & S2/68 ¶		
HR	ref	T_{eff}	$\log g$	S_{min}	T_{eff}	$\log g$	S_{min}	T_{eff}	$\log g$	S_{min}
63	a	8920	4.49	0.021	8740	4.26	0.032	8940	4.23	0.044
114	c	7210	3.51	0.038	7380	3.58	0.130	7670	3.91	0.266
269	a	7940	3.70	0.081	8150	3.78	0.099	8310	4.10	0.201
972	a	9720	3.56	0.005	9660	3.75	0.010	9690	4.00	0.041
1197	a	7750	3.48	0.048	8000	3.51	0.073	8200	3.72	0.161
1292	a	6680	3.36	0.020	6920	3.55	0.246	7270	4.01	0.539
1331	e	7280	3.65	0.023	7460	3.67	0.116	7790	3.97	0.219
1351	b	7210	3.83	0.052	7290	3.77	0.138	7610	4.21	0.238
1354	b	6780	3.84	0.024	6830	3.91	0.165	7220	4.42	0.268
1356	a	7560	3.68	0.035	7570	3.70	0.102	7840	4.04	0.208
1368	c	6960	3.49	0.039	7100	3.45	0.130	7450	3.83	0.233
1376	c	7060	3.34	0.032	7100	3.27	0.158	7430	3.65	0.242
1380	f	8150	3.82	0.023	8090	3.63	0.047	8240	3.97	0.093
1385	a	6540	3.50	0.035	6920	3.72	0.294	7280	4.16	0.672
1387	a	7990	3.58	0.045	8100	3.58	0.047	8230	3.80	0.109
1389	c	8750	4.38	0.014	8650	4.26	0.022	8880	4.21	0.032
1392	b	7280	3.46	0.047	7260	3.27	0.119	7550	3.71	0.185
1408	a	6830	3.64	0.055	7150	3.81	0.263	7500	4.23	0.570
1412	a	7630	3.47	0.055	7670	3.49	0.111	7900	3.79	0.211
1427	e	8010	3.69	0.024	7940	3.52	0.054	8150	3.79	0.099
1428	c	7420	3.57	0.024	7460	3.49	0.077	7750	3.78	0.123
1444	e	7550	3.77	0.029	7490	3.66	0.091	7810	3.95	0.143
1458	c	7940	3.89	0.036	7950	3.78	0.056	8180	4.06	0.103
1473	a	8060	3.78	0.054	8150	3.80	0.073	8280	4.15	0.168
1670	c	7210	3.35	0.023	7370	3.36	0.093	7670	3.68	0.201
1672	a	7420	3.33	0.021	7390	3.33	0.097	7650	3.70	0.201
2085	c	6950	3.95	0.027	7070	4.00	0.132	7450	4.38	0.255
2124	c	7960	3.82	0.036	7940	3.65	0.059	8150	3.92	0.096
3569	a	8260	4.34	0.044	7930	3.87	0.064	8190	4.13	0.091
3624	a	6780	2.53	0.041	6900	2.69	0.366	7190	3.16	0.616
3775	a	6330	3.61	0.011	6420	3.86	0.332	6850	4.25	0.481
3888	a	6980	3.50	0.055	7170	3.66	0.181	7500	4.05	0.397
4031	a	6940	2.87	0.040	6940	2.78	0.187	7250	3.24	0.268
4033	a	9080	3.76	0.008	8860	3.75	0.020	9010	3.69	0.034
4295	a	9750	3.58	0.007	9490	3.81	0.015	9550	3.88	0.021
4300	a	8320	4.66	0.053	8450	4.80	0.088	8640	4.97	0.200
4357	a	8310	3.85	0.010	8210	3.73	0.030	8400	3.92	0.091
4399	a	6600	3.40	0.021	6590	3.75	0.288	7010	4.25	0.398
4534	d	8490	4.27	0.017	8500	4.20	0.029	8640	4.37	0.087
4554	a	9490	3.16	0.038	9460	3.12	0.044	9500	3.45	0.085
4660	a	8910	4.01	0.011	8730	3.97	0.037	8960	3.75	0.052
4689	a	8450	2.69	0.010	8930	3.62	0.031	8960	4.31	0.046
4715	a	6790	2.92	0.039	7170	3.13	0.362	7450	3.47	0.633
4963	d	9150	4.15	0.020	9430	2.75	0.031	9390	3.50	0.053
7001	d	9410	4.03	0.013	9510	3.91	0.023	9570	4.00	0.075
7653	a	7720	3.35	0.033	7720	3.33	0.083	7910	3.60	0.159
8410	c	7470	3.30	0.027	7490	3.20	0.100	7760	3.53	0.184
8641	a	9570	4.16	0.008	9540	4.09	0.026	9490	3.92	0.020

¶ Fits using [M/H] = +0.5 models.

References: a Breger (1976b); b Ardeberg & Virdefors (1980); c Lane & Lester (1984); d Taylor (1984); e Adelman (1978); f Adelman (1980).

3.4 The determination of T_{eff} using the Infra-Red Flux Method

The Infra-Red Flux Method (IRFM) developed by Blackwell & Shallis (1977) allows for the simultaneous determination of T_{eff} and angular diameter (θ). The method relies on the comparative insensitivity to T_{eff} of the surface flux, F_{S,λ_0}, from a star at an infra-red wavelength, λ_0. Coupling the total integrated flux from the star at the Earth, F_E, with the observed monochromatic flux, F_{E,λ_0}, allows the setting up of two equations:

$$F_E = \frac{\theta^2}{4}\int_0^\infty F_{S,\lambda} d\lambda = \frac{\theta^2}{4}\sigma T_{eff}^4 \tag{3.5}$$

$$F_{E,\lambda_0} = \frac{\theta^2}{4}F_{S,\lambda_0} = \frac{\theta^2}{4}\phi(T_{eff}, \log g, \lambda_0) \tag{3.6}$$

where $\phi(T_{eff}, \log g, \lambda_0)$ is the stellar surface flux at λ_0, given by a model atmosphere. The simultaneous solution of equations 3.5 and 3.6 gives the values of θ and T_{eff}.

However, a modified system has been developed by Blackwell, Petford & Shallis (1980) in which equations 3.5 and 3.6 have been combined to remove the angular diameter dependance, giving a ratio:

$$R = \frac{F_E}{F_{E,\lambda_0}} \equiv \frac{F_S}{F_{S,\lambda_0}} = \frac{\sigma T_{eff}^4}{\phi(T_{eff}, \log g, \lambda_0)} \tag{3.7}$$

Comparison of the observed ratio with those from a grid of model atmospheres enables the T_{eff} of the star to be determined. The value of θ can also be obtained from either equation 3.5 or 3.6, if necessary.

The method is almost model independent, with only the stellar infra-red flux using models. Since the infra-red flux is almost devoid of absorption lines, the model values can to a fair approximation be given by the Planck function. Indeed, Blackwell, Shallis & Selby (1979) claimed that using a Planck function instead of a model atmosphere leads to an error of only 2% in T_{eff} at 6000 K, rising to 11% at 14000 K.

3.4.1 Application of Infra-Red Flux Method to Am stars

In their analysis of Ap stars Shallis & Blackwell (1979) suggested that the application of the IRFM to Am stars would be most interesting. The IRFM has only recently been applied to Am stars; Mégessier & Van't Veer (1991) presented a poster at IAU Symposium 145 in which they gave preliminary results for 63 Tau.

They used IUE low resolution images for the ultraviolet flux, and the optical spectrophotometry of Oke & Conti (1966). The IUE images were integrated directly to obtain the total ultraviolet flux. The total optical flux was determined by assuming the flux was the same as that of the best fit Kurucz model. Their total integrated flux for 63 Tau was $F_E = 1.3047 \times 10^{-7}$ erg cm^{-2} s^{-1}. The monochromatic infra-red flux was taken from Carney (1982) and on the Hayes (1979) absolute calibration the flux at 2.2μ was 3.990×10^{-13} erg cm^{-2} s^{-1} Å^{-1}. By comparison with Kurucz models they obtained $T_{eff} = 7160 \pm 70$ K.

However, they treated 63 Tau as a single star, whereas it is a well-known spectroscopic binary (Hundt, 1972; Batten, Fletcher & Mann, 1978; Hoffleit, 1982). The standard IRFM is invalid for such stars (Blackwell, Shallis & Selby, 1979). The cool companion will have relatively more flux in the infra-red, so the value of R will be smaller than for a single star. Hence, the IRFM will *underestimate* the T_{eff} of a spectroscopic binary. Cayrel, Burkhart & Van't Veer (1991) suggested that allowing for the cool companion to 63 Tau would raise the estimated T_{eff} of the primary by 100 K or so.

3.4.2 The Infra-Red Flux Method for spectroscopic binaries

The standard IRFM may be modified for use in the determination of the effective temperature for the primary component (T_{eff_1}) of a spectroscopic binary. The modification makes an allowance for the flux of the companion star by assuming its effective temperature (T_{eff_2}).

Equations 3.5 and 3.6 can be modified to include the flux from the secondary component, as follows:

$$F_E = \frac{\theta_1^2}{4}\sigma T_{eff_1}^4 + \frac{\theta_2^2}{4}\sigma T_{eff_2}^4 \tag{3.8}$$

$$F_{E,\lambda_0} = \frac{\theta_1^2}{4}\phi(T_{eff_1}, \log g_1, \lambda_0) + \frac{\theta_2^2}{4}\phi(T_{eff_2}, \log g_2, \lambda_0) \tag{3.9}$$

These two equations may be rearranged to obtain the ratio (R) as follows:

$$R = \frac{\theta_1^2\sigma T_{eff_1}^4 + \theta_2^2\sigma T_{eff_2}^4}{\theta_1^2\phi(T_{eff_1}, \log g_1, \lambda_0) + \theta_2^2\phi(T_{eff_2}, \log g_2, \lambda_0)} \tag{3.10}$$

$$R = \frac{\sigma(T_{eff_1}^4 + (\frac{\theta_2}{\theta_1})^2 T_{eff_2}^4)}{\phi(T_{eff_1}, \log g_1, \lambda_0) + (\frac{\theta_2}{\theta_1})^2\phi(T_{eff_2}, \log g_2, \lambda_0)} \tag{3.11}$$

The ratio of angular diameters $\frac{\theta_2}{\theta_1}$ can be replaced by the ratio of stellar radii $\frac{R_2}{R_1}$, as follows:

$$R = \frac{\sigma(T_{eff_1}^4 + (\frac{R_2}{R_1})^2 T_{eff_2}^4)}{\phi(T_{eff_1}, \log g_1, \lambda_0) + (\frac{R_2}{R_1})^2 \phi(T_{eff_2}, \log g_2, \lambda_0)} \tag{3.12}$$

where R_1 and R_2 are the stellar radii of the primary and secondary respectively.

The effective temperature of the secondary, T_{eff_2}, is generally unknown, but limits can often be placed on it from observations. The lack of identifiable absorption lines in the optical spectrum due to the companion gives an upper limit to T_{eff_2}; while the spectroscopic mass function gives a lower limit to the mass of the secondary and indirectly to T_{eff_2}. Estimates of stellar radii have to be applied when using this modified method. The values of $\log\left(\frac{R}{R_\odot}\right)$ from Allen (1973, pp.206-209) were used to provide main-sequence estimates.

Equation 3.12 was used to investigate the effect on the determination of T_{eff_1} for 63 Tau by varying the effective temperature of the secondary (see Figure 3.6). The effect of the cool companion on the derived value of T_{eff_1} is to raise it to around 7400 $\sim$ 7600 K, compared to the value 7240 K obtained by treating 63 Tau as a single star.

3.4.3 Application of Infra-Red Flux Method to programme stars

The values of the total integrated flux, F_E, for the JKT programme stars were obtained by integrating the ultraviolet and optical fluxes, previously used in the flux fitting work, along with infra-red fluxes taken from the Gezari, Schmitz & Mead (1987) catalogue and from Carney (1982) and Selby *et al.* (1988). All the fluxes were converted into wavelength flux units using Equation 3.3, thus placing them on the Hayes & Latham (1975) calibration scale. The infra-red magnitudes were placed on the Hayes (1979) absolute calibration.

The integrations were performed using the trapezoid rule with a Rayleigh-Jeans approximation added to account for the far infra-red flux. There were no ultraviolet flux measurements shortward of 1200Å, but for A and F stars there is very little flux in this region anyway and the contribution to F_E is negligible.

The S2/68 and optical fluxes were integrated numerically as described above. The Balmer Jump was approximated by a step-function integral:

$$\int_{\lambda^-}^{\lambda^+} F_\lambda d\lambda \simeq F^-(3646 - \lambda^-) + \frac{1}{2}(F^- + F^+)(\lambda^+ - 3646) \tag{3.13}$$

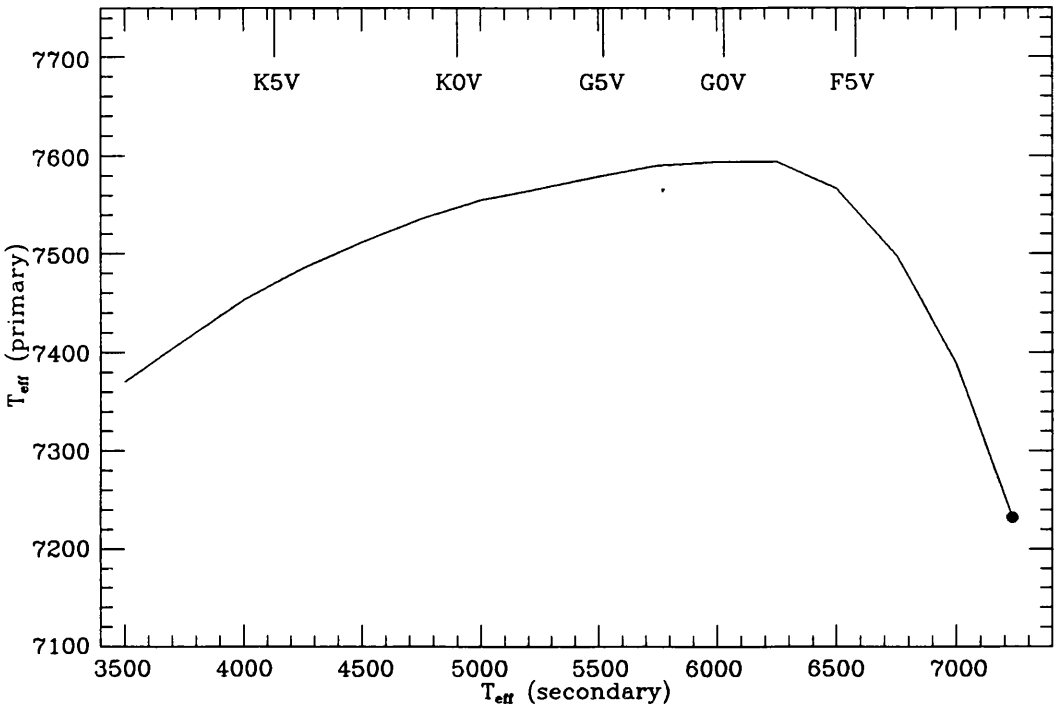

Figure 3.6: *The application of the Infra-Red Flux Method to a spectroscopic binary. Results for 63 Tau are given as an example of the effect of a cooler companion star on the derived effective temperature of the primary star. The filled circle is the* $T_{\rm eff}$ *obtained by treating the star as a single object.*

where F^- and F^+ are the fluxes below and above the Balmer Jump at wavelengths λ^- and λ^+ respectively.

The fluxes longward of $\lambda = 5000$Å were integrated differently so as to better approximate the shape of the continuum. In this region the flux variations with wavelength in log-log space tend to be essentially linear. The trapezoid rule overestimates the area. A log-log space interpolation was performed to obtain the flux at the mid-point between the two wavelength points. Then a Simpson's rule integration was performed. This was a much better approximation to the true integral.

A Rayleigh-Jeans approximation was added to account for the far infra-red flux. This was based on the longest available wavelength point. The approximation was:

$$\int_{\lambda_n}^{\infty} F_\lambda d\lambda \simeq \frac{1}{3} F_n \lambda_n \tag{3.14}$$

where F_n is the flux at the last wavelength point λ_n.

The errors on F_E were obtained by assuming errors on the ultraviolet, optical and infra-red fluxes. These were propagated through the integrations. There were

Table 3.4: *Values of Total Integrated Flux*

HR	F_E $\times 10^{-6}$ (erg s^{-1} cm^{-2}) Present work	Literature	Ref	HR	F_E $\times 10^{-6}$ (erg s^{-1} cm^{-2}) Present work	Literature	Ref
269	0.724±0.019	0.72	b	5404	0.421±0.011	0.66	a
		0.6844	c			0.62	b
509	1.144±0.037	1.148	c	5487	0.712±0.019	0.7222	c
1376	0.131±0.003	0.13047	d	5602	1.234±0.039	1.39	a
1380	0.298±0.008	0.2857	c			1.258	c
1473	0.493±0.013	0.4643	c	5681	1.309±0.042	1.37	a
2326	44.511±1.144	45.0	a	5933	0.721±0.021	0.77	a
2473	2.459±0.078	2.658	c	6493	0.323±0.008	0.39	b
2491	112.937±3.441	113.2	a			0.3885	c
2693	4.557±0.124	6.0	a	6556	3.657±0.095	3.61	a
2943	18.090±0.470	18.0	a			3.62	b
		18.1	b	6623	1.141±0.032	1.31	a
3569	1.372±0.042	1.39	b			1.42	b
3775	1.346±0.045	1.39	b			1.176	c
4031	1.016±0.035	1.02	b	7001	29.257±0.939	30.1	a
4295	3.207±0.112	3.25	b	7061	0.445±0.011	0.55	b
4357	2.383±0.062	2.37	b			0.5295	c
4399	0.559±0.013	0.76	b	7235	1.870±0.061	2.01	b
4554	2.984±0.098	3.02	a	7469	0.337±0.008	0.3995	c
4883	0.284±0.008	0.29	b	7557	12.114±0.311	12.20	a
5185	0.325±0.008	0.3997	c	7834	0.479±0.011	0.6098	c
5264	0.459±0.012	0.53	b	7924	8.052±0.236	8.21	a
5338	0.492±0.012	0.6118	c	8728	8.694±0.225	9.07	b

References: a Blackwell, Petford & Shallis (1980); b Malagnini *et al.* (1986); c Blackwell *et al.* (1990); d Mégessier & Van't Veer (1991).

relatively large uncertainties in the values of F_E due to uncertainties in the spectrophotometry. A typical uncertainty of 5 $\sim$ 10 % was found, consistent with that of the spectrophotometry as a whole.

The obtained values of total integrated flux were compared with those given in the literature. Table 3.4 shows the comparisons and there is a general agreement with only a few major discrepancies. Note that more stars than the JKT programme stars have been used to improve the statistics.

Using the available infra-red flux measurements and the total integrated flux, values of T_{eff} were obtained for the JKT programme stars using the *standard* IRFM. The results agree well with published values (Table 3.5). Note that although several of the stars are known to be binaries, they were treated as single in these calculations. The *modified* IRFM will be applied to binary stars in Chapter 7.

Table 3.5: *Results from Infra-Red Flux Method* §

HR	$F_E \times 10^{-6}$ (erg s^{-1} cm^{-2})	T_{eff}	n	Literature T_{eff}	Ref
269	0.724±0.019	8060±85	8	8028	b
1351	0.140±0.004	7280±117	7		
1354	0.090±0.002	6650±88	4		
1356	0.192±0.005	7860±52	4		
1368	0.128±0.004	7230±44	3		
1376	0.131±0.003	7240±61	3	7160	c
1380	0.298±0.008	8000±57	9	8025	b
1387	0.513±0.013	7970±97	4		
1389	0.516±0.016	8780±34	3		
1408	0.109±0.003	7020±30	3		
1412	1.089±0.032	7880±69	8		
1427	0.303±0.009	8000±37	3		
1428	0.158±0.005	7610±54	3		
1444	0.335±0.009	7550±67	7		
1473	0.493±0.013	8190±49	3	8118	b
1672	0.159±0.004	7600±138	5		
2085	0.814±0.022	7090±67	20		
3569	1.372±0.042	7740±280	9		
3775	1.346±0.045	6340±68	4		
3888	0.763±0.019	7070±91	29		
4031	1.016±0.035	6940±64	3		
4033	1.122±0.039	9040±31	2		
4295	3.207±0.112	9330±35	2		
4357	2.383±0.062	8280±124	10		
4534	3.642±0.094	8690±139	6		
4554	2.984±0.098	9140±88	9	9050	a
4660	1.229±0.040	8500±42	2		
4689	0.658±0.020	8480±81	27		
7001	29.257±0.939	9420±123	44	9468	a
8641	0.351±0.011	9510±85	7		

§No allowance made for companions (see text).

n is the number of infra-red flux points used.

References: a Blackwell, Petford & Shallis (1980), b Blackwell *et al.* (1990), c Mégessier & Van't Veer (1991).

3.5 Lane & Lester versus Moon & Dworetsky

As outlined in the Introduction there is a controversy concerning the T_{eff} and $\log g$ of Am stars. Lane & Lester (1984) using their spectrophotometric flux fitting technique, as described above, obtained T_{eff} and $\log g$ values which were systematically lower than those obtained using the *uvbyβ* calibration of Moon & Dworetsky (1985). Table 3.6 gives the T_{eff} and $\log g$ obtained by the two methods. The method of Lane & Lester yielded a T_{eff} for Procyon consistent with that of Code *et al.* (1976); while the Moon & Dworetsky grids gave values for giant Am star HR178 consistent with detailed analyses by Van't Veer-Menneret, Coupry & Burkhart (1985). Hence, there is an apparent conflict between the two methods - which method gives the correct T_{eff} and $\log g$?

Several papers have been published since the controversy arose in which the authors were undecided as to whether to use the Lane & Lester or Moon & Dworetsky parameters. Pyper & Adelman (1988) outlined the controversy but stated that it was impossible, at that time, to say who was correct. Additionally, Burkhart & Coupry (1989) briefly discussed the controversy and whilst citing some evidence against the Lane & Lester results, could not offer an explanation. Lemke (1989), in the analysis of early A-type stars, briefly outlined Lester's arguments but again offered no explanation.

Table 3.6: *Comparison of T_{eff} and $\log g$ deduced by Lane & Lester (LL) and Moon & Dworetsky (MD).*

		LL		MD		
name	HR	T_{eff}	$\log g$	T_{eff}	$\log g$	δm_0
60 Tau	1368	6900	3.6	7330	4.11	−0.017
63 Tau	1376	7000	3.4	7570	4.27	−0.042
68 Tau	1389	8700	4.3	9030	4.06	−0.017
81 Tau	1428	7300	3.8	7800	4.25	−0.032
88 Tau	1458	7800	4.0	8000	3.93	0.012
η Lep	2085	7000	4.1	7030	4.17	0.016
τ UMa	3624	6600	3.1	7390	4.17	−0.054
60 Leo	4300	8900	4.2	9050	4.35	−0.018
15 Vul	7653	7500	3.5	8040	3.67	−0.001

Dworetsky & Moon (1986) examined the systematic differences and found that they were correlated with the Strömgren metallicity index, δm_0. As can be seen

in Figure 3.7, the largest discrepancies occurred for stars with the strongest metallicity. They also showed that, apart from a small metallicity correction, the Moon & Dworetsky (1985) grids allow accurate determination of $\log g$ for Am as well as normal stars. They had shown that the values of $\log g$ calculated by Lane & Lester are systematically too low for metal-rich Am stars. An evaluation of the ΔT_{eff} trend was not possible due to lack of empirical T_{eff} values for Am stars. It was surprising that Lane & Lester found that solar-abundance models gave the best least-squares fits to the observed flux distributions for *all* 10 Am stars, including the supposedly metal-rich ones. This was even more surprising because solar-composition models have not been able to reproduce the observed line strength anomalies in Am stars (Wolff, 1983).

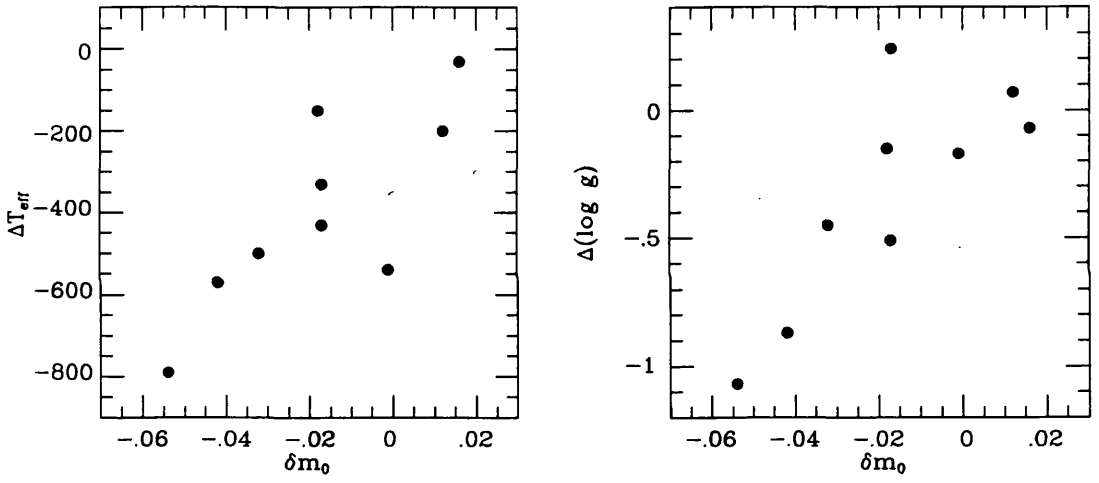

Figure 3.7: *Differences between the Lane & Lester (LL) and Moon & Dworetsky (MD) parameters as a function of* δm_0. *The are clear trends of* $\Delta T_{eff} = T_{eff}(LL) - T_{eff}(MD)$ *and* $\Delta \log g = \log g(LL) - \log g(MD)$ *with the metallicity index,* δm_0.

Lane & Lester found that their method tended to underestimate the value of $\log g$, for the cooler stars, by ~0.5 dex. This is consistent with the problem mentioned by Malagnini, Faraggiana & Morossi (1983). So, $\log g$ problems are not as serious as the T_{eff} discrepancy, in the first instance.

Lester (1987) found evidence that Am stars have a flux excess at 4785Å (2.1 μm^{-1}) compared with model fluxes and normal stars. This excess can be seen in Figure 3.1 for 63 Tau. Lester claimed that this excess would affect both the Strömgren *b*-magnitude and the β index making the T_{eff} of an Am star derived from *uvbyβ* photometry too high. Since the *b*-magnitude is contained in the c_1 and m_1 indices

these would lead to $\log g$ and metallicity being too large as well.

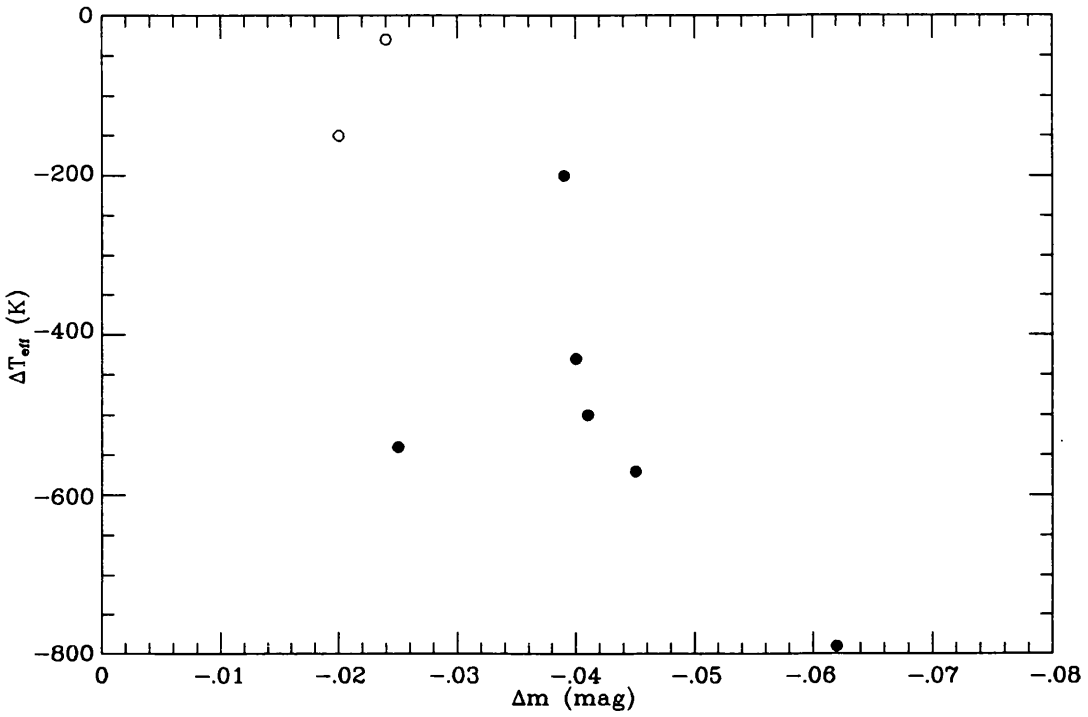

Figure 3.8: *The difference between the $T_{\rm eff}$ values of Lane & Lester (1984) and Dworetsky & Moon (1986) as a function of the observed flux excess at 4785 Å, measured relative to the predicted flux of the model with the effective temperature of Lane & Lester. The open circles are normal stars, and the filled circles are the Am stars. After Lester (1987).*

The proposed excess certainly appeared to be correlated with $\Delta T_{\rm eff}$ for the Am stars in his small sample (Figure 3.8) and could be the reason for the error in *uvbyβ* photometry. However much more work was needed on this problem, specifically looking at a much larger sample of stars and making spectroscopic observations of the region around 4785 Å to search for the possible cause of this excess.

3.6 Conclusion

Spectrophotometric flux fitting has been shown to give a very reasonable fit to the observed optical and ultraviolet flux distributions for A and F stars. However, the effects of metal line-blanketing must be considered in the analysis. The $T_{\rm eff}$ and $\log g$ obtained for late-A and F stars has been shown to be a strong function of metal abundance. Metal-rich stars give systematically too low a $T_{\rm eff}$ and $\log g$

when solar-abundance models are used. It is suspected that the reason for the discrepancy between the Lane & Lester and Moon & Dworetsky results is due to metal abundance.

The Infra-Red Flux Method yields excellent values of T_{eff} and is not significantly affected by metal abundance variations. However, the method is significantly affected by the presence of cool companion stars and hence allowance must be made for such companions, even if only approximately.

The combination of photometry, spectrophotometry and the IRFM should yield a consistent T_{eff} and $\log g$ value once the correct metal abundance and companion T_{eff} and $\log g$ are used. The problem of simultaneous determination of T_{eff}, $\log g$ and [M/H], and an attempt to resolve the controversy surrounding the different methods, are the subjects of Chapters 7 and 8.

Chapter 4

JKT observations and reduction procedure

4.1 Introduction

Owing to the paucity of Balmer line profiles in the literature, an observing programme was undertaken at the Observatorio del Roque de los Muchachos using the Richardson Brealey Spectrograph (RBS) on the 1.0m Jacobus Kapteyn Telescope (JKT). Details of the spectrograph can be found in Edwin (1988). The choice of spectrograph was dictated by the need to obtain the maximum wavelength coverage of the hydrogen-line profile wings, whilst using the highest possible resolution to resolve metal line profiles and locate continuum levels. This inevitably is a compromise and the RBS proved to be the most suitable spectrograph available. A 2400 l/mm holographic grating was used which provided a linear dispersion of 20Å/mm, and gave a wavelength coverage of ~230Å along a coated GEC CCD chip. The resolution, however, was only ~0.8Å which meant that the numerous metal lines in A- and F-type spectra could not be resolved. The resolution effects will be discussed in Chapter 5.

During a 10 night observing run, from 12^{th} to 21^{st} December 1989, over 230 stellar spectra were obtained. All in all, 455 CCD images were obtained. The target list included nearly twenty Am stars and included stars used by Lane & Lester (1984) in their fitting work. As well as taking spectra of the Hβ and Hγ profiles, several spectra were obtained of the region around 4700Å, to search for spectroscopic evidence concerning the flux excess at 4785Å (Lester, 1987). Table 4.1 gives the basic

data for the stars observed and also indicates the observations obtained for each star.

Owing to its brightness special precautions had to be taken when observing Vega. This involved the placing of a neutral density filter in front of the acquisition TV camera, so that the TV tube was not damaged due to over-illumination. This procedure did not in any way obstruct the spectrograph. Since Vega was observed at the beginning of a night the neutral density filter was inserted and removed by a technician. However, since this procedure was rather involved and a technician could not be present throughout the night, it was decided not to attempt to observed α CMi due to its brightness ($V = 0.38$) and because of the amount of observing time that would have been lost whilst inserting and removing the neutral density filter.

4.2 CCD image reduction and spectrum extraction

4.2.1 Introduction

A charge coupled device (CCD) is essentially the electronic equivalent of a photographic plate. CCDs are capable of detecting much lower light levels than those detectable by photographic plates; typically they are over 30 times more sensitive (Ridpath, 1988). This much-improved quantum efficiency allows images to be obtained in a fraction of the time required by photographic plates. The improved sensitivity is coupled with a large linear dynamic range which can, under ideal conditions, give a signal-to-noise ratio of $\sim$200. A third enhancement is the much larger wavelength response (see Argyle *et al.*, 1988).

Figure 4.1 shows a schematic of a CCD image as obtained using the RBS. The counts in the overscan region of the image do not come from an actual physical part of the CCD, but are caused by the clocking-out of a number of pixels on the chip from which the charge signal has already been extracted and measured. The counts in the underscan region are produced by 10 extra pixels at the beginning of row zero which are not illuminated but are clocked out when each row is read. Both the underscan and overscan can be used to provide a measure of the bias level and readout noise (see Section 4.2.2).

Light emerging from the spectrograph slit illuminated the pixel rows from 165 to 325 only. Also, columns 1 to 12 were not illuminated and were rejected during analysis. After the electronic bias had been removed from the images (see Section 4.2.2)

Table 4.1: *Basic data for the stars observed with the JKT*

HR		Star	HD	V	$B-V$	$U-B$	RV	$v \sin i$	Sp. Type
				Hyades Stars					
1254			25570	5.46	+0.37	0.00	+36V?	40	F2V
1292		45 Tau	26462	5.72	+0.36	+0.01	+37V?	6	F4V
1331	†	51 Tau	27176	5.65	+0.28	+0.08	+35SBO	97	kA5hF0mF2
1351	†	57 Tau	27397	5.59	+0.28	+0.08	+42SB1?	109	F0IV
1354			27429	6.12	+0.37	+0.02	+42SB	132	F2Vn
1356	†	58 Tau	27459	5.26	+0.22	+0.10	+36SB1	65	F0IV
1368	†	60 Tau	27628	5.72	+0.32	+0.10	+41SB1O	25	kA3hF2mF2
1376	†	63 Tau	27749	5.64	+0.30	+0.13	+35SB1O	10	kA2hF0mF3
1380	†	δ^2 Tau	27819	4.80	+0.15	+0.12	+39SB	59	A7V
1385			27901	5.98	+0.37	+0.04	+37SB?	125	F4V
1387	†	κ^1 Tau	27934	4.22	+0.13	+0.13	+40SB?	81	A7IV-V
1388		κ^2 Tau	27946	5.28	+0.25	+0.10	+32V	153	A7V
1389	†	68 Tau	27962	4.29	+0.05	+0.08	+35SB	18	A2IV-Vs
1392		υ Tau	28024	4.28	+0.26	+0.14	+35SB1	196	A9IVn
1394		71 Tau	28052	4.49	+0.25	+0.14	+38SBO	192	F0IV-Vn
1403	†		28226	5.72	+0.27	+0.10	+36SB2	88	kA5hF0mF2
1408	†	76 Tau	28294	5.90	+0.32	+0.06	+44V	102	F0IV
1412	†	θ^2 Tau	28319	3.40	+0.18	+0.13	+40SB1O	78	A7III
1414		79 Tau	28355	5.03	+0.23	+0.12	+33V?	104	kA5mF0III
1422		80 Tau	28485	5.58	+0.32	+0.10	+30SB	134	F0Vn
1427	†		28527	4.78	+0.17	+0.13	+38SB	71	A6IV
1428	†	81 Tau	28546	5.48	+0.26	+0.10	+39V?	21	kA5mF0III
1430		83 Tau	28556	5.40	+0.26	+0.10	+39V	95	F0IV
1444	†	ρ Tau	28910	4.65	+0.25	+0.08	+40SB2O	117	A9V
1472		89 Tau	29375	5.79	+0.31	+0.06	+38V	115	F0IV-V
1473	†	90 Tau	29388	4.27	+0.12	+0.13	+45SB1	79	A6V
1479		σ^2 Tau	29488	4.69	+0.15	+0.13	+36SB2	117	A5Vn
1480	†		29499	5.39	+0.26	+0.13	+36V	55	kA9hF0mF2
1507			30034	5.40	+0.25	+0.08	+40	86	A9IV
1519	†		30210	5.37	+0.19	+0.14	+41SB1?	47	A2m
1547		97 Tau	30780	5.10	+0.21	+0.12	+37V	141	A9V
1620	†	ι Tau	32301	4.64	+0.16	+0.15	+41	126	A7V
1670	†		33204	6.01	+0.27	+0.04	+41	27	kA7hA8mF1
1672	†	16 Ori	33254	5.43	+0.24	+0.16	+37SBO	15	kA2hA9mF2
1905	†	122 Tau	37147	5.54	+0.22	+0.10	+41	114	F0V
2124	†	μ Ori	40932	4.12	+0.16	+0.11	+45SB1O	24	kA3hA8mA7
				Lane & Lester Stars					
114	†	28 And	2628	5.23	+0.24	+0.09	−10	21	A9IV
1458	†	88 Tau	29140	4.25	+0.18	+0.11	+29SB2O	35	kA3hA5mA7
2085	†	η Lep	40136	3.71	+0.33	+0.01	−2	0	F1V
3624	†	τ UMa	78362	4.67	+0.35	+0.15	−9SBO	18	kA3hF2mF5
4300	†	60 Leo	95608	4.42	+0.05	+0.05	−10	24	A0.5mA3V
7001	†	α Lyr	172167	0.03	0.00	−0.01	−14V	15	A0Va
7653	†	15 Vul	189849	4.64	+0.18	+0.16	−21SB	23	kA6hA8mF5IV
8410	†	32 Aqr	209625	5.30	+0.23	+0.15	+20SB1O	19	kA5hA7mF0

† Also 4700 Å spectrum

Table 4.1: *Basic data for the stars observed with the JKT (continued)*

HR		Star	HD	V	$B-V$	$U-B$	RV	$v \sin i$	Sp. Type
				Field A and F Stars					
63		θ And	1280	4.61	+0.06	+0.04	+1V	107	A2IV
269		μ And	5448	3.87	+0.13	+0.15	+8	72	A5V
972		ζ Ari	20150	4.89	−0.01	−0.01	+7V	128	A0.5Va
984	†	ζ Eri	20320	4.80	+0.23	+0.09	−4SBO	66	kA2hA8mA7
1197			24167	6.25	+0.20	+0.14	−38	151	A5V
3569		ι UMa	76644	3.14	+0.19	+0.07	+9SBO	151	A7IV
3775		θ UMa	82328	3.17	+0.46	+0.02	+15SB1O	12	F6IV
3888		υ UMa	84999	3.80	+0.29	+0.10	+27V?	110	F0IV
4031		ζ Leo	89025	3.44	+0.31	+0.20	−16SB	84	F0IIIa
4033		λ UMa	89021	3.45	+0.03	+0.06	+18V	48	A1IV
4295	§	β UMa	95418	2.37	−0.02	+0.01	−12SB	39	A0mA1IV-V
4357	§	δ Leo	97603	2.56	+0.12	+0.12	−20V	181	A4V
4359		θ Leo	97633	3.34	−0.01	+0.06	+8V	20	A2IV
4399		ι Leo	99028	3.94	+0.41	+0.07	−10SB1O	20	F4IV
4534	§	β Leo	102647	2.14	+0.09	+0.07	−0V	121	A3V
4554	§	γ UMa	103287	2.44	0.00	+0.02	−13SB	168	A0Van
4660		δ UMa	106591	3.31	+0.08	+0.07	−13V	177	A2Van
4689	§	η Vir	107259	3.89	+0.02	+0.06	+2SB2O	34	A1IV
4715		4 CVn	107904	6.06	+0.33	+0.18	−0SB	73	F3III-IV
4963	¶	θ Vir	114330	4.38	−0.01	−0.01	−3SB	15	A1IV
8305	†	ι PsA	206742	4.34	−0.05	−0.11	+2SB2	47	A0IV
8641		o Peg	214994	4.79	−0.01	−0.01	+9V	12	A1IV
				HgMn Programme Stars					
364		87 Psc	7374	5.98	−0.08	−0.41	−16V	28	B8III
558		ϕ Phe	11753	5.11	−0.06	−0.15	+12SB	13	B9V
811		π Cet	17081	4.25	−0.14	−0.45	+15SB	18	B7V
1339		53 Tau	27295	5.35	−0.08	−0.25	+12SBO	2	B9IV
1702		μ Lep	33904	3.31	−0.11	−0.39	+28	12	B9pHgMn
1800			35548	6.57	−0.05	−0.18	−9V?	5	B9pHgSi
2010	†§	134 Tau	38899	4.91	−0.07	−0.17	+18V	22	B9IV
2519		33 Gem	49606	5.85	−0.13	−0.52	+13	35	B7III
2676	†		53929	6.11	−0.13	−0.47	+6V?	25	B9.5III
2844			58661	5.72	−0.10	−0.41	+21V	32	B9pHgMn
3595		ν Cnc	77350	5.45	−0.04	−0.10	−15SBO	23	A0pSi
3623		κ Cnc	78316	5.24	−0.11	−0.43	+24SB1O	9	B8IIIpMn
3652		36 Lyn	79158	5.32	−0.14	−0.48	+21V	29	B8IIIpMn
4072			89822	4.97	−0.06	−0.13	−0SB2O	15	A0pSiSr:Hg:
8404	§	21 Peg	209459	5.80	−0.07	−0.20	−0		B9.5V
8937		β Scl	221507	4.37	−0.09	−0.36	+2	37	B9.5IVpHgMnEu
				Flux Standard Stars					
	†		19445	8.04	+0.45	−0.25	−139		G5VI
	†		84937	8.30	+0.41	−0.24	−17		F5VI

† Also 4700 Å spectrum; § No Hβ spectrum; ¶ No Hγ spectrum.

their sizes were reduced to contain only the region illuminated by the slit. This not only reduced disk usage, but also speeded up processing.

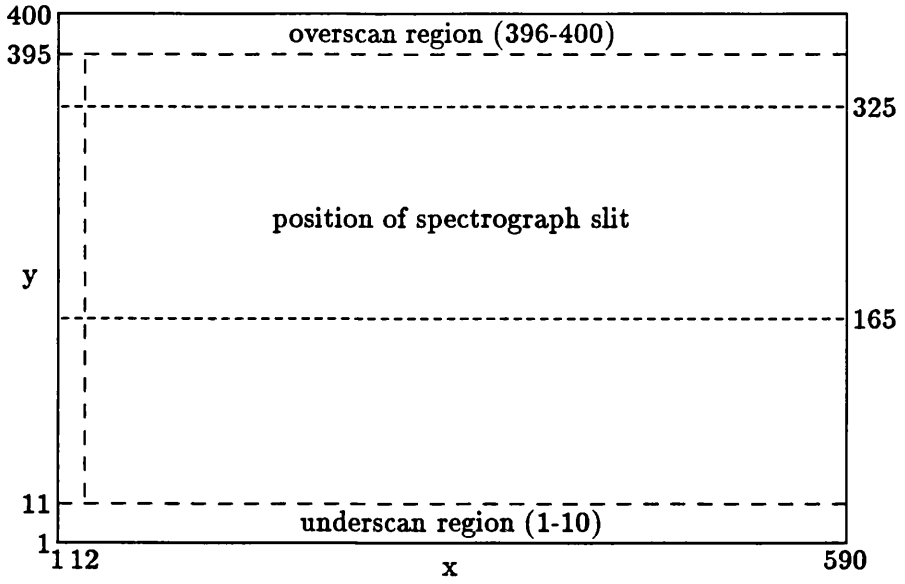

Figure 4.1: *Schematic of a JKT CCD image.*

To obtain the best from a CCD spectral image, several calibration procedures need to be performed, some of which involve the taking of ancillary frames over and above the usual stellar and arc spectra. These extra frames are described below, along with their use in the reduction procedure. The CCD reduction procedure was performed using standard *Starlink* FIGARO routines and recommended methods (Fuller, 1989).

4.2.2 Bias level

The bias is a DC level, preset electronically, to ensure that the noisy signal does not give a negative value during the digitizing process. The bias level is of the form, $a(t) + b(x, y)$ where $b(x, y)$, the pixel-position dependent term, is much less than the time dependent term, $a(t)$, and also small compared with the readout noise.

The value of $a(t)$ can vary by tens of counts over a period of a few hours, but the counts in the underscan region are only affected by $a(t)$ and readout noise. Hence the mean and standard deviation of the counts in the underscan region give a measure of $a(t)$ and readout noise respectively. So $a(t)$ can be easily subtracted from the counts in the whole CCD frame.

The value of $b(x, y)$ is small compared with the readout noise, but it is fixed and can be determined by adding several bias frames together, so as to reduce readout noise. A bias frame is a zero-second exposure performed with the shutter closed. During the observing run several bias frames were taken and 16 of them were added together to produce an image containing $b(x, y)$ and a much reduced value of readout noise.

The bias level forms a background which must be subtracted before multiplicative operations can be performed. In fact the subtraction of $b(x, y)$ in the present case made no noticeable change to the images, so only the value of $a(t)$ needed to be subtracted.

4.2.3 Dark frame

The dark-counts in a CCD frame arise from thermal motions in the CCD chip, but at liquid nitrogen temperatures, as used on La Palma, these are so small as to be negligible, except for long exposures. In the observations taken on La Palma the dark count was found to be negligible. A long, 10000 second, dark frame (exposure with the shutter closed) was taken on a cloudy night, and the counts were only marginally above those of the bias level by $\sim$5 counts. So, even though normal procedures require that a dark-count should have been subtracted from the individual frames, it was found to be unnecessary with the equipment used.

4.2.4 Flat-fielding

The individual pixels in a CCD array do not all have the same sensitivity due to several causes:

- Large-scale sensitivity variations due to changes in the thickness of the CCD coating.
- Individual pixel-to-pixel variations due to small variations in the electrode structure between pixels.
- Dust or grease marks on the surface of the chip.

These gain variations, $f(x, y)$, may be removed by a pixel-to-pixel gain calibration process known as flat-fielding. Flat fields are obtained by illuminating the spectrograph with a continuum light source (in this case, a tungsten-halogen flood lamp).

This gives an image which contains the instrumental, CCD and continuum source response functions.

Prior to use the flat field image is normalized to remove the large-scale variations and leave only the small-scale pixel-to-pixel sensitivity variations. This is performed by fitting a low order polynomial to the spectral response and dividing the flat field image by that fit. A 4^{th} order polynomial was used in the present work. The stellar spectrum was then divided by the balanced flat field to correct for the pixel-to-pixel sensitivity variations. The residual large-scale variations remaining in the image can be removed by the flux calibration procedure (see Section 4.3).

The flat-fielding procedure used on the JKT was very ad hoc. It involved removing the arc calibration lamp, placing several sheets of folded tissue paper over the hole and illuminating with a tungsten-halogen flood lamp. This procedure was thought at the time of observing to be woefully inadequate, but was the best that was available.

4.2.5 Cosmic rays

Unfortunately, CCDs are sensitive to cosmic rays. The passage of a cosmic ray through the CCD substrate leads to the random appearance of bright spots (extra counts) on the images. Natural background radiation also contributes to this problem. Fortunately, in the observations made with the JKT the exposure times were short enough for cosmic ray contamination of the stellar spectra to be relatively unlikely. Only a handful of spectra were found to contain significant cosmic ray contamination; these were mainly the fainter stars which required longer exposures.

Although there are cosmic ray cleaning routines in FIGARO these were not used as a general procedure due to lack of serious cosmic ray contamination. Instead, the positions of contaminating cosmic rays were noted so that they could be identified later in the final extracted spectra. The high count level in most of the spectra meant that only the strongest of cosmic ray blips were visible.

4.2.6 Spectrum extraction and wavelength calibration

Once a calibrated image had been obtained a 1-d spectrum could be extracted from the image. Since most of the spectra had very high counts and short exposure times, the sky background was found to be negligible and hence no background subtraction

was necessary.

A simple adding-up-of-the rows extraction was used, even though optimal procedures are available (Horne, 1986). Tests were made using optimal extraction, but no significant improvement was noted due to the high count level in the spectra.

Wavelength calibration was performed by identifying arc lines and then fitting a polynomial to those identifications to obtain the pixel to wavelength calibration, using the FIGARO automatic arc fitting procedure. The calibration was then copied onto the stellar spectrum. The wavelength calibrated spectrum was then re-binned onto an evenly spaced wavelength scale with a stepsize of 0.333Å, and finally converted into DIPSO format (Howarth & Murray, 1987).

The spectra were then normalized to 1.0 at the continuum level. This was performed by dividing by a straight line fitted to the points ±100Å from the Balmer core, or in the case of the 4700Å spectra at either end of the spectrum. This rectification was approximate in that it did not allow for depressions of the apparent continuum level due to line blanketing. Refinements to this procedure will be discussed in Chapters 5 and 6 when the spectra are used in temperature and metallicity determinations, respectively.

4.3 The photometric calibration of spectra

On comparing the JKT Hγ profile for Vega with those of Peterson (1969) and Kurucz (1979a), it was found that the JKT spectrum had more pronounced wings than expected. On further investigation it was found that this effect occurred in all the JKT Hγ spectra (Figure 4.2(a)). A similar effect was noticed in the JKT Hβ spectra, but to a much lesser degree. This effect was eventually traced to the large-scale instrumental and CCD response functions which remained in the spectra.

The two flux standard stars observed for flux calibration purposes could not be used to flux calibrate the stellar spectra reliably. This was due to the small wavelength range of the spectra and the presence of the Balmer lines. The large-scale responses had to be removed another way.

Instead of removing the large-scale response functions from the flat field, they were left in. The individual stellar spectra were divided by the raw flat fields. This meant that the instrumental and CCD responses were removed, leaving only the effect of the tungsten-halogen lamp spectrum. This response was modeled by

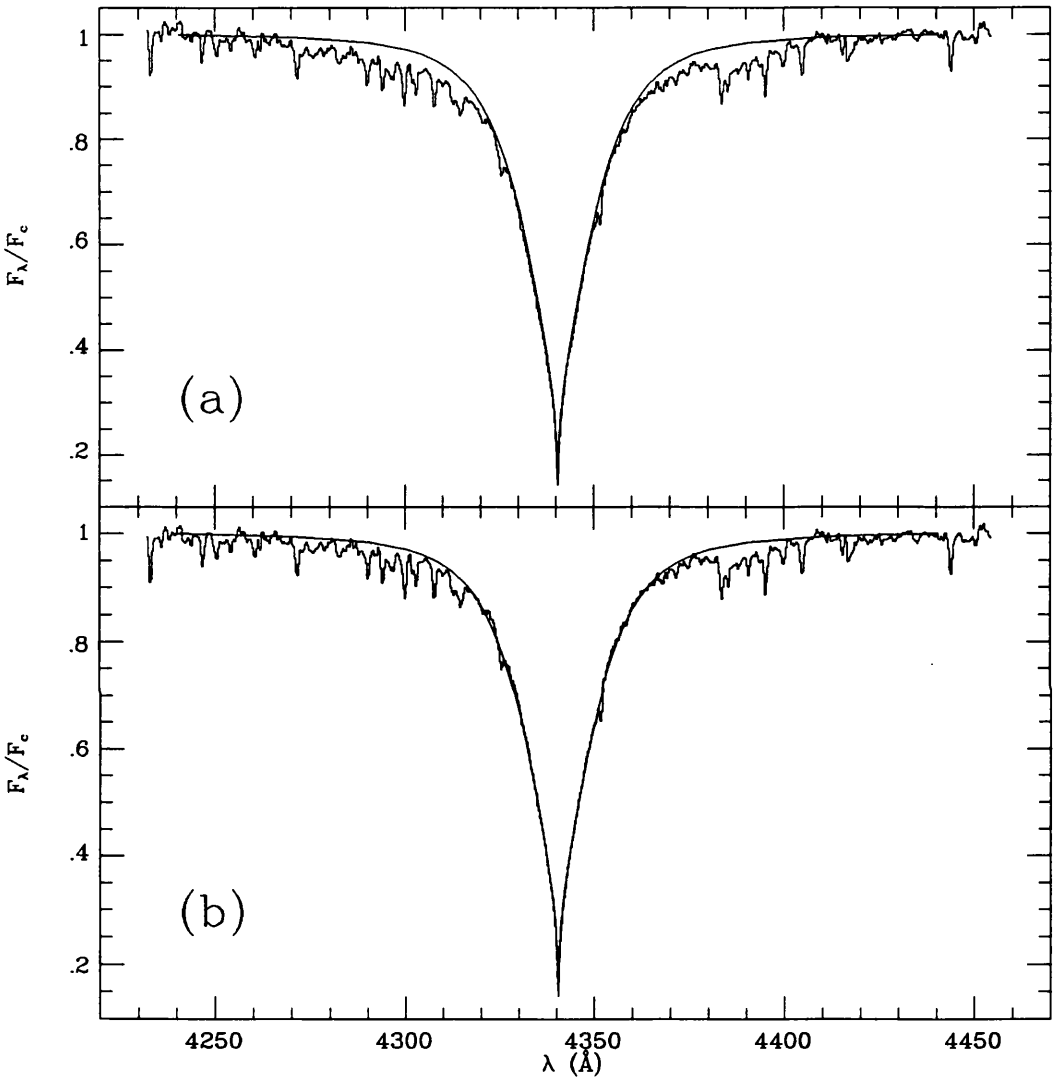

Figure 4.2: *The photometric calibration problem for the Hγ profiles. The Hγ profile of Vega (a) is shown with the expected Kurucz (1979a) profile ($T_{\rm eff}$ = 9500,* $\log g$ *= 4.0). Notice how the wings are much deeper either side of the core. Using the modified extraction process, described in the text, a much better profile shape (b) is obtained.*

assuming that the lamp was a black body with a temperature of 2500 K. The effect of the lamp was found to be negligible compared to the other responses. The effect on shape of the Hγ profile for Vega was most gratifying (Figure 4.2(b)).

Photometrically measured profiles of the Hγ and Hβ lines for several early A-type stars were presented by Gray & Evans (1973). Four of the stars were included in the JKT observing programme. A comparison between the two types of data is given in Figures 4.3 and 4.4. The agreement is excellent. Gray & Evans stated that the internal probable error for the profiles was less than 2%. These photoelectric results demonstrate the high photometric accuracy of the profiles given in Chapter 5. Importantly, Gray & Evans found that the scattered light in their profiles was well below 1% and could consequently be neglected. This agrees with the assumption of the low scattered light in the JKT spectra due to the use of a holographic grating (Tull, 1988). This also indicates that the calibration of the JKT spectra is certainly very good. Note the agreement in the core regions which are most affected by resolution and scattered light effects. The Gray & Evans Vega profiles are also consistent with the photoelectric profiles of Baschek & Oke (1965) and Peterson (1969).

4.4 Quality of final spectra

The overall quality of the final spectra is very good. The signal-to-noise ratio was estimated, using the Fourier techniques developed by Smith (1992), to be of the order of 100. This agreed very well with a visual estimate which revealed a noise level of the order of 1%. However, the absolute flux calibration of the spectra is less certain, due to the effects of the ad hoc flat-fielding procedure. Nonetheless, the photometric accuracy of the final spectra has been shown to be of the order of 1$\sim$2% (See previous Section).

Pixel variances were also estimated using:

$$V(x,y) = V_0 + \frac{D(x,y)}{Q} \tag{4.1}$$

where $\sqrt{V_0}$ = r.m.s. readout noise in data numbers

Q = effective number of photons per data number

$D(x,y)$ = image counts

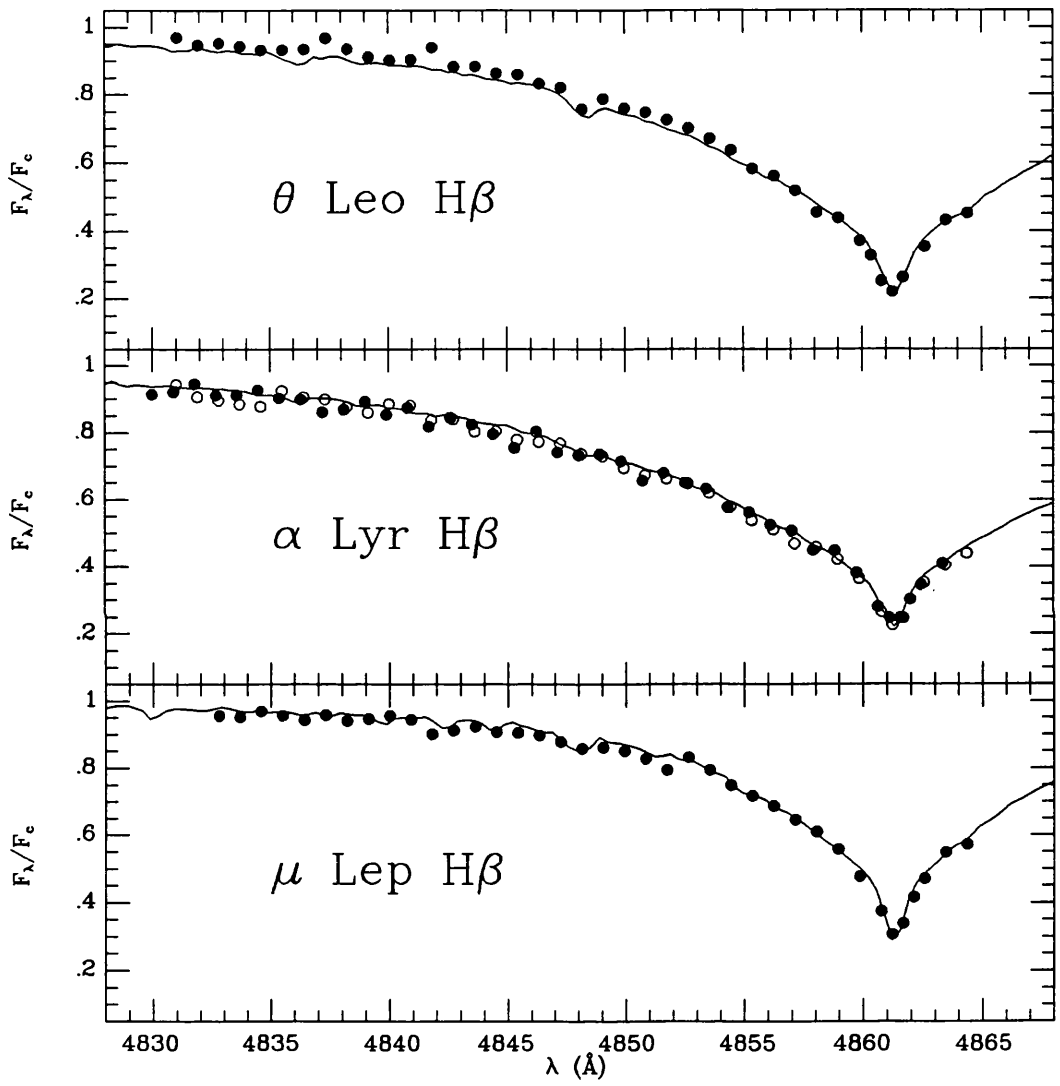

Figure 4.3: *Comparison with the Gray & Evans (1973) photoelectric Hβ profiles. The dots are the Gray & Evans measurements and the lines the JKT spectra.*

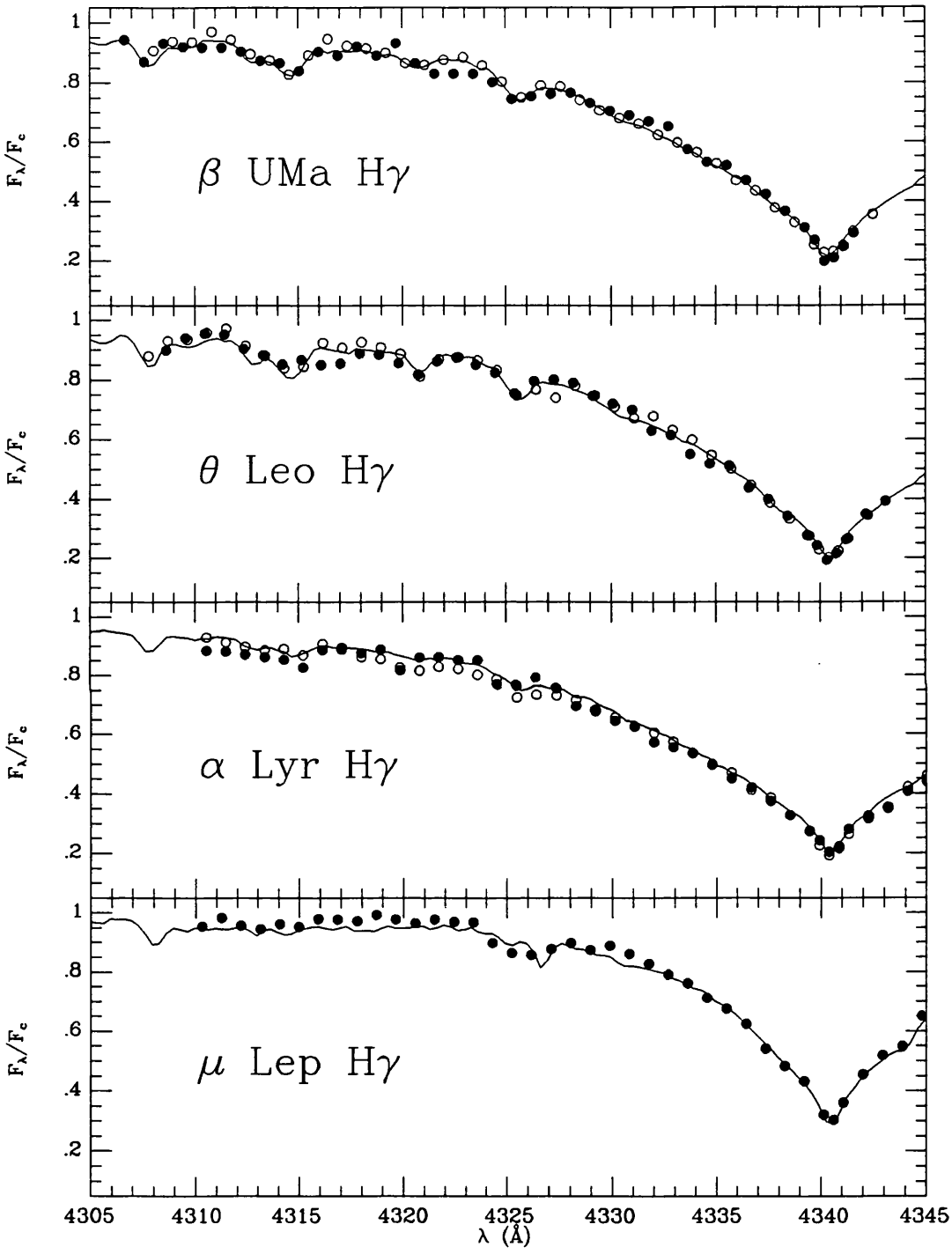

Figure 4.4: *Comparison with the Gray & Evans (1973) photoelectric Hγ profiles. The dots are the Gray & Evans measurements and the lines the JKT spectra.*

The values of V_0 and Q were determined from bias frames and flat fields by fitting a noise model to these images within the local FIGARO routine PAMNOISE. The model used was:

$$\log \sigma = \frac{1}{2} \log(V_0 + \frac{D(x,y)}{Q} + (D(x,y) \times G_n)^2) \tag{4.2}$$

where G_n = grain noise, which was assumed to be 0.5%. Grain noise is the small-scale pixel-to-pixel sensitivity variations in the raw flat fields. The following values were obtained: $V_0 = 460.10$, $Q = 1.6$. These compare well with the nominal values given by Argyle *et al.* (1988). Using these values in Equation 4.1, a nominal signal-to-noise ratio of ~200 was determined. This is larger than the actual observed S/N, due to uncertainties caused by the flat-fielding process. Nonetheless, the overall quality of the final spectra is certainly good enough for the present analyses.

The FWHM of the arc lines was found to be ~0.8Å which corresponds to the nominal value given by Edwin (1988). This value was taken to be the width of the instrumental profile and used in the calculation of synthetic spectra (Appendix A).

Chapter 5

The effective temperatures from Balmer line profiles

5.1 Introduction

The hydrogen Balmer lines provide an excellent T_{eff} diagnostic for stars cooler than about 8000 K due to their virtually nil gravity dependence (Gray, 1976, p.374). The JKT Hβ and Hγ spectra are used to obtain T_{eff} by the fitting of theoretical profiles. The fitting is hampered by the numerous metal lines in the spectra of late-A and F stars. A detailed investigation is made into the location of the true continuum level. To facilitate this, numerous synthetic spectra were calculated (See Appendix A). Several methods for fitting theoretical line profiles to observations have been used and each is explained in detail. In addition, the Hβ spectra are used in the determination of synthetic β indices and a comparison made with the Moon & Dworetsky (1985) and Lester, Gray & Kurucz (1986) values.

5.2 Standard profile extraction

For early A-type stars the Balmer lines are essentially free of contamination by metal lines, but for late-A and cooler stars the effects of metal lines become progressively more significant. The numerous metal lines make finding the true hydrogen line continuum level a problematic process for the stars under discussion here (Danford, 1975). Furthermore, Hγ is more severely affected by metal line blocking than Hβ, for the same T_{eff}.

Initially, each JKT spectrum was rectified by dividing it by a straight line fitted to the points at ±100Å from the Balmer core. A linear rectification had to be used since the shape of the Balmer line must be preserved in the rectified spectra (Smith & Van't Veer, 1987). The standard rectification technique is to fit a high order polynomial or perform a spline fit to the observational spectra. This technique could not be used, since it would remove the hydrogen line profiles. The linear rectification makes the assumption that the stellar continuum level does not deviate significantly from linear over the 200Å. A reference to Black Body and Kurucz (1979a) flux distributions shows that this assumption is indeed valid, with the stellar continuum curvature negligible over 200Å. Also, the Kurucz ATLAS6 program outputs continuum fluxes as well as line fluxes and these also verified the assumption.

A smooth curve was interactively fitted to the rectified spectra using CURSOR (Keith Smith, priv. comm.) which uses splines to produce a smooth curve through a set of points. An edit facility enabled the repositioning of points to obtain the best fit. The red and blue wings were fitted separately. At this stage no allowance was made for continuum depression due to line-blanketing and rotational effects.

On comparing the red and blue wings it was found that there were often significant differences, especially for stars with large rotational velocities. It was immediately obvious that the effects on the continuum level due to line-blanketing and rotation can be highly significant. The cause of the discrepancy between the two wings is due to:

- Depression of the apparent hydrogen line continuum due to the effects of blanketing and rotation.
- Uncertainties in the continuum level at the normalization points.

Both effects are related. To determine the effects of rotation on the apparent continuum level, the spectrum of the low $v \sin i$ star η Lep was artificially rotationally broadened to $v \sin i$ = 200 km/s. This revealed a significant depression in the apparent continuum level (see Figure 5.1). Note especially that the points at ±100Å are now well below the 1.0 level and thus rectification of stars with large $v \sin i$ must take this into account. This is shown dramatically in Figure 5.2 where the rectified spectrum of 71 Tau has the continuum level set too high compared to that predicted by the rotational broadened η Lep spectrum. There was a clear need to obtain

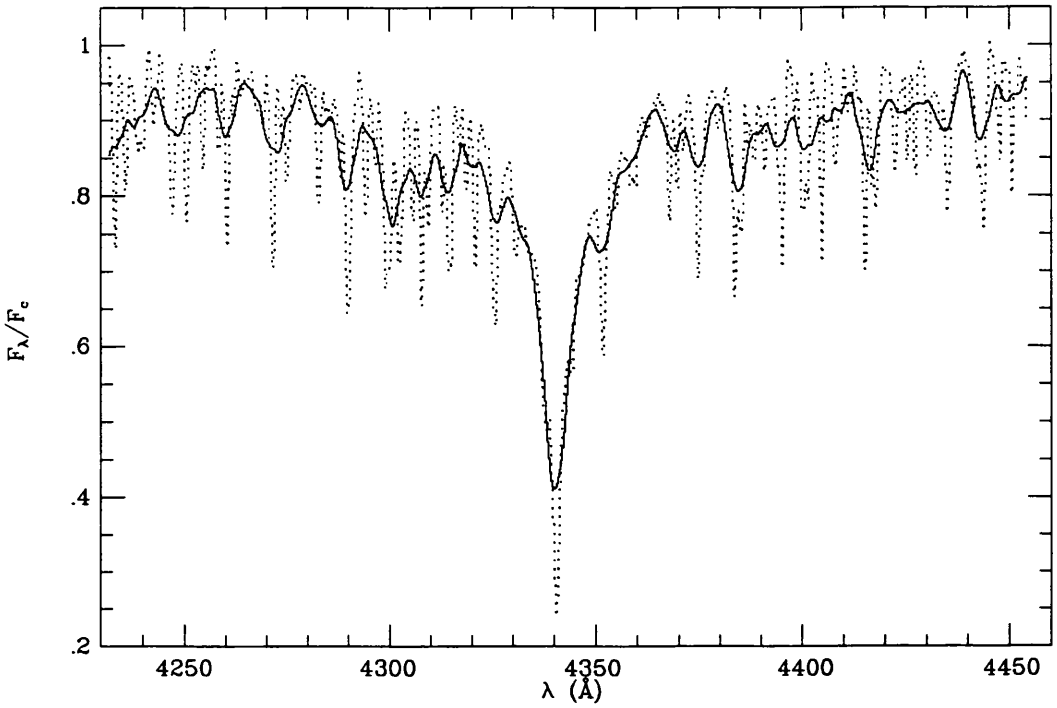

Figure 5.1: *Artificially rotationally broadened Hγ profile for η Lep (——) compared to the observed spectrum of η Lep (· · · · ·).*

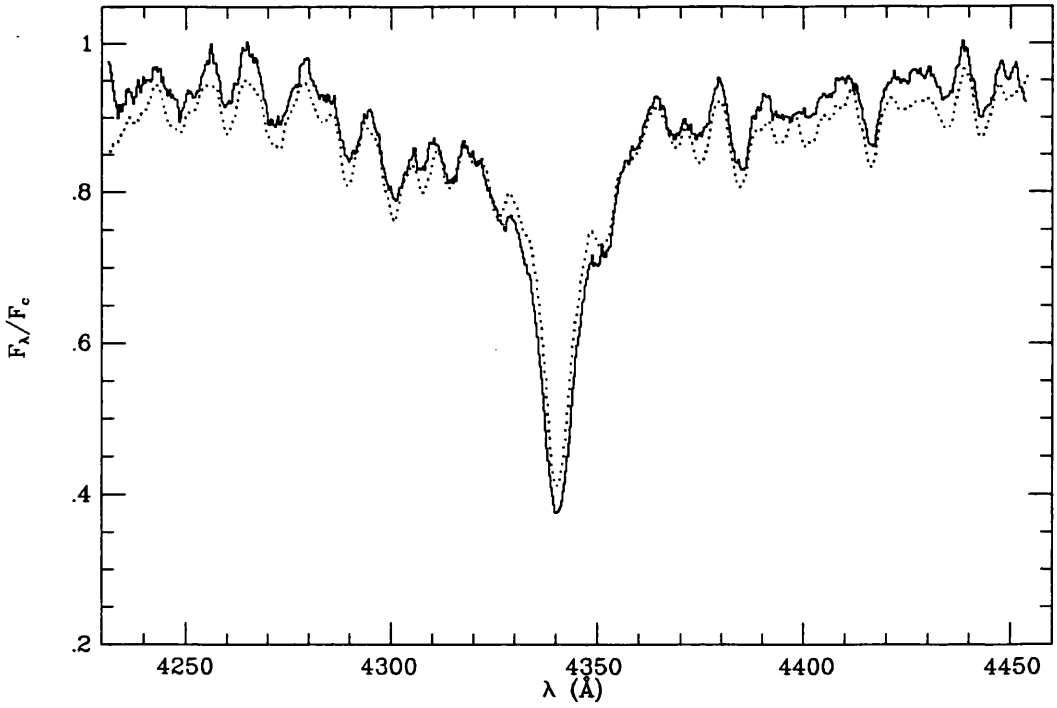

Figure 5.2: *Artificially rotationally broadened Hγ profile for η Lep (· · · · ·) compared to the observed spectrum of 71 Tau (——).*

a quantitative estimate of the effects of blanketing and rotation on the apparent continuum level in these relatively low-resolution spectra.

The relatively low resolution of the JKT spectra means that absorption lines are blended together and, often, what appears to be hydrogen-line profile continuum is not in fact continuum at all. This means that when the Balmer line profile is drawn across the JKT spectrum the apparent continuum points may indeed not be at hydrogen-line continuum level. Synthetic spectra were used to investigate the effects of both line-blanketing and rotation on the apparent continuum level. Blanketing and rotation effects are now outlined:

- The effect of increasing the amount of line-blanketing is shown in Figure 5.3. Increasing the amount of line-blanketing affects the location of the true hydrogen-line continuum level, with fewer and fewer points being close to the true level. Thus, when drawing the continuum level on the observations the depth of the Balmer line profile wings will be overestimated for heavily blanketed stars.

- Stellar rotation smears out lines and depresses the apparent continuum level (Figure 5.4). Stellar rotation will have a detrimental effect on the rectification and subsequent line fitting process for stars with high $v \sin i$. Not knowing where the continuum should be placed leads to systematic uncertainties in the fitting of the line profiles.

The use of synthetic spectra made it possible to estimate the effects of line-blanketing and rotation on the apparent continuum level. Each observational profile was re-extracted using synthetic spectra as a guide to where to place the continuum points. The red and blue wings were again extracted separately, but this time they agreed much better.

After extraction the red and blue wings were normalized to $\pm$40Å and averaged. This gave one-sided profiles, since both wings should be essentially symmetric. The value of $\Delta\lambda = 40$Å was chosen since it avoided the use of the far wings which were affected by residual calibration problems and because this is compatible with published profiles. The results are given in Tables 5.4 and 5.5 at the end of the chapter. The value of σ is an estimate of the relative uncertainty in the profiles. It is a measure of the overall discrepancy between the blue and red wings of the profile

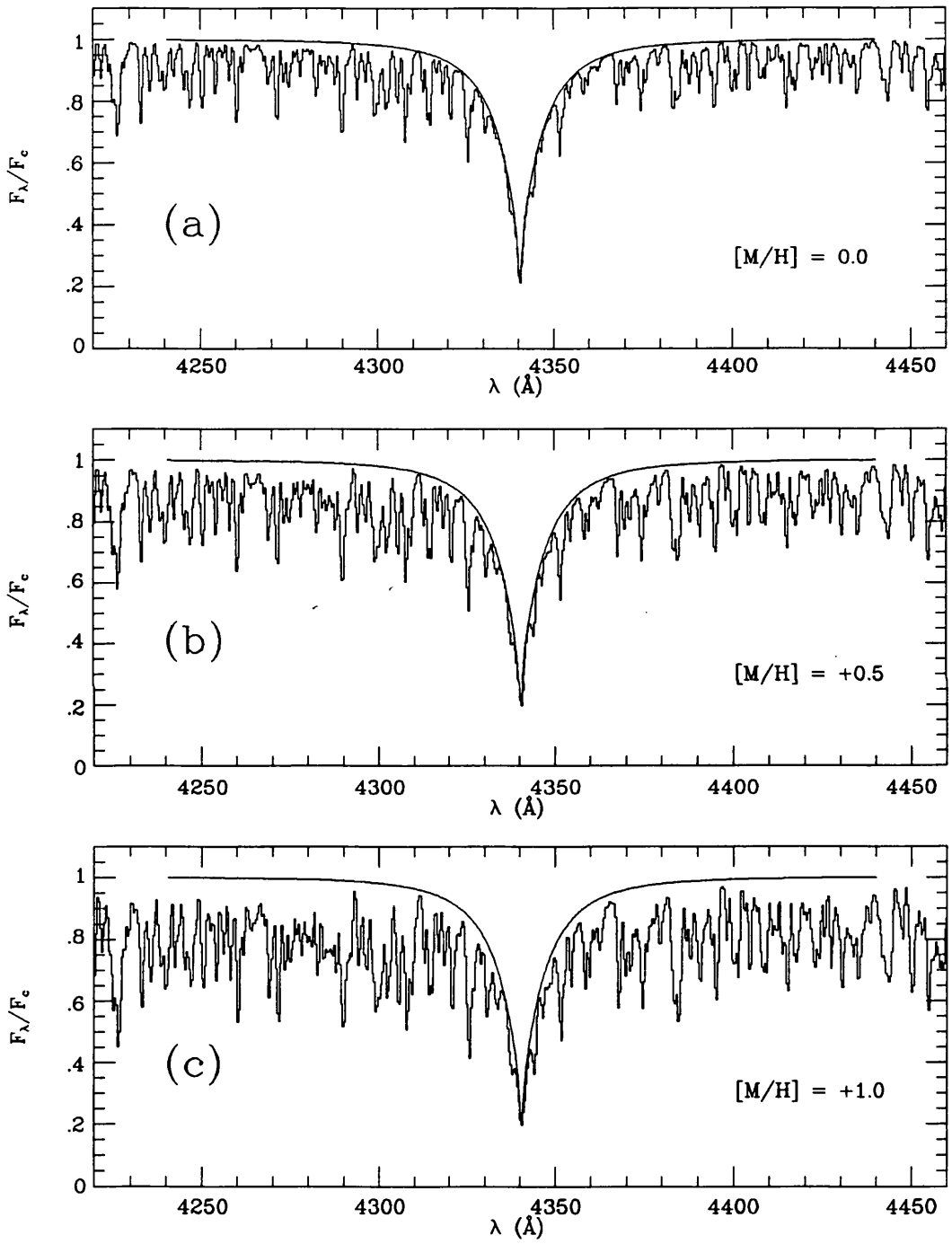

Figure 5.3: *The effect of increasing [M/H] on the apparent continuum level. Based on synthetic spectra with* $T_{\rm eff} = 7500$ *K and* $\log g = 4.0$.

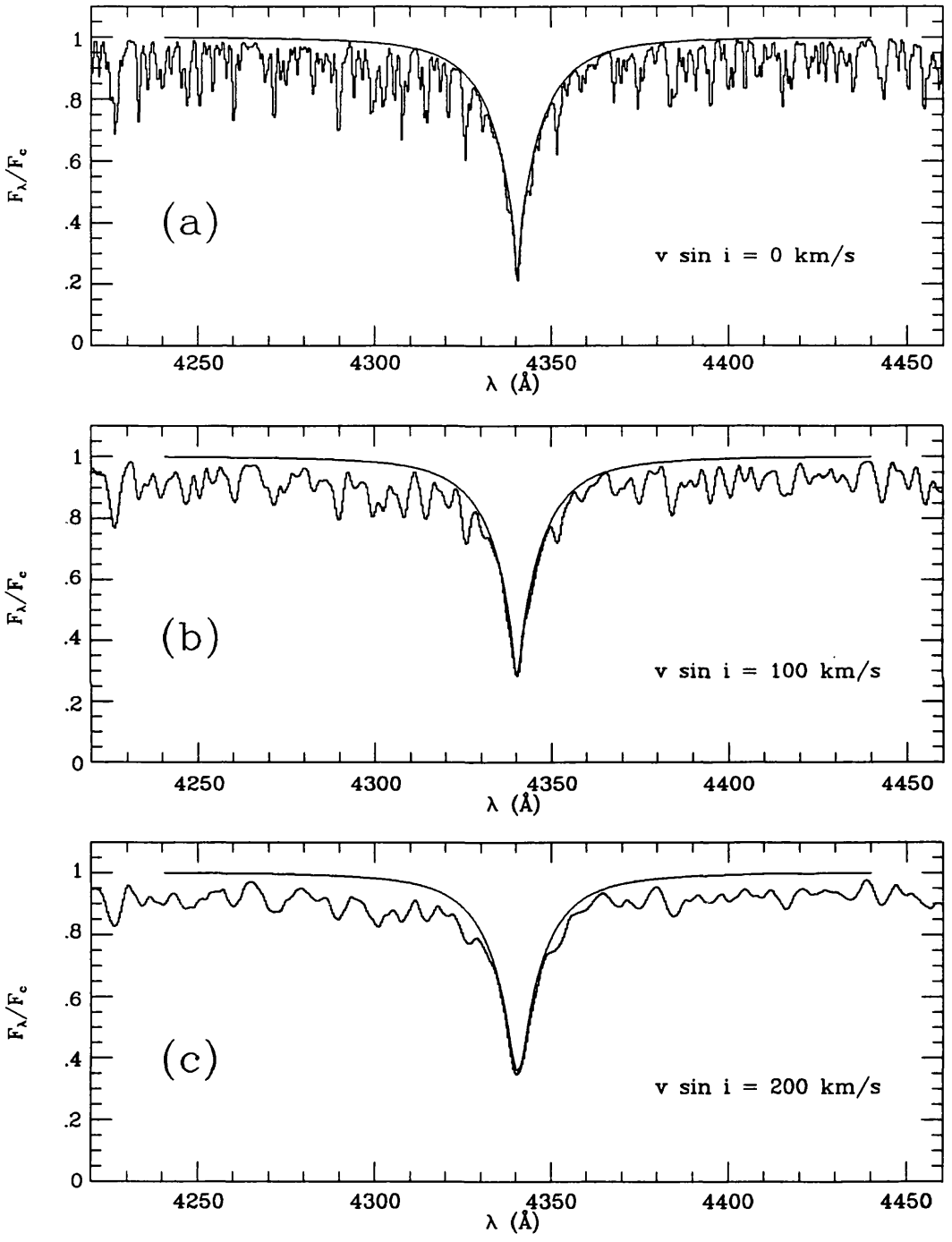

Figure 5.4: *The effect of increasing* $v \sin i$ *on the apparent continuum level. Based on synthetic spectra with* $T_{\rm eff} = 7500$ *K,* $\log g = 4.0$*, [M/H] = 0.0.*

and is defined as follows:

$$\sigma^2 = \frac{1}{N}\sum_{i=1}^{N}(R_i^+ - R_i^-)^2 \qquad (5.1)$$

where, R^+ is the residual flux of the blue wing, R^- that of the red wing and N the number of points in the profile. The values of σ indicate a typical uncertainty of only $1 \sim 2$ %.

5.3 Comparison between JKT and published profiles

A few of the JKT programme stars have published Balmer line profiles (See Figures 5.5 and 5.6). The majority of the published profiles were obtained from photographic spectra and, therefore, of poorer quality than the present profiles. Exceptions are the photoelectric profiles for Vega obtained by Peterson (1969). These are often used as the standard profiles. The JKT profiles are in excellent agreement.

The photographic profiles are shallower than the JKT ones due to the effects of scattered light in the spectrograph. Scattered light is caused by minor imperfections in the spectrograph diffraction grating rulings (Gray, 1976, p.283). The use of a holographic grating in the present work eliminated such imperfections (Tull, 1988).

5.4 Temperatures from smooth observational profiles

Effective temperatures were obtained by fitting theoretical profiles to the smoothed observational profiles. Kurucz (1979a) solar-composition Hβ and Hγ profiles were used, along with [M/H] = +0.5 profiles calculated using the BALMER programme written by Peterson. The hydrogen line profiles were calculated using the Stark-broadening tables of Vidal, Cooper & Smith (1973). All the theoretical profiles were calculated normalized to $\pm$100Å, but in the fitting they were re-normalized to $\pm$40Å to be compatible with the observations.

A least-squares fitting technique was used to obtain the best fit to the observed profiles, for the JKT programme stars cooler than 8500 K. The value of $\log g$ was assumed to be 4.0, because the variation in profile shape with $\log g$ is very small for stars in this temperature range. Above 8500 K, however, fits with varying $\log g$ would be required due to the significant variation of profile shape with $\log g$. Table 5.1 gives the values of $T_{\rm eff}$ obtained by fitting the model profiles to the smoothed Hβ and Hγ profiles and results agree very well. The Hγ results are slightly hotter by 70 $\pm$60 K,

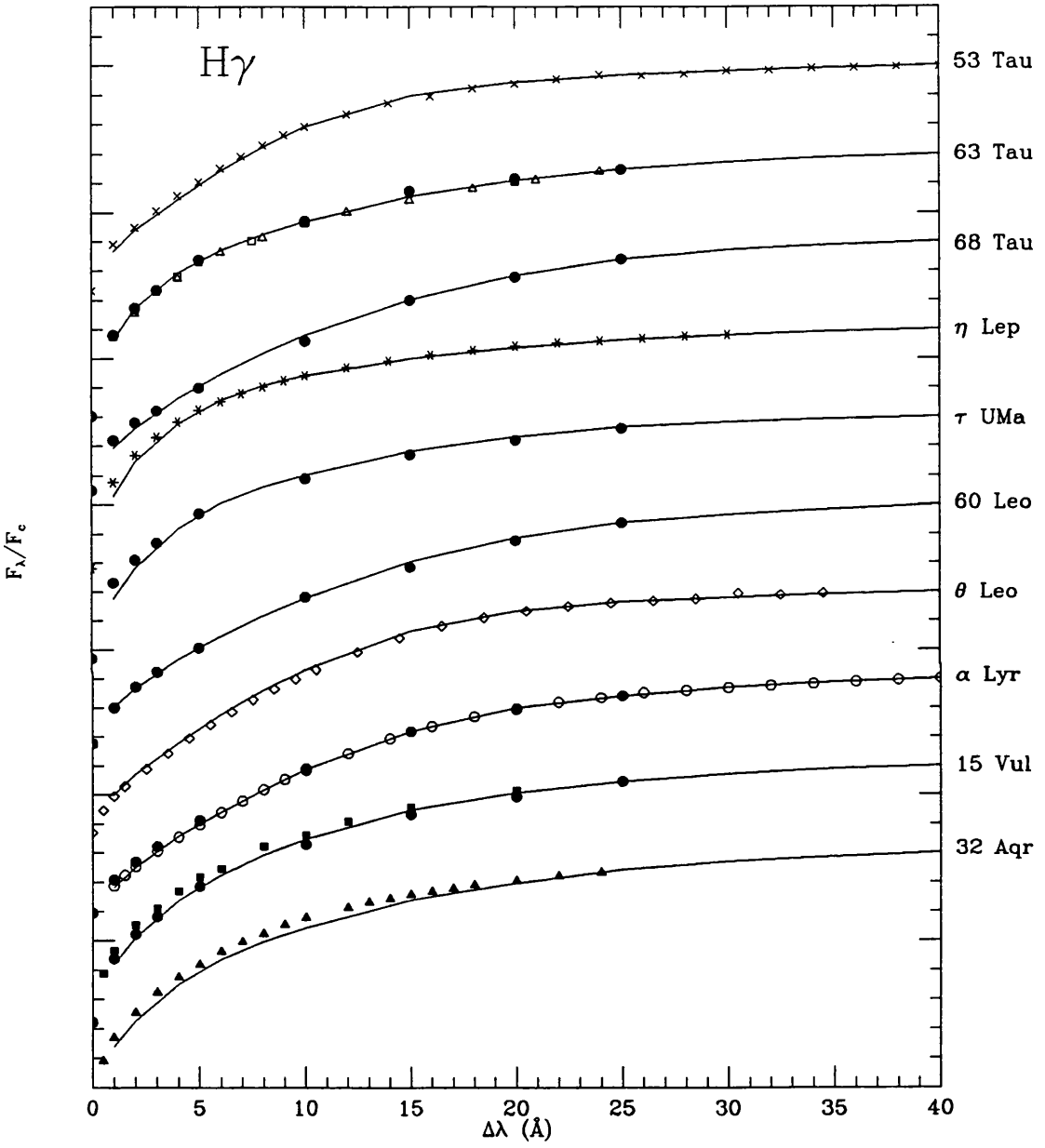

Figure 5.5: *Comparison with published Hγ profiles. Key: (◇) Adelman (1986), (*) Adelman (1987a), (×) Adelman (1987b), (•) Baschek & Oke (1965), (□) Hundt (1972), (▲) Kocer et al. (1987), (■) Miczaika et al. (1956), (○) Peterson (1969) and (△) Van't Veer-Menneret (1963).*

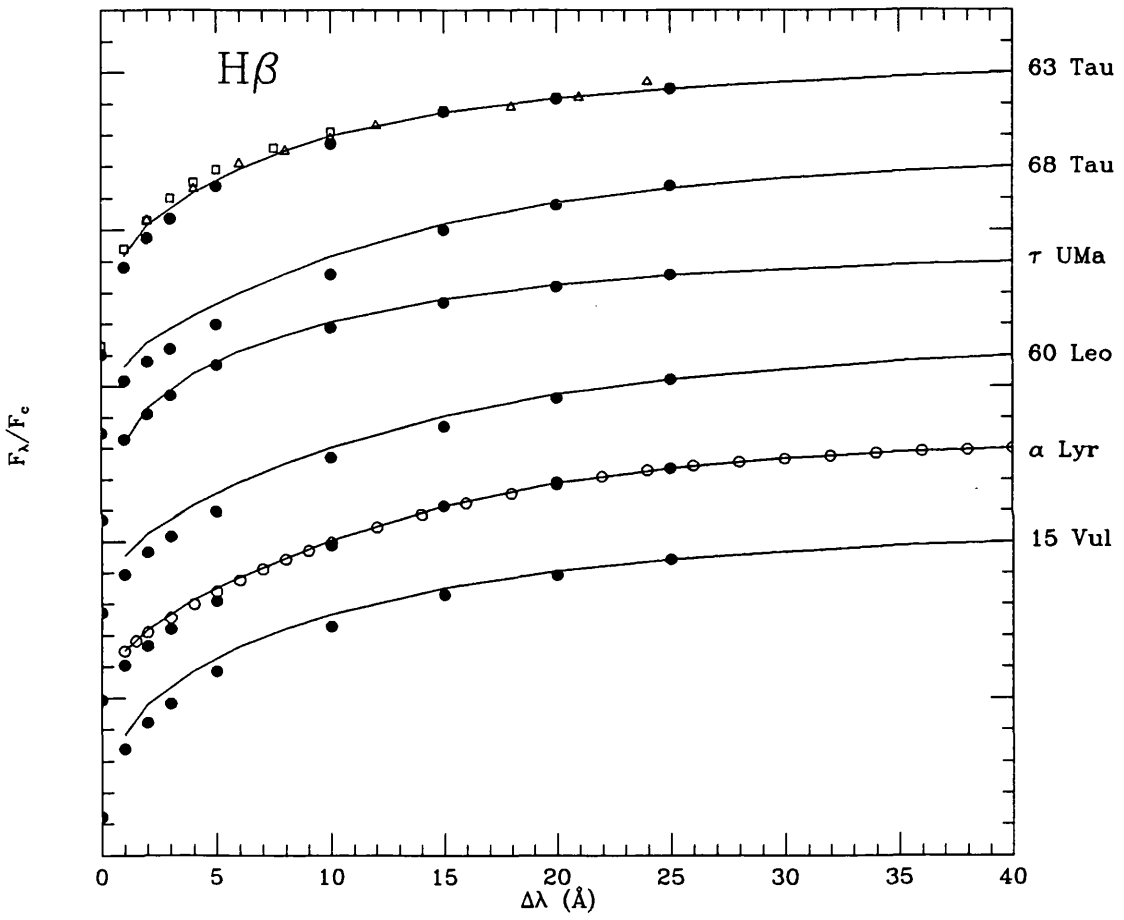

Figure 5.6: *Comparison with published Hβ profiles. Key: (•) Baschek & Oke (1965), (□) Hundt (1972), (○) Peterson (1969) and (△) Van't Veer-Menneret (1963).*

with no apparent change in the difference with T_{eff}. The difference appears to be due to the effects of line-blanketing not being completely removed. Using [M/H] = +0.5 models gave values of T_{eff} which were lower by 110 ±20 K for Hβ and 100 ±35 K for Hγ. Hence, increasing the metal abundance by 0.5 dex decreases the T_{eff} obtained from the Balmer lines by typically 100 K. Compared to spectrophotometric flux fitting, the sensitivity of the Balmer lines to blanketing effects is considerably less.

Table 5.1: *Results from fits to smoothed Balmer line profiles, for* $\log g = 4.0$ *and* $T_{eff} < 8500$ *K.*

	Hβ		Hγ			Hβ		Hγ	
HR	1×⊙	3×⊙	1×⊙	3×⊙	HR	1×⊙	3×⊙	1×⊙	3×⊙
114	7280	7160	7390	7270	1444	7670	7560	7770	7630
269	8210	8110	8210	8230	1458	7960	7840	8100	8030
984	7580	7470	7770	7640	1472	7320	7210	7400	7290
1197	8000	7880	8040	7950	1473	8230	8190	8230	8260
1254	6880	6740	6870	6740	1479	8180	8080	8200	8140
1292	7050	6920	7030	6900	1480	7770	7650	7870	7730
1331	7530	7420	7590	7480	1507	7570	7460	7600	7500
1351	7430	7320	7540	7440	1519	8160	8060	8190	8130
1354	7040	6900	7070	6940	1547	7860	7750	7940	7840
1356	7810	7690	7950	7850	1620	8160	8060	8210	8160
1368	7400	7280	7380	7270	1670	7690	7580	7850	7710
1376	7610	7500	7720	7610	1672	7940	7830	8040	7960
1380	8120	8020	8240	8180	1905	7750	7640	7910	7810
1385	7000	6860	7050	6920	2085	7020	6880	7140	7010
1387	8210	8170	8250	8210	2124	8030	7910	8140	8070
1388	7680	7580	7690	7590	3569	8010	7890	8040	7960
1392	7500	7390	7420	7310	3624	7480	7370	7500	7390
1394	7600	7490	7590	7480	3775	6480	6320	6460	6280
1403	7560	7450	7560	7450	3888	7160	7030	7320	7210
1408	7170	7040	7270	7160	4031	7120	6990	7270	7150
1412	7920	7800	8010	7930	4357			8250	8190
1414	8000	7890	8070	8000	4399	6850	6730	6840	6700
1422	7350	7230	7350	7240	4534			8310	8260
1427	8120	8020	8190	8120	4715	7160	7030	7210	7090
1428	7770	7650	7920	7820	7653	7920	7810	8080	8000
1430	7610	7510	7670	7570	8410	7880	7760	8040	7950

Figures 5.7 and 5.8 shows a selection of fits to the observed Hβ and Hγ profiles. The full set of Hβ and Hγ fits is given in Appendix C.1.

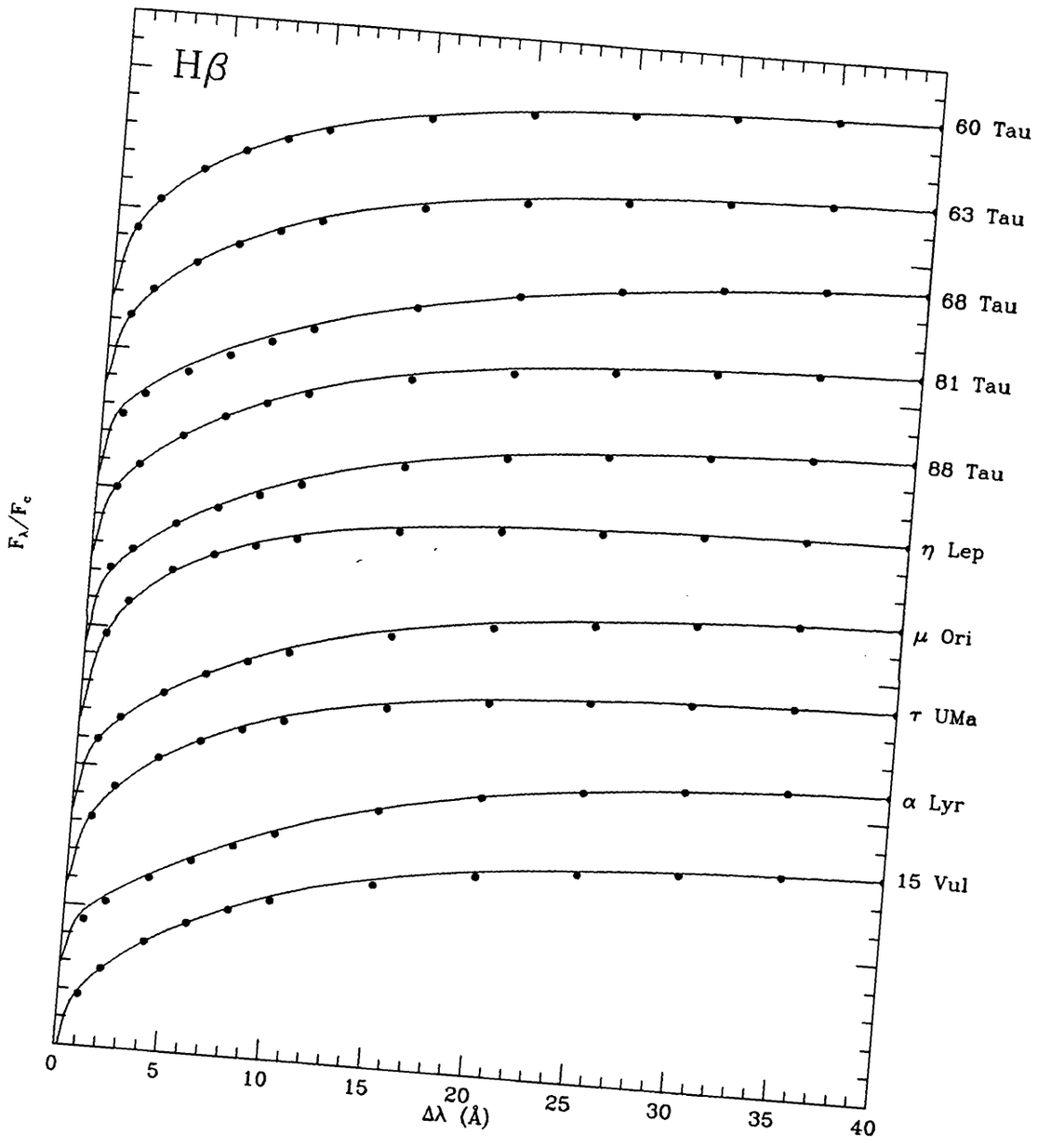

Figure 5.7: *Fits to Hβ profiles. Both the models and the observations are normalized to ±40 Å.*

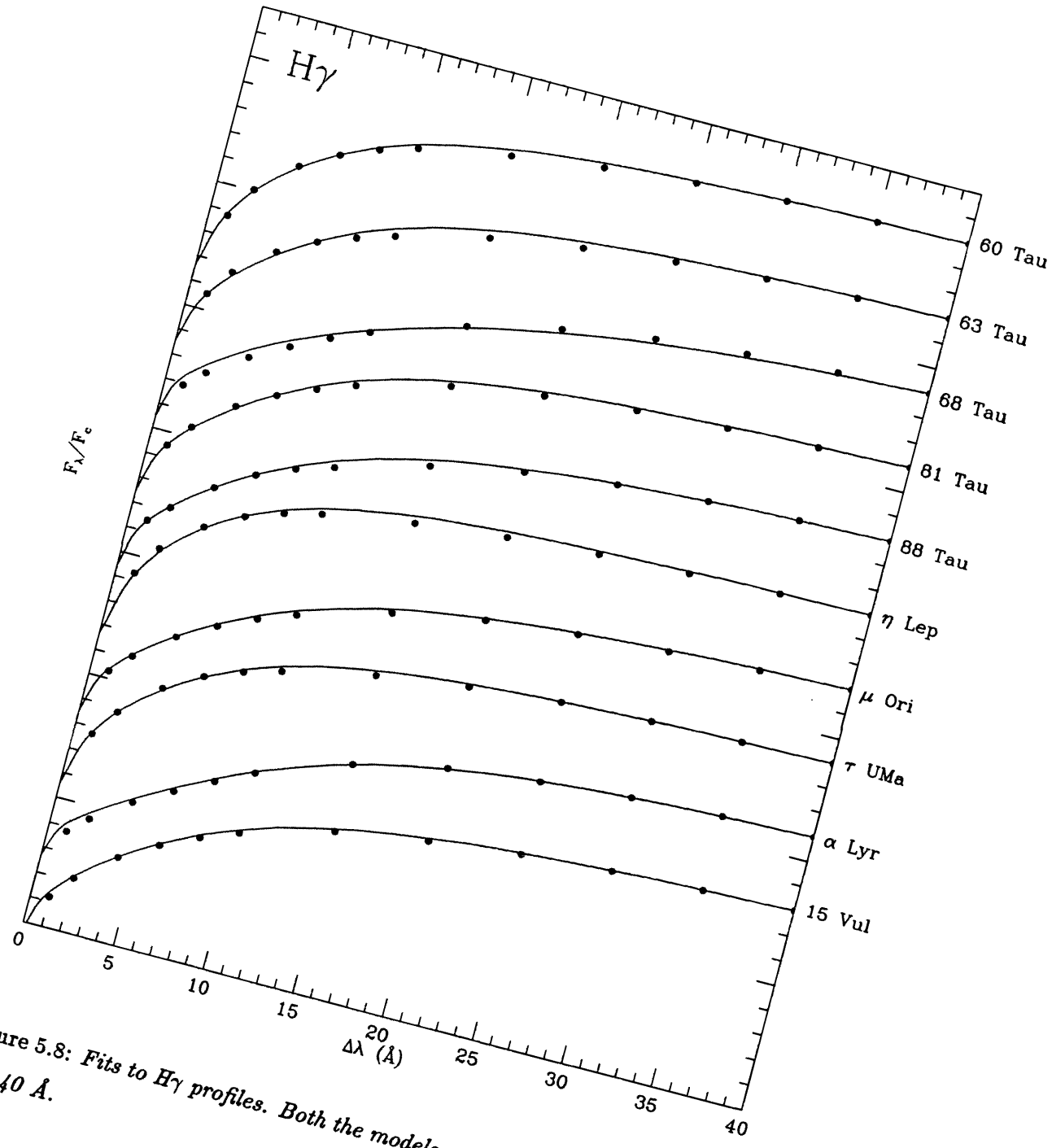

Figure 5.8: *Fits to Hγ profiles. Both the models and the observations are normalized to ±40 Å.*

5.5 Fitting model profiles directly to JKT spectra

An alternative method of obtaining T_{eff} from Balmer lines was also developed and tested. Instead of a least-squares fit to the smooth profiles, the models were fitted directly to the JKT spectra.

The principle of this procedure is illustrated in Figure 5.9. The theoretical profile shape is varied by changing T_{eff} until the profile which just touches the observed spectrum is found. Owing to noise in the spectrum, the theoretical profile is allowed to go a small amount, Δ, below the observations. A value of $\Delta = 0.01$ was used which corresponded to the estimated signal-to-noise ratio of the JKT spectra.

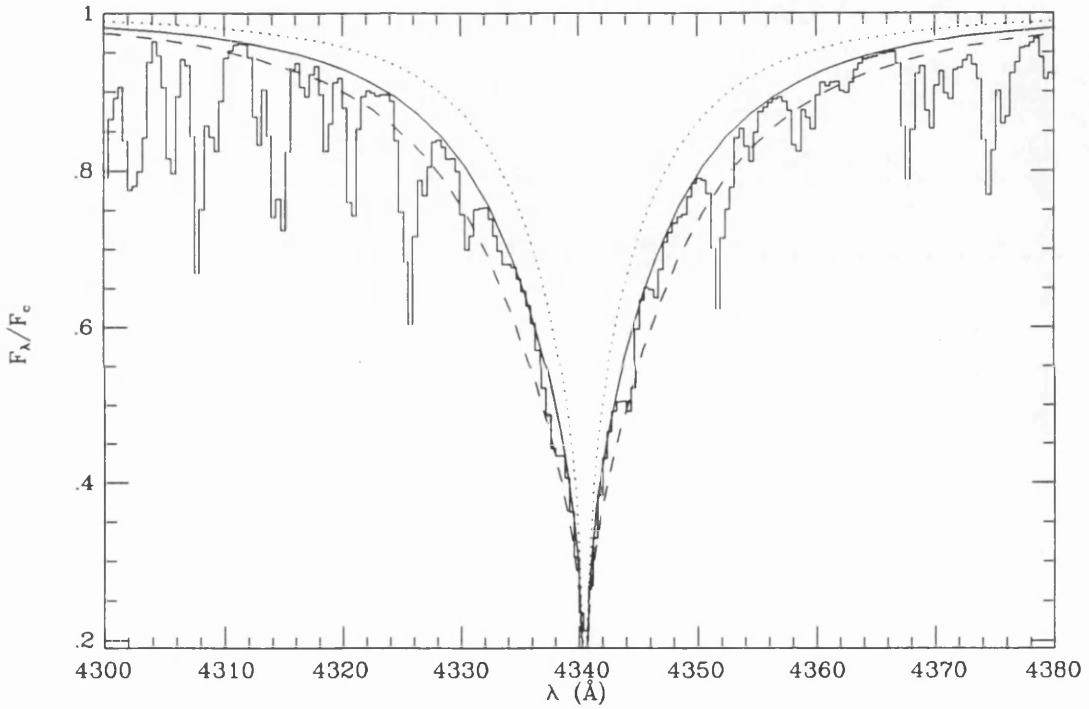

Figure 5.9: *The principle of the Balmer line fitting procedure. The theoretical profile is chosen so that it just fits the data with no points below the observed spectrum (——). Profiles that are too weak are rejected (· · · · ·) as are ones which fall below the observations (– – –).*

The theoretical profiles were interpolated onto the same wavelength points as the observations and then rotationally broadened to the $v \sin i$ of the star. Next, a Gaussian instrumental profile ($\sigma = 0.3$) was convolved with the profile to match the resolution of the observations. An iterative process was performed to obtain the T_{eff} of the profile that just touched the observed spectrum. The results for $\log g$

= 4.0 are given in Table 5.2. The Hγ results are slightly hotter by 100 $\pm$70 K. This agrees with the difference found in the previous section. Again, using [M/H] = +0.5 models gives lower values of T_{eff} by $\sim$100 K. Comparing this method with the standard fitting procedure reveals that the two give the same result to within $\pm$100 K.

Table 5.2: *Results obtained by fitting model Balmer line profiles to spectra (T_{eff} < 8500 K and* $\log g$ *= 4.0).*

	Hβ		Hγ			Hβ		Hγ	
HR	1×⊙	3×⊙	1×⊙	3×⊙	HR	1×⊙	3×⊙	1×⊙	3×⊙
114	7260	7140	7420	7320	1444	7660	7540	7730	7630
269	8140	8030	8250	8220	1458	7880	7770	8040	7940
984	7510	7400	7740	7640	1472	7280	7170	7340	7230
1197	7920	7810	8080	8000	1473	8250	8160	8250	8230
1254	6790	6680	6890	6750	1479	8110	8010	8190	8120
1292	6970	6850	7050	6910	1480	7700	7580	7780	7660
1331	7450	7330	7570	7470	1507	7510	7400	7630	7540
1351	7370	7250	7530	7420	1519	8090	7990	8140	8060
1354	6970	6840	6880	6750	1547	7780	7670	7840	7730
1356	7710	7600	7890	7790	1620	8110	8000	8190	8120
1368	7370	7250	7380	7270	1670	7720	7610	7780	7650
1376	7580	7470	7620	7520	1672	7910	7800	7960	7860
1380	8080	7970	8230	8150	1905	7720	7600	7920	7820
1385	6930	6800	6960	6820	2085	7010	6880	7130	7000
1387	8230	8130	8250	8240	2124	7930	7820	8150	8080
1388	7550	7430	7630	7530	3569	7950	7840	8090	8010
1392	7390	7280	7480	7390	3624	7370	7260	7440	7330
1394	7590	7470	7660	7580	3775	6380	6210	6460	6260
1403	7550	7430	7580	7480	3888	7060	6940	7230	7110
1408	7150	7030	7240	7120	4031	7040	6910	7120	6980
1412	7920	7820	8000	7910	4357			8250	8220
1414	7920	7810	8080	7990	4399	6760	6640	6790	6650
1422	7260	7150	7330	7230	4534			8420	8340
1427	8030	7930	8210	8130	4715	7070	6950	7000	6850
1428	7730	7620	7880	7780	7653	7820	7710	8090	8000
1430	7530	7410	7690	7590	8410	7830	7710	7980	7880

5.6 Using the ratio of two profiles

Van't Veer, Cayrel & Coupry (1991) gave the T_{eff} for 63 Tau based on the ratio of Hα and Hβ profiles with respect to those of Procyon (α CMi). This method avoided the need for absolute calibration of profiles, since instrumental responses largely cancel. However, the method does rely on the standard star T_{eff}, $\log g$ and [M/H] being known accurately. Procyon was chosen since its atmospheric parameters are reasonably well known (Steffen, 1985), and because the amount of line-blanketing is similar to that of 63 Tau. Not having Procyon in the present data set meant that this type of analysis could not be repeated. However, trials using Vega as the standard yielded values of T_{eff} consistent with the earlier methods.

5.7 Synthesis of β indices

As a by-product of the generation of synthetic line-blanketed spectra for the Hβ region, the calculation of synthetic β indices could be performed. This calculation was along the lines of that of Schmidt & Taylor (1979) and Schmidt (1979). The motivation for this work was to determine whether or not the empirically calibrated β indices of Moon & Dworetsky (1985) would agree with those obtained from line-blanketed synthetic spectra. Schmidt (1979) did not allow for metal lines in his calculations, but the effect should only be significant for cool stars. In this work, far more high-quality spectra are available with more extensive wings.

The rectified JKT Hβ spectra were used to obtain a spectroscopic value of the β index, $\beta_{\rm JKT}$. Two Gaussian response functions with widths of 30Å and 150Å were used to mimic the narrow and wide filters respectively. The spectral region $\pm$100Å from the Hβ core was integrated through both of the filters. The ratio of the two enabled $\beta_{\rm JKT}$ to be obtained:

$$\beta_{\rm JKT} = -2.5 \log_{10} \left(\frac{F_{\rm narrow}}{F_{\rm wide}} \right) \tag{5.2}$$

where $F_{\rm narrow}$ and $F_{\rm wide}$ are the integrated fluxes through the narrow and wide filters respectively.

The $\beta_{\rm JKT}$ values are in a natural system and must be transformed onto the standard system, $\beta_{\rm STD}$, using the transformation of Crawford & Mander (1966). Since photometric values of β are available for the JKT programme stars the transforma-

tion can be readily obtained:

$$\beta_{\rm STD} = 1.0094\ \beta_{\rm JKT} + 0.6634 \qquad (5.3)$$

The correlation is very tight with a typical scatter of ~0.01 in β. Figure 5.10 show the correlation and indicates that there is no clear evidence for bifurcation.

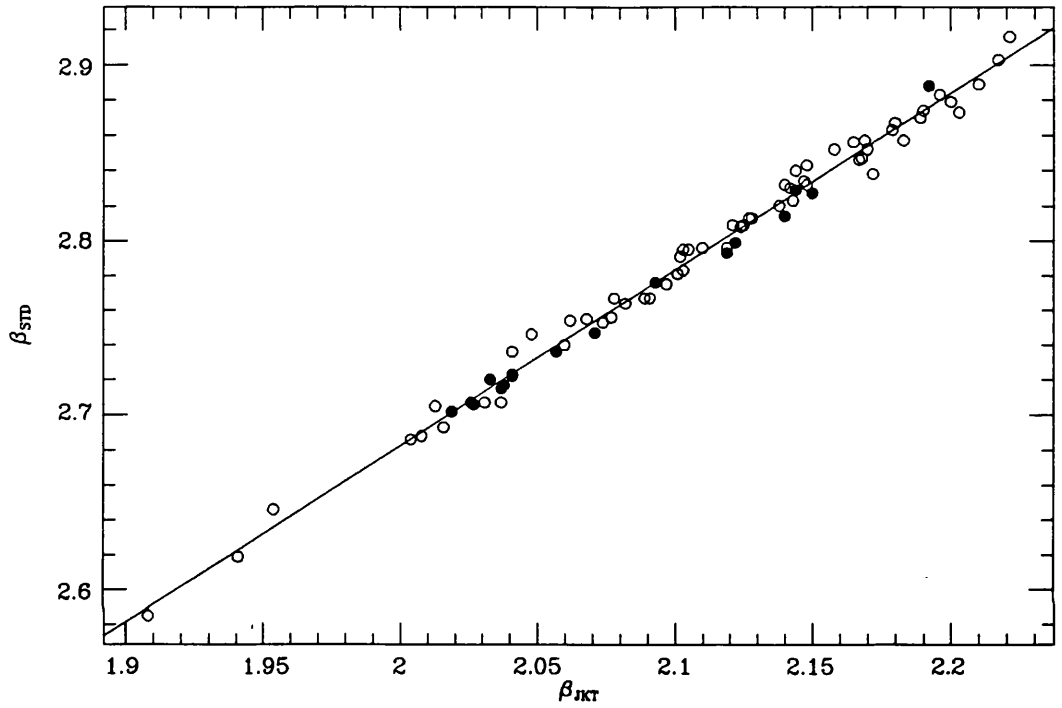

Figure 5.10: *Plot of $\beta_{\rm JKT}$ against $\beta_{\rm STD}$. The circles indicate stars with $T_{\rm eff} < 10000$ K and the dots are the hotter stars. There is no clear evidence for bifurcation, but there are only a few hot stars.*

Exactly the same integrations were applied to the synthetic spectra. After transformation onto the standard system, using Equation 5.3, a grid of β indices ($\beta_{\rm SYN}$) was obtained (Table 5.3). A similar calculation was performed using just the Kurucz (1979a) profiles (with no other absorption lines). The result was essentially the same, except for $T_{\rm eff} < 6500$ K when blanketing effects start to become significant. Neglecting the line-blanketing produced values of β that were too small.

A comparison with the various published β calibrations is shown in Figure 5.11. The Schmidt calibration is clearly deviant, especially at large values of β. The Moon & Dworetsky empirical correction to the Schmidt values is in good general agreement with $\beta_{\rm SYN}$ to within ± 0.02. The Lester, Gray & Kurucz calibration is much more discrepant especially for the lower (cool) values where, differences of up to 0.03 are

Table 5.3: *Synthetic β indices.*

	log g								
	[M/H] = −1.0			[M/H] = 0.0			[M/H] = +0.5		
T_{eff}	3.5	4.0	4.5	3.5	4.0	4.5	3.5	4.0	4.5
5500	2.546	2.543	2.546	2.580	2.576	2.572	2.603	2.602	2.598
6000	2.583	2.577	2.575	2.615	2.609	2.603	2.642	2.639	2.633
6500	2.640	2.630	2.623	2.665	2.656	2.648	2.689	2.681	2.675
7000	2.706	2.696	2.686	2.726	2.719	2.709	2.745	2.738	2.729
7500	2.774	2.765	2.757	2.791	2.784	2.775	2.801	2.797	2.789
8000	2.835	2.831	2.822	2.846	2.844	2.837	2.855	2.853	2.849
8500	2.889	2.893	2.887	2.894	2.906	2.906	2.896	2.912	2.916
9000	2.893	2.919	2.926	2.886	2.917	2.931	2.888	2.920	2.937
9500	2.870	2.914	2.937	2.866	2.910	2.937	2.863	2.908	2.937
10000	2.836	2.891	2.933	2.834	2.889	2.929	2.834	2.888	2.928
11000				2.777	2.834	2.887	2.778	2.835	2.888
12000				2.736	2.788	2.839	2.737	2.790	2.841
13000				2.708	2.754	2.800	2.707	2.754	2.802
14000				2.687	2.729	2.772	2.685	2.728	2.771
15000				2.670	2.710	2.749	2.667	2.707	2.747
16000				2.656	2.694	2.731	2.653	2.690	2.727
17000				2.644	2.680	2.715			
18000				2.632	2.668	2.705			

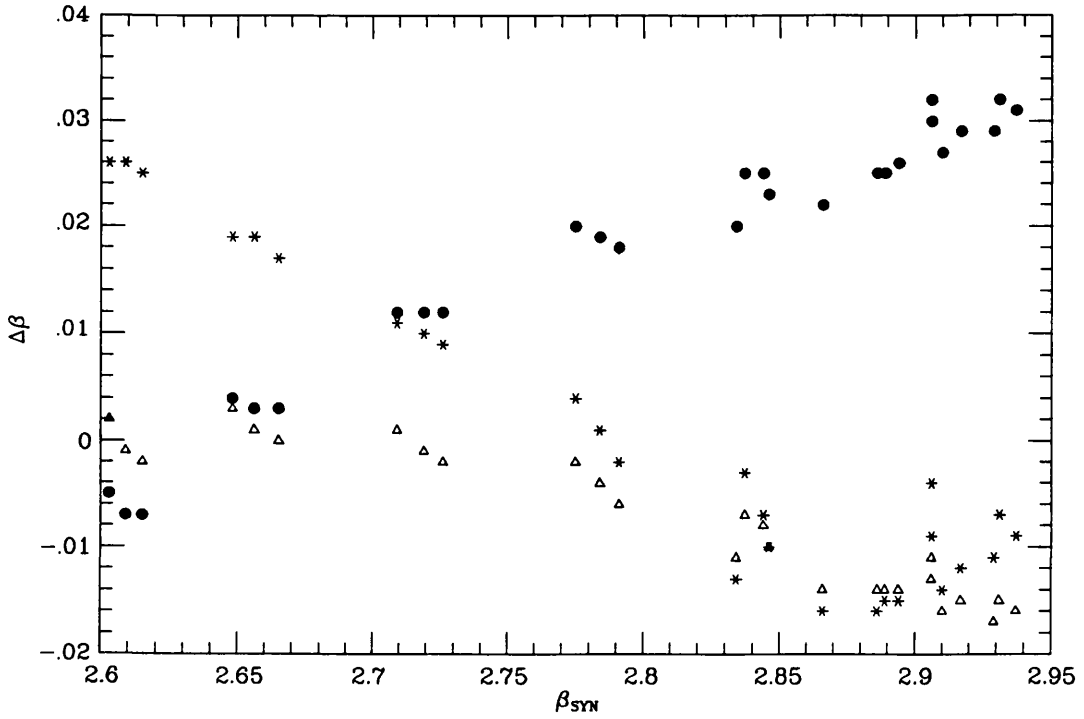

Figure 5.11: *Comparison between the various β calibrations. The difference, Δβ, is defined as* $\beta_{GRID} - \beta_{SYN}$. *The various* β_{GRID} *values are as follows: (•) Schmidt (1979), (△) Moon & Dworetsky (1985), (*) Lester, Gray & Kurucz (1986).*

found.

A comparison of the value of β calculated for the Sun using the new grid was made with that obtained by Olsen (1976). The new synthetic β value for the Sun (T_{eff} = 5777 K, $\log g$ = 4.44) is 2.589, which compares very well with $\beta_{\odot}$ = 2.595 given by Olsen. In contrast the Lester, Gray & Kurucz grid gives β = 2.618 for the solar model. This values is too large and indicates that for cool stars (T_{eff} < 6500 K) their grid gives too low a T_{eff} for a given β value. In fact, the Lester, Gray & Kurucz β values for 5500 K coincide with the values for 6000 K in the synthetic grid.

The Schmidt & Taylor transformation to the standard system appears to be the source of the discrepancy between Schmidt's results and the empirically corrected values of Moon & Dworetsky. Using higher-quality observations has produced a much better calibration. One suggestion for further work would be to extend the observations to stars earlier than A0 to check for colour bifurcation (Schmidt, 1979).

5.8 Conclusion

The Hβ and Hγ Balmer lines have been shown to be extremely reliable T_{eff} diagnostics for late-A and F stars. The effects of line-blanketing and stellar rotation on the apparent hydrogen line shapes have been investigated. After correction for such effects the 'true' hydrogen profiles agreed well with theoretical profiles. Two independent methods were used to obtain T_{eff} values for the JKT programme stars and the results agree to within ~100 K. The Hγ lines gave T_{eff} values which were slightly hotter than those obtained from Hβ, but by only ~70 K.

A calculation of synthetic β indices using line-blanketed spectra has been performed. A new grid of synthetic β indices has been determined for various metal abundances. The values were found to be in very good agreement with the empirically-corrected grid of Moon & Dworetsky (1985). The discrepancy between the Schmidt and Moon & Dworetsky calibrations has been traced, in part, to the transformation used by Schmidt. The use of higher-quality spectra enabled a much better transformation to be obtained.

Table 5.4: *Observed Hβ line profiles*

	Residual Flux at $\Delta\lambda$ (Å)											
Star	1.0	2.0	4.0	6.0	8.0	10.0	15.0	20.0	25.0	30.0	35.0	σ
63	.353	.424	.530	.607	.669	.720	.824	.893	.935	.965	.985	.005
114	.451	.551	.668	.740	.793	.831	.897	.937	.962	.979	.991	.016
269	.364	.447	.552	.631	.693	.742	.836	.893	.933	.962	.984	.006
364	.455	.541	.647	.727	.787	.837	.919	.955	.976	.987	.994	.007
558	.383	.456	.554	.646	.727	.782	.885	.938	.966	.981	.991	.011
811	.478	.563	.670	.758	.829	.873	.941	.971	.986	.994	.997	.005
972	.358	.412	.524	.609	.679	.735	.848	.913	.949	.972	.988	.005
984	.411	.505	.624	.700	.758	.803	.880	.927	.957	.976	.989	.005
1197	.415	.465	.575	.658	.713	.756	.843	.898	.935	.963	.984	.011
1254	.492	.617	.738	.805	.845	.876	.928	.956	.972	.984	.993	.020
1292	.457	.597	.715	.777	.821	.858	.915	.945	.965	.980	.991	.017
1331	.426	.524	.636	.708	.764	.805	.875	.921	.952	.972	.988	.012
1339	.425	.492	.579	.664	.736	.795	.889	.936	.965	.982	.993	.005
1351	.421	.517	.645	.725	.781	.822	.890	.929	.956	.975	.989	.008
1354	.481	.573	.710	.785	.834	.865	.912	.944	.966	.981	.992	.011
1356	.381	.484	.602	.681	.737	.782	.859	.904	.939	.964	.984	.009
1368	.428	.534	.650	.726	.780	.821	.890	.931	.957	.974	.988	.014
1376	.413	.512	.623	.698	.754	.797	.872	.919	.949	.970	.987	.015
1380	.374	.460	.562	.640	.701	.749	.841	.897	.935	.963	.984	.007
1385	.485	.577	.718	.794	.837	.867	.916	.947	.967	.982	.992	.011
1387	.355	.448	.542	.623	.688	.734	.831	.893	.935	.963	.984	.004
1388	.434	.484	.608	.692	.749	.791	.860	.904	.939	.966	.986	.012
1389	.361	.436	.527	.599	.660	.711	.817	.887	.932	.964	.985	.005
1392	.476	.511	.624	.714	.761	.798	.876	.920	.952	.975	.990	.014
1394	.467	.506	.608	.695	.752	.791	.866	.913	.947	.972	.989	.015
1403	.404	.506	.630	.708	.764	.804	.878	.923	.954	.975	.989	.010
1408	.449	.559	.699	.764	.809	.846	.907	.937	.958	.976	.989	.014
1412	.386	.471	.580	.664	.724	.772	.855	.910	.946	.969	.987	.012
1414	.367	.459	.577	.658	.719	.764	.848	.905	.943	.968	.987	.007
1422	.459	.524	.652	.736	.792	.826	.885	.925	.954	.975	.990	.016
1427	.367	.456	.566	.643	.701	.749	.838	.898	.936	.963	.984	.004
1428	.400	.487	.601	.682	.739	.783	.862	.911	.943	.967	.985	.007
1430	.400	.498	.622	.702	.757	.799	.878	.921	.951	.972	.988	.007
1444	.410	.486	.613	.695	.750	.793	.871	.917	.948	.970	.987	.009
1458	.411	.482	.582	.651	.708	.758	.850	.908	.944	.968	.985	.018
1472	.449	.526	.662	.742	.792	.829	.896	.933	.959	.977	.990	.006
1473	.365	.435	.541	.622	.687	.735	.829	.890	.930	.960	.983	.006
1479	.373	.442	.553	.637	.698	.747	.836	.892	.932	.962	.984	.010
1480	.386	.495	.603	.679	.738	.784	.866	.919	.951	.971	.987	.009
1507	.402	.506	.630	.709	.761	.803	.878	.919	.949	.970	.986	.008
1519	.357	.455	.558	.633	.694	.743	.843	.902	.941	.968	.986	.008
1547	.413	.470	.583	.671	.732	.775	.855	.906	.941	.967	.986	.014

Table 5.4: *Observed Hβ line profiles (Continued)*

Star	Residual Flux at Δλ (Å) 1.0	2.0	4.0	6.0	8.0	10.0	15.0	20.0	25.0	30.0	35.0	σ
1620	.368	.445	.556	.637	.700	.748	.841	.895	.935	.964	.985	.008
1670	.403	.501	.607	.683	.744	.791	.873	.919	.950	.971	.987	.011
1672	.383	.480	.578	.655	.715	.764	.853	.907	.944	.968	.985	.011
1702	.444	.538	.646	.736	.806	.858	.931	.963	.981	.990	.996	.004
1800	.413	.475	.585	.676	.751	.806	.895	.940	.967	.983	.993	.008
1905	.398	.485	.604	.687	.744	.787	.865	.911	.944	.968	.986	.010
2085	.471	.591	.712	.780	.826	.860	.916	.945	.965	.980	.991	.013
2124	.395	.475	.574	.653	.709	.752	.841	.897	.935	.963	.984	.012
2519	.500	.589	.702	.785	.847	.891	.947	.972	.984	.991	.996	.009
2676	.493	.579	.685	.776	.841	.883	.945	.970	.982	.990	.995	.006
2844	.471	.555	.664	.757	.822	.870	.935	.964	.980	.989	.995	.004
3569	.393	.460	.580	.661	.717	.760	.841	.894	.933	.962	.984	.007
3595	.388	.459	.560	.654	.734	.793	.896	.942	.968	.982	.992	.004
3623	.485	.562	.670	.757	.821	.867	.929	.961	.978	.988	.995	.015
3624	.417	.530	.642	.713	.765	.807	.882	.927	.957	.976	.989	.015
3652	.477	.567	.683	.768	.836	.877	.940	.966	.980	.989	.996	.007
3775	.553	.692	.813	.864	.896	.920	.950	.966	.978	.987	.994	.015
3888	.453	.557	.690	.767	.817	.854	.908	.938	.961	.977	.990	.008
4031	.452	.562	.690	.770	.826	.866	.922	.950	.971	.984	.993	.011
4033	.351	.426	.518	.599	.667	.721	.825	.895	.942	.973	.989	.008
4072	.381	.450	.553	.638	.713	.777	.876	.928	.961	.979	.991	.010
4300	.354	.426	.517	.592	.653	.703	.806	.877	.924	.956	.981	.006
4359	.358	.429	.529	.612	.684	.741	.852	.915	.951	.972	.988	.004
4399	.468	.621	.758	.813	.853	.885	.928	.955	.973	.984	.993	.020
4660	.398	.429	.527	.599	.660	.712	.809	.880	.928	.962	.984	.009
4715	.449	.552	.689	.769	.820	.857	.912	.943	.966	.982	.992	.007
4963	.357	.436	.539	.625	.701	.762	.868	.924	.957	.978	.991	.006
7001	.350	.417	.512	.585	.648	.704	.818	.892	.938	.968	.988	.009
7653	.386	.478	.579	.659	.720	.766	.855	.909	.945	.970	.987	.007
8410	.386	.482	.592	.668	.724	.769	.858	.914	.949	.971	.987	.007
8641	.355	.435	.534	.618	.689	.745	.857	.919	.954	.975	.990	.006
8937	.429	.508	.612	.701	.769	.824	.912	.952	.974	.985	.993	.005

Table 5.5: *Observed Hγ line profiles*

	Residual Flux at $\Delta\lambda$ (Å)											
Star	1.0	2.0	4.0	6.0	8.0	10.0	15.0	20.0	25.0	30.0	35.0	σ
63	.303	.370	.481	.572	.645	.706	.827	.906	.950	.972	.988	.010
114	.392	.500	.633	.719	.773	.818	.889	.934	.963	.980	.991	.010
269	.311	.381	.497	.586	.656	.708	.809	.885	.939	.971	.988	.008
364	.407	.490	.607	.704	.779	.834	.927	.964	.977	.986	.994	.008
558	.326	.395	.513	.615	.704	.773	.882	.938	.964	.980	.991	.013
811	.432	.513	.641	.746	.818	.869	.945	.974	.985	.991	.996	.005
972	.302	.358	.474	.567	.644	.713	.848	.920	.956	.977	.990	.009
984	.366	.456	.579	.663	.726	.776	.868	.924	.957	.977	.989	.009
1197	.361	.412	.532	.633	.703	.753	.843	.901	.938	.965	.984	.012
1254	.463	.590	.722	.800	.846	.877	.931	.960	.975	.985	.993	.014
1292	.438	.567	.697	.771	.820	.853	.917	.952	.970	.983	.992	.011
1331	.383	.457	.594	.700	.756	.794	.873	.921	.953	.975	.990	.016
1339	.365	.438	.544	.643	.723	.792	.897	.944	.969	.982	.992	.010
1351	.389	.472	.606	.701	.764	.809	.887	.935	.962	.978	.990	.014
1354	.449	.521	.679	.784	.831	.858	.910	.944	.967	.983	.994	.021
1356	.353	.430	.558	.653	.714	.759	.844	.901	.941	.968	.986	.015
1368	.382	.503	.636	.719	.778	.820	.885	.931	.964	.984	.993	.013
1376	.365	.472	.593	.671	.725	.769	.855	.910	.948	.973	.990	.015
1380	.318	.396	.514	.600	.665	.718	.819	.889	.937	.964	.984	.006
1385	.457	.535	.683	.777	.828	.860	.913	.947	.968	.983	.993	.021
1387	.313	.378	.490	.582	.652	.708	.814	.887	.935	.965	.986	.011
1388	.401	.455	.578	.675	.737	.779	.855	.914	.947	.970	.987	.025
1389	.292	.360	.462	.546	.618	.681	.802	.884	.939	.971	.989	.006
1392	.430	.474	.599	.704	.771	.814	.885	.933	.960	.977	.990	.019
1394	.410	.451	.578	.692	.759	.805	.876	.924	.953	.974	.989	.021
1403	.380	.457	.595	.695	.761	.808	.887	.934	.963	.981	.992	.014
1408	.416	.506	.651	.742	.792	.827	.896	.937	.961	.978	.991	.020
1412	.336	.406	.537	.642	.707	.759	.851	.909	.946	.970	.988	.014
1414	.337	.412	.533	.620	.689	.745	.848	.912	.950	.973	.988	.008
1422	.412	.479	.624	.733	.793	.832	.895	.935	.958	.974	.988	.018
1427	.334	.404	.520	.605	.671	.725	.831	.894	.936	.964	.985	.014
1428	.349	.440	.565	.647	.710	.762	.855	.911	.949	.971	.987	.010
1430	.375	.451	.582	.675	.741	.790	.876	.926	.958	.977	.990	.017
1444	.376	.439	.572	.671	.733	.782	.872	.923	.953	.972	.987	.020
1458	.350	.417	.531	.625	.691	.740	.839	.907	.948	.973	.989	.017
1472	.413	.475	.617	.723	.783	.822	.892	.935	.961	.977	.989	.014
1473	.313	.379	.498	.590	.655	.704	.811	.884	.936	.967	.986	.017
1479	.325	.387	.500	.599	.679	.735	.831	.896	.936	.963	.983	.015
1480	.343	.441	.574	.659	.718	.764	.853	.919	.956	.976	.990	.014
1507	.365	.448	.591	.693	.759	.806	.883	.929	.958	.976	.989	.017
1519	.305	.395	.524	.613	.676	.725	.827	.893	.938	.967	.985	.014
1547	.370	.422	.549	.649	.716	.765	.848	.905	.944	.969	.987	.026

Table 5.5: *Observed Hγ line profiles (Continued)*

	Residual Flux at $\Delta\lambda$ (Å)											
Star	1.0	2.0	4.0	6.0	8.0	10.0	15.0	20.0	25.0	30.0	35.0	σ
1620	.324	.388	.504	.598	.669	.724	.830	.903	.946	.968	.986	.013
1670	.354	.449	.569	.657	.724	.774	.857	.914	.949	.970	.987	.015
1672	.339	.431	.547	.635	.695	.741	.837	.901	.943	.970	.987	.018
1702	.399	.482	.624	.732	.812	.867	.939	.973	.983	.991	.996	.008
1800	.347	.423	.554	.658	.741	.810	.914	.955	.976	.986	.994	.008
1905	.354	.429	.557	.645	.714	.770	.863	.917	.953	.975	.989	.011
2010	.315	.382	.500	.603	.685	.757	.878	.935	.963	.979	.992	.006
2085	.430	.547	.676	.757	.807	.842	.900	.939	.964	.981	.993	.023
2124	.332	.408	.527	.611	.676	.730	.835	.902	.942	.966	.984	.009
2519	.452	.538	.668	.766	.834	.880	.944	.970	.984	.991	.996	.014
2676	.434	.518	.648	.750	.820	.869	.943	.972	.985	.993	.998	.007
2844	.422	.504	.646	.740	.808	.858	.932	.964	.981	.990	.996	.012
3569	.346	.408	.528	.630	.698	.752	.856	.910	.943	.966	.985	.011
3595	.328	.402	.527	.638	.729	.801	.909	.953	.973	.985	.994	.011
3623	.425	.517	.650	.753	.820	.869	.941	.970	.983	.991	.996	.005
3624	.374	.481	.619	.706	.761	.802	.882	.931	.965	.981	.992	.018
3652	.437	.522	.655	.762	.837	.889	.958	.981	.988	.993	.997	.009
3775	.516	.674	.813	.875	.905	.922	.954	.974	.984	.991	.996	.019
3888	.416	.487	.634	.734	.793	.831	.899	.941	.965	.979	.991	.016
4031	.400	.501	.651	.739	.796	.841	.911	.949	.972	.987	.995	.015
4033	.300	.366	.471	.562	.640	.704	.833	.909	.948	.972	.988	.009
4072	.326	.395	.514	.626	.721	.794	.902	.949	.971	.983	.992	.009
4295	.303	.366	.467	.559	.643	.716	.850	.920	.954	.976	.991	.009
4300	.303	.368	.465	.546	.616	.678	.804	.887	.939	.966	.985	.006
4357	.337	.386	.503	.596	.667	.721	.823	.896	.940	.966	.985	.014
4359	.300	.370	.479	.578	.662	.732	.865	.933	.965	.979	.991	.010
4399	.438	.588	.744	.815	.858	.890	.939	.965	.980	.988	.995	.021
4534	.319	.376	.482	.570	.637	.689	.802	.879	.933	.965	.983	.014
4554	.316	.366	.479	.568	.647	.716	.841	.919	.956	.974	.989	.007
4660	.341	.381	.483	.576	.649	.707	.825	.897	.933	.960	.982	.012
4689	.310	.382	.483	.570	.647	.715	.850	.914	.950	.973	.988	.006
4715	.412	.496	.652	.760	.816	.852	.916	.955	.975	.986	.994	.019
7001	.282	.350	.456	.540	.617	.687	.819	.899	.941	.970	.988	.007
7653	.320	.412	.536	.623	.691	.748	.848	.905	.945	.971	.988	.014
8404	.336	.406	.535	.651	.742	.812	.910	.957	.977	.987	.994	.007
8410	.340	.425	.551	.635	.696	.744	.839	.896	.942	.971	.987	.004
8641	.307	.372	.478	.576	.662	.737	.866	.933	.965	.980	.991	.010
8937	.378	.450	.566	.667	.751	.817	.908	.947	.970	.985	.994	.013

Chapter 6

The determination of stellar mean metal abundance

6.1 Introduction

A third stellar parameter, [M/H], is inextricably linked to the determination of T_{eff} and $\log g$ for A and F stars. The numerous metal lines have a significant effect on the emergent flux of stars later than mid A-type. Metal abundance must be known to allow for blanketing effects on photometry and spectrophotometry. It is vital that the mean metal abundance be accurately estimated prior to any detailed abundance analysis, since backwarming has a non-negligible effect on the atmospheric temperature structure. In this chapter various methods of obtaining an approximate value for [M/H] are discussed.

Line-blanketing plays a crucial role in determining both the emergent energy distribution and the physical structure of the atmosphere. Because the total flux in the atmosphere must be conserved, the flux blocked by the numerous metal lines must emerge at other frequencies, and the energy emitted in the continuum bands into which it is redistributed must rise above the value it would have had in the absence of lines. Furthermore, because the bandwidth of the spectrum in which energy transport occurs readily is restricted by lines, steeper temperature gradients are necessary to drive the flux through; as a result, temperatures in deeper layers rise, leading to the so-called backwarming effect. Finally, the lines alter the temperature in the outermost layers of the atmosphere, as shown in Figure 6.1.

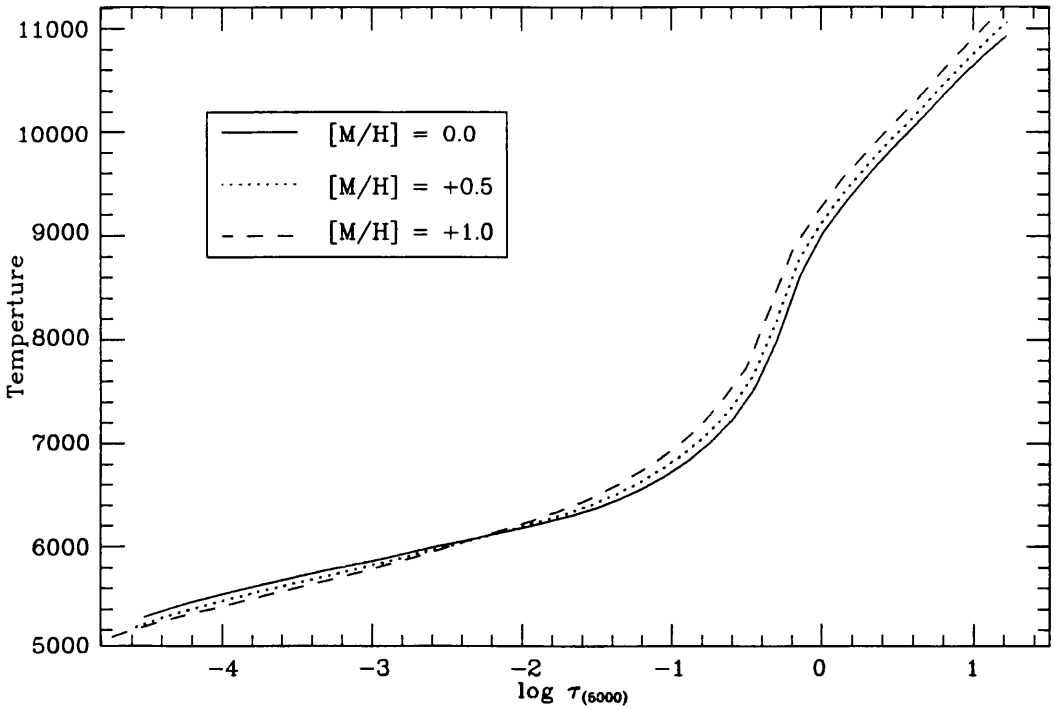

Figure 6.1: *The effect of line-blanketing on the atmospheric temperature structure. The variation of temperature with optical depth is shown. Increasing the metal abundance has the effect of increasing the temperature deep in the atmosphere, while lowering it in the surface layers.*

6.2 The determination of [M/H] from photometry

Photometric colour indices are sensitive to metal abundance to varying degrees and indeed some indices are deliberately designed to be particularly sensitive to metal abundances. Photometry can be used to obtain an approximate value for mean metal abundance, [M/H]. Of the three photometric systems being considered in this work, the UBV system has no metal abundance index and hence will not be considered in the following discussion.

6.2.1 [M/H] from *uvbyβ* photometry

The Strömgren-Crawford $uvby\beta$ system has a metallicity index, δm_0, defined in Chapter 2, which can be used to characterize Am stars. The m_1 colour is a metallicity or peculiarity indicator for A-type stars and a chemical composition indicator for F-type stars.

The calibration of [Fe/H] in terms of *uvby* photometry is long established. Ström-

gren (1966) in his review gave a calibration, based on the abundance determinations of Wallerstein (1962), for F8 – G2 stars:

$$[\mathrm{Fe/H}] = 0.3 - 13\delta m_0 + (\delta m_0 + \delta c_0) \tag{6.1}$$

where δm_0 and δc_0 have $(b-y)$ as the independent variable rather than β as used in the present work.

Crawford (1975) in his empirical calibration of $uvby\beta$ photometry for F stars reviewed the calibration of [Fe/H] in terms of δm_0. He gave the following calibration for F stars based on the [Fe/H] values compiled by Cayrel & Cayrel de Strobel (1966):

$$[\mathrm{Fe/H}] = -10\ \delta m_0 + 0.20 \tag{6.2}$$

He also repeated the fits obtained by Nissen (1970) and Gustafsson & Nissen (1972) using the new definition of δm_0, with β as the independent variable:

$$[\mathrm{Fe/H}] = -14\ \delta m_0 + 0.42 \qquad \text{for F1} - \text{F5 stars} \tag{6.3}$$

$$[\mathrm{Fe/H}] = -11\ \delta m_0 + 0.45 \qquad \text{for F5} - \text{G2 stars} \tag{6.4}$$

Crawford & Perry (1976) revised the Crawford relation obtaining for F1 – G2:

$$[\mathrm{Fe/H}] = -11\ \delta m_0 + 0.15 \tag{6.5}$$

Olsen (1984) gave a calibration for G and K dwarfs:

$$[\mathrm{Fe/H}] = -39\ \delta m_0{}^2 - 6\ \delta m_0 + 0.09. \tag{6.6}$$

However, the value of δm_0 in this equation was defined using $(b-y)$ as the independent variable, not β as used in the present work. Hence, the calibration is not directly compatible with the remaining ones.

Nissen (1988) produced a new calibration for F and G Stars (see also Nissen, 1981):

$$[\mathrm{M/H}] = -(10.5 + 50(\beta - 2.626))\ \delta m_0 + 0.12 \qquad \text{for } 2.59 < \beta < 2.72 \tag{6.7}$$

Hence, the correlation between δm_0 and [M/H] for F stars is well known. All the various calibrations for F-type stars give broadly the same [M/H] for a given δm_0.

Few calibrations have been published for A-type stars (A3 – F0, $2.72 < \beta < 2.88$) because m_1 is not usually considered to be primarily a composition index at these

temperatures. Using the published [Fe/H] values for 163 main sequence and giant stars, Berthet (1990b) obtained a calibration for A and F stars:

$$[\mathrm{Fe/H}] = -35.139\ \delta m_0{}^2 - 6.515\ \delta m_0 + 0.081 \tag{6.8}$$

with a standard error of ± 0.138 in [Fe/H]. The quadratic fit was required to fit the metal poor ([Fe/H] < -0.6) stars. A linear fit is adequate for stars with [Fe/H] > -0.6. Berthet showed that the Crawford & Perry (1976) calibration fitted the data for A and F stars fairly well, except for stars with low metal abundances. Stars with [Fe/H] > 0.0 were few and far between in his dataset and the calibration is not valid for metal-rich stars due to the turnover of the quadratic fit.

Since there is no adequate calibration available for A stars with large metallicity, the data from the Cayrel de Strobel *et al.* (1985) catalogue was used to obtain a relationship for A3 – F0 stars:

$$[\mathrm{M/H}] = -7.0\ \delta m_0 + 0.03 \tag{6.9}$$

where δm_0 was obtained using $uvby\beta$ from Hauck & Mermilliod (1980) and the codes of Moon (1985). The relation is independent of all the T_{eff} and $\log g$ calibrations currently being discussed and the values of [M/H] are also independent since they are taken directly from the Cayrel de Strobel *et al.* catalogue. However, it must be remembered that the value of [M/H] is itself dependent on the value of T_{eff} and $\log g$ used in the individual analyses that make up the catalogue. This could lead to systematic errors if, for example, the determinations of T_{eff} and $\log g$ for the metal-rich stars in the catalogue are in error due to the metallicity problems noted earlier (see Chapter 3). Hence, there is a need to determine a new calibration based on [M/H] values obtained using critically evaluated values of T_{eff} and $\log g$ that are independent of metallicity problems. Such a new calibration is determined in Section 6.4.

6.2.2 [M/H] from Geneva photometry

The Geneva m_2 index is sensitive to metallicity through the blanketing effect. The index is functionally equivalent to the Strömgren m_1 index and thus can be used to determine metallicity in a similar manner to δm_0.

Hauck (1986) determined a calibration for main-sequence A and F stars:

$$[\mathrm{Fe/H}] = 5.922\ \Delta m_2 + 0.070 \tag{6.10}$$

A similar calibration obtained for A and F giants by Berthet (1990a):

$$[\mathrm{Fe/H}] = 5.831\ \Delta m_2 + 0.034 \tag{6.11}$$

The similarity between these two calibrations led Berthet to conclude that a single calibration is valid of both main-sequence and giant A and F stars. He re-did the fit using his data and that used by Hauck (1986) and obtained:

$$[\mathrm{Fe/H}] = 5.553\ \Delta m_2 + 0.022 \tag{6.12}$$

which is valid for both main-sequence and giant stars.

Berthet (1990b) extended this study using the [Fe/H] values for 163 main-sequence and giant stars. He presented a calibration for A and F stars:

$$[\mathrm{Fe/H}] = -16.079\ \Delta m_2{}^2 + 5.935\ \Delta m_2 + 0.081 \tag{6.13}$$

This is similar to the fit he gave for the Strömgren δm_0 index. Again, the quadratic terms makes the calibration invalid for metal-rich stars.

6.3 The determination of [M/H] from spectrophotometry

The use of spectrophotometry in the determination of T_{eff} and $\log g$ has already been discussed fully in Chapter 3. It has already been shown that these results are affected by the atmospheric metal content [M/H] for late-A and F stars. However, if T_{eff} and $\log g$ can be independently determined, the value of [M/H] can be estimated from the ultraviolet fluxes.

The flux below the Balmer Jump is more sensitive to [M/H] than that at longer wavelengths due to the increased number of metal lines (See Figure 3.4 in Chapter 3, and the figures given by Kurucz (1979b)). A metal-rich star will have less flux in the ultraviolet than a solar-composition star of the same T_{eff} and $\log g$. Hence, the difference between observed ultraviolet flux and that predicted by a solar-composition model for the T_{eff} and $\log g$ of a star will provide a measure of metal abundance, [M/H].

Figure 6.2 illustrates the principle behind the proposed method for determining an ultraviolet measure of [M/H]. The observed ultraviolet flux points are compared

to the corresponding model fluxes and the mean difference is obtained:

$$\Delta UV = \frac{1}{n}\sum_{i=1}^{n}(o_i - m_i) \tag{6.14}$$

where o_i are the observed flux points and m_i the corresponding model values. The value of ΔUV is given in magnitude units. The flux points used in the present work are those obtained from the S2/68 database.

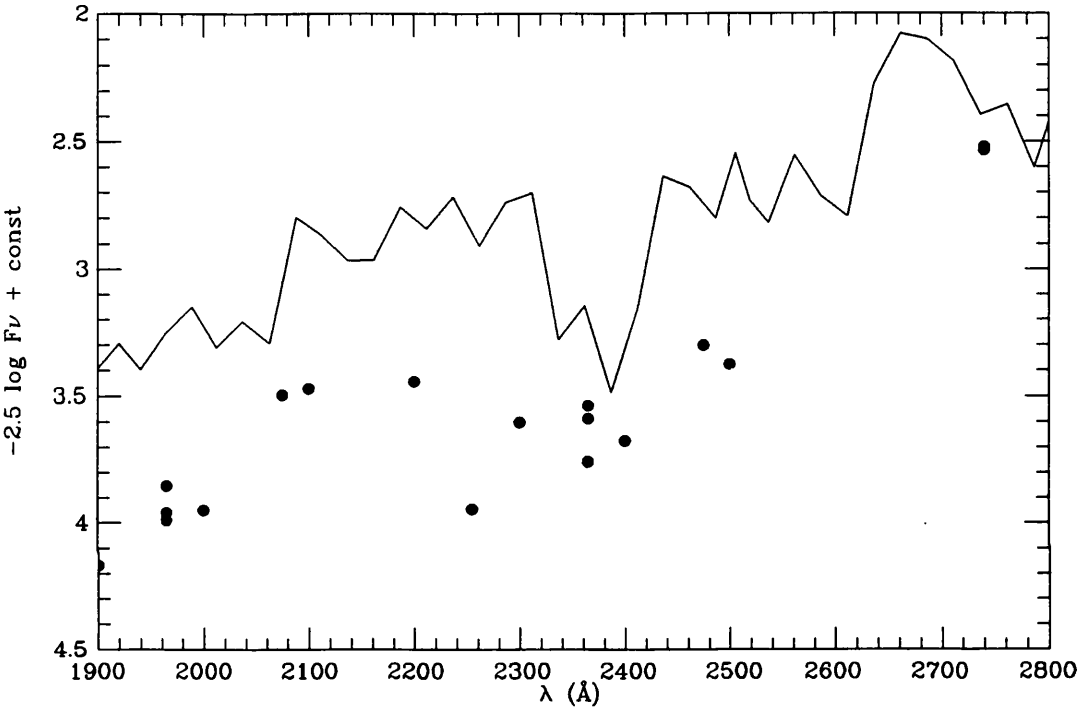

Figure 6.2: *The principle of the UV-method. The mean value of the difference in magnitude between the observations (•) and the solar abundance model (——) for that star gives a measure of metal abundance for late-A and F stars.*

The value of ΔUV can only provide an absolute measure of [M/H] if the differences are caused by line-blanketing only and not by opacity deficiencies or by errors in the T_{eff} or $\log g$. The Kurucz (1979a) models are known to have missing opacity. The values of ΔUV can be used differentially to compare metal-rich stars to normal stars. Errors in T_{eff} and $\log g$, however, will affect the result but this cannot be avoided unless absolute values are known empirically. Nevertheless, there is a correlation between ΔUV and δm_0, for stars in the range $6000 < T_{eff} < 8500$ K, when the Moon & Dworetsky (1985) calibration is used to obtain T_{eff} and $\log g$ (See Figure 6.3). This indicates that, if the Moon & Dworetsky results are correct, ΔUV measures metallicity with considerable accuracy. If ΔUV could be calibrated

in terms of [M/H] then spectrophotometry could be used to obtain stellar metal abundances. This method is valid only for stars in which the effects of interstellar reddening are negligible or properly removed.

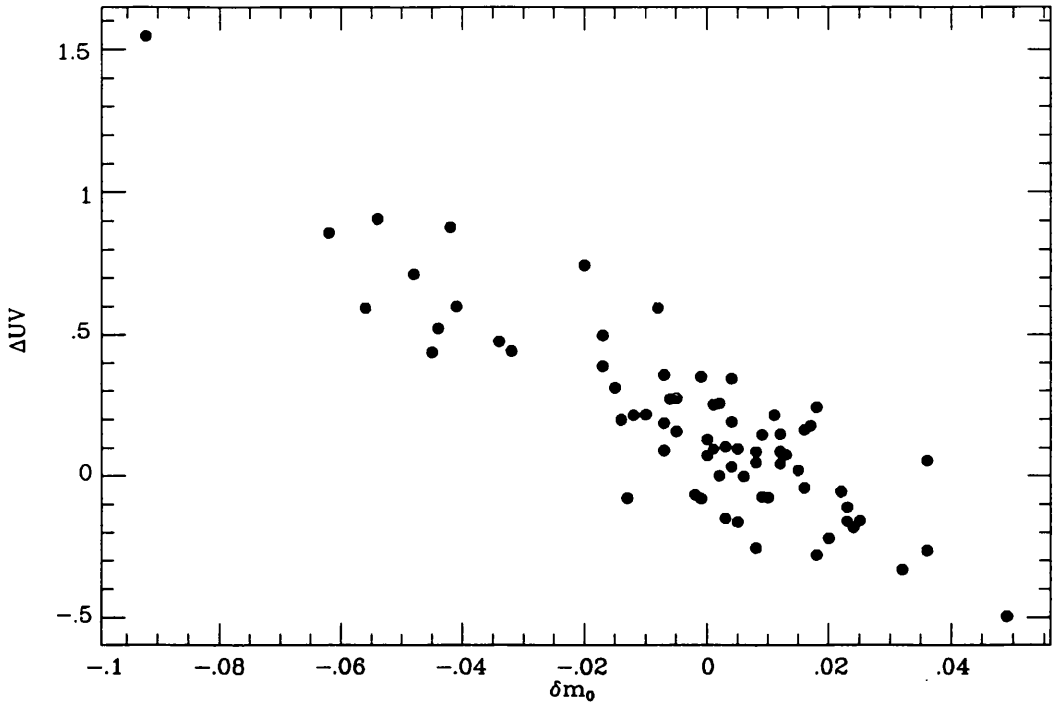

Figure 6.3: *The correlation between ΔUV and δm_0 for stars in the range 6000 < $T_{\rm eff}$ < 8500 K. There is a strong correlation between the ultraviolet metallicity index ΔUV and the Strömgren photometric index δm_0. This clearly shows that, provided the stellar $T_{\rm eff}$ and* $\log g$ *are known, the metal abundance can be estimated from the ultraviolet flux deviation. The $T_{\rm eff}$ and* $\log g$ *are from the Moon & Dworetsky (1985) calibration.*

Because the effects of line-blanketing varying with temperature, the value of ΔUV may not be correlated linearly with [M/H]. A $T_{\rm eff}$ term in the calibration is to be expected. Using [M/H] = +0.5 models as synthetic observations, a theoretical value of ΔUV was obtained as a function of $T_{\rm eff}$. Figure 6.4 shows the variation of ΔUV with $T_{\rm eff}$ for [M/H] = +0.5 along with the observed values of ΔUV. The value of ΔUV is insensitive to $\log g$, with a change of only 0.05 dex in ΔUV going from $\log g$ = 4.5 to 3.5. For $T_{\rm eff}$ < 8500 K, stars with ΔUV greater than the theoretical [M/H] = +0.5 line ought to have metal abundances greater than [M/H] = +0.5.

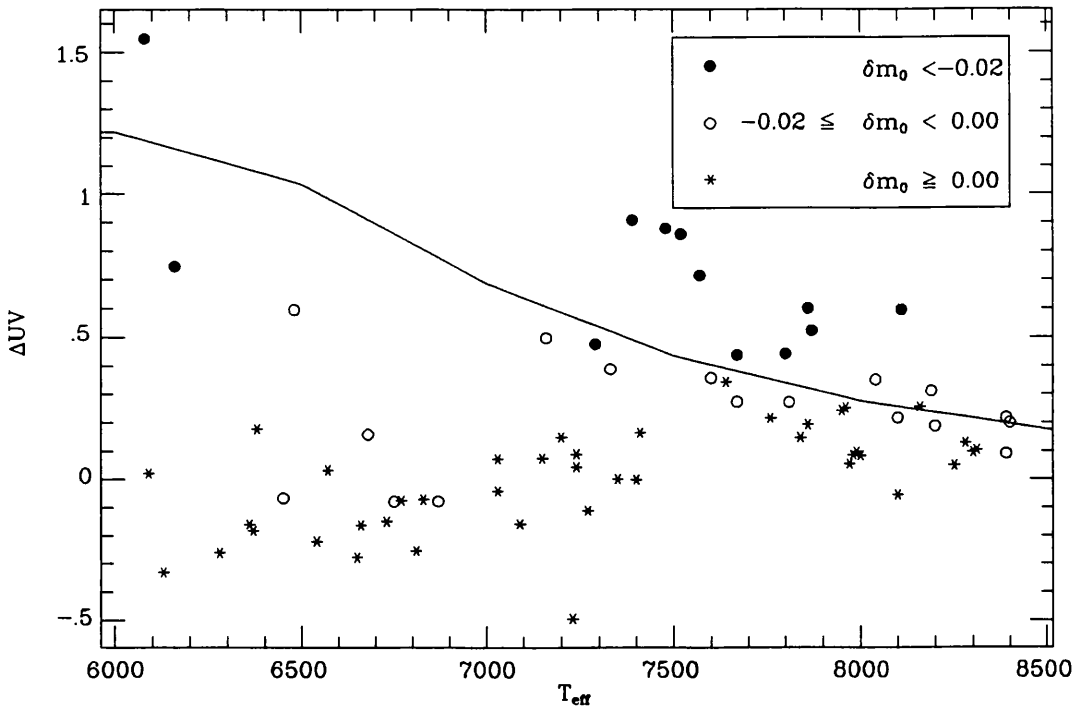

Figure 6.4: *The variation of ΔUV with $T_{\rm eff}$. The line indicates the theoretical ΔUV values for [M/H] = +0.5 and $\log g$ = 4.0.*

6.4 The determination of [M/H] from JKT spectra

The relatively low resolution of the JKT spectra precludes the use of detailed line profile fitting or indeed the measuring of individual line equivalent widths with any degree of accuracy. However, as is shown below the spectra can still be used to obtain a gross value of [M/H] by the comparison with synthetic spectra. The procedure is essentially a comparison of the amount of line blocking in a region of the JKT spectrum with that predicted by synthetic spectra, computed with a range of values of [M/H]. Knowing $T_{\rm eff}$ and $\log g$ allows the value of [M/H] to be determined.

The 4700Å region JKT spectra were used for this analysis. The region from 4600 – 4700Å was selected to have its amount of line-blocking measured. The 100Å sections of spectrum were integrated numerically to obtain a line-blocking coefficient:

$$\Lambda = \log_{10}\left[\int_{4600}^{4700}(1 - R_\lambda)d\lambda\right] \tag{6.15}$$

where R_λ is the residual flux at λ. However, Λ cannot directly give a value of [M/H] since it has to be related to model atmospheres.

Owing to the sensitivity of the proposed method to uncertainties in the continuum level location, the simple linear two-point rectification used for the Balmer line

profiles could not be used. Instead, each of the spectra was carefully rectified by fitting a smooth curve to the apparent or expected continuum level. This procedure used the CURSOR routine to draw a smooth curve through continuum points, as previously used in Section 5.2. The same problems caused by blanketing and rotation were encountered and treated as before. The rectification process is illustrated in Figure 6.5. The value of Λ for Vega is the lowest of all the JKT programme stars observed at 4700Å. Hence, any systematic error in the evaluation of the continuum level will have the largest effect on the value of Λ obtained for Vega. The carefully rectified spectra reduce the systematic errors considerably.

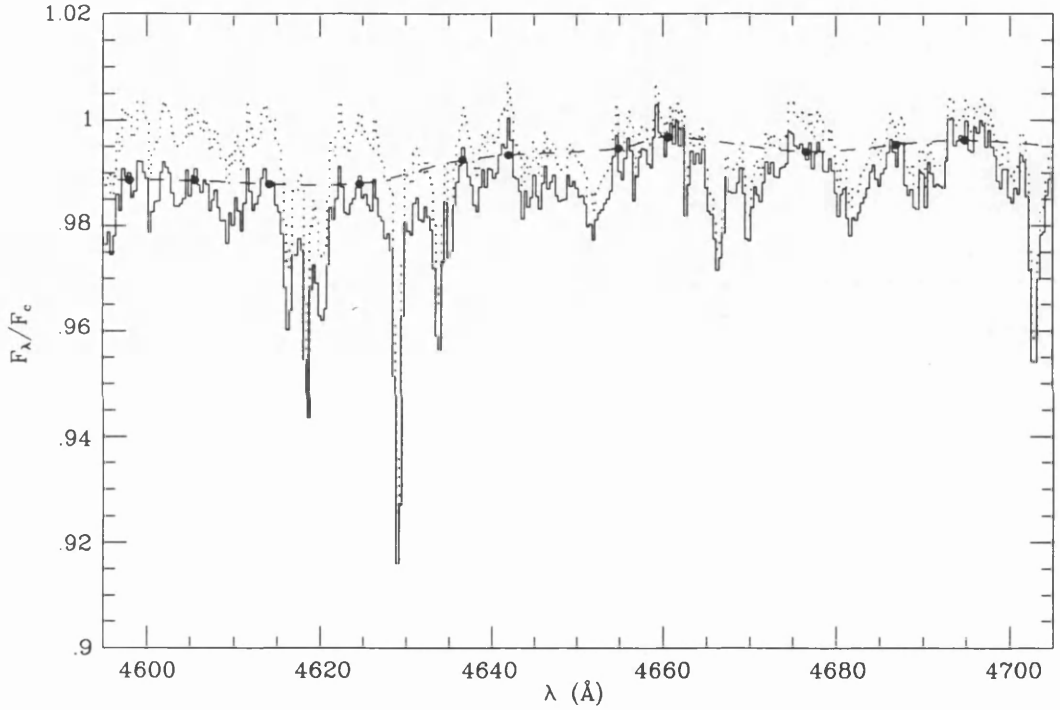

Figure 6.5: *The rectification of the Vega spectrum. Several continuum points (•) were selected along the raw spectrum (——) and a smooth curve drawn through them (– – –). The spectrum was then divided by this curve to obtain a rectified spectrum (· · · · ·).*

A grid of 150 synthetic spectra was calculated covering the ranges, $5500 < T_{eff} < 10000$, $3.5 < \log g < 4.5$, and $-1.0 < [M/H] < +1.0$, in steps of 500 K, 0.5 dex and 0.5 dex respectively. A value of Λ for each of these synthetic spectra was obtained for the same wavelength range as the observational spectra. This yielded a 3-dimensional grid of Λ in terms of T_{eff}, $\log g$ and [M/H](Figure 6.6). A series of 2^{nd} order polynomial least-squares fits was made to these coefficients to obtain an

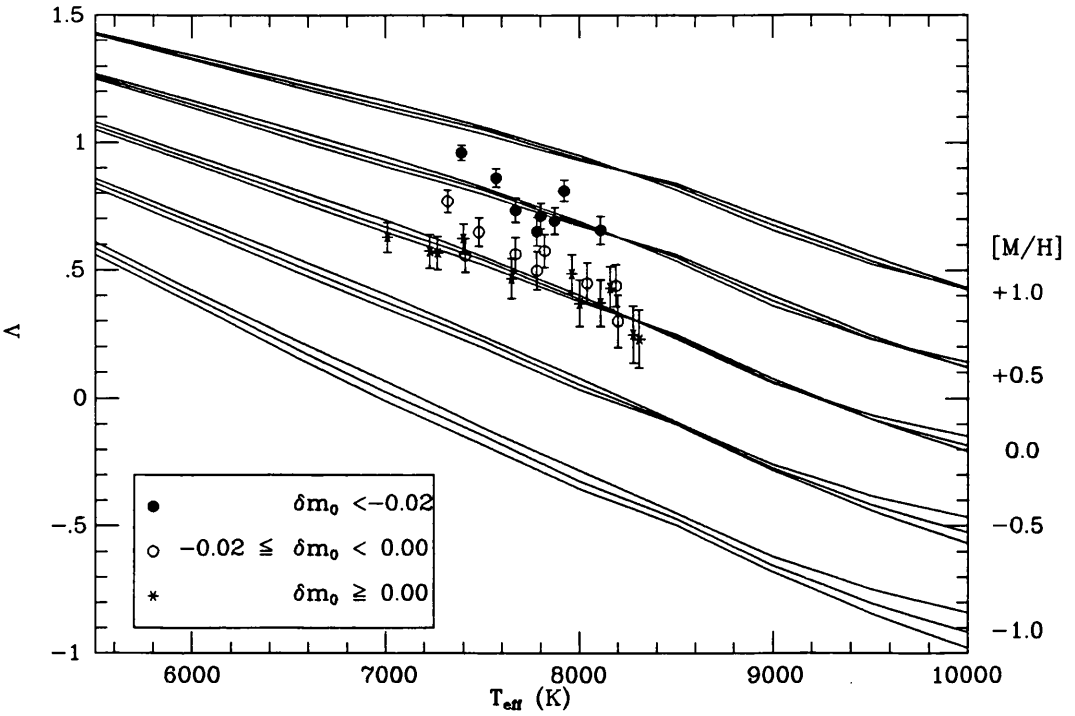

Figure 6.6: *The observed and calculated line-blocking coefficients, Λ. The grid lines are the predicted Λ tracks for various abundances. The three lines indicate the Λ tracks for* $\log g$ *values of 3.5, 4.0 and 4.5. The stars are represented by various symbols according to* δm_0*. Note that, for the Moon & Dworetsky (1985)* $T_{\rm eff}$ *values, stars with different* δm_0 *values are well segregated into corresponding metal abundance groups.*

explicit calibration in terms of $T_{\rm eff}$, $\log g$ and [M/H]:

$$\Lambda = A[\mathrm{M/H}]^2 + B[\mathrm{M/H}] + C \tag{6.16}$$

where,

$$\begin{aligned}
C &= E_{(1,1,1)} + E_{(1,2,1)}\log g + E_{(1,3,1)}\log g^2 \\
&\quad +(E_{(1,1,2)} + E_{(1,2,2)}\log g + E_{(1,3,2)}\log g^2)X \\
&\quad +(E_{(1,1,3)} + E_{(1,2,3)}\log g + E_{(1,3,3)}\log g^2)X^2 \\
B &= E_{(2,1,1)} + E_{(2,2,1)}\log g + E_{(2,3,1)}\log g^2 \\
&\quad +(E_{(2,1,2)} + E_{(2,2,2)}\log g + E_{(2,3,2)}\log g^2)X \\
&\quad +(E_{(2,1,3)} + E_{(2,2,3)}\log g + E_{(2,3,3)}\log g^2)X^2 \\
A &= E_{(3,1,1)} + E_{(3,2,1)}\log g + E_{(3,3,1)}\log g^2 \\
&\quad +(E_{(3,1,2)} + E_{(3,2,2)}\log g + E_{(3,3,2)}\log g^2)X \\
&\quad +(E_{(3,1,3)} + E_{(3,2,3)}\log g + E_{(3,3,3)}\log g^2)X^2
\end{aligned}$$

$X = T_{eff} - 5500$

$E_{(i,j,k)}$ are the coefficients determined from the polynomial fitting

For any given stellar T_{eff} and $\log g$ the value of [M/H] can be obtained directly using the quadratic formula:

$$[M/H] = \frac{-B + \sqrt{B^2 - 4A(C - \Lambda)}}{2A} \tag{6.17}$$

The calibration was able to recover the grid point [M/H] values to within ± 0.025 dex.

The values of [M/H] determined by this method will be significantly more uncertain than the formal fitting error of ± 0.025, due to uncertainties in T_{eff} and Λ. The values of Λ determined from the JKT spectra are rather uncertain due to noise and uncertainties in continuum shape and location. A typical error of 1% in the continuum level was adopted as the uncertainty in the rectification process.

The final values of [M/H] obtained from this method are given in Table 6.1. The T_{eff} and $\log g$ values used were obtained from the Moon & Dworetsky (1985) calibration. Using T_{eff} values from Hβ profiles and an approximate $\log g$ of 4.0 gave basically the same results. If the T_{eff} and $\log g$ values given by solar-abundance spectrophotometric fits are used, values of [M/H] $\sim$0.0 are obtained, as one might expect.

When the values of [M/H] are plotted against δm_0 an excellent correlation was obtained (see Figure 6.7). An unweighted least-squares fit to these points gave:

$$[M/H] = -10.56\ \delta m_0 + 0.081 \qquad \text{for } 2.72 < \beta < 2.88 \tag{6.18}$$

with a linear correlation coefficient of $r = -0.923$ for 28 points. There was no noticeable change in the slope of the fit with T_{eff}, though the present sample is rather small. Such an effect was expected to be present and could have been hidden in the general scatter. This calibration has a gradient consistent with those obtained by Crawford (1975) and Nissen (1988). The strong correlation was rather surprising since for A-type stars m_1 is not sensitive to metal abundance alone.

This work shows conclusively that for A3 – F0 stars there is a strong correlation of δm_0 with metal abundance, indicating that Am stars are indeed metal-rich objects. The above relationship is based on the solar abundances adopted by Kurucz(1979a). The Anders & Grevesse (1989) solar abundances would give lower values of [M/H]

Table 6.1: *Metal abundances obtained from the JKT spectra*

HR	β	δm_0	δc_0	T_{eff}	$\log g$	Λ	[M/H]
114	2.755	0.023	0.179	7270	3.54	0.567 ± 0.065	−0.059 ± 0.122
984	2.795	0.009	0.076	7650	3.97	0.468 ± 0.078	−0.031 ± 0.136
1331	2.767	0.006	0.072	7400	3.94	0.623 ± 0.059	0.114 ± 0.115
1351	2.767	−0.001	0.057	7410	4.00	0.557 ± 0.066	0.005 ± 0.122
1356	2.813	−0.003	0.064	7820	4.03	0.577 ± 0.064	0.234 ± 0.121
1368	2.756	−0.017	0.026	7320	4.10	0.770 ± 0.044	0.346 ± 0.099
1376	2.783	−0.042	−0.009	7570	4.27	0.862 ± 0.037	0.651 ± 0.095
1380	2.857	−0.007	0.097	8200	3.98	0.301 ± 0.102	−0.044 ± 0.166
1387	2.867	0.000	0.149	8280	3.84	0.249 ± 0.110	−0.093 ± 0.176
1389	2.889	−0.017		9030	4.06	0.188 ± 0.120	0.158 ± 0.193
1403	2.775	−0.017	0.041	7480	4.07	0.650 ± 0.056	0.203 ± 0.111
1408	2.746	0.012	0.027	7230	4.08	0.573 ± 0.065	−0.050 ± 0.120
1412	2.830	0.001	0.183	7960	3.73	0.486 ± 0.075	0.139 ± 0.135
1427	2.856	−0.015	0.082	8190	4.02	0.439 ± 0.082	0.174 ± 0.143
1428	2.809	−0.032	−0.002	7800	4.25	0.713 ± 0.050	0.472 ± 0.107
1444	2.796	−0.005	0.051	7670	4.06	0.564 ± 0.066	0.142 ± 0.123
1458	2.834	0.014	0.113	8000	3.93	0.371 ± 0.091	−0.026 ± 0.152
1473	2.870	0.003	0.137	8310	3.87	0.231 ± 0.113	−0.105 ± 0.180
1480	2.808	−0.028	0.031	7780	4.14	0.653 ± 0.056	0.351 ± 0.113
1519	2.846	−0.048	0.093	8110	3.99	0.656 ± 0.055	0.511 ± 0.113
1620	2.847	0.001	0.167	8110	3.79	0.372 ± 0.091	0.023 ± 0.154
1670	2.796	−0.045	0.031	7670	4.13	0.736 ± 0.048	0.450 ± 0.105
1672	2.823	−0.044	0.023	7920	4.20	0.811 ± 0.041	0.715 ± 0.100
1905	2.809	−0.002	0.052	7780	4.07	0.500 ± 0.074	0.085 ± 0.132
2085	2.720	0.018	0.023	7010	4.15	0.628 ± 0.058	−0.058 ± 0.112
2124	2.852	0.002	0.105	8160	3.96	0.431 ± 0.083	0.145 ± 0.145
3624	2.764	−0.054	0.011	7390	4.17	0.960 ± 0.030	0.765 ± 0.090
4300	2.916	−0.018		9050	4.34	0.374 ± 0.091	0.466 ± 0.158
7001	2.903	−0.002		9550	4.06	−0.395 ± 0.218	−0.462 ± 0.303
7653	2.840	−0.001	0.212	8040	3.67	0.449 ± 0.080	0.113 ± 0.142
8410	2.820	−0.048	0.097	7870	3.94	0.693 ± 0.052	0.463 ± 0.110

by ~0.067 dex. To be consistent with the newer solar abundances the constant in Equation 6.18 would be changed to +0.014.

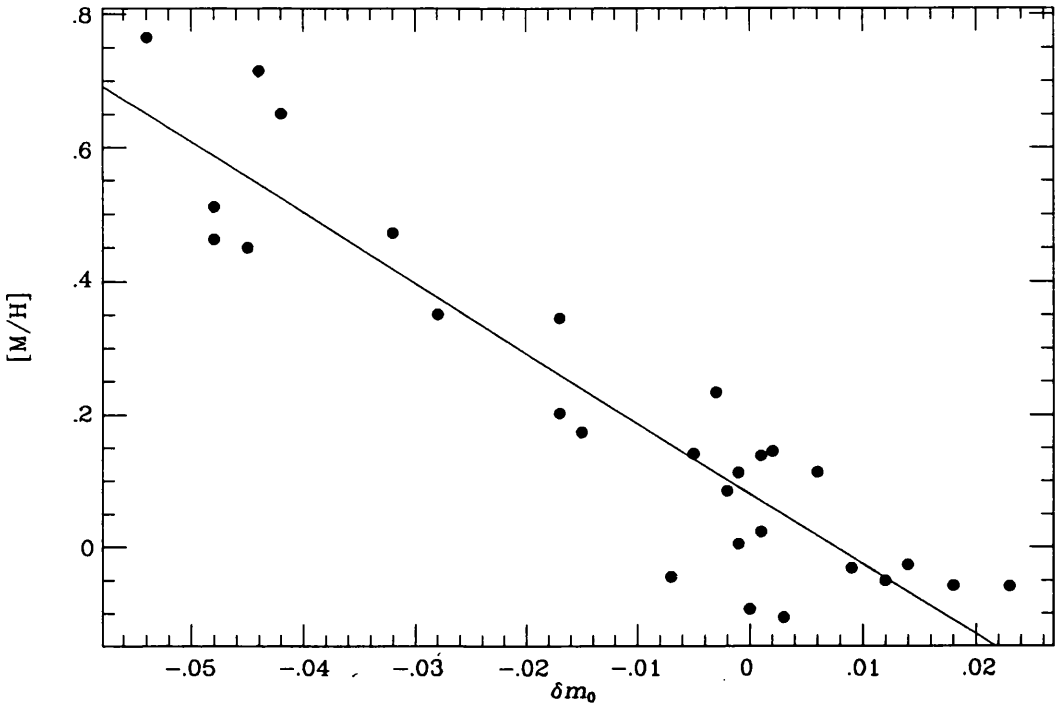

Figure 6.7: *Correlation between [M/H] obtained from the JKT spectra with the Strömgren metallicity index δm_0, for $T_{\rm eff} < 8500$ K. The line is the least-squares fit to the data points.*

6.5 The importance of microturbulence

Microturbulence is a fitting parameter, originally introduced to make abundance results from weak and strong lines agree. The microturbulent velocity ξ_t is added quadratically to the thermal velocity of the lines:

$$v_D^2 = \frac{2kT}{m} + {\xi_t}^2 \tag{6.19}$$

Microturbulence is modelled as a non-thermal movement of individual elements of gas that are small compared to the mean free path of the photon, *i.e.* small compared to the optical depth scale of the photosphere. Those masses of gas moving with different velocities absorb at different Doppler shifts from the line centre and a broadened profile with increased equivalent width results. The flat part of the curve-of-growth will lie above that predicted for the line broadened by thermal motions

only (See Figure 6.8). The increased equivalent width means that if too low a value of microturbulence is used in an abundance determination, the abundance will be overestimated. However, microturbulence remains as a free parameter without a full hydrodynamic explanation.

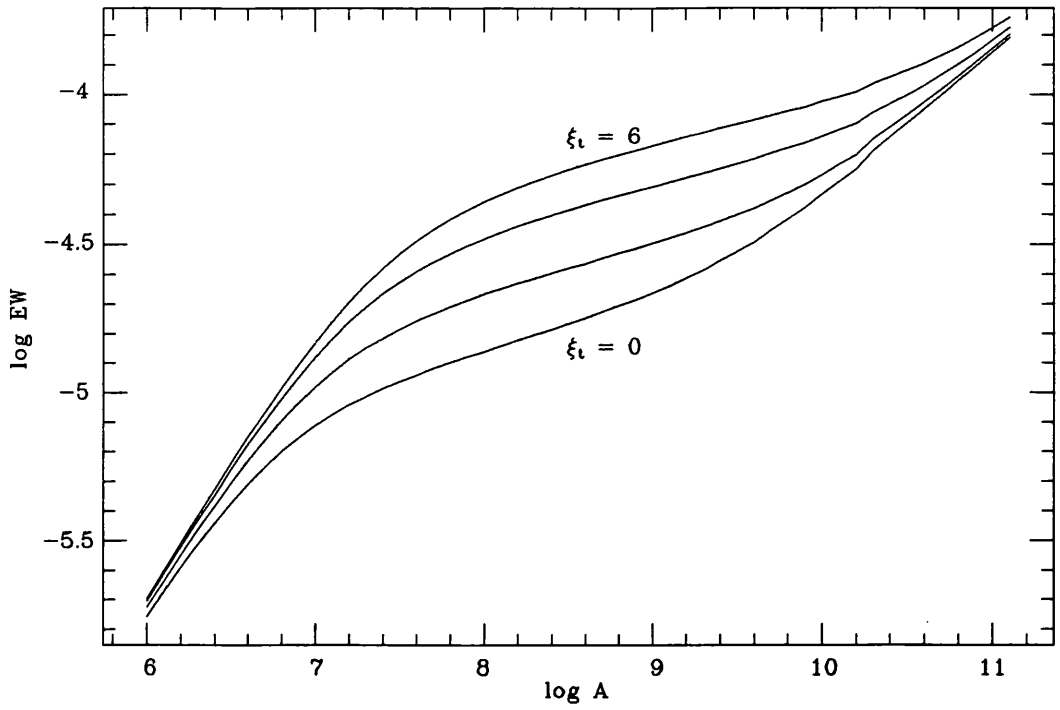

Figure 6.8: *The effect of microturbulence on the curve-of-growth.*

The value of microturbulence is crucial to the accurate determination of metal abundance of A and F stars. So far, all models and syntheses have used a value for the microturbulent velocity ξ_t of 2 km/s and indeed all published UBV, $uvby\beta$ and Geneva calibrations have implicitly assumed that value. Yet, values of 4 – 5 km/s have been obtained by several workers in the analyses of Am stars (Smith, 1973; Takeda, 1984; Guthrie, 1987). It is important to recognize the role of microturbulence since changing it by 0.5 km/s can change the calculated abundances by 0.1 dex, or more.

The variation of microturbulence with spectral type was studied by Chaffee (1970). It was found that the value of ξ_t varied from 2 km/s for $(b-y) = 0$, rose to 4 km/s around $(b-y) = 0.15$, then fell to around 2 km/s again for $(b-y) = 0.30$. For $(b-y) > 0.30$ the value of ξ_t rose, reaching over 4 km/s for $(b-y) = 0.40$. This work was in general agreement with the values of $\xi_t \sim 5$ - 6 km/s found

for Am stars. (Smith, 1971; 1973).

Recent analyses using fully line-blanketed model atmospheres, more accurate $\log gf$ values, and higher-quality spectra have revealed that the value of ξ_t is lower. Nissen (1988) produced a calibration for ξ_t in terms of T_{eff} and $\log g$ for F0 – G2 stars:

$$\xi_t = 3.2 \times 10^{-4}(T_{eff} - 6390) - 1.3(\log g - 4.16) + 1.7 \qquad (6.20)$$

This calibration is valid for $5800 < T_{eff} < 7200$ K, $3.5 < \log g < 4.4$ and $-0.5 <$ [M/H] < 0.2. No significant dependence of ξ_t on [M/H] was found, but the [M/H] range used was rather small. For early A-type stars a values of ξ_t around $1 - 3$ km/s has been obtained (Gigas, 1986; Lemke, 1989). Coupry & Burkhart (1992) found values of around $\xi_t = 2 - 4$ km/s for late A-type stars, including Am stars. They also suggested that microturbulence may be a unique function of T_{eff} along the main sequence.

Kurucz (1975) gave the preliminary results of an investigation into the differential effects of changing the microturbulent velocity on both flux distribution and photometric colours. He found that the effect on flux distributions of changing the microturbulent velocity from 2 to 4 km/s, while keeping the abundance fixed, was very small and only really affected the flux below the Balmer Jump: increasing the microturbulent velocity reduces the flux, as is to be expected.

Kurucz also gave his preliminary results on the effect of abundance and microturbulence changes on *UBV* and *uvby* photometry. He found that the effect of changing microturbulence cannot be photometrically distinguished from abundance changes. The two effects follow the same photometric track. He estimated that, for the main sequence, doubling the microturbulent velocity from 2 to 4 km/s has about the same effect as doubling the abundance, *i.e.* a change of 0.3 dex in log abundance.

Changing the value of microturbulence directly affects the synthesis calculations. Increasing microturbulence in the synthesis increases the equivalent widths of the component lines, this leads to a general increase in the total amount of line-blocking. The Λ-method described above will be affected by such microturbulence changes. A value of $\xi_t = 2$ km/s was assumed in the calculations. Table 6.2 shows the effect of microturbulence on the abundance obtained from the Λ-method. It is clear that if the stellar microturbulence is higher than 2 km/s the Λ-method will overestimate the value of [M/H]. This is especially true for the cooler stars. Alas, due to the low

resolution of the JKT spectra, it was impossible to obtain values of microturbulence from them. Therefore, the value of [M/H] can be regarded as a blanketing parameter which not only reflects abundance variations, but also reflects microturbulence.

Table 6.2: *The effect of microturbulence on the derived value of [M/H] using the Λ-method. All models have* $\log g = 4.0$.

	[M/H]		
T_{eff}	$\xi_t = 0$	$\xi_t = 2$	$\xi_t = 4$
5500	−0.324	−0.011	0.278
6000	−0.265	−0.005	0.236
6500	−0.218	−0.005	0.199
7000	−0.175	0.005	0.181
7500	−0.144	0.008	0.158
8000	−0.123	0.001	0.130
8500	−0.104	0.003	0.123
9000	−0.109	−0.011	0.103
9500	−0.103	−0.007	0.108
10000	−0.093	0.005	0.118

If, as proposed by Coupry & Burkhart (1992), microturbulence is a unique function of T_{eff} then for late-A and F stars a value of 4 km/s would imply an increase in the value of m_0 for model grids. This would be in the correct direction to reduce the discrepancy between model colours and observations (see Figure 2.4).

6.6 Conclusion

The stellar mean metal abundance has been obtained for several A and F stars, including a number of Am stars. The low-resolution JKT spectra were used to obtain values of [M/H] by comparison with synthetic spectra. Using these results it was found that the photometric metallicity indices are very robust stellar [M/H] parameters for late-A and F stars. For star in the range A3 – F0 a very tight linear correlation has been obtained:

$$[\mathrm{M/H}] = -10.56\ \delta m_0 + 0.081 \qquad (6.21)$$

which is valid for metal-rich stars, including classical Am stars. The results are also consistent with those obtained for metal-poor stars and later-type stars.

Interestingly, Luck (1991) reviewed the [Fe/H] ratios for Population II stars. He found that the [Fe/H] determinations have varied significantly in the past, but

with no systematic improvement with time. He concluded that the differences were primarily due to systematically different T_{eff} and $\log g$ determinations and not necessarily the accuracy of the measurements. This is exactly what is found for the A and F stars in the present work.

Chapter 7

Comparison of the various methods

Having obtained the stellar atmospheric parameters from photometry and spectrophotometry, and the effective temperatures from Balmer line profiles, detailed comparisons can now be made between the various methods and calibrations. Many reservations have already been raised; but as yet no inter-comparisons have been made. In this chapter the comparisons will be performed and the systematic differences between the various methods evaluated.

The initial reason for this work was to resolve the discrepancies between the works of Lane & Lester (1984) and Moon & Dworetsky (1985). This was extended into a study of the broader aspects of the methods of determining the atmospheric parameters of normal A and F stars, as well as Am stars.

7.1 Comparison of the results of Lane & Lester and Moon & Dworetsky

As explained in Chapter 3 it was the work of Lane & Lester (1984) which gave rise to the controversy concerning the $T_{\rm eff}$, $\log g$ and [M/H] of Am stars. Lane & Lester (LL) fitted model atmosphere flux distributions to the optical and ultraviolet spectrophotometry of Am stars. Their results were systematically lower than those previously obtained using photometry. They argued that the earlier results were too high due to the use of unblanketed model atmosphere calculations. However, Moon & Dworetsky (MD) presented empirically-calibrated $uvby\beta$ photometry grids. These

were based on the line-blanketed models of Kurucz (1979a). Such models match the observed fluxes of stars much better than the earlier unblanketed models. The MD grids gave values of T_{eff} and $\log g$ that were in agreement with earlier results. The LL results remained discrepant and a controversy arose. This controversy was investigated.

As well as for the JKT programme stars, optical spectrophotometry for other A and F stars was taken from Breger (1976b), ultraviolet fluxes from the S2/68 database and *uvbyβ* photometry from the catalogue of Hauck & Mermilliod (1980). Solar-abundance spectrophotometric fits were made using the procedure described in Chapter 3 to reproduce the LL results for a much larger number of stars. The codes of Moon (1985) were again used to obtain dereddened *uvbyβ* colours and to obtain fits to the MD grids.

The differences between the spectrophotometric fits and the results from the MD grids were examined. Figures 7.1 and 7.2 show that, for stars cooler than 8500 K, there is a clear systematic trend with δm_0. The fits give lower values of T_{eff} and $\log g$ for stars with large negative δm_0 values. The δm_0 index is known to be strongly correlated with metal abundance (See Chapter 6) and a negative δm_0 indicates a metal-rich star with [M/H] > 0. Hence the observed trends with δm_0 are very likely to be trends with stellar metal abundance. In Chapter 3 it was shown that fitting a solar-abundance model to a metal-rich star yields systematically too low a T_{eff} and $\log g$ (See Figure 3.5). Spectrophotometric fits using models with a composition of [M/H] $= +0.5$ yield higher temperatures and gravities. The open circles in the two figures are the differences obtained when such models are used. The trend of difference with δm_0 is significantly reduced. Therefore, it appears that the problem lies with the spectrophotometric fits and not the *uvbyβ* photometry. This seems to cast doubt on the Lane & Lester results and to validate the calibration of Moon & Dworetsky.

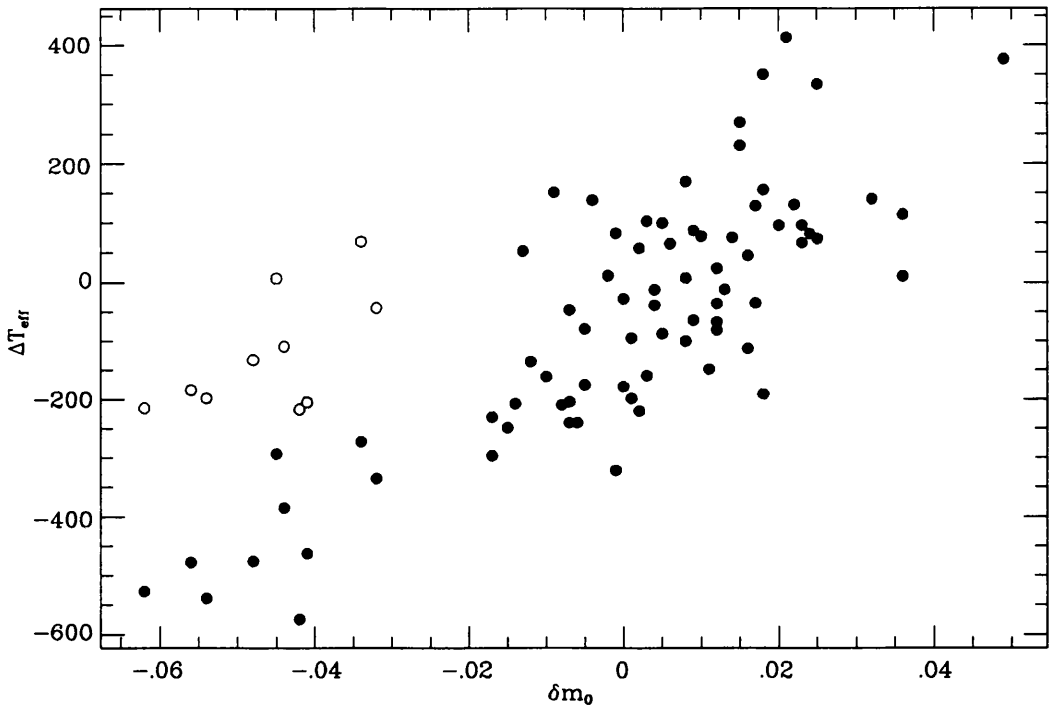

Figure 7.1: *Plot of* $\Delta T_{\rm eff} = T_{\rm eff}(fit) - T_{\rm eff}(MD)$ *against* δm_0 *for stars cooler than 8500 K. The open circles indicate the results obtained using [M/H] = +0.5 models.*

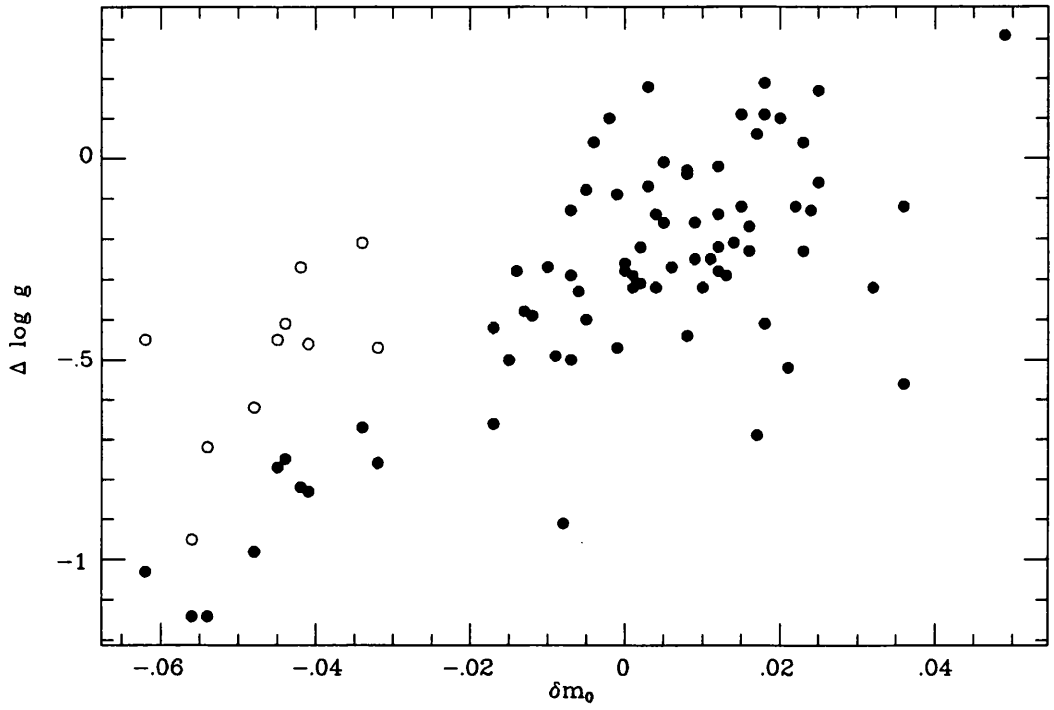

Figure 7.2: *Plot of* $\Delta \log g = \log g(fit) - \log g(MD)$ *against* δm_0 *for stars cooler than 8500 K. The open circles indicate the results obtained using [M/H] = +0.5 models.*

7.2 The flux excess at 4785Å

Lester (1987), in defending the Lane & Lester results, found evidence for an excess of observed flux at 4785Å for Am stars compared to that predicted by model atmospheres and that observed in normal stars. The value of the flux excess is defined in terms of a difference in observed and model magnitudes:

$$\Delta m = m_{\rm obs} - m_{\rm model} \tag{7.1}$$

where $m_{\rm obs}$ is the observed magnitude at 4785Å and $m_{\rm model}$ is the predicted magnitude from a solar-composition model atmosphere. Both the observations and the models are normalized to 5556Å.

Lester assumed that the spectral region around 4785Å was the only source of the flux excess. He argued that since the excess will be contained in the Strömgren b filter, the observed b-magnitude would be smaller (brighter) than the expected model value by an amount Δb. Hence, atmospheric parameters for Am stars obtained from *uvby* would be erroneous due to this excess. Also, since the excess is included in the wide filter of the β index, this will cause the value of β for Am stars to be larger by an amount $\Delta\beta$. The effects of this excess on the *uvbyβ* indices would be as follows:

$$\begin{aligned} (b-y) &\Longrightarrow (b-y)+\Delta b \\ m_1 &\Longrightarrow m_1 - 2\Delta b \\ c_1 &\Longrightarrow c_1 + \Delta b \\ \beta &\Longrightarrow \beta - \Delta\beta \end{aligned}$$

where Δb and $\Delta\beta$ take the same sign as the value of Δm, *i.e.* negative.

The consequences of these changes on the $T_{\rm eff}$, $\log g$ and [M/H] obtained from the photometry is that they would <u>all</u> be overestimated. Hence, Lester concluded that this excess makes Am stars appear to be hotter and more metal-rich that they ought to be. The MD $T_{\rm eff}$ is based on the β index, which may well be affected by this excess. But, the effects ought to be smaller since the excess lies in the wing of the β filter.

Lester's sample of stars was rather small and biased towards Am stars. To rectify this, the large dataset described in Section 7.1 was used to obtain values of Δm. Figure 7.3 shows a clear systematic trend of flux excess with the difference ($\Delta T_{\rm eff}$) between spectrophotometric and MD $T_{\rm eff}$ values. The flux excess increases as the

spectrophotometric fits get progressively cooler than the photometry values. The Am stars ($\delta m_0 < -0.02$) form a group with large ΔT_{eff} and $\Delta m < -0.05$.

There is a lot of scatter, but the relationship appears very similar to Figure 7.1 and possibly deviates from a linear relationship. A linear relationship between ΔT_{eff} and Δm would be expected if the excess is the sole cause of the differences, since increasing Δm would increase Δb by the same relative amount and this would have a linear effect on T_{eff} obtained from $(b-y)$ or β. The possible deviation from linearity indicates that flux excess may not directly affect the T_{eff} obtained from *uvbyβ* photometry. There may be another reason for the excess and the differences between the methods.

Burkhart & Coupry (1989) pointed out that the Geneva $(B_2 - V_1)$ colour should not be affected by the excess. The B_2 filter lies nearly outside the region of the excess flux. There is a tight correlation between $(b-y)_0$ and $(B_2 - V_1)$ with no sign of a metallicity effect. This indicates that the excess ought not have any effect on the *uvbyβ* colours.

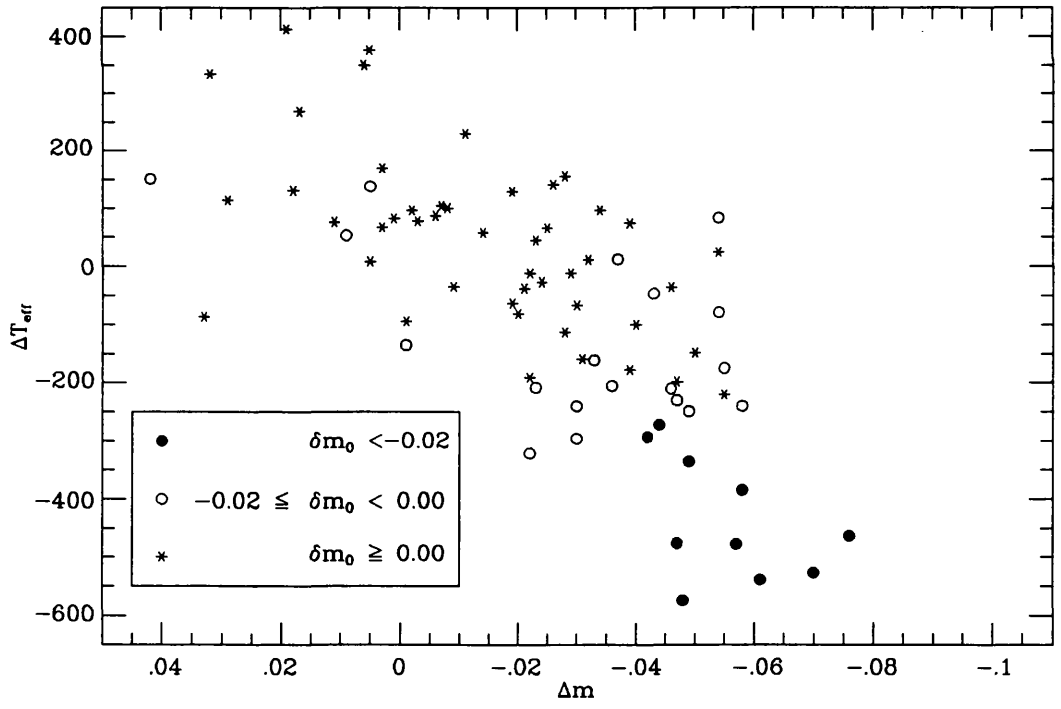

Figure 7.3: *Plot of Δm against ΔT_{eff} of Figure 7.1.*

A plot of Δm against spectrophotometric T_{eff} appears to show a peak in excess around 7000 – 7500 K (see Figure 7.4). Note, however, that Am stars dominate this region, so a selection effect could be responsible for this apparent peak. There is

a lot of scatter, but the peak may be real. If the possibility of a selection effect is ignored, it can be concluded that the excess is a T_{eff} effect rather than a δm_0 effect. However, metal abundance must not be completely ignored since spectrophotometric T_{eff} values are significantly affected by changes in [M/H]. Hence, it was concluded that the excess is a function of both T_{eff} and δm_0, although the two effects may be closely related.

Values of Δm were also calculated using solar-abundance models with the T_{eff} and $\log g$ given by the Moon & Dworetsky grids, denoted by Δm(MD) to distinguish it from the spectrophotometric value of Δm. Interestingly, the trend with δm_0 disappears indicating that part of the Δm must be due to the selection of T_{eff} and $\log g$. Additionally, plotting Δm(MD) against T_{eff} (Figure 7.5) shows no sign of a peak. The variation with T_{eff} is now fairly smooth with much less scatter than in Figure 7.4. An average value of Δm(MD) appears to be approximately -0.03 mag for stars in the range $6500 < T_{eff} < 8000$ K. Only for the cooler stars does the value of Δm(MD) decrease.

Figure 7.6 shows the flux excess as a function of $\Delta\log g$. The majority of stars appear to have a $\Delta\log g$ of ~ 0.3 dex, which is independent of Δm. The Am stars, however, tend to have larger $\Delta\log g$, with the spectrophotometric $\log g$ much lower than the $uvby\beta$ value. However, $\Delta\log g$ is clearly correlated with δm_0 (Figure 7.2), indicating that the majority of the difference is due to metallicity effects and not Δm.

These results indicate that the excess is mainly a T_{eff} effect with a secondary component due to metallicity effects. Lester (1987) suggested that the excess was possibly caused by an iron-group line strength anomaly. He stated that an explanation of the excess must await a detailed analysis of the spectral region in question. This is what was done during the JKT observing run.

7.2.1 Observations of the flux excess region

During the JKT observing run, many spectra were obtained of the region centred upon 4700Å. These spectra show <u>no</u> obvious sign of any flux excess anywhere near 4785Å. The Am stars have the same continuum shape as the normal A stars. The spectra looked normal and there was no apparent change to the amount of line-blanketing in the region.

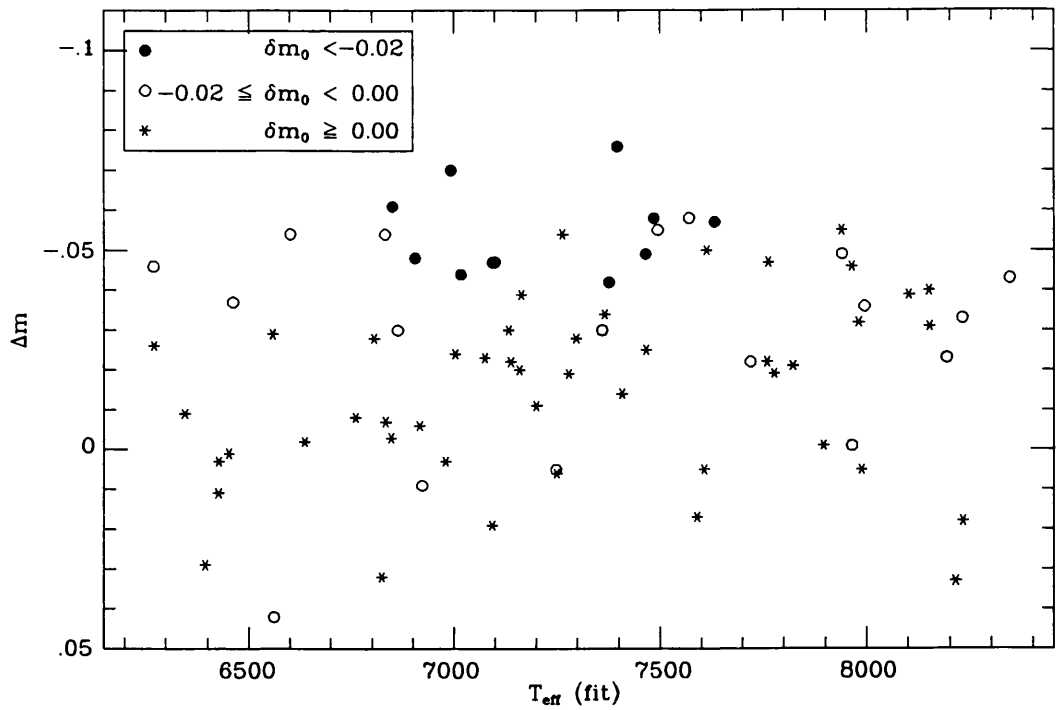

Figure 7.4: *Plot of Δm against spectrophotometric $T_{\rm eff}$*

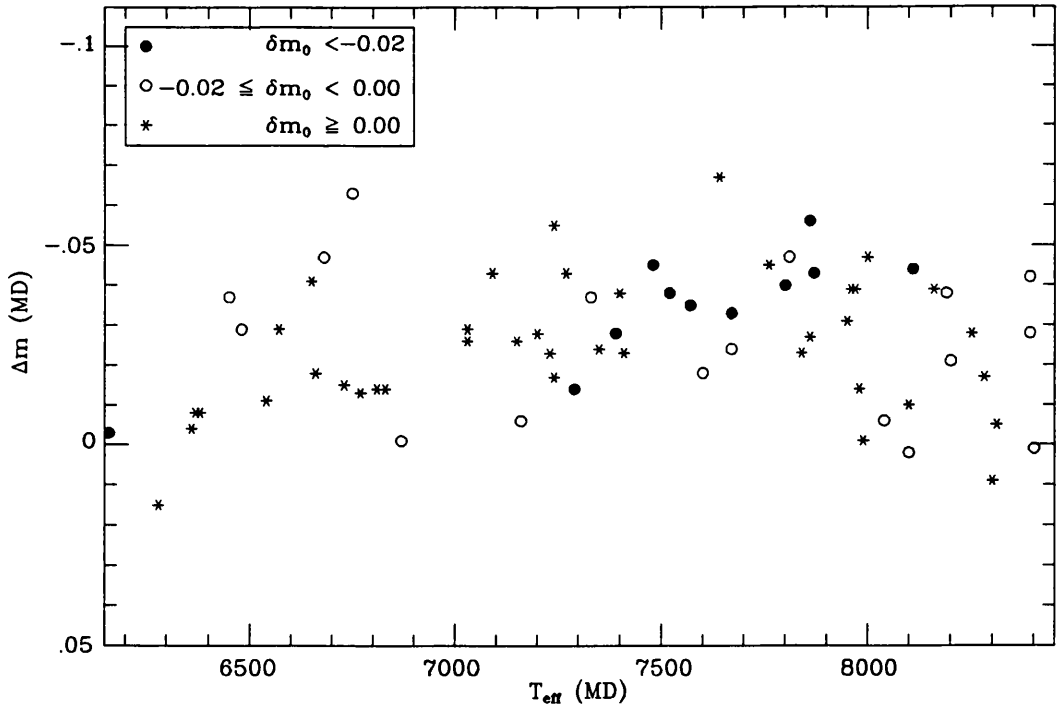

Figure 7.5: *Plot of Δm against Moon & Dworetsky (1985) $T_{\rm eff}$.*

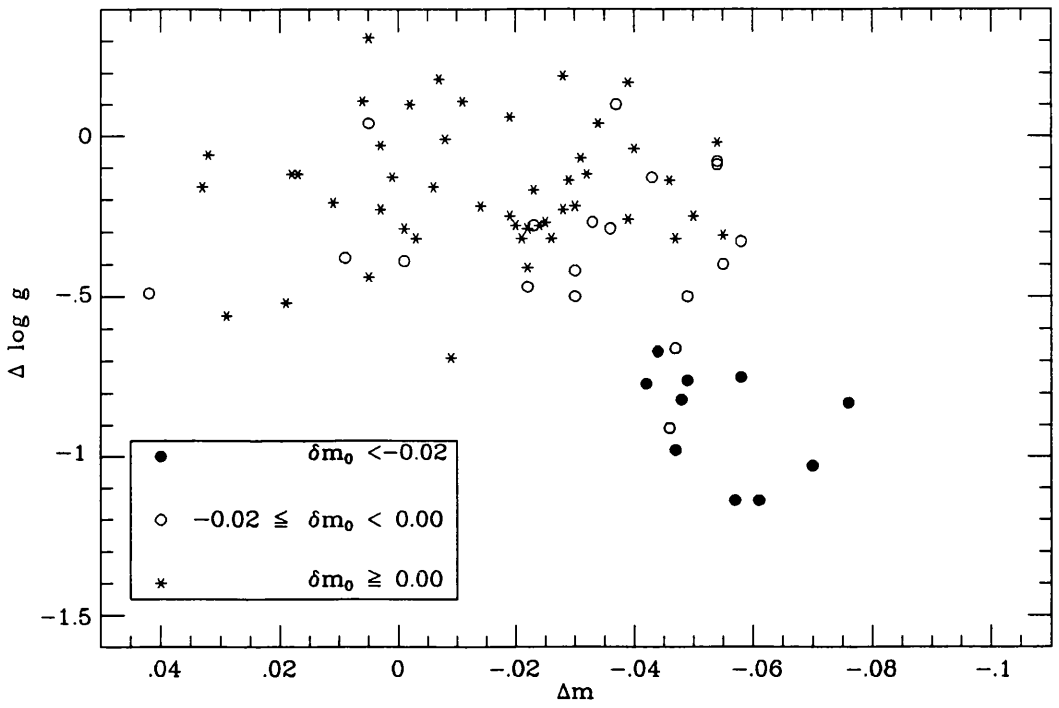

Figure 7.6: *Plot of* Δm *against* $\Delta \log g$.

7.2.2 Identification of the cause of the flux excess

In the course of investigations with synthetic spectra, a curious line strength anomaly was observed. The synthetic spectra contained two groups of lines around 4740 Å and 4790 Å which were not present in the observed spectrum of Vega (See Figure 7.7). These two groups of lines were identified as the following C I multiplets:

$$2p^3\ {}^3\mathrm{D}^\mathrm{o} - 5p\ {}^3\mathrm{P}$$

$$2p^3\ {}^3\mathrm{D}^\mathrm{o} - 5p\ {}^3\mathrm{D}$$

The very strong features cannot be due to an abundance error because the $[C/H]$ abundance of -0.5 used in the synthesis agrees with that obtained by Adelman & Gulliver (1990). Since these lines are too strong in the synthesis and because other C I lines appear to be the correct strength, it was concluded that the $\log gf$ values for the lines of these two multiplets in the Kurucz & Peytremann (1975) (KP) line list must be seriously wrong.

Oscillator strengths for C I have been calculated as part of the Opacity Project (Seaton, 1987; Berrington *et al.*, 1987). Multiplet gf values for C I lines in the $4600 \sim 4800$ Å range were obtained from Paul Crowther (priv. comm.). The relative

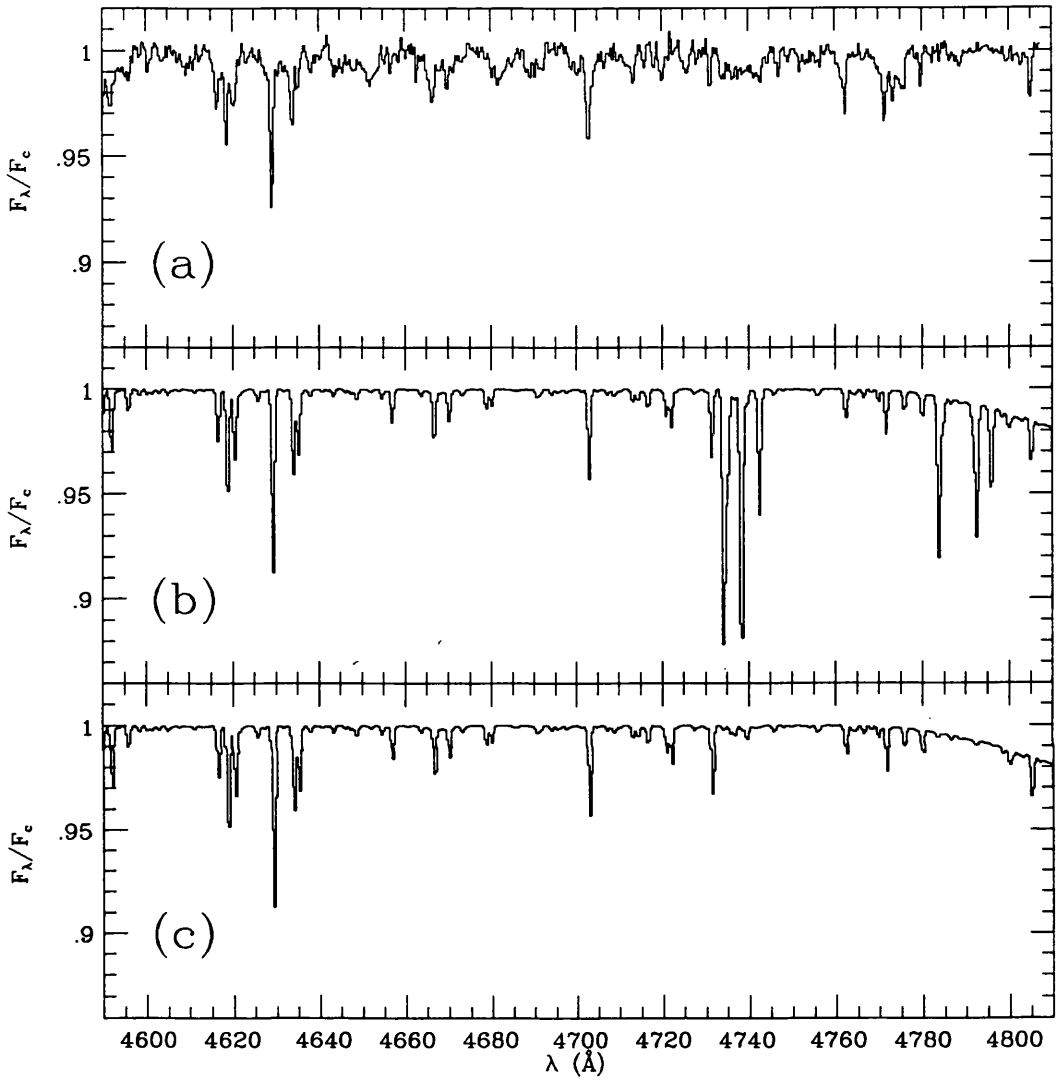

Figure 7.7: *Comparison between the observed spectrum of Vega (a) and the corresponding synthetic spectra (9500, 4, −0.5) using the Kurucz & Peytremann (1975) C I* $\log gf$ *values (b) and the Opacity Project C I* $\log gf$ *values (c). Clearly, the Kurucz & Peytremann C I* $\log gf$ *values produce far too strong C I lines around 4740 Å and 4790 Å. The curvature on the right-hand side of the synthetic spectra is caused by the wing of the Hβ line, which has been normalized out of the Vega spectrum.*

strengths were calculated using *LS* coupling (Allen, 1973, p.61). The individual $\log gf$ values are given in Table 7.1. The two anomalous multiplets have $\log gf$ values in KP that are over 2 dex larger than the Opacity Project values. The KP values are severely wrong for these lines. Interestingly, one of these multiplets lies around 4785Å, which is the wavelength region of the flux excess.

Table 7.1: *Line oscillator strengths of C I multiplets.*

Multiplet (Number)	λ (Å)	EP Low	log gf values KP	OP	WSG
$2p^3\ ^3D^o - 5p\ ^3P$	4734.260	7.9458	−0.09	−2.36	
(18.05)	4734.917	7.9462	−2.10	−4.28	
	4735.163	7.9463	−0.89	−3.11	
	4738.213	7.9462	−0.87	−3.11	
	4738.459	7.9463	−0.36	−2.63	
	4742.561	7.9462	−0.72	−2.98	
$3s\ ^3P^o - 4p\ ^3P$	4762.313	7.4805	−2.21	−2.58	−2.28
(6)	4762.532	7.4828	−2.04	−2.48	−2.20
	4766.673	7.4828	−2.38	−2.70	−2.40
	4770.027	7.4828	−2.16	−2.58	−2.28
	4771.741	7.4879	−1.56	−2.01	−1.70
	4775.898	7.4879	−1.97	−2.48	−2.20
$2p^3\ ^3D^o - 5p\ ^3D$	4783.799	7.9458	−0.56	−3.40	
(18.04)	4784.721	7.9463	−1.47	−4.30	
	4791.735	7.9458	−1.58	−4.30	
	4792.407	7.9462	−1.47	−4.32	
	4792.660	7.9463	−0.79	−3.65	
	4795.859	7.9462	−1.02	−3.84	
	4796.112	7.9463	−1.60	−4.32	
$3s\ ^3P^o - 4p\ ^3S$	4812.921	7.4805	−2.69	−3.87	−2.99
(5)	4817.373	7.4828	−2.34	−3.39	−2.53
	4826.796	7.4879	−2.50	−3.17	−2.31

Multiplet and number are from Moore (1970); KP = Kurucz & Peytremann (1975), OP = Opacity Project, WSG = Wiese, Smith & Glennon (1966).

The Kurucz (1979 a,b) model flux distributions are based on opacity distribution functions calculated using the KP line list, which contains the anomalous C I oscillator strengths. The Kurucz fluxes are integrated over a bandpass of 25Å, so the relative contribution to the total line-blanketing by these anomalous lines over such a small bandpass will be significant. This will lead to a depression in the model flux at that point.

The model flux point nearest to 4785Å is 4787Å. The relative effect of the C I opacity was determined by calculating two sets of synthetic spectra, one with the

KP $\log gf$ values for C I and the other with the new Opacity Project values. The ratio of the integrated fluxes for the two synthetic spectra gives the flux excess due to the C I anomaly:

$$\Delta m(\text{C I}) = -2.5 \log \left(\frac{F_{\text{new}}}{F_{\text{old}}} \right) \tag{7.2}$$

where F_{old} is the flux calculated using the KP line list and F_{new} is the flux obtained after correcting the anomalous C I $\log gf$ values. Table 7.2 shows that at 7500 K an excess of almost 0.03 mag is generated just by the anomalous C I multiplet. Hence, the mean value of Δm, at least, is due to a depression in the model flux-level, and *not* due to any enhancement in the observed stellar fluxes. Figure 7.8 shows the predicted Δm values compared to the observed values using the Moon & Dworetsky T_{eff} and $\log g$ values. The solid line fits the observations very well.

Table 7.2: *Values of Δm obtained from C I lines. Based on synthetic spectra with $\log g$ = 4.0 and [M/H] = 0.0.*

	T_{eff}						
$\log g$	5500	6000	6500	7000	7500	8000	8500
3.5	−0.013	−0.018	−0.023	−0.027	−0.029	−0.029	−0.026
4.0	−0.010	−0.015	−0.020	−0.025	−0.027	−0.028	−0.027
4.5	−0.008	−0.013	−0.017	−0.022	−0.025	−0.026	−0.027

The metallicity dependent component to the excess is due to the fitting of a solar-composition model flux distribution to a non-solar-composition stellar flux distribution. This is shown in Table 7.3. Solar-composition flux distributions have been fitted to [M/H] = +0.5 synthetic spectrophotometric 'observations'. These 'observations' were binned onto the wavelength points typical of S2/68 and Breger (1976b). Clearly, the δm_0-dependent component to the flux excess was caused by the fitting of solar-composition fluxes to spectrophotometry from metal-rich atmospheres.

A combination of the two components to the flux excess can, therefore, explain the phenomenon found by Lester (1987). The flux excess is an artefact caused by the combined effects of anomalous model opacity and inappropriate use of spectrophotometry to derive T_{eff} and $\log g$.

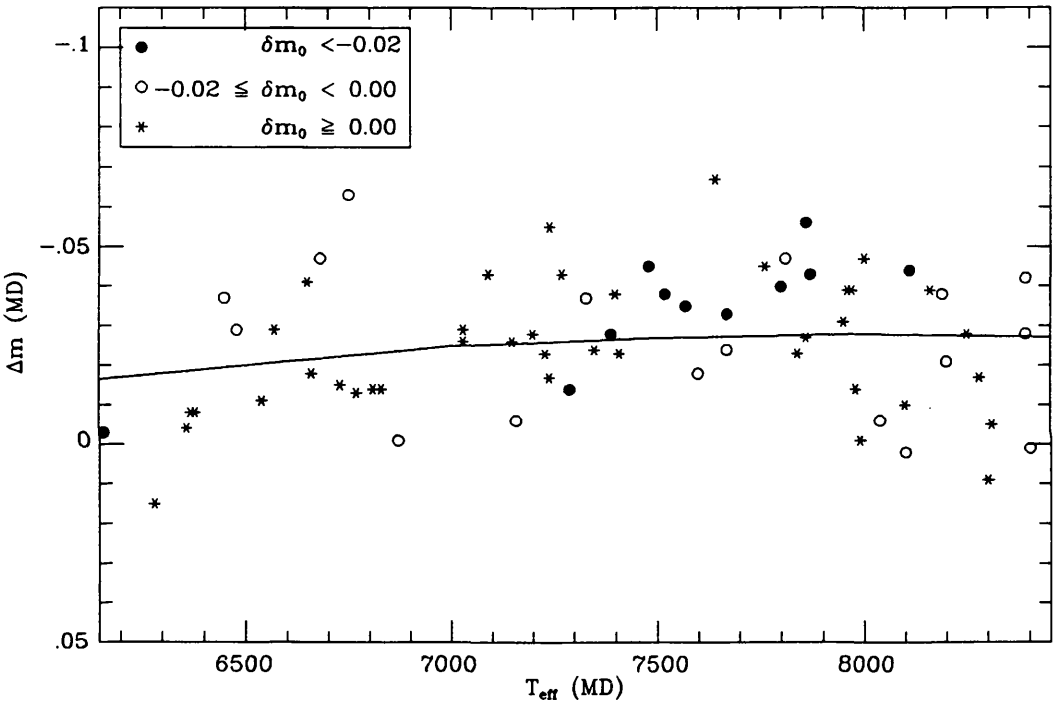

Figure 7.8: *The variation of theoretical Δm values with $T_{\rm eff}$. The line shows the value of Δm predicted from the C I line strength anomaly. There is a good fit to the observed Δm values, based on the Moon & Dworetsky (1985) $T_{\rm eff}$ values.*

Table 7.3: *Values of Δm obtained from fitting [M/H] = 0.0 models to [M/H] = +0.5 synthetic spectrophotometric 'observations'. The $T_{\rm eff}$ is that of the [M/H] = +0.5 'observations'. The values of Δm are those obtained when [M/H] = 0.0 models are fitted to these 'observations'.*

	$T_{\rm eff}$						
$\log g$	5500	6000	6500	7000	7500	8000	8500
3.5	−0.045	−0.035	−0.031	−0.021	−0.013	−0.004	−0.001
4.0	−0.059	−0.039	−0.032	−0.023	−0.013	−0.008	+0.000
4.5	−0.073	−0.046	−0.034	−0.025	−0.015	−0.008	+0.001

7.2.3 Conclusion

The flux excess at 4785Å has been shown to have been caused by an error in the model flux level. The anomalously strong C I lines in the Kurucz & Peytremann (1975) line list gave rise to a mean value of Δm = -0.03, for late-A and F stars. Larger values of flux excess have been shown to be caused by fitting a solar-composition model flux distribution to fluxes of metal-rich stars. The correlations of Δm with $\Delta T_{\rm eff}$ and $\Delta \log g$ have been shown to be caused by metallicity effects on the spectrophotometry and not by an effect on the *uvbyβ* photometry. Therefore, Lester's explanation of the differences between Lane & Lester (1984) and Moon & Dworetsky (1985) is not correct.

7.3 Comparison with the $T_{\rm eff}$ obtained from Balmer line profiles

Having shown that the apparent flux excess is an artefact with no effect on *uvbyβ* photometry, an independent measure of $T_{\rm eff}$ was needed to resolve the discrepancy with spectrophotometry. The Balmer lines provide such an independent $T_{\rm eff}$ diagnostic for late-A and F stars. Using the solar-abundance Balmer line results and the solar-abundance spectrophotometric results a comparison with Moon & Dworetsky was performed.

Figure 7.9 shows the correlation between MD and Hβ results; there is a broad agreement. Figure 7.10 shows the correlation between spectrophotometric $T_{\rm eff}$ and Hβ $T_{\rm eff}$; it is immediately obvious that the Am stars ($\delta m_0 < -0.02$) have a spec-

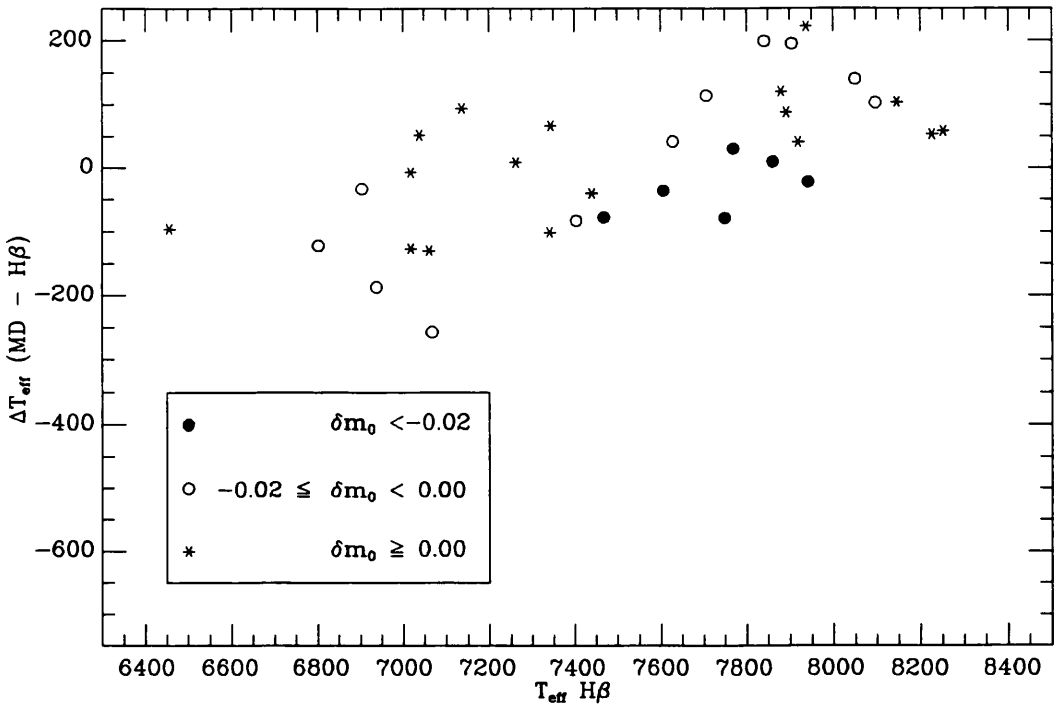

Figure 7.9: *Comparison between the $T_{\rm eff}$ obtained from Hβ profiles and the Moon & Dworetsky (1985) grids.*

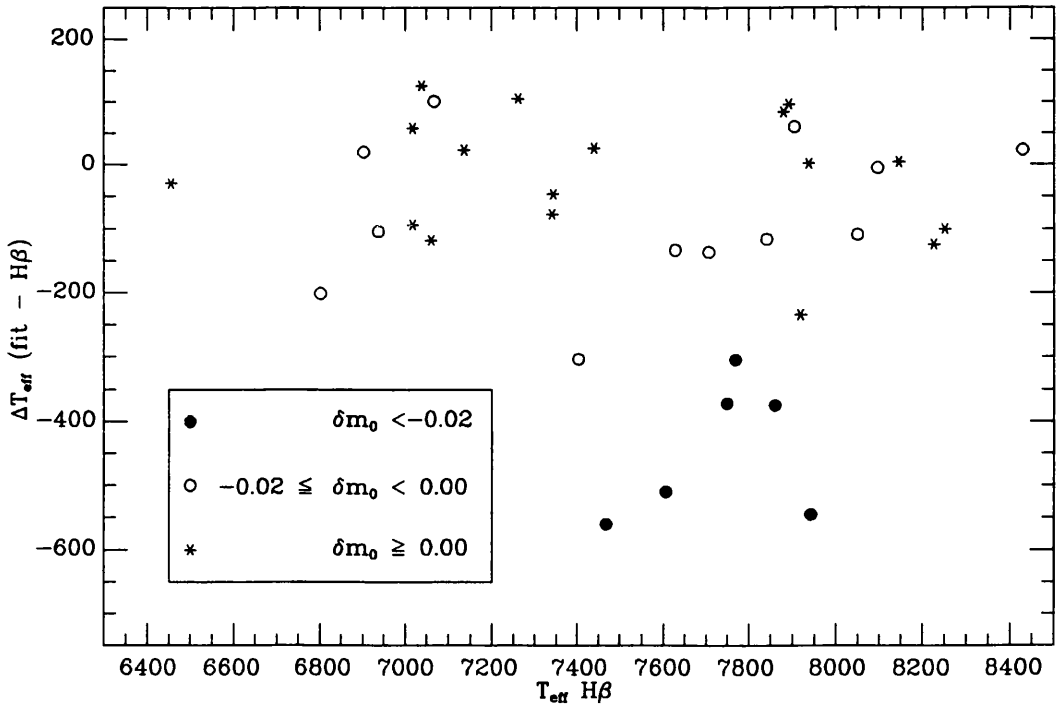

Figure 7.10: *Comparison between the $T_{\rm eff}$ obtained from the Hβ profiles and spectrophotometric flux fitting.*

trophotometric T_{eff} much cooler than the Balmer line value. The stars with $\delta m_0 < -0.02$ have been shown to be genuinely metal-rich in Chapter 6. Enhanced abundance models are required to fit these stars. The use of [M/H] = +0.5 models significantly reduces the discrepancy between spectrophotometry and Balmer lines. The Balmer lines are relatively insensitive to metal abundance and thus provide an excellent T_{eff} diagnostic for these stars (Chapter 5). Therefore, the hydrogen-line profiles have shown that the calibration of Moon & Dworetsky gives reliable temperatures and that the results of Lane & Lester seriously underestimated the temperatures of metal-rich Am stars.

7.4 T_{eff} - log g relationship from mass and luminosity

From their fundamental definitions it is possible to obtain a relationship between T_{eff} and $\log g$ in terms of mass and luminosity. By combining Equations 1.1 and 1.2 the stellar radius cancels:

$$\log g = \log\left(\frac{M}{M_\odot}\right) - \log\left(\frac{L}{L_\odot}\right) + 4\log T_{eff} - 10.607 \qquad (7.3)$$

Knowing mass and luminosity allows a relationship between T_{eff} and $\log g$ to be established. The T_{eff} and $\log g$ of the star will lie somewhere on that line.

Luminosity can be obtained directly from the absolute bolometric magnitude:

$$M_{bol} = 4.69 - 2.5\log\left(\frac{L}{L_\odot}\right). \qquad (7.4)$$

The value of M_{bol} can be obtained from the apparent bolometric magnitude, provided the distance and reddening are known. The apparent bolometric magnitude can be obtained from total integrated flux (F_E):

$$M_{bol} = -2.5\log F_E - 11.514 + 5 + 5\log\pi - A_V \qquad (7.5)$$

where π is the parallax and A_V the absorption due to interstellar reddening. For the majority of the JKT programme stars the interstellar reddening is negligible since they are closer than 100 pc (see Table 2.4). If no value of F_E is available directly then an estimate can be made from:

$$\log_{10} F_E = -0.4(V + BC + 11.514) \qquad (7.6)$$

where BC, the bolometric correction, for A and F stars can be estimated from a fit to the values given by Popper (1980):

$$BC = -3.104 + 9.328 \times 10^{-4}\mathrm{T_{eff}} - 8.245 \times 10^{-8}\mathrm{T_{eff}^2} + 1.768 \times 10^{-12}\mathrm{T_{eff}^3} \quad (7.7)$$

Substituting for M_{bol} we get:

$$\log g = \log\left(\frac{M}{M_\odot}\right) + 0.4\ M_{\mathrm{bol}} + 4\log \mathrm{T_{eff}} - 12.483 \quad (7.8)$$

The stellar mass cannot be obtained directly. However, it is an empirical law that mass and luminosity are related. For main-sequence stars the mass-luminosity relation can be used (Smith, R.C., 1983, *Observatory*, **103**, 29; Andersen, J., 1991, *Astr. Astrophys. Rev.*, **3**, 91):

$$\log\left(\frac{L}{L_\odot}\right) \simeq 4.0 \log\left(\frac{M}{M_\odot}\right). \quad (7.9)$$

Thus assuming that the mass-luminosity relation is the same for both Am and normal A and F stars we get:

$$\log g = 0.3\ M_{\mathrm{bol}} + 4\log \mathrm{T_{eff}} - 12.014 \quad (7.10)$$

This sort of relationship between $\mathrm{T_{eff}}$ and $\log g$ was used by Hundt (1972) and Cayrel, Burkhart & Van't Veer (1991) in their discussions of 63 Tau. Further use of this relationship will be made in Chapter 8.

For evolved stars the luminosity will be higher for a given mass. Hence, the value of $\log g$ will be lower. The mass-luminosity relationship discussed above will give too large a value for $\log g$ and hence is effectively an upper-limit.

7.4.1 Comparison with $\log g$ values obtained from photometry and spectrophotometry

The values of $\log g$ obtained using the mass-luminosity relationship were compared to those obtained from spectrophotometric fits and the Moon & Dworetsky grid. The Hyades stars contained in the JKT programme were selected for this comparison, because they are essentially main-sequence objects with very well-determined distances. The field stars were not used since their distances were generally less well known. Figure 7.11 shows the deviations from the mass-luminosity $\log g$ values of the values obtained from spectrophotometric flux fitting and the Moon & Dworetsky (1985) $uvby\beta$ calibration. The MD $\log g$ values are very close to the

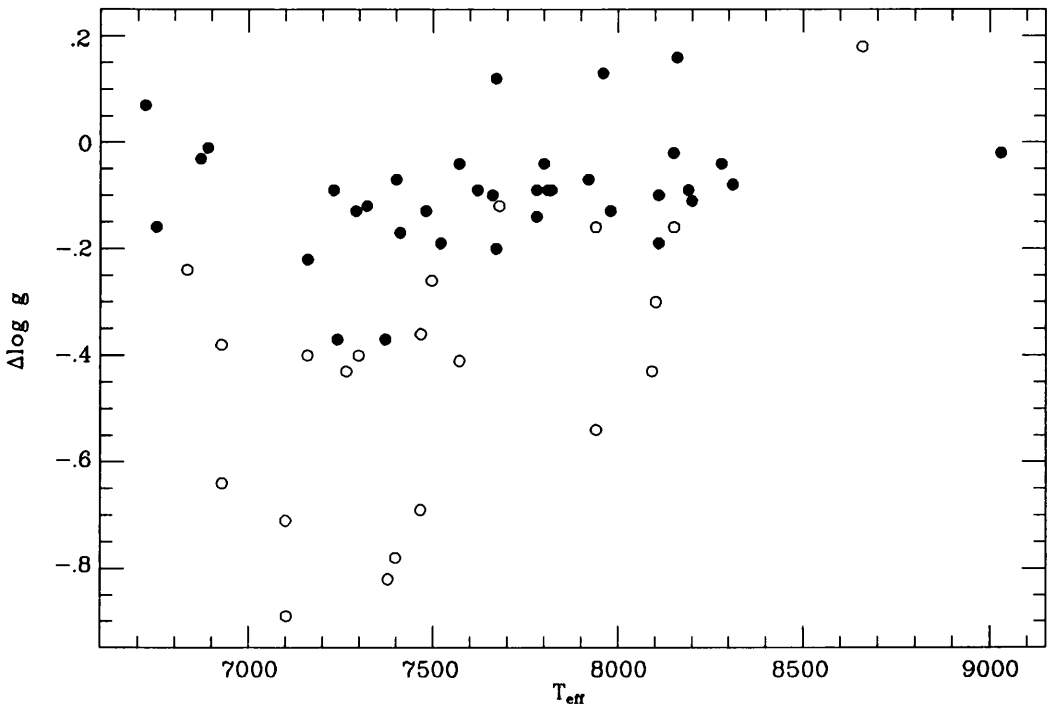

Figure 7.11: *Comparison with* $\log g$ *obtained from the mass-luminosity relationship. Values of* $\Delta\log g = \log g(calib) - \log g(M - L)$ *for the Hyades stars. The circles are the spectrophotometric values and the dots those from the Moon & Dworetsky calibration. The Moon & Dworetsky values are in good agreement with the mass-luminosity values.*

mass-luminosity values, with a systematic difference of $0.1 \sim 0.2$ dex visible. The $\log g$ values obtained from spectrophotometric fits, however, are wildly discrepant.

The use of the mass-luminosity relationship to obtain estimates of $\log g$ has revealed that the photometric $\log g$ values are considerably more reliable than that obtained by spectrophotometric fits. This confirms the result that the $\log g$ values obtained by Lane & Lester (1984) for Am stars are too low. The Am stars in the Hyades are essentially main-sequence objects and not evolved as the Lane & Lester results would indicate.

7.5 Conclusion

The systematic differences between the results of Lane & Lester and Moon & Dworetsky have been resolved. The atmospheric parameters obtained by Lane & Lester are too low for metal-rich Am stars. Their spectrophotometric fits did not adequately

account for the effects of line-blanketing in these metal-rich stars. The adequate allowance for metal abundance gives spectrophotometric atmospheric parameters that are in better agreement with the photometric values of Moon & Dworetsky. The use of hydrogen-line profiles confirmed the T_{eff} values obtained by Moon & Dworetsky.

Strömgren-Crawford *uvbyβ* photometry is not adversely affected by a flux excess at 4785Å. The proposed flux excess, suggested by Lester (1987), has been shown to be an artefact caused by anomalously strong C I lines appearing in the model fluxes. The systematic trend of flux excess with the difference between the results of Lane & Lester and Moon & Dworetsky was caused by the incorrect results of Lane & Lester.

The use of photometry as accurate estimators of T_{eff}, $\log g$ and [M/H] has been confirmed. Nevertheless, further work need to be performed on the calibration of photometry and this will be discussed in Chapter 9.

Please note that pp. 132-135 have been revised. The changes have a slight effect on the temperature-gravity diagrams given in Appendix D. However, the effect is so small as to be hardly noticeable.

Chapter 8

The atmospheric parameters of A and F stars

8.1 Introduction

The critically evaluated methods for determining the T_{eff}, $\log g$ and [M/H] for A and F stars can be used to determine the best values for the JKT programme stars. However, several of these stars are known to be double, a few are even triple or multiple systems, and many of the stars warrant special discussion. It was felt that all the stars should be discussed individually for the sake of completeness.

All the JKT programme stars were examined for evidence concerning companions. Allowances were then made for the effects of the companions in the determination of T_{eff} and $\log g$. These allowances are discussed together with methods of detecting companion stars and estimating their atmospheric parameters. The final adopted atmospheric parameters of the JKT programme stars are presented along with values of $\log L$, $\log R$ and M. An observational HR diagram is given for those stars with reliable distance determinations.

8.2 The detection of cool companion stars

The presence of cool companions can have a significant effect on the apparent flux distribution of a star. Hence, it is vital to know whether or not a star is a binary prior to a detailed analysis. In this section the methods for detecting and estimating the mass, luminosity, etc. of cool companions are outlined.

The most common case is that of a single-lined spectroscopic binary in which the orbital elements are known from radial velocity variations alone. The relevant elements are: P the orbital period in days, K the semi-amplitude of radial velocity variations in km/s, e the orbital eccentricity, i the orbital inclination (i=90° for an eclipsing system), $a \sin i$ the projected semi-major axis of the primary in km, and $f(m)$ the mass function of the system given in solar masses. The mass function is of specific use in the present analysis and is defined:

$$f(m) = \frac{3.985 \times 10^{-20}(a \sin i)^3}{P^2} = \frac{M_2^3 \sin^3 i}{(M_1 + M_2)^2} \tag{8.1}$$

where M_1 and M_2 are the masses of the primary and secondary respectively. The orbital inclination in a spectroscopic binary is generally indeterminate. However, $\sin^3 i \leq 1$ so the mass function can be used to obtain a lower-limit on the mass of the secondary:

$$M_2^3 \geq f(m)\,(M_1 + M_2)^2 \tag{8.2}$$

The non-detection of absorption lines due to the companion in the visible region implies an upper limit on the relative brightness of the secondary compared to the primary. This upper limit, ΔV, can be used to obtain a further constraint on the mass of the secondary, via the mass-luminosity relationship for main-sequence stars:

$$\left(\frac{M_2}{M_1}\right) < 10^{(-0.1 \quad \Delta V)} \tag{8.3}$$

Hence, for any given value of M_1 the mass of the secondary M_2 can be constrained. The use of the mass-luminosity relationship implies that the companion is not under-luminous for its mass, *i.e.* not a white dwarf.

A detection of the secondary spectrum in a double-lined spectroscopic binary enables the mass ratio of the two stars to be determined, once the relative orbits of the two stars have been obtained:

$$\frac{M_2}{M_1} = \frac{K_1}{K_2} \tag{8.4}$$

Even a single detection can give an approximate mass ratio from the radial velocities of the two components, assuming that the orbit for the primary is known. Even if the orbit is not known, several observations can enable the mass ratio to be determined. Triple, quadruple and even quintuple systems have been identified using very high signal-to-noise spectra (Fekel, Lacy & Tomkin, 1980; Burkhart & Coupry, 1988).

A star may, however, be double but not an identifiable spectroscopic binary. This can be due to unfavourable orbital inclination, very small radial velocity changes, large $v \sin i$ masking the radial velocity changes, etc. In such cases no estimate can be obtained for the spectral type of the secondary unless it can be observed. Lunar occultations can provide evidence for duplicity. Observations of occultations can reveal the presence of a companion from the shape of the photoelectric light-curve. Estimates of the magnitude difference (Δm) and the vector separation can be obtained. The vector separation is not the true separation, but the projected separation along the line of motion of the Moon's limb with respect to the stars. It gives a lower-limit to the separation.

Detections of companions have been made using speckle interferometry (McAlister & Hartkopf, 1988). A series of such measurements can reveal orbital motion, in exactly the same way as for 'classical' visual binaries. The orbital elements relevant to the present work are: P the period in years, e the eccentricity, a the semi-major axis in arc seconds and i the orbital inclination. The total mass of the system is given by:

$$M_1 + M_2 = \frac{a^3}{\pi^3 P^2} M_\odot \qquad (8.5)$$

where π is the trigonometric parallax. Knowing the distance to the system enables the total mass to be determined. In the relatively rare case in which both spectroscopic and visual orbital elements can be determined both M_1 and M_2 can be explicitly obtained.

8.3 Modifications to techniques to allow for companion stars

The techniques and calibrations previously discussed can be modified to allow for the effects of cooler companion stars in binary and multiple systems.

In the analysis of multiple systems the atmospheric parameters of the companions are assumed or estimated. The adopted $T_{\rm eff}$, $\log g$ and [M/H] of each companion were used to obtain the grid values for that companion. These model values are denoted (i), with N being the total number of companions. The main grid points are denoted (o), and the superscript $'$ indicates that the grid has been adjusted.

The assumption is made that values of M_V, $\log R$ and $(B-V)$ can be estimated

from the main-sequence values given by Allen (1973). Of course, the values of M_V and $\log R$ are significantly affected by evolutionary effects. The flux from a primary evolved off the main sequence will be relatively less affected by the flux from a main-sequence companion and the effects on the determination of T_{eff} and $\log g$ of the primary will consequently be lower.

The evolutionary tracks of Maeder & Meynet (1988) can be used to provide values of mass (M). Once the T_{eff} and luminosity of a star have been established, the stellar radius can be readily obtained:

$$\log\left(\frac{R}{R_\odot}\right) = 7.522 + \frac{1}{2}\log\left(\frac{L}{L_\odot}\right) - 2\log T_{eff} \tag{8.6}$$

By comparison with the evolutionary tracks, M can be interpolated and $\log g$ determined from:

$$\log g = \log\left(\frac{M}{M_\odot}\right) - 2\log\left(\frac{R}{R_\odot}\right) + 4.4377. \tag{8.7}$$

or from Equation 7.3.

The analysis of multiple systems was performed by adding in the expected contributions of the companions into the model grid values. These corrections are now described.

8.3.1 Adjustments to the photometry grids

The *uvbyβ* indices for each companion were obtained. Main sequence estimates of M_V for each companion were obtained from Allen (1973). Where there was more than one companion star, the combined values for the *uvbyβ* photometry and M_V were obtained. The routine ADDCOLOURS (written by Terry Moon) was used to combine the photometry of two stars. For multiple companions this routine was used recursively.

The original model grid may be adjusted to allow for the effects of the companion stars. The *uvbyβ* photometry of each model grid point was replaced by the combined photometry of the original grid point and the companion. This was performed using ADDCOLOURS, with the grid point M_V values obtained from Allen (1973). The observed photometry of the star may be applied to the new grid and the T_{eff} and $\log g$ of the primary obtained.

8.3.2 Adjustments to the spectrophotometry grids

A model flux distribution for each companion was obtained. Each model flux distribution was then adjusted to include the light from the companions:

$$F'_{(o,\lambda)} = R_o^2 F_{(o,\lambda)} + \sum_{i=1}^{N} R_i^2 F_{(i,\lambda)} \tag{8.8}$$

where radius replaces angular diameter since the effects of distance will be cancelled out by subsequent calculations. Main sequence values of radius were obtained from Allen (1973). This means that for low-gravity models the stellar radius will be severely underestimated. However, since we are mainly concerned with near main-sequence stars the effects will be minimal.

In the case of flux fitting the F' grid values were converted into magnitude units and normalized to 5556Å. The spectrophotometric flux fitting technique described in Section 3.2.1 may now be used to obtain the $T_{\rm eff}$ and $\log g$ of the primary. Metallicity effects on the results are still present and must, as before, be carefully accounted for in the fitting.

In the case of the Infra-Red Flux Method the values of total integrated model flux have to be adjusted:

$$F'_E(o) = R_o^2 \sigma\ T_{\rm eff}^4(o) + \sum_{i=1}^{N} R_i^2 \sigma\ T_{\rm eff}^4(i) \tag{8.9}$$

where, again, the radius replaces the angular diameter. The ratio for the IRFM was then obtained:

$$R'(o) = \frac{F'_E(o)}{F'_{(o,\lambda_0)}} \tag{8.10}$$

where λ_0 is an infra-red wavelength point. The IRFM may now be applied to obtain the $T_{\rm eff}$ of the primary. This is the more general case of the modified IRFM described in Section 3.4.2.

8.3.3 Adjustments to the Balmer line grids

A model Balmer line profile for each companion was obtained. To adjust the whole grid of Balmer line profiles the relative residual flux contributions were determined. Each profile was thus adjusted:

$$R'_{(o,\Delta\lambda)} = \frac{\left(F_{V(o)} + a(F_{B(o)} - F_{V(o)})\right)R_{(o,\Delta\lambda)} + \sum_{i=1}^{N}\left[\left(F_{V(i)} + a(F_{B(i)} - F_{V(i)})\right)R_{(i,\Delta\lambda)}\right]}{F_{V(o)} + a(F_{B(o)} - F_{V(o)}) + \sum_{i=1}^{N}\left[F_{V(i)} + a(F_{B(i)} - F_{V(i)})\right]} \tag{8.11}$$

where R is the residual flux at $\Delta\lambda$ from the Balmer line core, F_V and F_B are the fluxes at the V and B wavelengths (Allen, 1973) given by:

$$\log_\lambda F_V = -0.4M_V - 8.43 \tag{8.12}$$

$$\log_\lambda F_B = -0.4M_B - 8.17 \tag{8.13}$$

and a is a constant introduced to allow for the relative effects of the different wavelengths of the Hβ and Hγ lines: $a = 0.58$ for Hβ and $a = 1.05$ for Hγ.

The observed Balmer line may now be fitted by the new grid of adjusted profiles to obtain the $T_{\rm eff}$ of the primary as a function of $\log g$.

8.3.4 Adjustments to the synthetic β grid

Adjustments to the synthetic β grid obtained in Section 5.7 were made. The adjustments were the same as for $uvby\beta$ except that values of $(b-y)$, required by ADDCOLOURS, were obtained differently. Values of $(B-V)$ were obtained from Allen (1973) and converted into $(b-y)$ colours using:

$$(b-y) = 0.58(B-V) + 0.025 \tag{8.14}$$

This relationship was based on the observed photometry of the JKT programme stars. A very similar relationship was obtained from the model calibrations of Relyea & Kurucz (1978) and Kurucz (1991b). The empirical relationship was preferred since it is model independent. By comparison with the observed value of β the $T_{\rm eff}$ of the primary may be determined as a function of $\log g$.

8.3.5 Adjustments to the mass-luminosity relationship

The mass-luminosity relationship obtained in Section 7.4 could be easily modified to allow for the effects of companion stars. The total observed luminosity of the star and its companions was obtained from the total integrated flux and the parallax value. The luminosities of the companion stars were obtained from Allen (1973) and subtracted from the total observed luminosity to leave only the luminosity of the primary. The corrected luminosity was converted into $M_{\rm bol}$ and the mass-luminosity relationship used as before.

8.4 Discussion of the programme stars

The binary nature of the JKT programme stars has been investigated. A literature search was made for evidence concerning the binary nature of each star. This was aided by the SIMBAD data bank maintained by the Centre de Données Stellaires in Strasbourg.

HR63 θ And A2IV

Based on speckle-interferometric observations, McAlister *et al.* (1989) reported that this star is double with a separation of 0.″057. Further observations are needed to confirm this and detect orbital motion. There have been no other reports of binarity.

HR114 28 And A9IV

There is a faint common-proper-motion (13.3v) companion B at 3″, but otherwise not known to be a binary.

HR269 μ And A5V

Not known to be double.

HR972 ζ Ari A0.5Va

The radial velocity measurements given by Abt & Biggs (1972) showed no sign of any variability.

HR984 ζ Eri kA2hA8mA7

A well-known single-lined spectroscopic binary, with elements determined by Abt & Levy (1985):
$P = 17.9297$d, $K = 21.5$ km/s, $e = 0.14$, $a \sin i = 5.249 \times 10^6$ km, $f(m) = 0.0180 M_\odot$.

HR1197 A5V

Not known to be double.

HR1254 F2V

Abt & Levy (1976) concluded that the radial velocity was constant.

HR1292 45 Tau F4V

Plaskett *et al.* (1922) reported that the radial velocity was variable, but there have been no other reports of variability (Abt & Biggs, 1972). Unresolved by speckle interferometry, separation <0.″033 (Hartkopf & McAlister, 1984).

HR1331 51 Tau kA5hF0mF2

A spectroscopic binary comprising a strong broad-lined A8V type primary and a faint sharp-lined secondary of about type G0. Unfortunately the lines of the primary are too broad ($v \sin i$ = 97 km/s) for accurate radial velocity measurement and so the faint sharp lines of the secondary were used by Deutsch, Lowen & Wallerstein (1971) to determine the orbital elements:
P = 4035d, K_2 = 9.1 km/s, e = 0.34, $a \sin i = 475 \times 10^6$, $f(m) = 0.26 M_\odot$.
Note that the K value is for the secondary, not the primary.

The system was resolved by McAlister (1977a) using speckle interferometry and has been well-studied thereafter (McAlister & Hartkopf, 1988). Peterson & Solensky (1988) obtained orbital elements from a simultaneous solution to both the spectroscopic and interferometric observations:
P = 4125d, e = 0.170, a = 0.″129, i = 125°, K_2 = 9.30 km/s.
They also gave the V-magnitudes of the two stars as 5.81 and 7.81

The total mass of the system, based on the visual orbit and the distance given by Schwan (1990), is 3.0 $M_\odot$, which is consistent with the spectral types; A8 (1.9 $M_\odot$) and G0 (1.1 $M_\odot$) according to Allen (1973).

HR1351 57 Tau F0IV

Stilwell (1949) found a large variation in the radial velocity measurements for this star. Abt & Biggs (1972) state that the radial velocity has been reported as variable by several workers. But $v \sin i$ = 109 km/s is rather large and could account for the variability. Unresolved by speckle interferometry, separation <0.″033 (Hartkopf & McAlister, 1984).

HR1354 F2Vn

There are several reports of variable radial velocity for this star. Also, there have been reports of double lines (Christie & Wilson, 1938; Wilson, 1948; Abt, 1970).

However, no orbital elements have been published. The relatively large rotational velocity of $v \sin i = 132$ km/s makes the detection of small radial velocity variations problematical.

Unresolved by speckle interferometry, separation <0.″033 (Hartkopf & McAlister, 1984). Additionally, in observations of a lunar occultation, Eitter & Beavers (1979) found no sign of duplicity.

HR1356 58 Tau F0IV

Lee (1910a) found that the radial velocity was variable, but Stilwell (1949) reported a constant radial velocity. Unresolved by speckle interferometry, separation <0.″033 (Hartkopf & McAlister, 1984).

HR1368 60 Tau kA3hF2mF2

A single-lined spectroscopic binary with preliminary orbital elements determined by Abt (1961):
$P = 2.1433$d, $K = 26.6$ km/s, $e = 0.04$, $a \sin i = 0.783 \times 10^6$ km, $f(m) = 0.00418 M_\odot$.

HR1376 63 Tau kA2hF0mF3

A well-known single-lined spectroscopic binary with orbital elements given by Abt & Levy (1985):
$P = 8.4130$d, $K = 36.6$ km/s, $e = 0.0$, $a \sin i = 4.237 \times 10^6$, $f(m) = 0.04285 M_\odot$.
The companion has not been seen spectroscopically (Hundt, 1972), implying a secondary of G5V type or later. A lunar occultation observation by Africano *et al.* (1978) showed no sign of the companion, but the companion is expected to be very close to the primary.

HR1380 δ^2 Tau A7V

Lee (1909) found that the radial velocity measures indicated a period of 12 days, but the range in velocity of only 12 km/s was rather small. Stilwell (1949) found that the radial velocity was constant. Abt (1965) concluded that the radial velocity was probably constant, but could not rule out an extremely slow variation. Unresolved by speckle interferometry, separation <0.″033 (Hartkopf & McAlister, 1984). A lunar occultation observation by Africano *et al.* (1978) showed no sign of duplicity.

HR1385 F4V

Abt (1970) found that the radial velocity was constant. Unresolved by speckle interferometry, separation <0.″033 (Hartkopf & McAlister, 1984).

HR1387 κ^1 Tau A7IV-V

Both Harper (1937) and Abt (1965) concluded that the radial velocity was constant. However, the star is a suspected occultation double (Appleby, 1980) with a vector separation of 0.″1 (Hartkopf & McAlister, 1984). However, the pair could not resolved by speckle interferometry, separation <0.″030 (Hartkopf & McAlister, 1984). This would imply orbital motion or a large Δm.

HR1388 κ^2 Tau A7V

Harper (1937) and Abt & Biggs (1972) found that the radial velocity was constant. Unresolved by speckle interferometry, separation <0.″033 (Hartkopf & McAlister, 1984).

HR1389 68 Tau A2IV-Vs

Abt & Biggs (1972) gave a constant radial velocity, but according to Hoffleit (1982) the star is a single-lined spectroscopic binary with orbital elements:
$P = 57.25$d, $K = 68.8$ km/s, $a \sin i = 50.6 \times 10^6$ km, $f(m) = 1.58\ M_\odot$.
The mass function for this orbit is rather large and thus the elements may be bogus. Additionally, the orbital elements are not listed in the Batten, Fletcher & MacCarthy (1989) catalogue, nor could the original source used by Hoffleit be found. The elements are consequently ignored. Unresolved by speckle interferometry, separation <0.″033 (Hartkopf & McAlister, 1984). Radick & Lien (1980) reported that there was no sign of a companion in observations made during a cloud-affected occultation.

Jeffers, van den Bos & Greeby (1963) listed a companion at 1.″3 and $\Delta m = 3\overset{m}{.}3$, but this is not a spectroscopic companion. However, the photometry and spectrophotometry will be for the combined light.

HR1392 υ Tau A9IVn

Frost (1909) found that the spectrum was apparently composite and confirmed this by the measures of subsequent plates. Stilwell (1949) reported that the radial veloc-

ity was probably constant in spite of a velocity range of 33 km/s due to the difficulty in measuring the very broad lines of this star ($v \sin i$ = 196 km/s). He concluded that "the evidence in favour of the binary nature of the star was too uncertain".

Kraft (1965) listed the star as a single-lined spectroscopic binary, but gave no period. He stated that it could be a double-lined spectroscopic binary, which would account for its anomalous position in the HR diagram. Hoffleit (1982) stated that the star is a close occultation double, separation 0".020 and $\Delta m = 1^{m}.9$. Unresolved by speckle interferometry, separation <0".030 (Hartkopf & McAlister, 1984).

HR1394 71 Tau F0IV-Vn

Frost, Barrett & Struve (1929) reported close double lines, but these have not been confirmed by other observers. Abt (1965) obtained uncertain orbital elements: P = 5200d, K = 15.1 km/s, e = 0.241, $a \sin i = 1048 \times 10^6$ km, $f(m) = 1.70 M_{\odot}$. The rather large mass function led Hoffleit (1982) to conclude that there is a "massive invisible component", but the large value is likely to be due to the uncertain orbital elements. Abt & Levy (1974), however, concluded that the radial velocity was constant. Hence, there is uncertainty as to the binary nature of this star. The star has a large rotational velocity ($v \sin i$ = 192 km/s) and small periodic changes in radial velocity will be difficult to detect. Batten, Fletcher & MacCarthy (1989) stated that the star should be further observed to improve the orbital elements.

Occultation observations by Dunham (1980) and Peterson *et al.* (1981a) revealed the presence of a companion but there were large discrepancies in Δm ($2^{m}.0$ and $3^{m}.5$ respectively). Radick *et al.* (1982) concluded that, if the observations were of the same companion, it must lie about 0".1 east of the primary. However, the star has not been resolved by speckle interferometry, separation <0".030 (Hartkopf & McAlister, 1984), but this could be due to orbital motion or a large Δm.

HR1403 kA5hF0mF2

Reported by Abt (1961) to be a double-lined spectroscopic binary with generally inseparable lines, but there were not enough observations to determine an orbit or even a good mass ratio. Abt & Levy (1985), however, found that their spectra showed no line doubling and concluded that the radial velocity was constant.

The star was discovered to be a close double, separation 0".01, by occultation

(Hoffleit, 1982; Hartkopf & McAlister, 1984). However, the system remains unresolved by speckle interferometry, separation <0.″030 (Hartkopf & McAlister, 1984).

HR1408 76 Tau F0IV

Stilwell (1949) concluded that the radial velocity was constant. However, Abt (1970) concluded that the radial velocity was variable. Unresolved by speckle interferometry, separation <0.″033 (Hartkopf & McAlister, 1984).

HR1412 θ^2 Tau A7III

A well-known single-lined spectroscopic binary with elements given by Ebbighausen (1959):
$P = 140.728$d, $K = 31.0$ km/s, $e = 0.75$, $a \sin i = 39.7 \times 10^6$ km, $f(m) = 0.126 M_\odot$. No detections of secondary spectrum have been made and the possibility of a third body in the system cannot be ruled out (Batten, Fletcher & MacCarthy, 1989).

The separation was determined to be about 0.″021 based on three occultation measurements by Evans & Edwards (1980), Peterson *et al.* (1981b) and Evans (1983). However, the pair has not been resolved by speckle interferometry, separation <0.″030 (Hartkopf & McAlister, 1984).

Peterson *et al.* (1981b) found that $\Delta V = 1.^{\mathrm{m}}1$ and that the secondary was marginally bluer than the primary. They suggested that the system comprises an A7IV primary and an A5V secondary. Breger *et al.* (1987) used the Peterson *et al.* results together with photometric observations to determine the following parameters for the binary:

Primary $V = 3.75$, $B - V = 0.17$, $M_1 = 2.0 M_\odot$, A7IV.
Secondary $V = 4.85$, $B - V = 0.16$, $M_2 = 1.6 M_\odot$, A5V.

They found a mass ratio of $M_2/M_1 = 0.8$ and an inclination of $i \sim 47°$.

HR1414 79 Tau kA5mF0III

Abt & Levy (1985) reported constant radial velocity. No detection of a companion using speckle interferometry, separation <0.″035 (Hartkopf & McAlister, 1984).

HR1422 80 Tau F0Vn

A well-known visual binary system consisting of a F0V primary and a G2V secondary. The orbital elements were given by Peterson & Solensky (1988):
P = 177.9y, e = 0.90, a = 0.″85, i = 119°
who also gave the V-magnitudes for the primary and secondary as 5.70 and 7.98 respectively. The total mass of the system based on the parallax of Eggen (1985) is 1.62 $M_{\odot}$. This value is clearly too low. However, there is a large uncertain in long period orbits which could account for the low total mass. For example, the orbital elements given by Baize (1980):
P = 180.0y, e = 0.82, a = 1.″00, i = 107.6°
give a total mass of 2.82 $M_{\odot}$which is more consistent with the spectral types: F0V (1.7 $M_{\odot}$) and G2V (1.0 $M_{\odot}$).

Heintz (1981) found that the radial velocity of the primary showed a distinctive periodic variation and gave the following circular orbital elements:
P = 30.50d, K = 11.5 km/s, $a \sin i = 4.82 \times 10^6$ km, $f(m) = 0.0048 M_{\odot}$.
This would make the system triple. However, the rotational velocity is rather large ($v \sin i$ = 134 km/s) and small radial velocity variations would be difficult to detect.

HR1427 A6IV

Barrett (1910) found that the radial velocity was variable. However, Abt (1965) failed to find any periodic changes in radial velocity and tentatively concluded that the velocity was constant. Peterson *et al.* (1981b) report marginal occultation evidence of a binary. White (1979) and Radick & Lien (1982) report none. No clear evidence for a companion.

HR1428 81 Tau kA5mF0III

A possible single-lined spectroscopic binary, according to Abt & Levy (1985) who gave marginal elements:
P = 106.3d, K = 3.3 km/s, e = 0.52, $a \sin i = 4.07 \times 10^6$ km, $f(m) = 0.00024 M_{\odot}$.
The low values of K and $f(m)$ along with the large eccentricity of the orbit, indicate a very poor fit and possibly not real (see for example, Morbey & Griffin, 1987).

Unresolved by speckle interferometry, separation <0.″035 (Hartkopf & McAlister, 1984). Radick *et al.* (1982) found no sign of a companion from a lunar occultation

observation.

HR1430 83 Tau F0IV

Abt & Biggs (1972) give constant radial velocity measures. No companion detected by speckle interferometry, separation <0.″035 (Hartkopf & McAlister, 1984).

HR1444 ρ Tau A9V

A single-lined spectroscopic binary, although Lee (1910b) reported double lines, but this has not been confirmed by others. Uncertain elements were given by Abt (1965): $P = 488.5$d, $K = 18.5$ km/s, $e = 0.094$, $a \sin i = 123.7 \times 10^6$ km, $f(m) = 0.317 M_\odot$. However, Abt & Levy (1974) could not confirm the period. Unresolved by speckle interferometry, separation <0.″030 (McAlister, 1978; Hartkopf & McAlister, 1984).

HR1458 88 Tau kA3hA5mA7

Identified as a double-lined spectroscopic binary by Harper (1913) and Abt (1961). Abt & Levy (1985) found that although their spectra at elongations showed weak secondary Balmer lines, they were too difficult to measure and so determined orbital elements for the primary:
$P = 3.5712$d, $K = 76.3$ km/s, $e = 0.0$, $a \sin i = 3.75 \times 10^6$ km, $f(m) = 0.16 M_\odot$.
These elements are in agreement with those determined by Wilson (1913). The mass ratios determined by Harper and Abt were 0.47 and 0.61 respectively. Combining these with the mass function gives:
$m_1 \sin^3 i = 3.4 \sim 1.8 M_\odot$ and $m_2 \sin^3 i = 1.6 \sim 1.1 M_\odot$
There is considerable uncertainty in the mass values, due to the difficulty in obtaining measurements of the faint secondary lines (Abt, 1961).

This apparently simple and well-understood spectroscopic binary was found by Burkhart & Coupry (1988) to be a quintuple system! Around the same time, McAlister *et al.* (1987) resolved the star with speckle interferometry, separation 0.″107. Since then three further observations have been obtained by McAlister *et al.* (1989), who reported a change of 100° in position angle in 2.4y. This would appear to indicate a period of the order of a decade, but no orbital elements can be obtained until further observations are obtained. Burkhart & Coupry found that all five of their lines varied from night-to-night indicating that the system is either sextuple

with the wide star not observed or that the two wide stars are both spectroscopic binaries in the quintuple system. Not unreasonably, they concluded that this system requires much more detailed spectroscopic and speckle-interferometric study.

HR1472 89 Tau F0IV-V

The radial velocity is possibly variable (Abt, 1970). No companion detected by speckle interferometry, separation <0.″035 (Hartkopf & McAlister, 1984).

HR1473 90 Tau A6V

Stilwell (1949) reported that the radial velocity was variable. Abt (1965), however, was unable to find a consistent period and concluded that the velocity is probably constant.

HR1479 σ^2 Tau A5Vn

Stilwell (1949) concluded that the radial velocity was constant. Abt (1965) confirmed this stating that there was "no convincing evidence for binary motion".

HR1480 kA9hF0mF2

Both Stilwell (1949) and Abt (1970) concluded that the radial velocity was constant.

HR1507 A9IV

Abt & Biggs (1972) report constant radial velocity measures.

HR1519 A2m

Stilwell (1949) concluded that the radial velocity was probably constant. However, Abt & Levy (1985) found that the star was a single-lined spectroscopic binary and gave uncertain elements:
$P = 18.102$d, $K = 11.7$ km/s, $e = 0.44$, $a \sin i = 2.62 \times 10^6$ km, $f(m) = 0.00218 M_\odot$.
An alternative set with $P = 34.10$d gave slightly less scatter but much less well defined elements. The use of published measures, they stated, did not resolve the ambiguity.

HR1547 97 Tau A9V

Stilwell (1949) concluded that the radial velocity was probably constant, but with an "element of uncertainty".

HR1620 ι Tau A7V

The radial velocity is constant according to Abt (1965). Reported to be an occultation double with vector separation of 0.″1 (Hartkopf & McAlister, 1984). However, Hartkopf & McAlister could not resolve the pair with speckle interferometry, separation <0.″030.

HR1670 kA7hA8mF1

The radial velocity is constant (Harper, 1937; Wilson, 1948; Abt, 1970).

There is a common-proper-motion companion companion at 11.″6, but it is too distant to affect photometry and spectrophotometry. The companion was seen on the aquisition TV screen during the JKT observing run, but not included in the Balmer line spectra.

HR1672 16 Ori kA2hA9mF2

A single-lined spectroscopic binary with orbital elements given by Conti (1969a): $P = 155.83$d, $K = 8.2$ km/s, $e = 0.67$, $a \sin i = 13.0 \times 10^6$ km, $f(m) = 0.0037 M_\odot$.

HR1905 122 Tau F0V

Harper (1937) found that the radial velocity was constant, but noted that the lines were fuzzy.

HR2085 η Lep F1V

No evidence for radial velocity variability (Abt, 1965).

HR2124 μ Ori kA3hA8mA7

This system comprises a single-lined spectroscopic binary A and a close visual component B. Spectroscopic orbital elements for A were determined by Bourgeois (1929) who also determined an eccentricity of $e = 0.76$ for the visual orbit from the long term variations in the radial velocity of A. Alden (1942) pointed out that the high

eccentricity of the visual orbit leads to an unexpectedly high value for the mass of star B; Popper (1949) suggested that the mass discrepancy could be removed if star B had a large bolometric correction. In fact the reason is that star B is itself a double-lined binary with equal mass components (Fekel, 1980).

Spectroscopic orbital elements for this quadruple system were given by Batten, Fletcher & MacCarthy (1989) based on the work by Fekel:

A: $P = 4.4476$d, $K = 29.5$ km/s, $a \sin i = 1.80 \times 10^6$ km, $f(m) = 0.012 M_\odot$

B: $P = 4.7838$d, $K_1 = 82.0$ km/s, $a_1 \sin i = 5.39 \times 10^6$ km, $M_1 \sin^3 i = 1.13 M_\odot$

$K_2 = 83.3$ km/s, $a_2 \sin i = 5.48 \times 10^6$ km, $M_2 \sin^3 i = 1.11 M_\odot$

The orbits were taken as circular.

The visual orbital elements have been given by Finsen & Worley (1970):

$P = 18.25$y, $e = 0.76$, $a = 0''.28$, $i = 95.1°$.

Using speckle interferometry measurements, Morgan *et al.* (1978) found that a period of 20.2y gave a better fit to the data. However, Batten, Fletcher & MacCarthy (1989) gave a period of 18.86y, but stated that there is not a satisfactory set of spectroscopic elements for the visual pair. They quoted the following elements:

$P = 6883.8$d, $K_1 = 14.4$ km/s, $a_1 \sin i = 886 \times 10^6$ km, $M_1 \sin^3 i = 2.9 M_\odot$

$K_2 = 15.9$ km/s, $a_2 \sin i = 978 \times 10^6$ km, $M_2 \sin^3 i = 2.6 M_\odot$.

The magnitudes and colours for the photometry and spectrophotometry are for the combined light. The value of ΔV for the visual pair is rather uncertain (Fekel, 1980); Alden (1942) quoted $2^m.3$, while Finsen & Worley (1970) listed $1^m.6$. However, the masses of the components can be used to estimate the T_{eff} of the constituent stars. Using the visual orbital elements and the trigonometric parallax of $0''.029$ (Jenkins, 1963) a total mass for the system of $2.7 M_\odot$ was obtained. This is not consistent with the spectroscopic orbital elements. These require a parallax of $\simeq 0''.022$ to get the required total mass of $5.5 M_\odot$. A re-determination of the parallax is required. Using the spectroscopic orbital elements the following mass estimates were obtained:

$1.8 < M(\mathrm{Aa}) < 2.4 M_\odot$

$0.5 < M(\mathrm{Ab}) < 1.1 M_\odot$

$M(\mathrm{Ba}) \simeq M(\mathrm{Bb}) \simeq 1.3 M_\odot$

The mass of Ab must be somewhat less than those of Ba and Bb since lines of Ab

have not been detected. The components Ba and Bb are ~F5V type (6500 K) and Ab is later than G0V type (<6000 K).

HR3569 ι UMa A7IV

This system comprises a single-lined spectroscopic binary A ($V = 3\overset{m}{.}14$) and a faint visual binary pair BC ($V = 10\overset{m}{.}2$). The orbit for this wide system was given by Baize & Petit (1989):

$P = 817.9$y, $e = 0.79$, $a = 9''.09$, $i = 57.8°$.

The orbital elements for the dM1 pair BC were derived by Eggen (1967):

$P = 39.69$y, $e = 0.32$, $a = 0''.68$, $i = 108°$.

The spectroscopic binary A was discussed by Abt (1965) who gave uncertain elements:

$P = 4028$d, $K = 6.0$ km/s, $e = 0.36$, $a \sin i = 311 \times 10^6$ km, $f(m) = 0.074 M_\odot$.

However, Abt & Levy (1974) concluded that "the radial velocity was probably constant, but the data from various observatories was rather discordant". The rotational velocity for A is rather large ($v \sin i = 151$ km/s) making the detection of small radial velocity movements difficult. The elements for the spectroscopic binary must be viewed with some scepticism.

Morgan, Beckmann & Scaddan (1980) detected a companion, separation $1''.0$, using speckle interferometry, which they could not identify as a known member of the system. They concluded that they had detected a previously unknown member of system A. However, Balega, Bonneau & Foy (1984) reported that A was unresolved by speckle interferometry, separation $<0''.028$. This discrepancy could be due to orbital motion, but further observations are required to confirm this. Additionally, the uncertain nature of the spectroscopic orbital elements means that speckle companion could be the spectroscopic companion. Further radial velocity measurements are required to revise the orbital elements.

The pair BC is too faint and distant to have any measurable effect on the analysis, but the orbital elements for the wide system were used to put limits on the mass of the spectroscopic binary. Using the parallax $\pi = 0.066$, the mass of A was determined to be 3.2 $M_\odot$. From the spectroscopic mass function the following limits were placed on the masses of the components:

M(Aa) $\lesssim 2.5\ M_\odot$ and M(Ab) $\gtrsim 0.8\ M_\odot$. This, of course, assumes that the Abt &

Levy mass function is reliable.

HR3624 τ UMa kA3hF2mF5

A single-lined spectroscopic binary with good quality orbital elements determined by Bretz (1961):
$P = 1062.4$d, $K = 3.9$ km/s, $e = 0.48$, $a \sin i = 50.0 \times 10^6$ km, $f(m) = 0.0044 M_\odot$.
Unresolved by speckle interferometry, separation <0.″022 (Balega & Balega, 1985).

HR3775 θ UMa F6IV

Reported to be a single-lined spectroscopic binary with uncertain elements determined by Abt & Levy (1976):
$P = 371.0$d, $K = 4.3$ km/s, $e = 0.25$, $a \sin i = 21.24 \times 10^6$ km, $f(m) = 0.00278 M_\odot$.
However, Morbey & Griffin (1987) found that the above elements are spurious and should be rejected, Abt (1987) agreed. Abt & Willmarth (1987), also, obtained constant radial velocity.

No sign of a companion with speckle interferometry, separation <0.030 (Merrill, 1922). Gómez & Abt (1982) found no sign of a secondary spectrum based on CCD observations of the region near 6420Å. Their results implied that any secondary would be later than G7.

HR3888 υ UMa F0IV

Abt (1965) concluded that the velocity was constant.

HR4031 ζ Leo F0IIIa

Harper (1937) measured "numerous fuzzy lines" and considered the radial velocity to be variable. Wilson & Joy (1950) made no mention of variability, but Abt (1970) found some scatter in the radial velocity measures. No conclusive proof either way.

No companion resolved by speckle interferometry, separation <0.″030 (Merrill, 1922; Balega, Bonneau & Foy, 1984).

HR4033 λ UMa A1IV

Abt & Biggs (1972) gave radial velocities that were generally constant. No companion detected by speckle interferometry, separation <0.″030 (Merrill, 1922).

HR4295 β UMa A0mA1IV-V

Abt & Biggs (1972) gave a constant radial velocity.

HR4300 60 Leo A0.5mA3V

Reported as possible single-lined spectroscopic binary with P = 6.4244d by Abt & Levy (1985), but otherwise has been regarded as having a constant radial velocity (Abt & Biggs, 1972). Unresolved by speckle interferometry, separation <0.″030 (McAlister *et al.*, 1989).

HR4357 δ Leo A4V

The radial velocity of this broad-lined star was concluded to be constant (Abt, 1965). No companion found by speckle interferometry, separation <0.″030 (Merrill, 1922; McAlister *et al.*, 1989).

HR4359 θ Leo A2IV

Abt & Biggs (1972) gave generally constant radial velocity. No companion detected by speckle interferometry, separation <0.″030 (McAlister *et al.*, 1989).

HR4399 ι Leo F4IV

A visual binary with orbital elements determined by Baize (1952):
P = 192.00y, e = 0.55, a = 1.″92, i = 130°.
Worley (1969) gave ΔV = 2.^{m}67 and the companion has been identified as G3V (Hoffleit, 1982).

From radial velocity variations, Abt & Levy (1976) determined uncertain orbital elements after assuming the other elements from Baize:
P = 192.00y, K = 2.5 km/s, e = 0.54, $a \sin i$ = 2029 × 10^6 km, $f(m) = 0.0678 M_{\odot}$.
However, Batten, Fletcher & MacCarthy (1989) urged caution in accepting these elements.

Baize (1980) suspected that there is a third star in the system, associated with the primary. He gave the following elements:
P = 16.0y, e = 0.24, a = 0.″324, i =129°.
However, Heintz (1986) reviewed the available data and found no indication that ι Leo is triple. He also gave a new set of orbital elements:

P = 183.4y, e = 0.532, a = 1″.931, i = 127.7°.

Additionally, he stated that $K_1 \simeq 2.5$ km/s and that the companion B is not observable spectroscopically with current techniques. The new orbital elements and the parallax value of π = 0″.0522 (Malagnini & Morossi, 1990) give a total mass of the system of 1.5 $M_\odot$, which is clearly too low. A value of $\sim$ 2.5 $M_\odot$ is more probable.

HR4534 β Leo A3V

Abt & Biggs (1972) found some scatter in the radial velocity measures, but no individual reports of variability. No companion detected using speckle interferometry, separation <0″.030 (Merrill, 1922). A Code *et al.* (1976) fundamental star.

HR4554 γ UMa A0Van

Petrie (1951) found a large scatter in radial velocity measures, but had "very poor lines" due to large rotational velocity, $v \sin i$ = 168 km/s. Abt & Biggs (1972) gave a generally constant velocity. Unresolved by speckle interferometry, separation <0.030 (Merrill, 1922).

HR4660 δ UMa A2Van

Petrie (1951) found a large scatter in radial velocity measures, but had "very poor lines" due to large rotational velocity, $v \sin i$ = 177 km/s. No companion detected by speckle interferometry, separation <0″.030 (Merrill, 1922).

HR4689 η Vir A1IV

A well-known double-lined spectroscopic binary with orbital elements determined by Harper (1935):

$$P = 71.9\text{d}, \; K_1 = 30.5 \text{ km/s}, \; e = 0.34, \; a_1 \sin i = 28.4 \times 10^6 \text{ km}, \; M_1 \sin^3 i = 1.5 M_\odot$$
$$K_2 = 43.7 \text{ km/s}, \qquad a_2 \sin i = 40.6 \times 10^6 \text{ km}, \; M_2 \sin^3 i = 1.0 M_\odot.$$

The binary was discussed by Conti (1969b) who concluded that the mass ratio ($M_1/M_2 = 1.5$) implied that the primary is above the main sequence if the secondary is on it. Both stars could not be on the main sequence, as in that case the secondary would be type F0, which was clearly at odds with the observations.

The binary was first resolved using speckle interferometry by McAlister (1977b), separation 0″.12. However, this component is not the double-lined binary because

the maximum separation predicted by Halbwachs (1981) was 0.″012. Thus the star is a triple system. The wide system has since been extensively studied by speckle interferometry (McAlister & Hartkopf, 1988) and preliminary orbital elements have been determined by Balega, Bonneau & Foy (1984):

P = 13.0y, e = 0.08, a = 0.″135, i = 49.4°

Baize (1986) used more interferometric observations and gave:

P = 13.499y, e = 0.07, a = 0.″132.

From the orbital elements and the parallax of π = 0.″010 (Jenkins, 1952) the total mass of the system 12 $M_{\odot}$. The parallax of π = 0.″016 quoted by Hoffleit (1982) gives a total mass of 3 $M_{\odot}$. Hence, the total mass of this triple system is difficult to establish.

HR4715 4 CVn F3III-IV

Wilson & Joy (1950) found some variability in radial velocity. Crampton & Fernie (1967) found that the star is a δ Sct variable, with both magnitude and radial velocity variation over a few hours. King & Liu (1990) discussed the variability of this star and concluded that it had been mis-classified as a spectroscopic binary by Hoffleit (1982).

HR4963 θ Vir A1IV

Beardsley & Zizka (1977) analysed the radial velocity variations and determined orbital elements for the spectroscopic binary:

P = 17.84y, K = 3.18 km/s, e = 0.33, $a \sin i = 268.9 \times 10^6$, $f(m) = 0.018 M_{\odot}$.

Superimposed on this is a short period variation of 0.15d, which they attributed to pulsation.

The long-period binary was resolved by speckle interferometry at 4-meter Mayall telescope, separation 0.″485 (McAlister, 1977b). Numerous speckle observation were catalogued by McAlister & Hartkopf (1988), but no orbital elements have been determined. Hoffleit (1982) stated that Δm = 1.0 for the interferometric binary and that the system could be triple.

HR7001 α Lyr A0Va

The primary standard star for spectrophotometric and photometric systems. A Code *et al.* (1976) fundamental star.

HR7653 15 Vul kA6hA8mF5IV

A single-lined spectroscopic binary with ill-defined orbital elements given by Abt (1961):
P = 3606d, K = 4.5 km/s, e = 0.48, $a \sin i = 198 \times 10^6$ km, $f(m) = 0.0238 M_\odot$.
Additionally, Rudd & Stickland (1977) gave another poorly defined orbit:
P = 3195d, K = 4.6 km/s, e = 0.76, $a \sin i = 131 \times 10^6$ km, $f(m) = 0.0088 M_\odot$.
Hence, the star needs a long series of observations made with the same equipment and telescope to determine the true nature of the orbit. Unresolved by speckle interferometry, separation <0.″030 (Hartkopf & McAlister, 1984).

HR8305 ι PsA A0IV

A double-lined spectroscopic binary. Dworetsky (priv. comm.) obtained several spectrograms in the late 1970's which show that the period is a few days or weeks and that the components are of nearly equal brightness. The Hγ spectrum taken with the RBS showed a double-lined Balmer core; ΔRV = 120 km/s. The other two spectra taken showed no sign of double lines. Unresolved by speckle interferometry, separation <0.″041 (Bonneau *et al.*, 1980).

HR8410 32 Aqr kA5hA7mF0

A single-lined spectroscopic binary with elements given by Abt & Levy (1985):
P = 7.8330d, K = 7.5 km/s, e = 0.05, $a \sin i = 0.808 \times 10^6$ km, $f(m) = 0.000343 M_\odot$.

HR8641 *o* Peg A1IV

The radial velocity generally constant (Abt & Biggs, 1972).

8.5 The adopted parameters of the JKT programme stars

The plotting of a temperature-gravity (Kiel) diagram allows for the visual evaluation of the atmospheric parameters. The relative effects of changing [M/H] and companion stars can be readily evaluated. Such diagrams were used in the investigation of the JKT programme stars. Owing to the size of the dataset (66 stars) the final temperature-gravity diagrams are not presented here, but are given in Appendix D.

Having investigated the binary nature of the JKT programme stars, the $T_{\rm eff}$ and $\log g$ of the stars were determined. The modifications to the various techniques described in Section 8.3 were used to obtain the $T_{\rm eff}$ and $\log g$ for the primary star in binary and multiple systems. Several stars proved very difficult, in that the various methods would not give a unique solution, these will be discussed individually. The majority, however, gave very consistent solutions.

The adopted atmospheric parameters of the programme stars are given in Table 8.1. Unless otherwise indicated, a single star solution was adopted. In addition, for the stars with reliable distance and total integrated flux determinations, values of $\log R$, $\log L$ and M are included in the table. The values of M were obtained by interpolation within the evolutionary tracks of Maeder & Meynet (1988).

Table 8.1: *Adopted parameters of JKT programme stars*

HR	T_{eff}	$\log g$		$\log L$	$\log R$	M
63	9000±200	4.0±0.2	†			
114	7300±150	3.7±0.2				
269	8150±100	3.9±0.2				
972	9700±200	3.8±0.2				
984	7700±200	4.1±0.2	†			
1197	7900±100	4.1±0.1				
1254	6800±100	4.2±0.1				
1292	7000±100	4.1±0.1				
1331	7650±100	4.0±0.2	†	1.49±0.06	0.50±0.03	2.0
1351	7500±150	4.1±0.1	†	0.96±0.06	0.26±0.03	1.7
1354	7000±100	4.1±0.2	†	0.77±0.06	0.22±0.03	1.6
1356	7750±150	4.1±0.1		1.15±0.06	0.32±0.03	1.8
1368	7250±100	4.1±0.1	†¶	0.95±0.06	0.27±0.03	1.6
1376	7500±100	4.1±0.1	†¶	1.00±0.06	0.27±0.03	1.7
1380	8200±100	4.1±0.1	†	1.33±0.06	0.37±0.03	2.0
1385	6900±100	4.0±0.1				
1387	8300±100	3.9±0.1	†	1.59±0.06	0.48±0.03	2.1
1388	7500±100	4.1±0.1				
1389	9000±200	4.0±0.2	†¶	1.53±0.06	0.38±0.03	2.2
1392	7300±150	3.5±0.2	†	1.75±0.06	0.67±0.03	2.3
1394	7500±150	3.8±0.1	†			
1403	7500±100	4.0±0.1				
1408	7300±100	4.2±0.1	†	0.85±0.06	0.22±0.03	1.6
1412	8200±100	3.8±0.1	†	1.87±0.06	0.63±0.03	2.5
1414	8000±100	4.0±0.1				
1422	7450±100	4.1±0.1	†¶			
1427	8000±100	4.0±0.2	¶	1.33±0.06	0.38±0.03	2.0
1428	7650±100	4.1±0.1	¶	1.05±0.06	0.28±0.03	1.7
1430	7600±100	4.1±0.1				
1444	7950±150	4.0±0.2	†¶	1.36±0.06	0.40±0.03	2.0
1458	7900±100	4.0±0.2	†			
1472	7300±100	4.0±0.1				
1473	8200±100	3.9±0.1		1.50±0.06	0.45±0.03	2.0
1479	8150±100	3.9±0.1				
1480	7650±100	4.0±0.1	¶			
1507	7600±100	4.1±0.1				
1519	8000±100	3.9±0.2	¶			
1547	7750±100	4.0±0.1				
1620	8100±100	3.9±0.1				
1670	7600±150	3.9±0.1	¶	1.30±0.06	0.41±0.03	1.9
1672	7900±100	4.1±0.1	†¶	1.17±0.06	0.31±0.03	1.8
1905	7800±150	4.1±0.1				
2085	7050±100	4.2±0.1		0.69±0.20	0.17±0.10	1.6
2124	9000±200	4.0±0.2	†			

¶ indicates [M/H] = +0.5 models used to obtain solution.

† indicates note follows table.

Table 8.1: *Adopted parameters of JKT programme stars (continued)*

HR	T_{eff}	$\log g$		$\log L$	$\log R$	M
3569	8050±150	4.3±0.2	†¶	0.90±0.10	0.16±0.05	1.8
3624	7400±100	3.9±0.1	†¶			
3775	6400±150	4.0±0.2		0.94±0.06	0.38±0.03	1.5
3888	7100±150	3.7±0.1				
4031	6950±100	3.1±0.1				
4033	9200±200	3.6±0.2		1.54±0.22	0.36±0.11	2.3
4295	9500±200	3.8±0.2		1.64±0.15	0.38±0.08	2.4
4300	9200±150	4.1±0.2				
4357	8200±100	4.0±0.1		1.53±0.12	0.46±0.06	2.0
4359	9500±200	3.6±0.2				
4399	6700±100	3.7±0.2	†	0.82±0.17	0.28±0.09	1.5
4534	8600±100	4.2±0.2		1.25±0.08	0.28±0.04	2.0
4554	9600±150	3.8±0.2				
4660	8500±250	4.3±0.2		1.89±0.06	0.19±0.06	1.9
4689	9400±250	3.6±0.2	†			
4715	6900±150	3.1±0.2				
4963	9700±250	3.5±0.2	†			
7001	9500±150	3.9±0.1		1.78±0.04	0.46±0.02	2.5
7653	8000±150	3.7±0.2	†¶			
8305	10500±200	4.0±0.2	†			
8410	7900±100	3.8±0.2	†¶			
8641	9700±150	3.6±0.2				

¶ indicates [M/H] = +0.5 models used to obtain solution.

† indicates note follows table.

Notes to Table 8.1:

HR63 Companion of 6500 K was adopted.

HR984 A companion of 5500 K was adopted.

HR1331 Companion of 6000 K was adopted to be consistent with the observed spectral type of G0V.

HR1351 A companion of 4500 K was adopted.

HR1354 A companion of 5500 K was adopted.

HR1368 A solution was adopted which did not require the presence of the companion. The companion must be very faint, later than K0 (5000 K).

HR1376 A companion of 5000 K was adopted.

HR1380 A companion of 5000 K was adopted.

HR1387 A companion of 5000 K was adopted.

HR1389 A companion of 6000 K was adopted.

HR1392 No companion required to get a consistent solution.

HR1394 No companion required to get a consistent solution.

HR1408 A companion of 5500 K was adopted.

HR1412 A companion of 6000 K was adopted.

HR1422 A companion of 5700 K was adopted.

HR1444 A companion of 6300 K was adopted.

HR1458 A quintuple system. No consistent solution could be found. Solution given is for a single system.

HR1672 A companion of 5000 K was adopted.

HR2124 A quadruple system. Two companions with T_{eff} = 6500 K were adopted. Resultant parameters are very uncertain.

HR3569 A companion of 5000 K was adopted.

HR3624 A companion of 5500 K was adopted.

HR4399 A companion of 5500 K was adopted.

HR4689 A triple system. Solution is for a companion of 6500 K. Analysis uncertain.

HR4963 A possible triple system. Solution is for a single star. Analysis uncertain.

HR7653 A companion of 5500 K was adopted.

HR8305 A double-lined spectroscopic binary. Not analysed since it is too hot for the present work. Solution is for a single star.

HR8410 A companion of 5500 K was adopted.

This work has shown that the binary nature of stars can have a significant effect on the derived atmospheric parameters of the visual primary. Several of the programme stars have only recently been discovered to be double, or even multiple systems. High signal-to-noise spectra will continue to reveal the presence of companion stars. Such an observing programme is clearly required for several of the JKT programme stars. Only by the accurate measurement of the secondary spectra can the true atmospheric parameters of multiple systems be ascertained. The stars HR1458, HR2124, HR4689 and HR4963 require a detailed spectroscopic analysis to determine the atmospheric parameters of the companion stars.

8.6 HR Diagram for the JKT programme stars

The adopted temperatures and luminosities of the JKT programme stars can be used to generate an HR diagram. Only stars with accurate distance determinations could be used since the value of $\log L$ is highly sensitive to distance. Figure 8.1 shows the HR diagram for the JKT programme stars. In the case of stars which were found or known to be double or multiple systems, the luminosities of the companions have been subtracted from the observed value of $\log L$. The evolutionary tracks of Maeder & Meynet (1988) indicate that the majority of the stars do lie along the main sequence. There are a few evolved stars in the programme list and they are clearly visible.

The Am stars in the Hyades do not appear any different from the normal stars, they are not evolved objects within the Hyades. The $\log g$ values obtained by Lane & Lester (1984) are clearly at odds with this notion and cannot be correct.

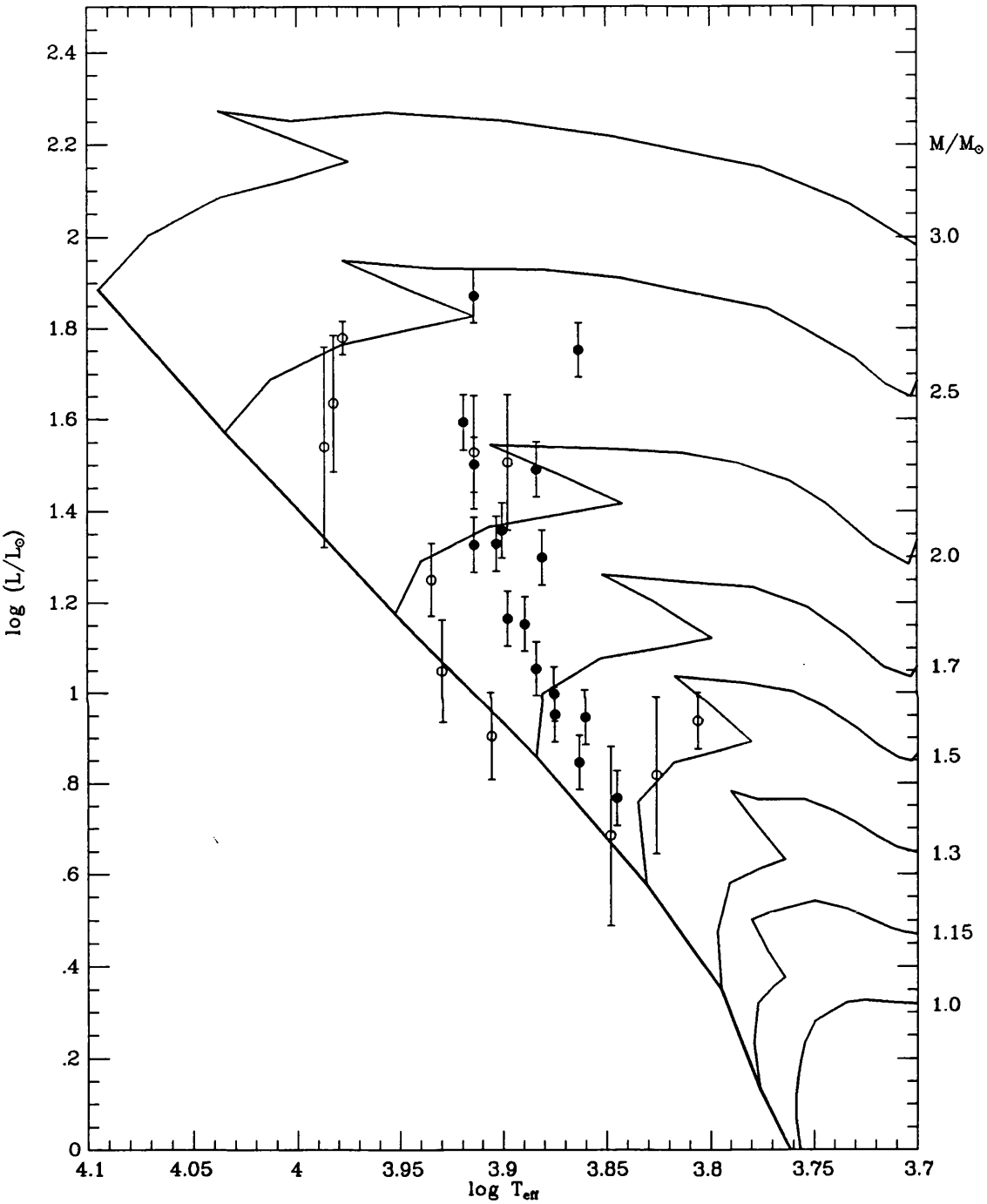

Figure 8.1: *HR Diagram for the JKT programme stars. Only the Hyades stars (•) and selected field stars (o) with accurate parallax measurements are included. The evolutionary tracks are from Maeder & Meynet (1988). The ZAMS is indicated by the thick line.*

Chapter 9

Conclusions

This work has shown that the effective temperatures and surface gravities of metallic-lined Am stars are consistent with those of normal A- and F-type stars of similar colours and ages. The atmospheric metal abundances have been shown to be enhanced compared to the Sun, confirming the generally-held views of Am stars, namely that the abundance anomalies are caused by atmospheric processes such as radiative diffusion and gravitational settling.

The various published photometry calibrations have been reviewed. The present generation of $uvby\beta$ calibrations, based on the Kurucz (1979a) models, all gave essentially the same values of $T_{\rm eff}$ and $\log g$ to within $\pm$200 K and $\pm$0.2 dex, respectively. However, none of the present photometry calibrations were able to reproduce the observed m_1 colours for late-A and F stars. Several reasons for this were discussed by Relyea & Kurucz (1978), but as yet no true explanation has been found. Changes in convective treatment, microturbulence values and missing opacity have all been proposed, and all can to some extent overcome the deficiencies. The newly-determined preliminary $uvby$ calibration by Kurucz (1991b) has significantly reduced the discrepancy. Nevertheless, the values of $T_{\rm eff}$ and $\log g$ determined from such photometry are extremely reliable and not significantly affected by metallicity.

The spectrophotometric flux fitting technique employed by Lane & Lester (1984) in their analysis of Am stars has been shown to be seriously affected by the effects of atmospheric metal abundance. Solar-abundance models give very good formal fits to the observed optical and ultraviolet energy distributions. Such fits give less scatter than when enhanced-abundance models are used, because the present generation of model-atmosphere fluxes contain ultraviolet opacity deficiencies. These deficiencies

are exaggerated when non-solar-composition fluxes are used. Hence, Lane & Lester were led to conclude that solar-abundance fits were the most reliable and adopted T_{eff} and $\log g$ values for Am stars from such models. However, it has been shown that Am stars are metal-rich and consequently enhanced-abundance models must be used to fit to the observed spectrophotometry of these stars, even though the formal fit is not as good. Future developments in the model fluxes are expected to reduce the errors in the ultraviolet opacity and produce better fits.

Observations of the Hβ and Hγ Balmer lines were obtained using a medium-resolution spectrograph. Upon correction for instrumental effects, the resultant spectra were found to be extremely reliable and consistent with published photoelectric results. The effects of metal line-blanketing and stellar rotation on the apparent hydrogen-line continuum level were investigated with the aid of synthetic spectra. Having taken due account of these effects, smoothed line profiles were extracted and found to be in excellent agreement with theoretical profiles. The Balmer lines proved to be excellent T_{eff} diagnostics for the late-A and F stars considered in the present work. The resultant temperatures were in close agreement with those obtained for *uvbyβ* photometry. Spectrophotometric fits were also in very good agreement, provided the metal abundance was adequately allowed for in such fits.

The flux excess at 4785Å, identified by Lester (1987) as detrimentally affecting *uvbyβ* photometry, has been fully investigated spectroscopically. No sign of the flux excess was found in high-quality spectra of the region around the flux excess. The flux excess was identified as being caused by anomalously strong C I lines in the model flux distributions. The oscillator strengths for these lines were updated using results from the Opacity Project and were then found to agree with the observations. The C I line-strength anomaly explained the mean value of the flux excess. The metallicity-dependent component to the flux excess was caused by the use of spectrophotometric T_{eff} and $\log g$ values by Lane & Lester (1984).

Line-blocking coefficients (Λ) for several A and F stars were obtained from the JKT spectra. A large grid of synthetic spectra was calculated to enable the observed Λ-values to be calibrated in terms of mean metal abundance. Such a method produced remarkably reliable values of [M/H] and enabled a calibration in terms of δm_0 to be obtained. For A3 to F0 stars an excellent correlation between the spectroscopic

metal abundance and the Strömgren metallicity indicator was obtained:

$$[\mathrm{M/H}] = -10.56\ \delta m_0 + 0.081$$

This calibration is valid for Am stars, something which previous published calibrations are not. The calibration is also consistent with published calibrations for mildly metal-poor stars.

A new grid of synthetic β indices has been determined for various values of [M/H]. These values of β were obtained using line-blanketed synthetic spectra and better represent the observed values for cooler stars. A close agreement with the solar β value was found. The new calibration has significantly reduced the discrepancy with observed β values. The calibration gave values of T_{eff} in very good agreement with those obtained from Hβ and Hγ profiles.

The simultaneous use of photometry, spectrophotometric flux fitting, the Infra-Red Flux Method, Balmer line profiles and the mass-luminosity relationship has enabled the critical evaluation of the T_{eff} and $\log g$ of the JKT programme stars. Allowances and modifications have been made to correct for the relative flux contributions of cooler companion stars. Such adjustments, along with the proper selection of metal abundance, gave very consistent solutions for most of the programme stars. Only the most complex multiple systems remain problematical.

The critically evaluated T_{eff} and $\log g$ values for the JKT programme stars were used to construct an HR diagram. The stellar parameters of mass, luminosity and radius were obtained for the stars with accurately known distances. These results confirmed that the metallic-lined stars in the Hyades cluster lie along the main sequence. No systematic differences between them and normal stars were found.

9.1 Further work

Several areas of further study and work have been identified.

New model atmospheres

The new Kurucz (1991b) model atmosphere calculations have only recently become available and have consequently been only very briefly utilized in the present work. The new models use much-improved opacity distribution functions containing a considerably larger number of atomic transitions. The model flux distributions are in

better agreement with the observations of Vega and the Sun. The inclusion of molecular opacity has enabled models to be calculated to lower temperatures (3500 K).

Modifications to the treatment of convection in the new models are of specific interest. Convection plays an important role in determining the atmospheric structure of late-A and F stars. However, the new models give inconsistent flux distributions and Balmer line profiles in the temperature and gravity range covered by the present work. There is a marked jump in the Balmer line profile as $\log g$ is changed. This effect is clearly not a real stellar effect and appears to be due to convergence problems with the new models. This effect needs to be fully evaluated. Until it is, the new models cannot be safely used in the study of late-A and F stars. The models for hotter and cooler stars are in excellent agreement with observations.

Microturbulence has been recognized by Kurucz as an important model parameter. The new model atmosphere code, ATLAS9, allows for the explicit varying of the microturbulent velocity. The varying of microturbulence will enable the suspected unique variation with T_{eff} (Coupry & Burkhart, 1992) to be fully evaluated. The effects of the treatment of stellar convection remains a problem to be solved.

The use of these models, once fully evaluated, will be advantageous. Based on the new colours, the changes to the atmospheric parameters obtained here should be small (~200 K at most).

New photometry calibrations

A new empirical calibration of *uvbyβ* photometry, based on Kurucz (1991b) colours is required. The inclusion of microturbulence variations in the calibration is needed. An increase in ξ_t from 2 km/s to 4 km/s around 7500 K will further reduce the discrepancy between observational and theoretical m_0 colours.

An empirical calibration along the lines of Moon & Dworetsky (1985) or Lester, Gray & Kurucz (1986) ought to be performed. A larger set of fundamental stars needs to be used. The Infra-Red Flux Method could be used to obtain accurate temperatures of stars which are definitely single. Values of the total integrated flux coupled with accurate distance determinations can be used to give values of $\log L$. Knowing T_{eff} and $\log L$ enables $\log g$ to be obtained by comparison with theoretical evolutionary tracks. These values of T_{eff} and $\log g$ will not be model-independent fundamental values but should be of sufficient quality to be regarded

as such. Additionally, any new calibration must adequately allow for the variation of metal abundances in the cooler fundamental stars. Changes in metal abundance significantly affect the model colours of cool stars.

The synthetic β values obtained in the present work will need to be recalculated using Balmer lines profiles obtained from the new models. Further observations are required to secure the transformation to the standard system. More hot stars are especially required to enable a search for bifurcation.

The search for companion stars

The binary nature of many of the stars in the JKT programme list is very uncertain. The literature search revealed that many of the stars have been inadequately studied for evidence of binarity. The use of high-resolution, high signal-to-noise spectra will allow the detection of many more companions. Long term radial velocity studies need to be undertaken to confirm the orbital elements of many of the known binary systems.

The IRFM, being extremely sensitive to the presence of cool companion stars, can be used to detect the existence of close companions. To this end several of the JKT programme stars need to have infra-red flux measurements obtained and some require optical spectrophotometric measurements.

Detailed abundance analyses of Am stars

The use of the Λ-method for determining [M/H] could be extended to other A and F stars. One ideal case would be the study of metal abundances in other open clusters, such as Coma, Præsepe, M34, etc. A medium-resolution spectrograph, such as the RBS, would be ideal in such a study. The new larger-format CCD chips would allow the Hβ line to be obtained simultaneously. This would allow the determination of $T_{\rm eff}$ and Λ from the same spectrum, and since the Λ-method is relatively insensitive to $\log g$ a values of [M/H] could be readily obtained. Such a study would be most rewarding, since many of the Am stars in fainter open clusters have not been adequately classified by low-dispersion surveys.

There is an urgent need to obtain high-quality, high-resolution, wide-wavelength coverage spectra of Am and normal A and F stars. Detailed abundance analyses using photographic data have now become dated. Many of the marginal Am stars

have abundance anomalies that are rather mild and need high signal-to-noise for precisely determine the elemental abundances. Coupling the accurate T_{eff} and $\log g$ values of Am stars with precise abundances and microturbulence values will enable stringent limits to be placed on the theoretical models of these most-interesting of objects.

Acknowledgments

I am deeply indebted to my supervisor, Dr. Mike Dworetsky, for introducing me to the Am stars and for providing excellent guidance and assistance throughout the course of this work.

My gratitude goes to Keith Smith for providing UCLSYN, without which this work would have been more difficult. His other pearls of wisdom are acknowledged.

A special mention goes to Pepe Vilchez and Roy Wallis for their excellent support during the JKT observing run.

Several people have made useful contributions to this work and they are thanked: Tony Lynas-Gray for the useful discussion on model atmospheres and CRAY computers; Paul Crowther and the Opacity Project for kindly giving me the C I oscillatory strengths; Simon Jeffery and CCP7 for providing the new Kurucz model fluxes; Ian Howarth for his DIPSO $v \sin i$ routine; Adrian Fish for help with *Starlink* and *Starlink* itself for providing several catalogues of data on tape.

The support of an SERC studentship is gratefully acknowledged; as is the financial support of the department.

A mention goes to my colleagues and friends: Dave, Mike, Andy, Tim, Alisdair, Robin, Howard, Paul and everyone else!

I owe a great debt of thanks to my parents for all the support they have given me over the years. Their contribution is warmly acknowledged. As is that of my brother, John.

Finally, a very special thankyou goes to my beloved Carol for putting-up with me!

References

Abt, H.A., 1961. *Astrophys. J. Suppl.*, **6**, 37.

Abt, H.A., 1965. *Astrophys. J. Suppl.*, **11**, 429.

Abt, H.A., 1970. *Astrophys. J. Suppl.*, **19**, 387.

Abt, H.A., 1987. *Astrophys. J.*, **317**, 353.

Abt, H.A. & Bidelman, W.P., 1969. *Astrophys. J.*, **158**, 1091.

Abt, H.A. & Biggs, E.S., 1972. *Bibliography of Stellar Radial Velocities*, Latham Process Corp, New York.

Abt, H.A. & Levy, S.G., 1974. *Astrophys. J.*, **188**, 291.

Abt, H.A. & Levy, S.G., 1976. *Astrophys. J. Suppl.*, **30**, 273.

Abt, H.A. & Levy, S.G., 1985. *Astrophys. J. Suppl.*, **59**, 229.

Abt, H.A. & Moyd, K.I., 1973. *Astrophys. J.*, **182**, 809.

Abt, H.A. & Willmarth, D.W., 1987. *Astrophys. J.*, **318**, 786.

Adelman, S.J., 1978. *Astrophys. J.*, **222**, 547.

Adelman, S.J., 1980. *Astrophys. J. Suppl.*, **43**, 491.

Adelman, S.J., 1986. *Astr. Astrophys. Suppl.*, **64**, 173.

Adelman, S.J., 1987a. *Astr. Astrophys. Suppl.*, **67**, 353.

Adelman, S.J., 1987b. *Mon. Not. R. astr. Soc.*, **228**, 573.

Adelman, S.J. & Gulliver, A.F., 1990. *Astrophys. J.*, **348**, 712.

Adelman, S.J. & Pyper, D.M., 1983. *Astrophys. J.*, **266**, 732.

Adelman, S.J., Bolcal, C., Hill, G. & Koçer, D., 1991. *Mon. Not. R. astr. Soc.*, **252**, 329.

Africano, J.L., Evans, D.S., Fekel, F.C., Smith, B.W. & Morgan, C.A., 1978. *Astr. J.*, **83**, 1100.

Alden, H.L., 1942. *Astr. J.*, **50**, 73.

Allen, C.W., 1973. *Astrophysical Quantities*, Athlone Press, London, 3rd edition.

Anders, E. & Grevesse, N., 1989. *Geochimica et Cosmochimica Acta*, **53**, 197.

Appleby, G.M., 1980. *J. Brit. Astr. Assoc.*, **90**, 572.

Ardeberg, A. & Virdefors, B., 1980. *Astr. Astrophys. Suppl.*, **40**, 307.

Argyle, R.W., Mayer, C.J., Pike, C.D. & Jorden, P.R., 1988, *A User Guide to the JKT CCD Camera, ING User Manual, XVIII.*

Baize, P., 1952. *J. Observateurs*, **31**, 35.

Baize, P., 1980. *Astr. Astrophys. Suppl.*, **39**, 83.

Baize, P., 1986. *Astr. Astrophys. Suppl.*, **65**, 551.

Baize, P. & Petit, M., 1989. *Astr. Astrophys. Suppl.*, **77**, 497.

Balega, Y., Bonneau, D. & Foy, R., 1984. *Astr. Astrophys. Suppl.*, **57**, 31.

Balega, Yu.Yu. & Balega, I.I., 1985. *Sov. Astron. Lett.*, **11**, 47.

Barrett, S.B., 1910. *Astrophys. J.*, **32**, 183.

Baschek, B. & Oke, J.B., 1965. *Astrophys. J.*, **141**, 1404.

Batten, A.H., Fletcher, J.M. & Mann, P.J., 1978. *Publ. Dom. Astrophys. Obs.*, **15**, 121.

Batten, A.H., Fletcher, J.M. & MacCarthy, D.G., 1989. *Publ. Dom. Astrophys. Obs.*, **17**, 1.

Beardsley, W.R. & Zizka, E.R., 1977. *Rev. Mex. Astron.*, **3**, 109.

Berrington, K.A., Burke, P.G., Butler, K., Seaton, M.J., Storey, P.J. & Taylor, K.T., 1987. *J. Phys. B: At. Mol. Phys.*, **20**, 6379.

Berthet, S., 1990a. *Astr. Astrophys.*, **227**, 156.

Berthet, S., 1990b. *Astr. Astrophys.*, **236**, 440.

Blackwell, D.E. & Shallis, M.J., 1977. *Mon. Not. R. astr. Soc.*, **180**, 177.

Blackwell, D.E., Shallis, M.J. & Selby, M.J., 1979. *Mon. Not. R. astr. Soc.*, **188**, 847.

Blackwell, D.E., Petford, A.D. & Shallis, M.J., 1980. *Astr. Astrophys.*, **82**, 249.

Blackwell, D.E., Petford, A.D., Arribas, S., Haddock, D.J. & Selby, M.J., 1990. *Astr. Astrophys.*, **232**, 396.

Blanco, V.M., Demers, S., Douglass, G.G. & Fitzgerald, M.P., 1970. *Publ. U.S. Naval Obs.*, **21**.

Bonneau, D., Blazit, R., Foy, R. & Labeyrie, A., 1980. *Astr. Astrophys. Suppl.*, **42**, 185.

Bourgeois, P., 1929. *Astrophys. J.*, **70**, 256.

Breger, M., 1976a. *Astrophys. J. Suppl.*, **32**, 1.

Breger, M., 1976b. *Astrophys. J. Suppl.*, **32**, 7.

Breger, M., Huang, Lin, Jiang, Shi-yang, Guo, Zi-he, Antonello, E. & Mantegazza, L., 1987. *Astr. Astrophys.*, **175**, 117.

Bretz, M.C., 1961. *Astrophys. J.*, **133**, 139.

Burkhart, C. & Coupry, M.F., 1988. *Astr. Astrophys.*, **200**, 175.

Burkhart, C. & Coupry, M.F., 1989. *Astr. Astrophys.*, **220**, 197.

Buser, R. & Kurucz, R.L., 1978. *Astr. Astrophys.*, **70**, 555.

Carney, B.W., 1982. *Astr. J.*, **87**, 1527.

Cayrel, R. & Cayrel de Strobel, G., 1966. *Ann. Rev. Astr. Astrophys.*, **4**, 1.

Cayrel, R., Burkhart, C. & Van't Veer, C., 1991. In: *Evolution of Stars: The Photospheric Abundance Connection, IAU Symp. No. 145*, eds. Michaud, G. & Tutukov, A., p. 99, Kluwer, Dordrecht, Holland.

Cayrel de Strobel, G., Bentolila, C., Hauck, B. & Duquennoy, A., 1985. *Astr. Astrophys. Suppl.*, **59**, 145.

Chaffee, F.H., Jr, 1970. *Astr. Astrophys.*, **4**, 291.

Chandrasekhar, S., 1950. *Radiative Transfer*, Oxford University Press.

Charbonneau, P. & Michaud, G., 1988. *Astrophys. J.*, **327**, 809.

Christie, W.H. & Wilson, O.C., 1938. *Astrophys. J.*, **88**, 34.

Code, A.D., 1975. In: *Multicolor Photometry and the Theoretical H-R Diagram, Dudley Obs. Rept. No. 9*, eds. Philip, A.G., Davis & Hayes, D.S., p. 221.

Code, A.D., Davis, J., Bless, R.C. & Hanbury Brown, R., 1976. *Astrophys. J.*, **203**, 417.

Conti, P.S., 1969a. *Astrophys. J.*, **156**, 661.

Conti, P.S., 1969b. *Astrophys. J.*, **158**, 1085.

Conti, P.S., 1970. *Publ. astr. Soc. Pacif.*, **82**, 781.

Conti, P.S., Wallerstein, G. & Wing, R.F., 1965. *Astrophys. J.*, **142**, 999.

Coupry, M.F. & Burkhart, C., 1992. *Astr. Astrophys. Suppl.* in press.

Cowley, A., Cowley, C., Jaschek, M. & Jaschek, C., 1969. *Astr. J.*, **74**, 375.

Cowley, C.R., Sears, R.L., Aikman, G.C.L. & Sadakane, K., 1982. *Astrophys. J.*, **254**, 191.

Crampton, D. & Fernie, J.D., 1967. *Publ. astr. Soc. Pacif.*, **79**, 330.

Crawford, D.L., 1975. *Astr. J.*, **80**, 955.

Crawford, D.L., 1979. *Astr. J.*, **84**, 1858.

Crawford, D.L. & Barnes, J.V., 1970. *Astr. J.*, **75**, 978.

Crawford, D.L. & Mander, J., 1966. *Astr. J.*, **71**, 114.

Crawford, D.L. & Perry, C.L., 1976. *Publ. astr. Soc. Pacif.*, **88**, 454.

Danford, S.C., 1975. In: *Multicolor Photometry and the Theoretical H-R Diagram, Dudley Obs. Rept. No. 9*, eds. Philip, A.G., Davis & Hayes, D.S., p. 177.

Deutsch, A.J., Lowen, L. & Wallerstein, G., 1971. *Publ. astr. Soc. Pacif.*, **83**, 298.

Dreiling, L.A. & Bell, R.A., 1980. *Astrophys. J.*, **241**, 736.

Dunham, D.W., 1980. *Occultation Newsl.*, **2**(8).

Dworetsky, M.M. & Moon, T.T., 1986. *Mon. Not. R. astr. Soc.*, **220**, 787.

Ebbighausen, E.G., 1959. *Publ. Dom. Astrophys. Obs.*, **11**, 235.

Edwin, R., 1988, *The St Andrews RBS User Manual, ING User Manual, XI.*

Eggen, O.J., 1967. *Ann. Rev. Astr. Astrophys.*, **5**, 105.

Eggen, O.J., 1985. *Astr. J.*, **90**, 1046.

Eitter, J.J. & Beavers, W.I., 1979. *Astrophys. J. Suppl.*, **40**, 475.

Evans, D.S., 1983. In: *Current Techniques in Double and Multiple Star Research, IAU Coll. No. 62*, eds. Harrington, R.S. & Franz, O.G., p. 73, Lowell Obs. Bull. No. 167, Vol IX, No. 1.

Evans, D.S. & Edwards, D.A., 1980. *Observatory*, **100**, 206.

Fekel, F., Jr, Lacy, C.H. & Tomkin, J., 1980. In: *Close Binary Stars: Observations and Interpretation, IAU Symp. No. 88*, eds. Plavec, M.J., Popper, D.M. & Ulrich, R.K., p. 53, Reidel, Dordrecht, Holland.

Fekel, F.C., 1980. *Publ. astr. Soc. Pacif.*, **92**, 785.

Finsen, W.S. & Worley, C.E., 1970. *Republic Obs. Johannesburg Circ.*, **7**, 203.

Frost, E.B., 1909. *Astrophys. J.*, **29**, 233.

Frost, E.G., Barrett, S.B. & Struve, O., 1929. *Publ. Yerkes Obs.*, **7**(1).

Fuller, N.M.J., 1989, *FIGARO — A General Data Reduction System, Starlink User Note, No. 86.*

Gezari, D.Y., Schmitz, M. & Mead, J.M., 1987. *Catalog of Infrared Observations, NASA Reference Publication*, **1196**.

Giddings, J. & Rees, P., 1989, *IUEDR — IUE Data Reduction Package, Starlink User Note, No. 37.*

Gigas, D., 1986. *Astr. Astrophys.*, **165**, 170.

Golay, M., 1972. *Vistas in Astronomy*, **14**, 13.

Gómez, A.E. & Abt, H.A., 1982. *Publ. astr. Soc. Pacif.*, **94**, 650.

Gray, D.F., 1976. *The Observation and Analysis of Stellar Photospheres*, Wiley.

Gray, D.F. & Evans, J.C., 1973. *Astrophys. J.*, **182**, 147.

Gray, R.O. & Garrison, R.F., 1989. *Astrophys. J. Suppl.*, **69**, 301.

Greenstein, J.L., 1948. *Astrophys. J.*, **107**, 151.

Greenstein, J.L., 1949. *Astrophys. J.*, **109**, 121.

Gustafsson, B. & Nissen, P.E., 1972. *Astr. Astrophys.*, **19**, 261.

Guthrie, B.N.G., 1987. *Mon. Not. R. astr. Soc.*, **226**, 361.

Halbwachs, J.L., 1981. *Astr. Astrophys. Suppl.*, **44**, 47.

Harper, W.E., 1913. *Publ. Dom. Astrophys. Obs.*, **1**, 115.

Harper, W.E., 1935. *Publ. Dom. Astrophys. Obs.*, **6**, 217.

Harper, W.E., 1937. *Publ. Dom. Astrophys. Obs.*, **7**, 1.

Hartkopf, W.I. & McAlister, H.A., 1984. *Publ. astr. Soc. Pacif.*, **96**, 105.

Hauck, B., 1968. *Publ. Obs. Genève*, **75**.

Hauck, B., 1973. In: *Problems of Calibration of Absolute Magnitudes and Temperatures of Stars, IAU Symp. No. 54*, eds. Hauck, B. & Weterlund, B.E., p. 117, Reidel, Dordrecht, Holland.

Hauck, B., 1975. In: *Multicolor Photometry and the Theoretical H-R Diagram, Dudley Obs. Rept. No. 9*, eds. Philip, A.G., Davis & Hayes, D.S., p. 143.

Hauck, B., 1986. *Astr. Astrophys.*, **155**, 371.

Hauck, B. & Mermilliod, M., 1980. *Astr. Astrophys. Suppl.*, **40**, 1.

Hauck, B. & Mermilliod, M., 1990. *Astr. Astrophys. Suppl.*, **86**, 107.

Hauck, B. & Van't Veer-Menneret, C., 1970. *Astr. Astrophys.*, **7**, 219.

Hayes, D.S., 1979. In: *Problems of Calibration of Multicolor Photometric Systems, Dudley Obs. Rept. No. 14*, ed. Philip, A.G., Davis, p. 297.

Hayes, D.S. & Latham, D.W., 1975. *Astrophys. J.*, **197**, 593.

Heck, A., Egret, D., Jaschek, C. & Jaschek, M., 1984. *Reference Atlas of IUE Low-Dispersion Spectra, ESA*, **Sp. 1052**.

Heintz, W.D., 1981. *Astrophys. J. Suppl.*, **46**, 247.

Heintz, W.D., 1986. *Astrophys. J. Suppl.*, **64**, 1.

Hilditch, R.W., Hill, G. & Barnes, J.V., 1983. *Mon. Not. R. astr. Soc.*, **204**, 241.

Hoffleit, D.H., 1982. *Bright Star Catalogue*, Yale University Observatory, New Haven, 4th revised edition.

Holweger, H., Gigas, D. & Steffen, M., 1986. *Astr. Astrophys.*, **155**, 58.

Holweger, H., Steffen, M. & Gigas, D., 1986. *Astr. Astrophys.*, **163**, 333.

Horne, K., 1986. *Publ. astr. Soc. Pacif.*, **98**, 609.

Howarth, I.D. & Murray, J., 1987, *DIPSO — A friendly spectrum analysis program, Starlink User Note, No. 50.*

Hundt, E., 1972. *Astr. Astrophys.*, **21**, 413.

Jamar, C., Macau-Hercot, D., Monfils, A., Thompson, G.I., Houziaux, L. & Wilson, R., 1976. *Ultraviolet Bright-Star Spectrophotometric Catalogue, ESA*, **SR-27.**

Jaschek, C. & Jaschek, A., 1987. *The Classification of Stars*, Cambridge University Press.

Jeffers, H.M., van den Bos, W.H. & Greeby, F.M., 1963. *Index Catalogue of Double Stars, Pub. Lick Obs.*, **Vol. XXI.**

Jenkins, L.F., 1952. *General Catalogue of Trigonometric Stellar Parallaxes*, Yale University Observatory, New Haven.

Jenkins, L.F., 1963. *Supplement to the General Catalogue of Trigonometric Stellar Parallaxes*, Yale University Observatory, New Haven.

Johnson, H.L., 1958. *Lowell Obs. Bulletin*, **90.**

Johnson, H.L. & Morgan, W.W., 1953. *Astrophys. J.*, **117**, 313.

King, J.R. & Liu, T., 1990. *Publ. astr. Soc. Pacif.*, **102**, 328.

Kobi, D. & North, P., 1990. *Astr. Astrophys. Suppl.*, **85**, 999.

Koçer, D., Bolcal, C., Inelmen, E. & Adelman, S.J., 1987. *Astr. Astrophys. Suppl.*, **70**, 49.

Kohl, K., 1964. *Zeitschr. Astrophys.*, **60**, 115.

Kraft, R.P., 1965. *Astrophys. J.*, **142**, 681.

Kurucz, R.L., 1970. *Smithsonian Ap. Obs. Spec. Rept.*, **309.**

Kurucz, R.L., 1975. In: *Multicolor Photometry and the Theoretical H-R Diagram, Dudley Obs. Rept. No. 9*, eds. Philip, A.G., Davis & Hayes, D.S., p. 271.

Kurucz, R.L., 1979a. *Astrophys. J. Suppl.*, **40**, 1.

Kurucz, R.L., 1979b. In: *Problems of Calibration of Multicolor Photometric Systems, Dudley Obs. Rept. No. 14*, ed. Philip, A.G., Davis, p. 363.

Kurucz, R.L., 1988. Private communication.

Kurucz, R.L., 1991a. In: *Stellar Atmospheres: Beyond Classical Models, NATO ASI Series*, eds. Crivellari, L., Hubeny, I. & Hummer, D.G., Kluwer, Dordrecht, Holland.

Kurucz, R.L., 1991b. In: *Precision Photometry: Astrophysics of the Galaxy*, eds. Philip, A.G., Davis, Upgren, A.R. & Janes, K.A., p. 27, L. Davis Press, Schenectady.

Kurucz, R.L. & Peytremann, E., 1975. *Smithsonian Ap. Obs. Spec. Rept.*, **362**.

Lane, M.C. & Lester, J.B., 1980. *Astrophys. J.*, **238**, 210.

Lane, M.C. & Lester, J.B., 1984. *Astrophys. J.*, **281**, 723.

Lane, M.C. & Lester, J.B., 1987. *Astrophys. J. Suppl.*, **65**, 137.

Lee, O.J., 1909. *Astrophys. J.*, **29**, 240.

Lee, O.J., 1910a. *Astrophys. J.*, **31**, 176.

Lee, O.J., 1910b. *Astrophys. J.*, **32**, 300.

Lemke, M., 1989. *Astr. Astrophys.*, **225**, 125.

Lester, J.B., 1987. *Mon. Not. R. astr. Soc.*, **227**, 135.

Lester, J.B., Lane, M.C. & Kurucz, R.L., 1982. *Astrophys. J.*, **260**, 272.

Lester, J.B., Gray, R.O. & Kurucz, R.L., 1986. *Astrophys. J. Suppl.*, **61**, 509.

Luck, R.E., 1991. In: *Evolution of Stars: The Photospheric Abundance Connection, IAU Symp. No. 145*, eds. Michaud, G. & Tutukov, A., p. 247, Kluwer, Dordrecht, Holland.

Macau-Hercot, D., Jamar, C., Monfils, A., Thompson, G.I., Houziaux, L. & Wilson, R., 1978. *Ultraviolet Bright-Star Spectrophotometric Catalogue, ESA*, **SR-28**.

Maeder, A. & Meynet, G., 1988. *Astr. Astrophys. Suppl.*, **76**, 411.

Malagnini, M.L. & Morossi, C., 1990. *Astr. Astrophys. Suppl.*, **85**, 1015.

Malagnini, M.L., Faraggiana, R., Morossi, C. & Crivellari, L., 1982. *Astr. Astrophys.*, **114**, 170.

Malagnini, M.L., Faraggiana, R. & Morossi, C., 1983. *Astr. Astrophys.*, **128**, 375.

Malagnini, M.L., Morossi, C., Rossi, L. & Kurucz, R.L., 1986. *Astr. Astrophys.*, **162**, 140.

Matsushima, S., 1969. *Astrophys. J.*, **158**, 1137.

McAlister, H.A., 1977a. *Astrophys. J.*, **212**, 459.

McAlister, H.A., 1977b. *Astrophys. J.*, **215**, 159.

McAlister, H.A., 1978. *Publ. astr. Soc. Pacif.*, **90**, 288.

McAlister, H.A. & Hartkopf, W.I., 1988. *Second Catalog of Interferometric Measurements of Binary Stars, CHARA Contributions*, **2**.

McAlister, H.A., Hartkopf, W.I., Hutter, D.J. & Franz, O.G., 1987. *Astr. J.*, **93**, 688.

McAlister, H.A., Hartkopf, W.I., Sowell, J.R., Dombrowski, E.G. & Franz, O.G., 1989. *Astr. J.*, **97**, 510.

Mégessier, C. & Van't Veer, C., 1991. In: *Evolution of Stars: The Photospheric Abundance Connection, Posters presented at IAU Symposium 145*, eds. Michaud, G., Tutukov, A. & Bergevin, M., p. 35, University of Montreal.

Merrill, P.W., 1922. *Astrophys. J.*, **56**, 43.

Michaud, G., 1970. *Astrophys. J.*, **160**, 641.

Michaud, G., 1976. In: *Physics of Ap Stars*, eds. Weiss, W.W., Jenkner, H. & Wood, H.J., p. 81, Universitatssternwarte Wien, Vienna.

Michaud, G., 1991. In: *Evolution of Stars: The Photospheric Abundance Connection, IAU Symp. No. 145*, eds. Michaud, G. & Tutukov, A., p. 111, Kluwer, Dordrecht, Holland.

Miczaika, G.R., Franklin, F.A., Deutsch, A.J. & Greenstein, J.L., 1956. *Astrophys. J.*, **124**, 134.

Moon, T.T., 1985. *Commun. Univ. London Obs.*, **78**.

Moon, T.T. & Dworetsky, M.M., 1985. *Mon. Not. R. astr. Soc.*, **217**, 305.

Moore, C.E., 1970. *Nat. Stand. Ref. Data Ser., Nat. Bur. Stand. (U.S.)*, **3, Sec. 3**.

Morbey, C.L. & Griffin, R.F., 1987. *Astrophys. J.*, **317**, 343.

Morgan, B.L., Beddoes, D.R., Scaddan, R.J. & Dainty, J.C., 1978. *Mon. Not. R. astr. Soc.*, **183**, 701.

Morgan, B.L., Beckmann, G.K. & Scaddan, R.J., 1980. *Mon. Not. R. astr. Soc.*, **192**, 143.

Morgan, W.W. & Keenan, P.C., 1973. *Ann. Rev. Astr. Astrophys.*, **11**, 29.

Morossi, C. & Malagnini, M.L., 1985. *Astr. Astrophys. Suppl.*, **60**, 365.

Napiwotzki, R., Schönberner, D. & Wenske, V., 1991. In: *Proceedings Kiel/CCP7 Workshop on Atmospheres of Early-type Stars*, Springer, Germany. in press.

Nicolet, B., 1978. *Astr. Astrophys. Suppl.*, **34**, 1.

Nicolet, B., 1981. *Astr. Astrophys.*, **97**, 85.

Nissen, P.E., 1970a. *Astr. Astrophys.*, **6**, 138.

Nissen, P.E., 1981. *Astr. Astrophys.*, **97**, 145.

Nissen, P.E., 1988. *Astr. Astrophys.*, **199**, 146.

North, P. & Hauck, B., 1979. In: *Problems of Calibration of Multicolor Photometric Systems, Dudley Obs. Rept. No. 14*, ed. Philip, A.G., Davis, p. 183.

North, P. & Kobi, D., 1991. In: *Precision Photometry: Astrophysics of the Galaxy*, eds. Philip, A.G., Davis, Upgren, A.R. & Janes, K.A., p. 327, L. Davis Press, Schenectady.

North, P. & Nicolet, B., 1990. *Astr. Astrophys.*, **228**, 78.

Oke, J.B. & Conti, P.S., 1966. *Astrophys. J.*, **143**, 134.

Oke, J.B. & Gunn, J.E., 1983. *Astrophys. J.*, **266**, 713.

Olsen, E.H., 1976. *Astr. Astrophys.*, **50**, 117.

Olsen, E.H., 1984. *Astr. Astrophys. Suppl.*, **57**, 443.

Olson, E.C., 1974. *Publ. astr. Soc. Pacif.*, **86**, 80.

Peterson, D.M., 1969. *Smithsonian Ap. Obs. Spec. Rept.*, **293**.

Peterson, D.M. & Solensky, R., 1988. *Astrophys. J.*, **333**, 256.

Peterson, D.M., Baron, R.L., Dunham, E. & Mink, D., 1981a. *Astr. J.*, **86**, 1090.

Peterson, D.M., Baron, R.L., Dunham, E., Mink, D., Weekes, T.C. & Elliot, J.L., 1981b. *Astr. J.*, **86**, 280.

Petrie, R.M., 1951. *Publ. Dom. Astrophys. Obs.*, **8**, 117.

Philip, A.G., Davis & Egret, D., 1980. *Astr. Astrophys. Suppl.*, **40**, 199.

Philip, A.G., Davis & Relyea, L.J., 1979. *Astr. J.*, **84**, 1743.

Philip, A.G., Davis, Miller, T.M. & Relyea, L.J., 1976. In: *Dudley Obs. Rept. No. 12.*

Plaskett, J.S., Harper, W.E., Young, R.K. & Plaskett, H.H., 1922. *Publ. Dom. Astrophys. Obs.*, **1**, 287.

Popper, D.M., 1949. *Astrophys. J.*, **109**, 100.

Popper, D.M., 1980. *Ann. Rev. Astr. Astrophys.*, **18**, 115.

Press, W.H., Flannery, B.P., Teukolsky, S.A. & Vetterling, W.T., 1989. *Numerical Recipes*, Cambridge University Press, Cambridge.

Pyper, D.M. & Adelman, S.J., 1988. In: *New Directions in Spectrophotometry*, eds. Philip, A.G., Davis, Hayes, D.S. & Adelman, S.J., p. 113, L. Davis Press, Schenectady.

Radick, R. & Lien, D., 1980. *Astr. J.*, **85**, 1053.

Radick, R. & Lien, D., 1982. *Astr. J.*, **87**, 170.

Radick, R.R., Africano, J.L., Rogers, W.F., Schneeberger, T.J. & Tyson, E.T., 1982. *Astr. J.*, **87**, 885.

Relyea, L.J. & Kurucz, R.L., 1978. *Astrophys. J. Suppl.*, **37**, 45.

Ridpath, I., 1988. *Popular Astronomy*, **35**(4), 18.

Roman, N.G., Morgan, W.W. & Eggen, O.J., 1948. *Astrophys. J.*, **107**, 107.

Rudd, P.J. & Stickland, D.J., 1977. *Observatory*, **97**, 2.

Rufener, F., 1981. *Astr. Astrophys. Suppl.*, **45**, 207.

Rufener, F. & Maeder, A., 1971. *Astr. Astrophys. Suppl.*, **4**, 43.

Sadakane, K., 1981. *Publ. astr. Soc. Pacif.*, **93**, 587.

Schmidt, E.G., 1979. *Astr. J.*, **84**, 1739.

Schmidt, E.G. & Taylor, D.J., 1979. *Astr. J.*, **84**, 1193.

Schwan, H., 1990. *Astr. Astrophys.*, **228**, 69.

Seaton, M.J., 1987. *J. Phys. B: At. Mol. Phys.*, **20**, 6363.

Selby, M.J., Hepburn, I., Blackwell, D.E., Booth, A.J., Haddock, D.J., Arribas, S., Leggett, S.K. & Mountain, C.M., 1988. *Astr. Astrophys. Suppl.*, **74**, 127.

Shallis, M.J. & Blackwell, D.E., 1979. *Astr. Astrophys.*, **79**, 48.

Smith, K.C. PhD thesis, University of London, 1992.

Smith, K.C. & Van't Veer, C., 1987. In: *Elemental Abundance Analyses*, eds. Adelman, S.J. & Lanz, T., p. 133, Institut d'Astronomie de l'Universite de Lausanne.

Smith, M.A., 1971. *Astr. Astrophys.*, **11**, 325.

Smith, M.A., 1973. *Astrophys. J.*, **182**, 159.

Steffen, M., 1985. *Astr. Astrophys. Suppl.*, **59**, 403.

Stilwell, W.H., 1949. *Publ. Dom. Astrophys. Obs.*, **7**, 337.

Strömgren, B., 1963a. *Quart. J. R. astr. Soc.*, **4**, 8.

Strömgren, B., 1963b. In: *Basic Astronomical Data*, ed. Strand, K.Aa., p. 123, University of Chicago Press.

Strömgren, B., 1966. *Ann. Rev. Astr. Astrophys.*, **4**, 433.

Takeda, Y., 1984. *Publ. astr. Soc. Japan*, **36**, 149.

Taylor, B.J., 1984. *Astrophys. J. Suppl.*, **54**, 259.

Titus, J. & Morgan, W.W., 1940. *Astrophys. J.*, **92**, 256.

Tull, R.G., 1988. In: *Instrumentation for Ground Based Optical Astronomy, Present & Future*, ed. Robinson, L.B., p. 104, Springer-Verlag.

Van't Veer, C., Cayrel, R. & Coupry, M.F., 1991. In: *Evolution of Stars: The Photospheric Abundance Connection, Posters presented at IAU Symposium 145*, eds. Michaud, G., Tutukov, A. & Bergevin, M., p. 49, University of Montreal.

Van't Veer-Menneret, C., 1963. *Ann. Astrophys.*, **26**, 289.

Van't Veer-Menneret, C., Coupry, M.F. & Burkhart, C., 1985. *Astr. Astrophys.*, **146**, 139.

Vidal, C.R., Cooper, J. & Smith, E.W., 1973. *Astrophys. J. Suppl.*, **25**, 37.

Wallerstein, G., 1962. *Astrophys. J. Suppl.*, **6**, 407.

White, N.M., 1979. *Astr. J.*, **84**, 872.

Wiese, W.L., Smith, M.W. & Glennon, B.M., 1966. *Nat. Stand. Ref. Data Ser., Nat. Bur. Stand. (U.S.)*, **4 vol. 1.**

Wilson, R.E., 1913. *Lick Obs. Bull.*, **7**, 104.

Wilson, R.E., 1948. *Astrophys. J.*, **107**, 119.

Wilson, R.E. & Joy, A.H., 1950. *Astrophys. J.*, **111**, 221.

Wolff, S.C., 1983. *The A Stars: Problems and perspectives*, NASA, Washington, DC.

Worley, C.E., 1969. *Astr. J.*, **74**, 764.

Appendix A

The generation and use of synthetic spectra

A.1 Introduction

The appearance of a stellar spectrum is determined by the physical processes occurring in the stellar atmosphere. In the absence of any selective absorption, the shape of a stellar flux distribution would be essentially given by the Planck function. (Technically, one would obtain the grey atmosphere flux distribution which is slightly less peaked near λ_{max}. See Chandrasekhar (1950) for details). However, selective absorption or opacity has a significant effect on the shape of the emergent flux distribution on a large as well as a small wavelength range. The sources of opacity are:

- bound-bound absorption which gives rise to absorption lines
- bound-free absorption which gives rise to, *e.g.*, the Balmer Jump
- free-free absorption
- scattering

All these processes combine together to produce the characteristic shapes of stellar flux distributions, both on the large scale (shapes of Balmer and Paschen continua, Balmer jump, etc.) and on the small scale (shape of Balmer lines, individual absorption lines, etc.). The gross atmospheric structure, such as the depth dependence of temperature, pressure, etc. and the shape of flux distributions, is obtained from model atmosphere calculations. The fine detail is the province of spectrum synthesis.

A.2 The calculation of synthetic spectra

The generation of a synthetic spectrum is essentially a two part process; 1. the generation of a model atmosphere and 2. the production of the synthetic spectrum itself.

The production of line-blanketed model atmospheres was performed using the ATLAS6 code running on the Cray COS1M at ULCC. The code has been discussed in detail by Kurucz (1970, 1979a) and will not be treated here.

Various codes have been developed for the generation of synthetic spectra. The present work was undertaken using UCLSYN. The code was discussed in detail by Smith (1992), who extensively modified and upgraded the original code written by J.E. Ross around 1970. Another, more widely used code is SYNTHE written by Kurucz. This is specifically designed for the generation of large amounts of synthetic spectra, as required in the present work. However, this code only runs on the Cray at RAL due to the enormous size of the datasets used.

To calculate synthetic spectra UCLSYN was used in VAX overnight batch mode, rather than using SYNTHE on the Cray at RAL. The choice of UCLSYN was made because it was much easier to use than SYNTHE and because the Cray turnaround times were hampered by network transfer problems.

UCLSYN requires a model atmosphere structure to be able to calculate line profiles. The plane-parallel line-blanketed model atmospheres of Kurucz (1979a) were used throughout, with additional [M/H] = +0.5 models calculated using the ATLAS6 code.

The necessary absorption line data was obtained from the Kurucz & Peytremann (1975) line list, except for the transition group (Ca to Ni) where the Kurucz (1988) enhanced line list was used. These enormous line lists were trimmed down to contain only the lines in the wavelength range 4200 – 5000Å. The wavelength, $\log gf$, lower-level excitation potential and ionization stage for each element were extracted. The damping constants required were calculated using the Kurucz WIDTH defaults:

- The radiative damping constant for the line is taken as the classical damping constant:

$$\gamma_{cl} = 2.223 \times 10^{15}/\lambda^2 \qquad \text{(A.1)}$$

  where λ = wavelength in Å.

- The Stark-broadening damping constant is obtained from:

$$\gamma/n_e = 1.0 \times 10^{-8}\, n_{\rm eff}^5 \tag{A.2}$$

where $n_{\rm eff}^2 = 13.595 Z_{\rm eff}^2/(I - EP_{\rm upper})$

I = ionization energy in eV

$EP_{\rm upper}$ = upper-level excitation potential in eV

$Z_{\rm eff}$ = effective charge (neutral = 1, etc.)

- The Van der Waals damping constant is obtained from:

$$\Delta\bar{r}^2 = \frac{5}{2}(n_{\rm eff}^2/Z_{\rm eff})^2 \tag{A.3}$$

except for transition elements in the range $20 < n_{\rm seq} < 29$ when,

$$\Delta\bar{r}^2 = (45 - n_{\rm seq})/Z_{\rm eff} \tag{A.4}$$

is used, where $n_{\rm seq} = A - Z_{\rm eff} + 1$

A = atomic number of element

The elemental solar abundances used were those adopted by Kurucz (1979a). They could be scaled to any value of [M/H] as required. A microturbulence of ξ_t = 2 km/s was adopted to be consistent with the published model calculations.

The synthesis was performed in 5Å segments using the lines in that segment, plus 1Å either side to allow for line wings. There were no very strong absorption lines in the regions synthesized for the present work. A step size of 0.01Å was used. A total of 230Å-worth of spectrum segments were calculated and joined together to form one long spectrum. The long spectrum had the continuum level set to 1.00. This was because UCLSYN was designed for use in abundance analyses. However, UCLSYN does include approximate hydrogen-line wing opacity when calculating the synthetic spectra. The true shape of the hydrogen-line was obtained by multiplying the spectrum by the Kurucz (1979a) line profiles. Additional Balmer line profiles for [M/H] = +0.5 were calculated using Peterson's BALMER code.

The synthetic spectrum was then convolved with the JKT instrumental profile, taken to be a Gaussian profile with σ = 0.3. This profile corresponded to the 0.8Å FWHM resolution of the RBS spectrograph as measured from arc spectra and given by Edwin (1988). The spectrum was then binned onto a uniform grid with bin sizes of 0.4Å corresponding to the 22μm CCD pixel sizes.

Strictly speaking, rotational broadening should be applied to the synthetic spectrum before the instrumental effects are added. But after extensive testing it was found that rotational broadening could be applied to the final binned spectrum with an error of less than 1%. This saved an enormous amount of computing time. Rotational broadening to a given $v \sin i$ was applied using a routine supplied by Ian Howarth (priv. comm.).

A.3 Comparison with a SYNTHE spectrum

To test that UCLSYN gave reliable synthetic spectra a comparison was made with a SYNTHE spectrum (Figure A.1). The SYNTHE spectrum was found to have put the hydrogen line in the wrong place. The core was at the vacuum wavelength, whereas the absorption lines were at their expected air wavelengths. Consequently, when comparing the two outputs the UCLSYN spectrum had to have the Balmer profile added with the core at the vacuum wavelength. The two codes produced spectra that were in good agreement with each other. There are a few minor differences due to partition functions of rare elements not being present in the UCLSYN code or vice versa.

A.4 Comparison with JKT observations

The synthetic spectra agree fairly well with the JKT observations. There are, of course, differences due to imperfections in the synthetic spectra. There are several sources: $\log gf$values, microturbulence, abundances, etc. Hence, one cannot expect the observations and syntheses to agree exactly. The general agreement is more than adequate for the purposes required in the present work, such as the study of blanketing effects.

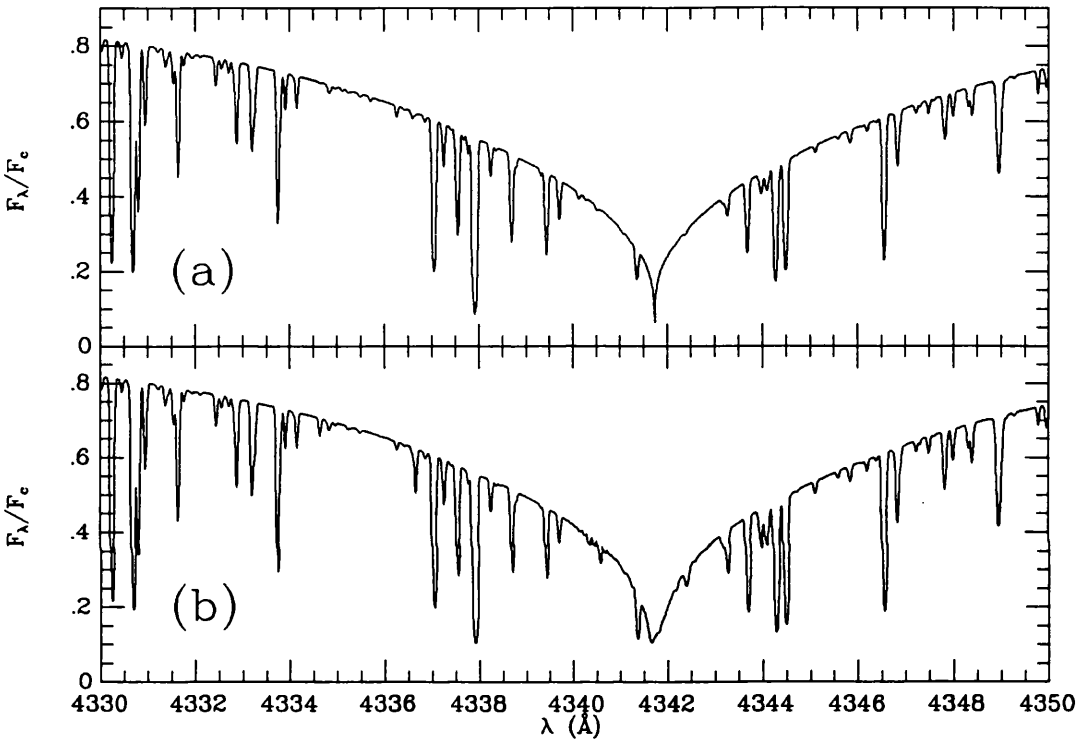

Figure A.1: *Comparison between* SYNTHE *(a) and* UCLSYN *(b). Both syntheses are for* $T_{\rm eff} = 7500$ *K,* $\log g = 4.0$*,* $[M/H] = +0.5$ *and* $\xi_{\rm t} = 2$ *km/s. The absorption lines are of very similar strength, but the core of the hydrogen line is markedly different. This is due to the inclusion of Doppler broadening in the Kurucz (1979a) profile, which is not present in the* SYNTHE *profile. Note, also, a small amount of numerical noise at 4340.5Å, the center of the true position of Hγ.*

Appendix B

Fits to spectrophotometry

B.1 Plots of fits to spectrophotometry

The following pages contain the solar-abundance spectrophotometric fits to the JKT programme stars. The $T_{\rm eff}$ and $\log g$ of the models are the best fit solutions given in Table 3.3. The sources of optical spectrophotometry were given in the same table and the ultraviolet fluxes were obtained from the S2/68 database. All the fits were normalized to 5556Å.

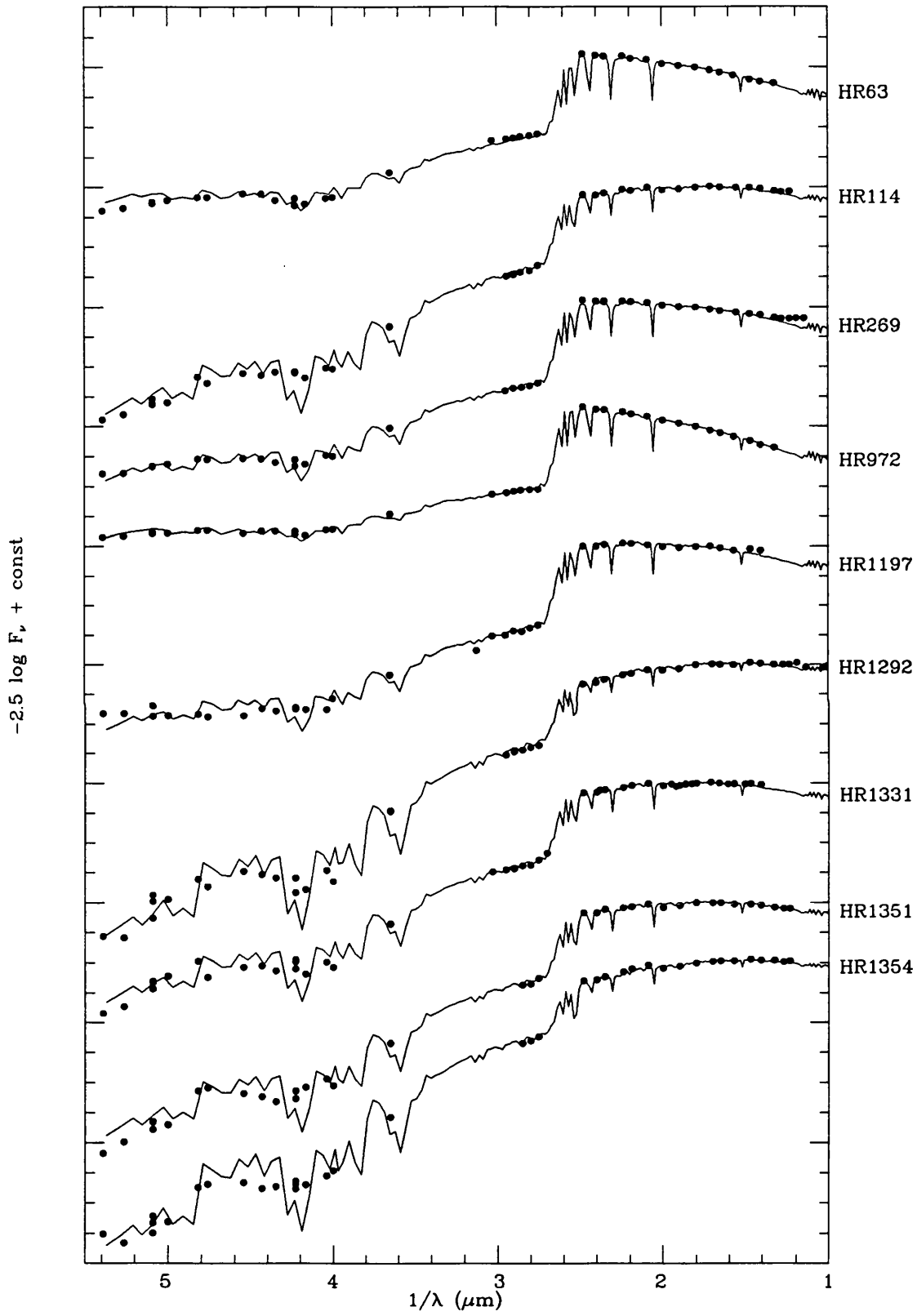

Figure B.1: *[M/H] = 0.0 fits to the JKT programme stars*

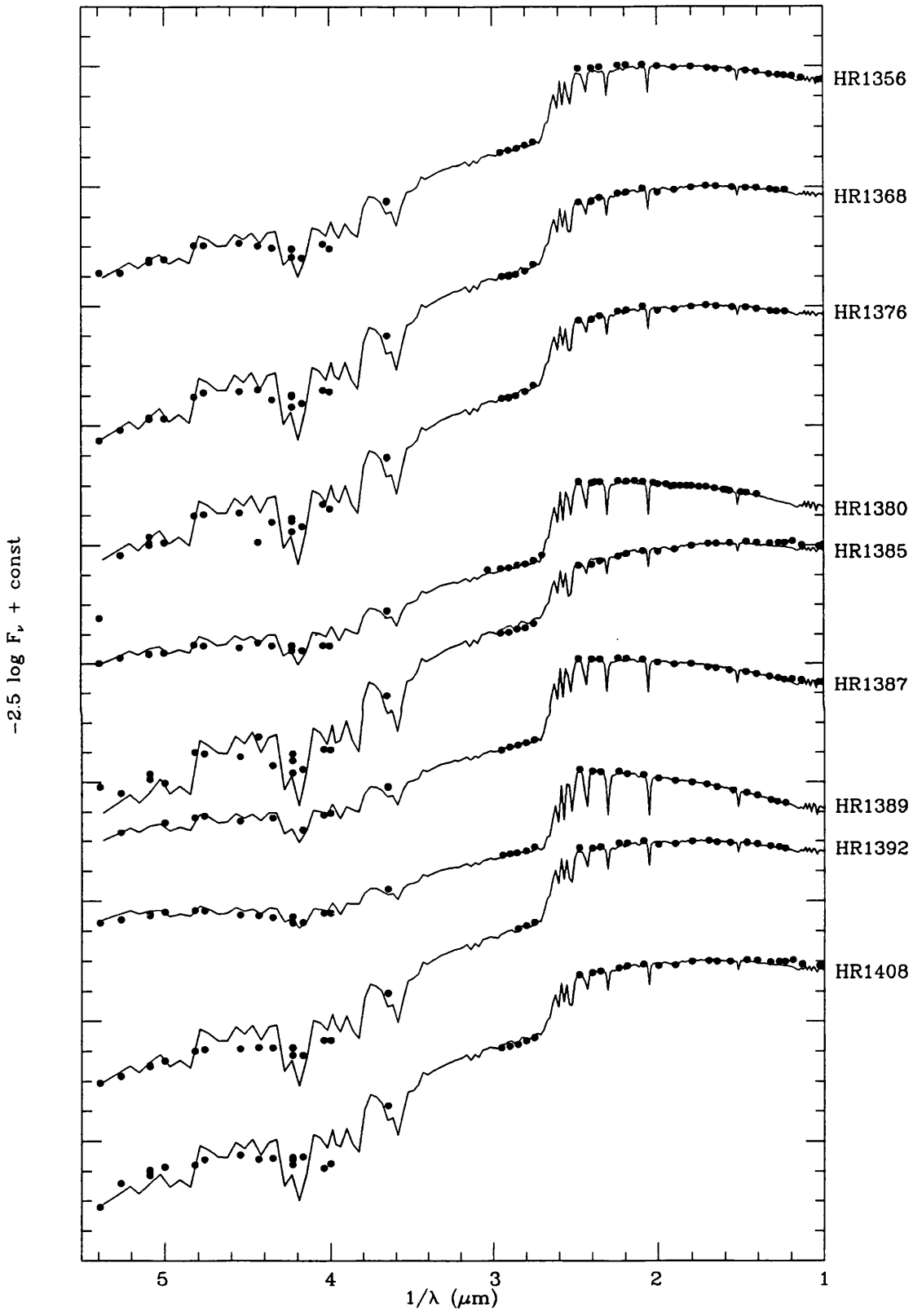

Figure B.1: *[M/H] = 0.0 fits to the JKT programme stars (continued)*

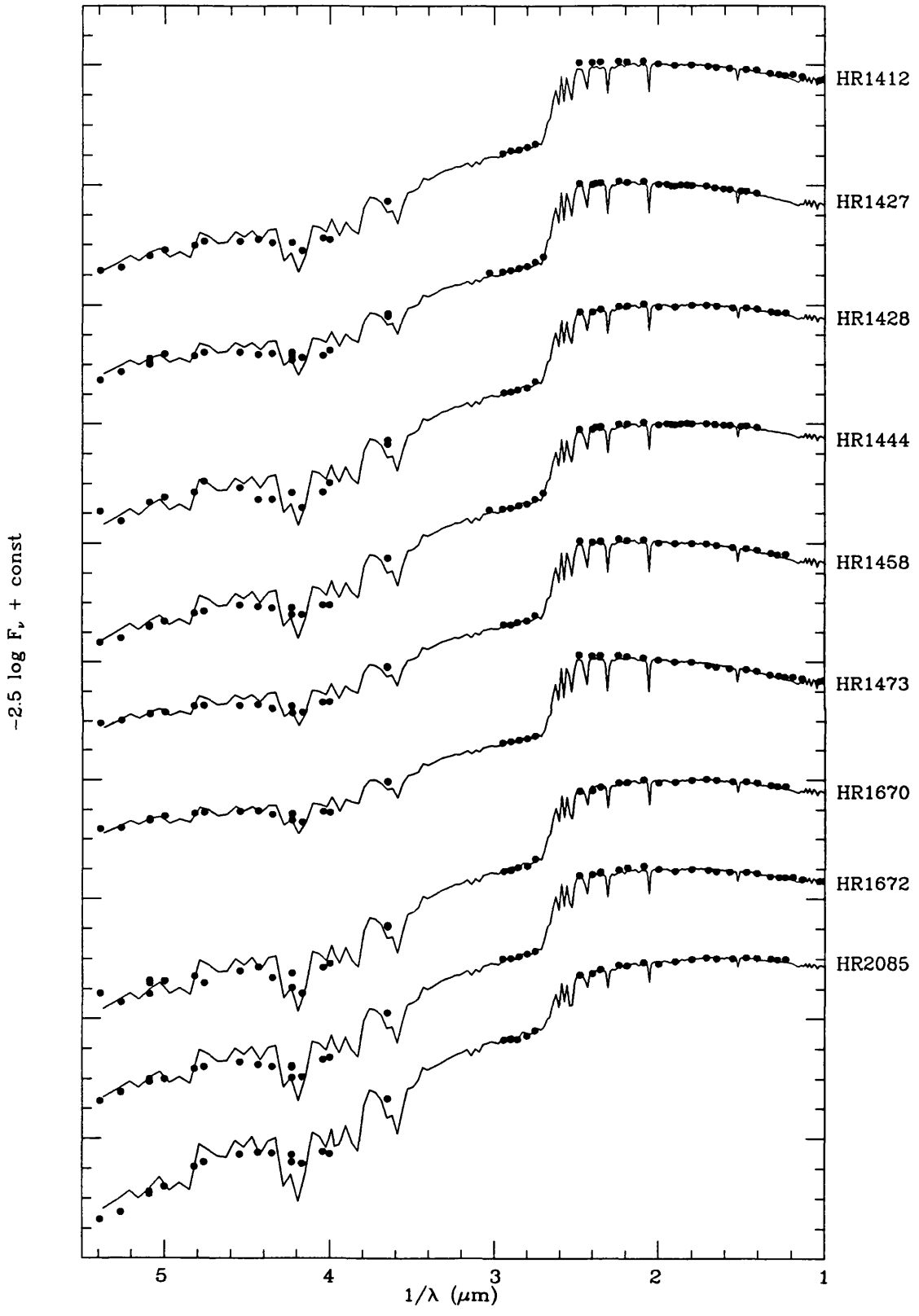

Figure B.1: *[M/H] = 0.0 fits to the JKT programme stars (continued)*

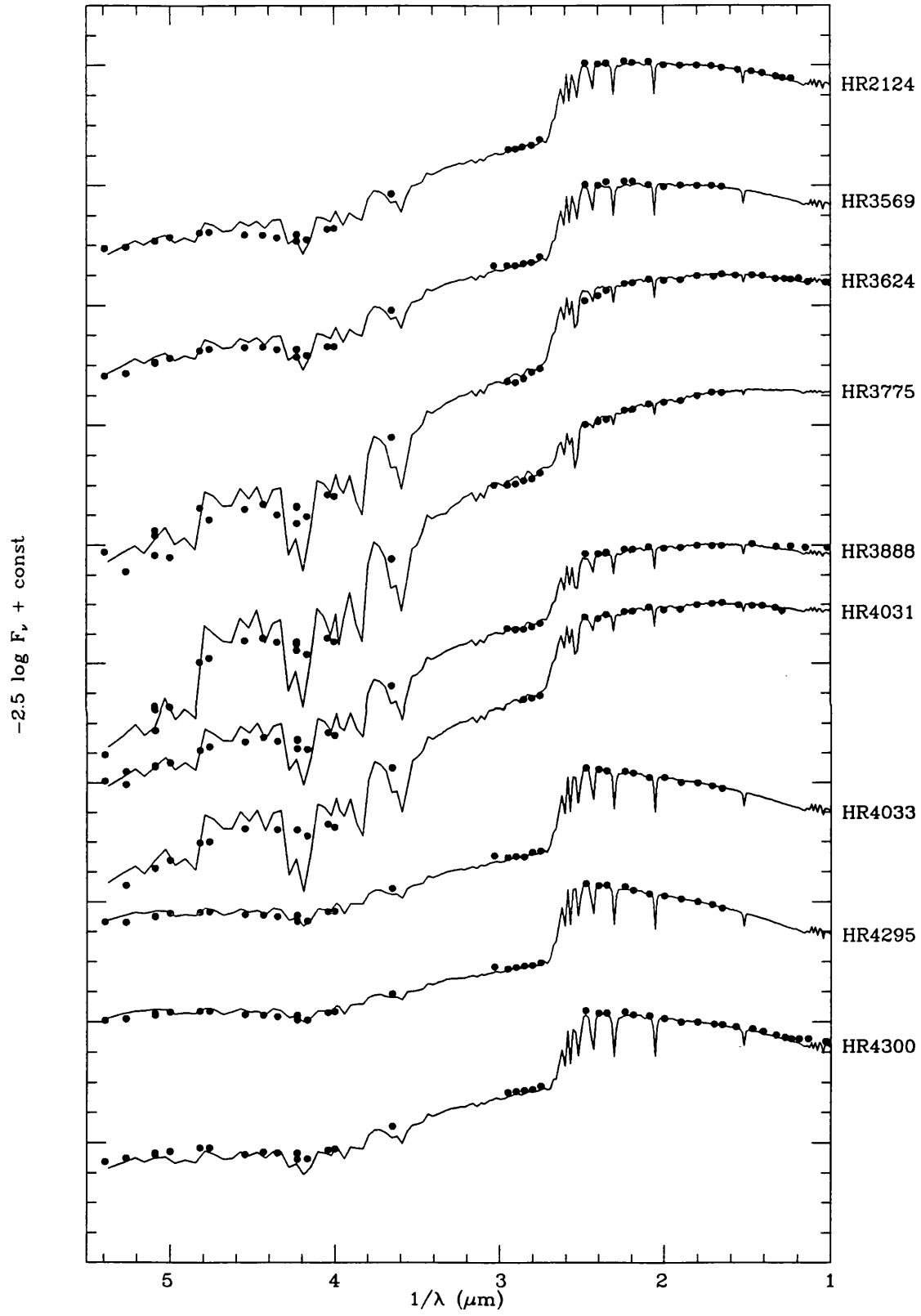

Figure B.1: *[M/H] = 0.0 fits to the JKT programme stars (continued)*

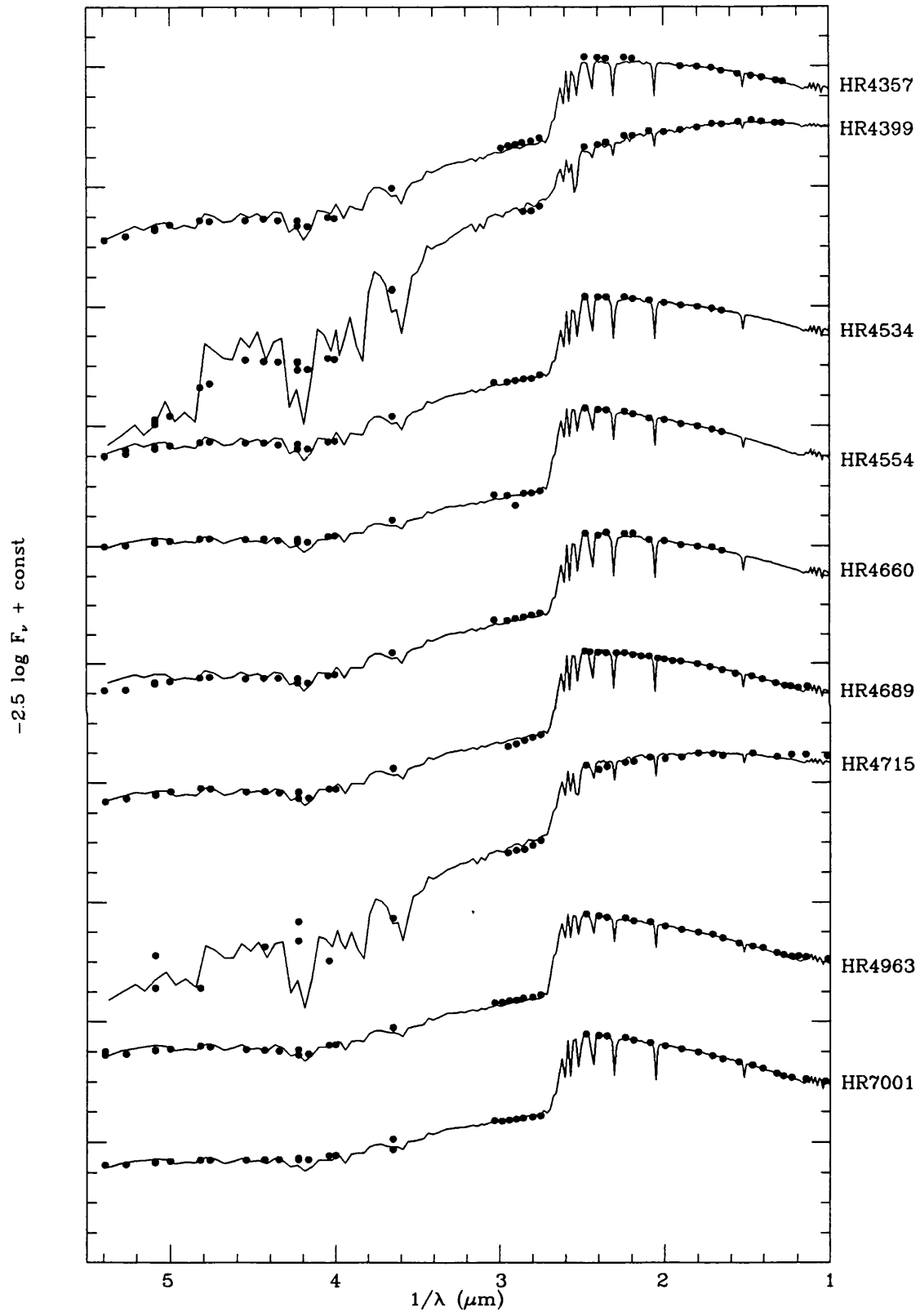

Figure B.1: *[M/H] = 0.0 fits to the JKT programme stars (continued)*

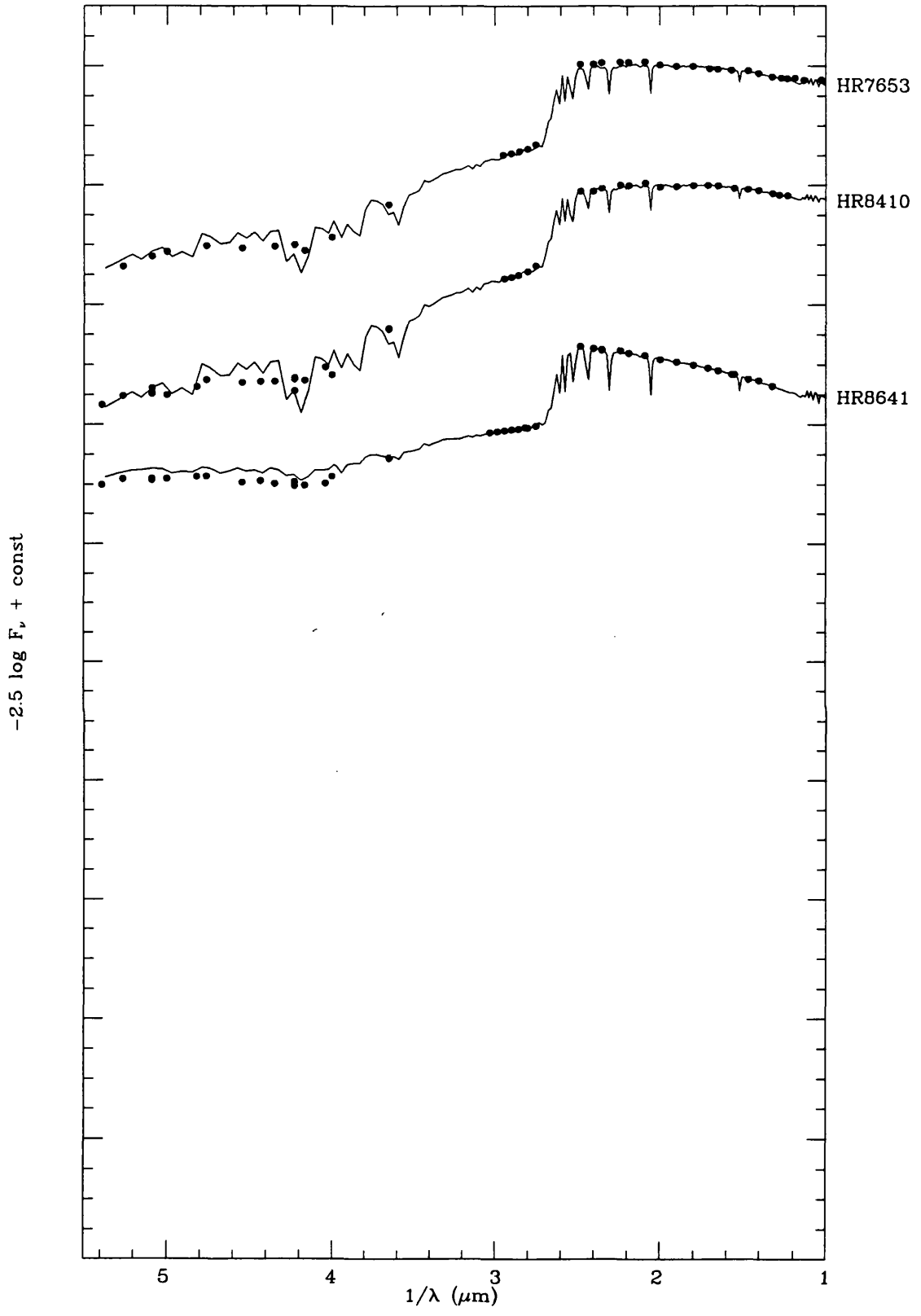

Figure B.1: *[M/H] = 0.0 fits to the JKT programme stars (continued)*

Appendix C

Fits to Balmer line profiles

C.1 Plots of fits to Hβ and Hγ profiles

The following pages contain the solar-abundance fits to the smoothed Hβ and Hγ profiles. The T_{eff} of the model profiles are the best fit solutions given in Table 5.1 and $\log g = 4.0$. All the profiles have been normalized to ± 40Å.

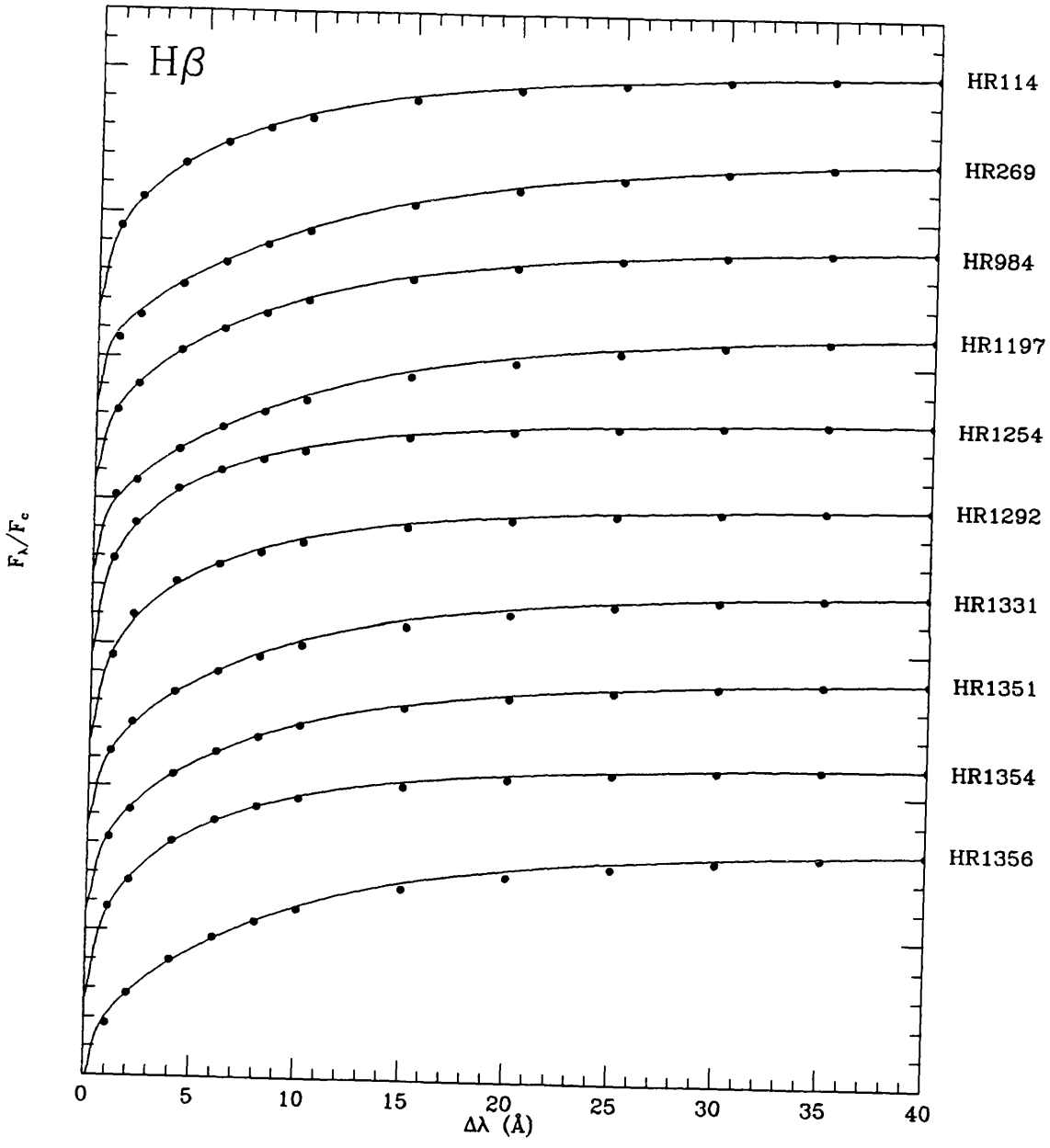

Figure C.1: *[M/H] = 0.0 fits to Hβ profiles*

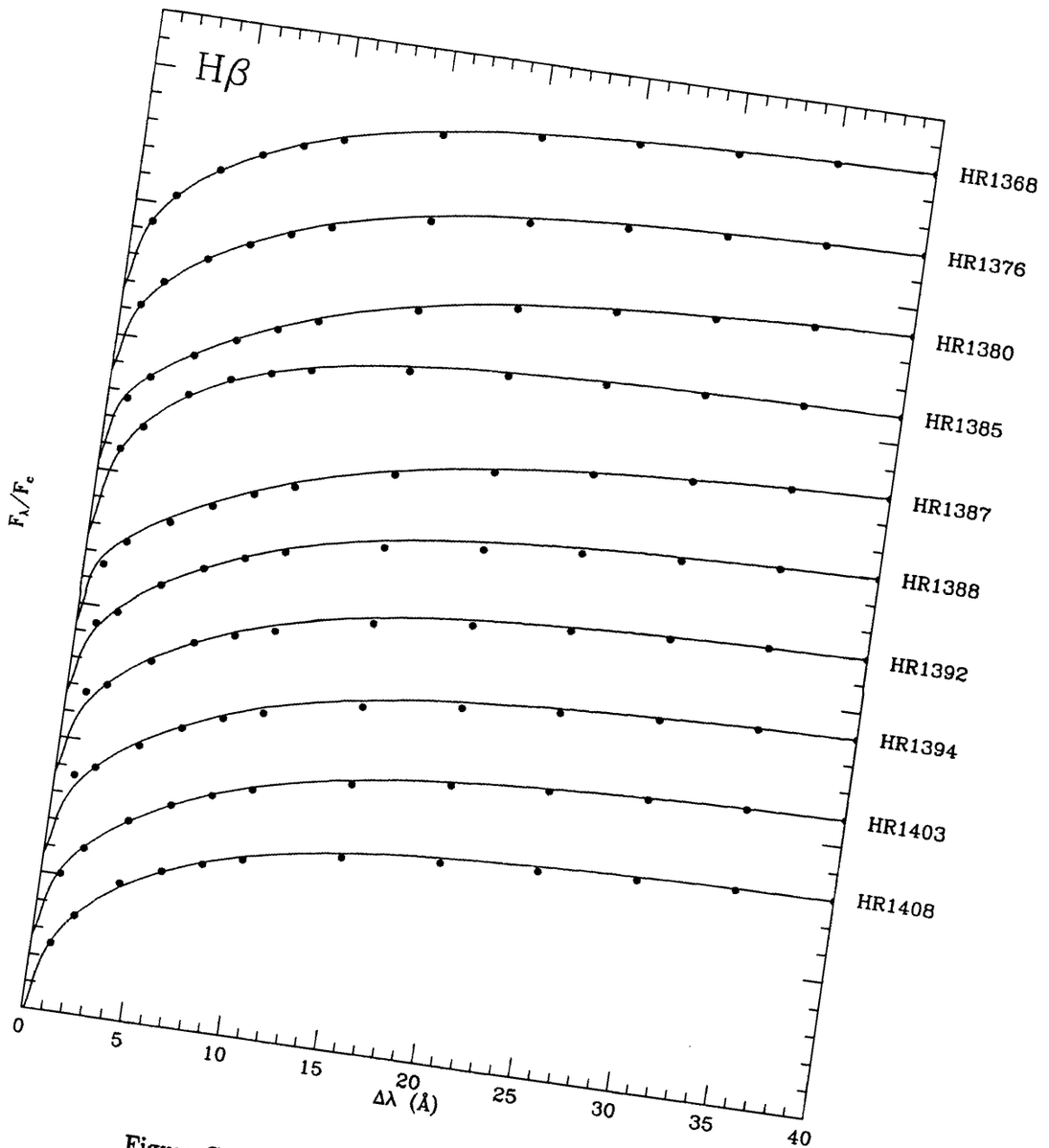

Figure C.1: *[M/H] = 0.0 fits to Hβ profiles (continued)*

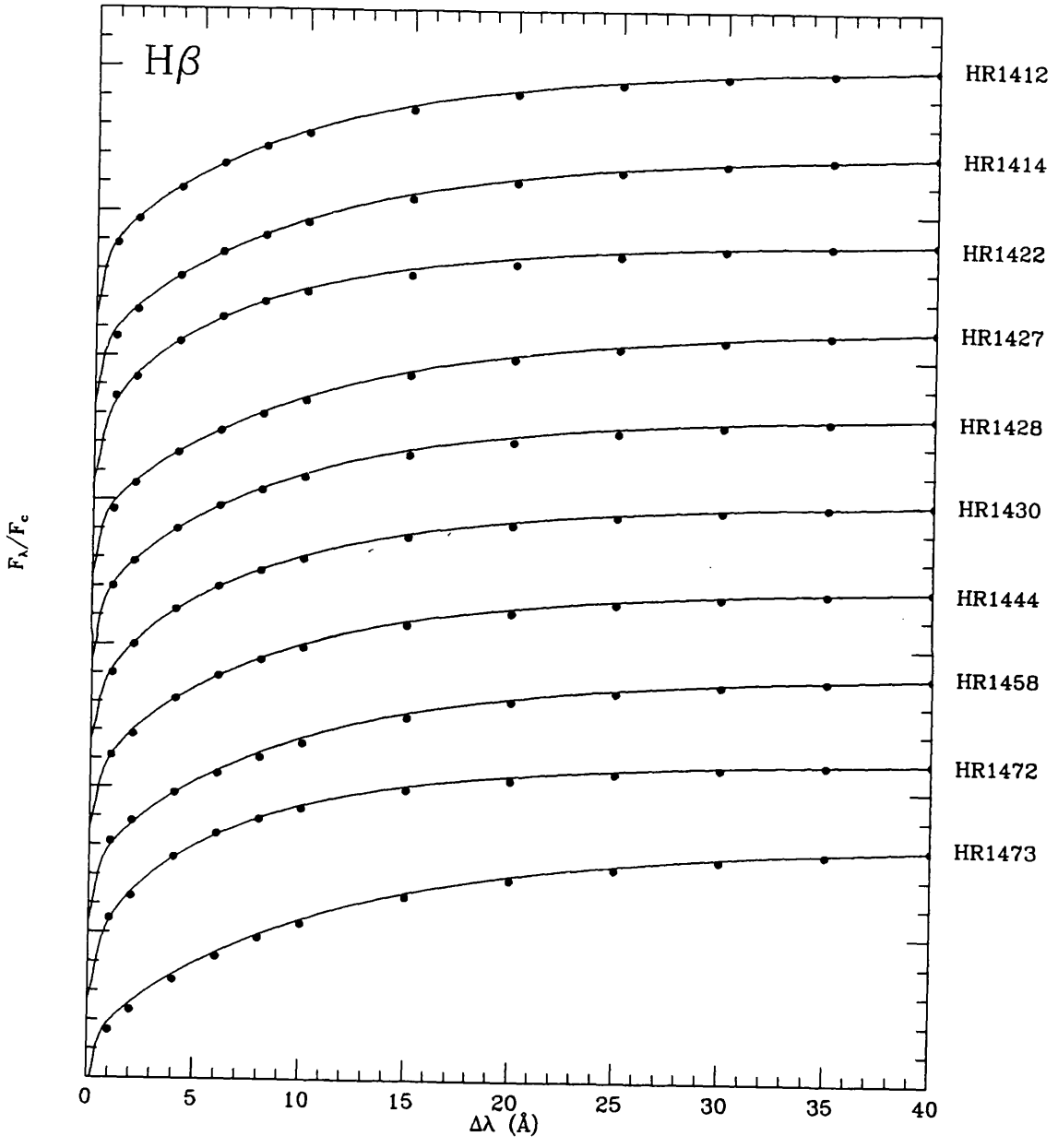

Figure C.1: *[M/H] = 0.0 fits to Hβ profiles (continued)*

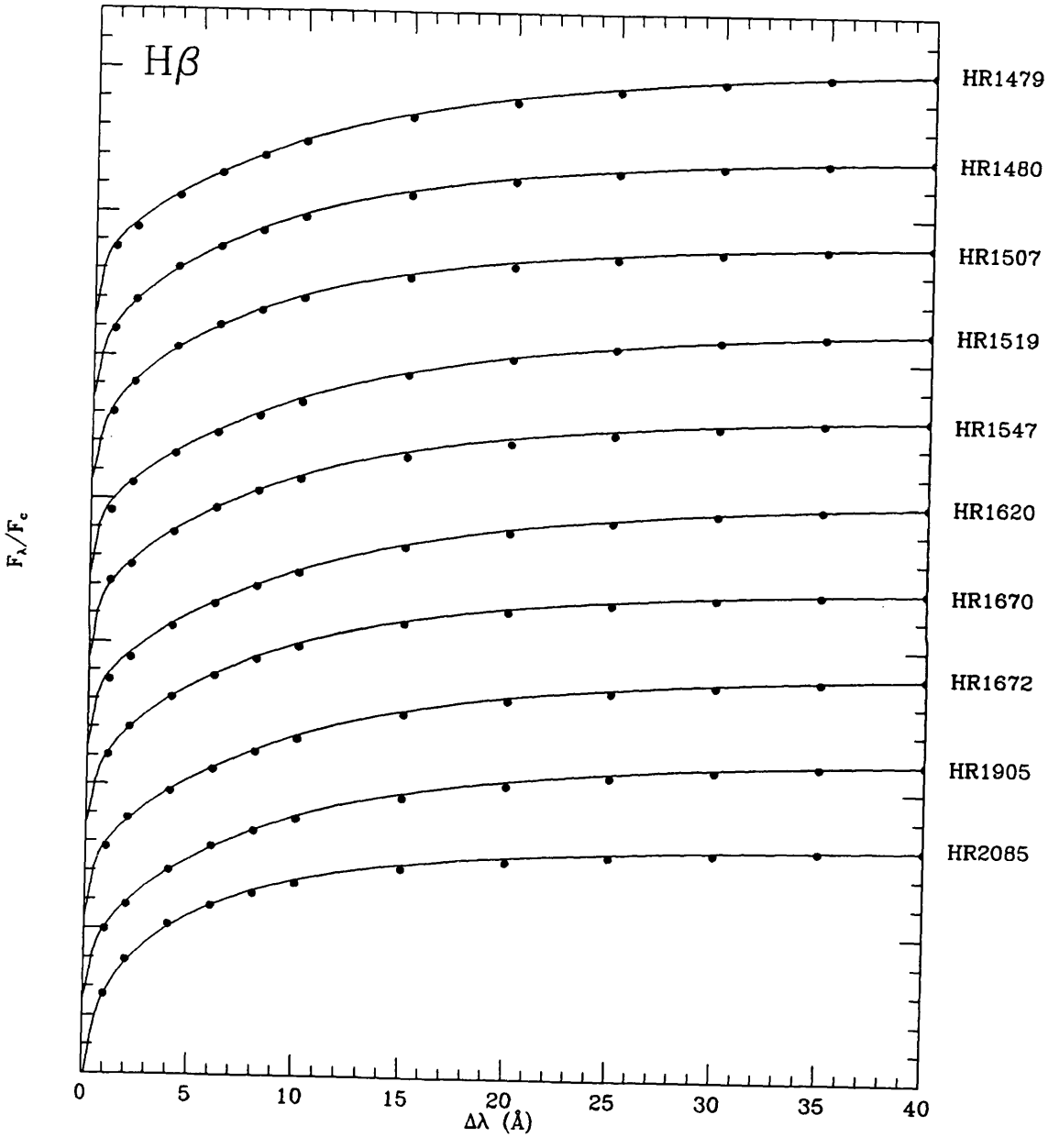

Figure C.1: *[M/H] = 0.0 fits to Hβ profiles (continued)*

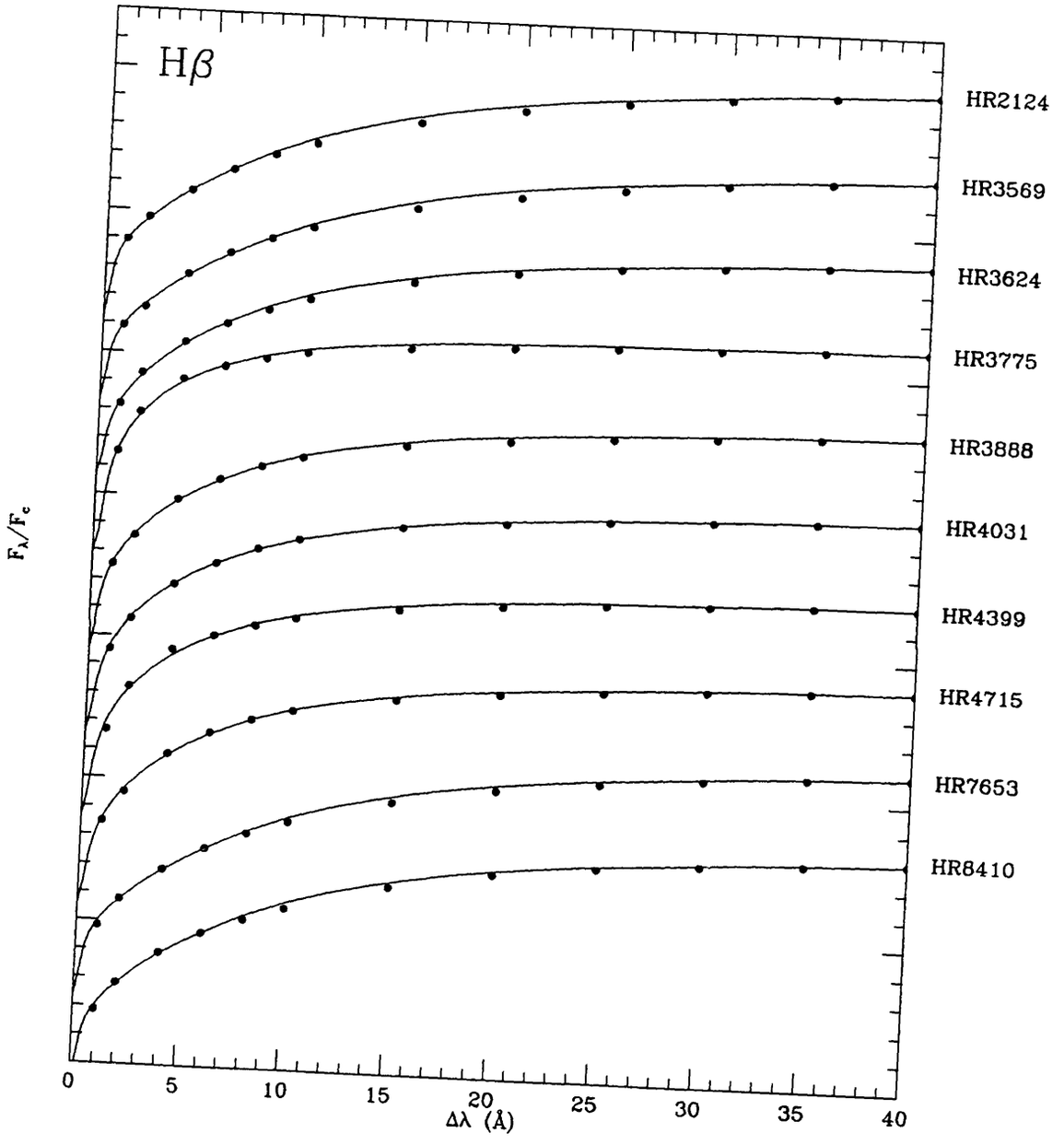

Figure C.1: *[M/H] = 0.0 fits to Hβ profiles (continued)*

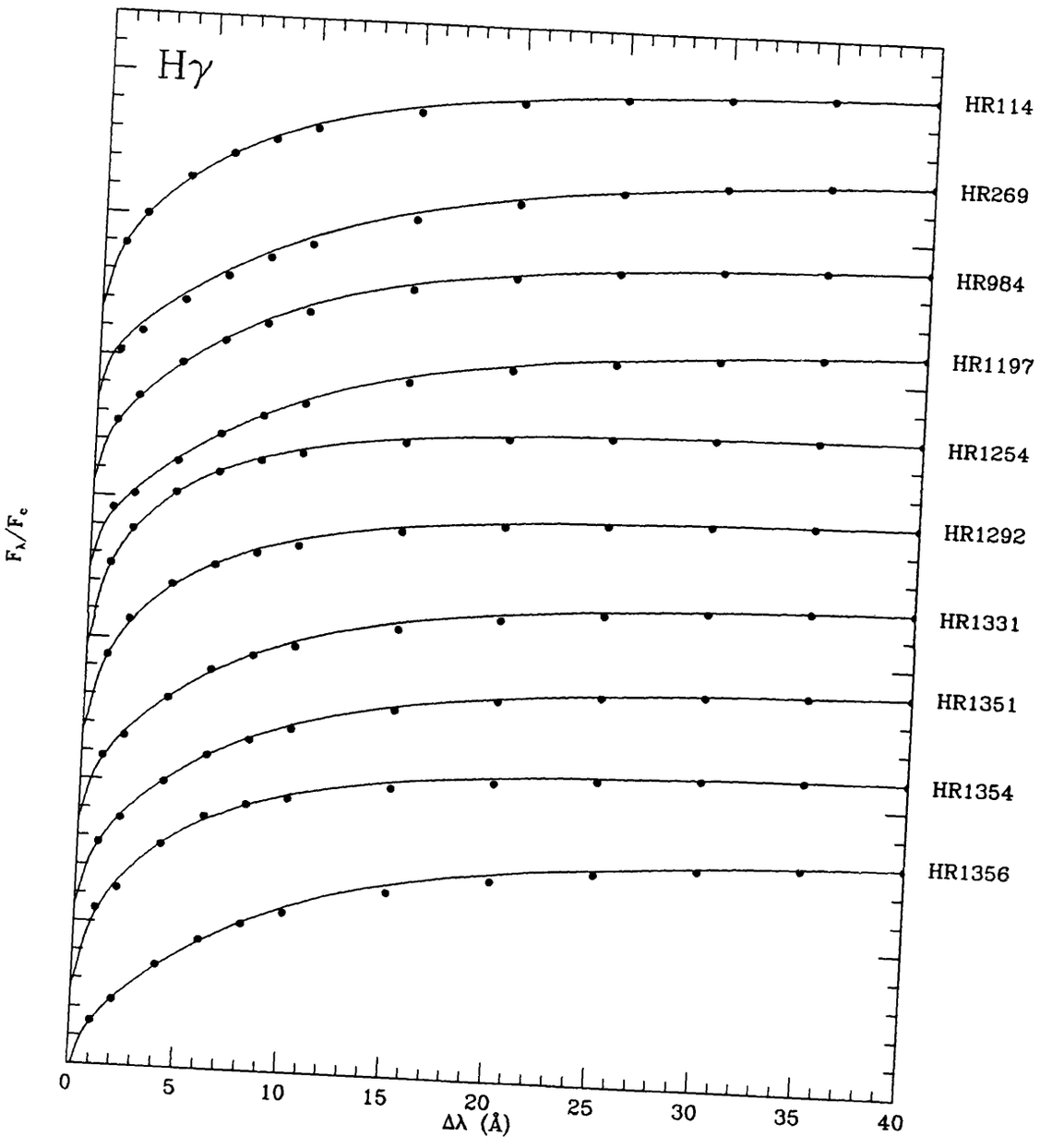

Figure C.2: *[M/H] = 0.0 fits to Hγ profiles*

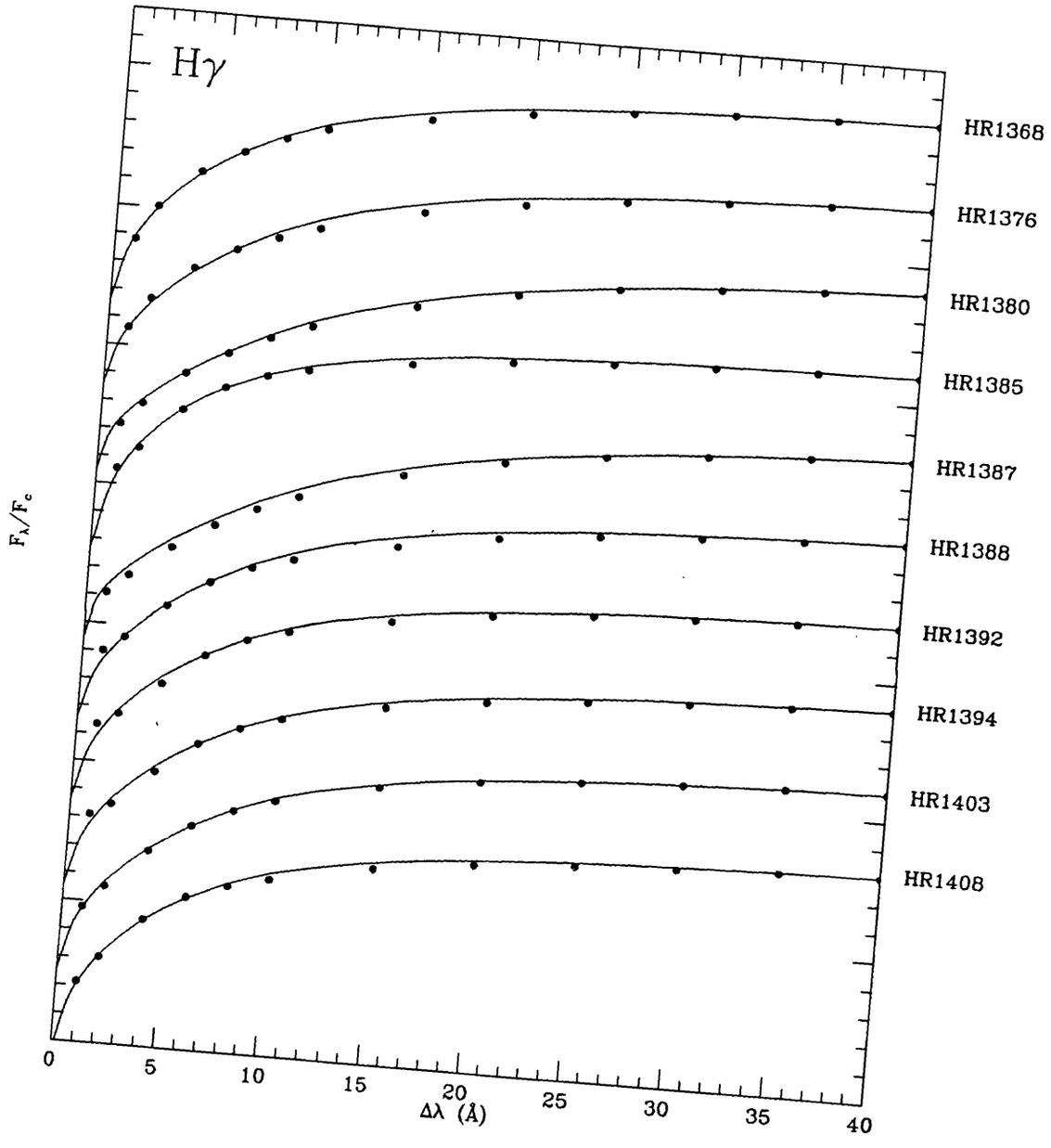

Figure C.2: *[M/H] = 0.0 fits to Hγ profiles (continued)*

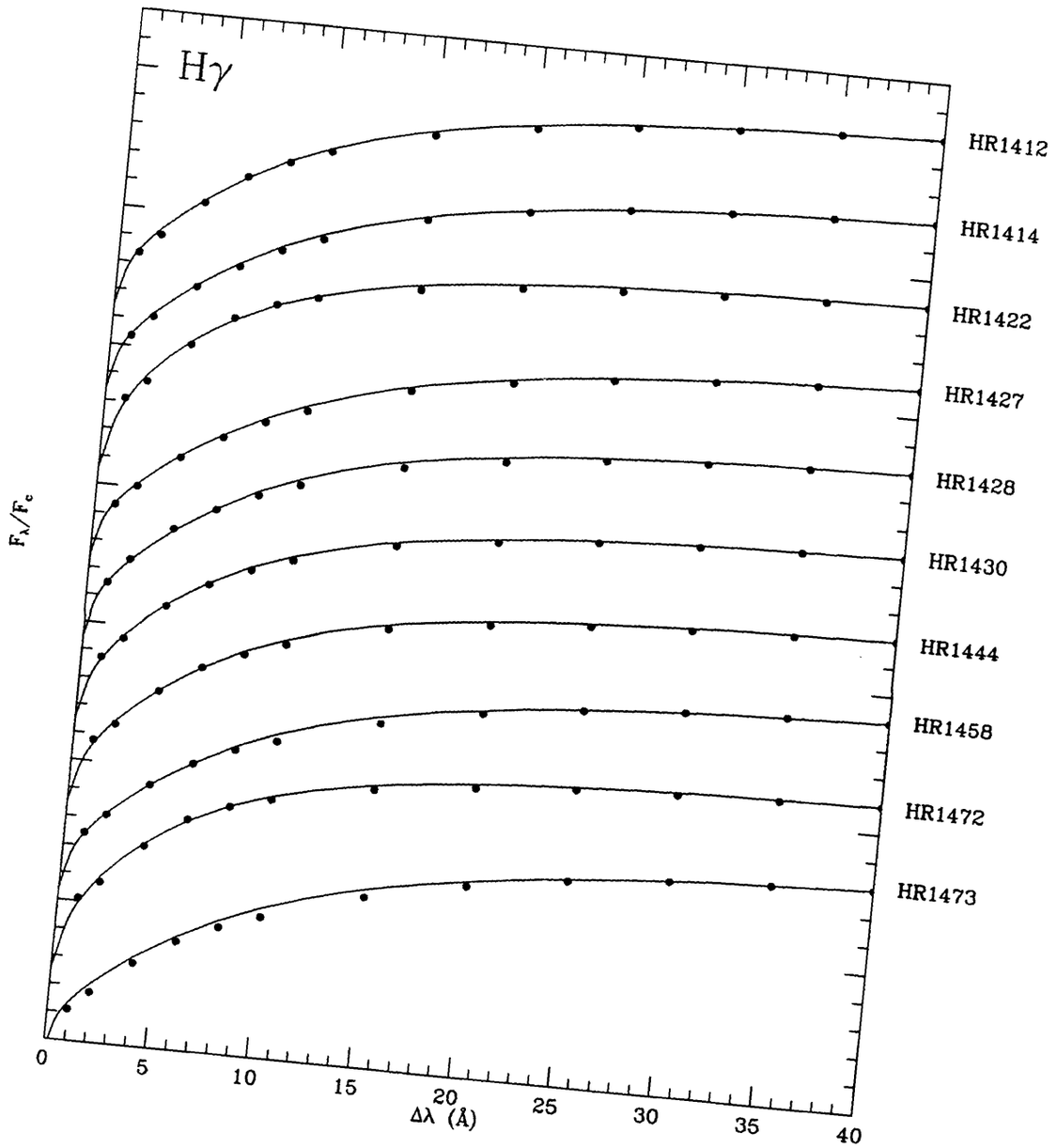

Figure C.2: *[M/H] = 0.0 fits to Hγ profiles (continued)*

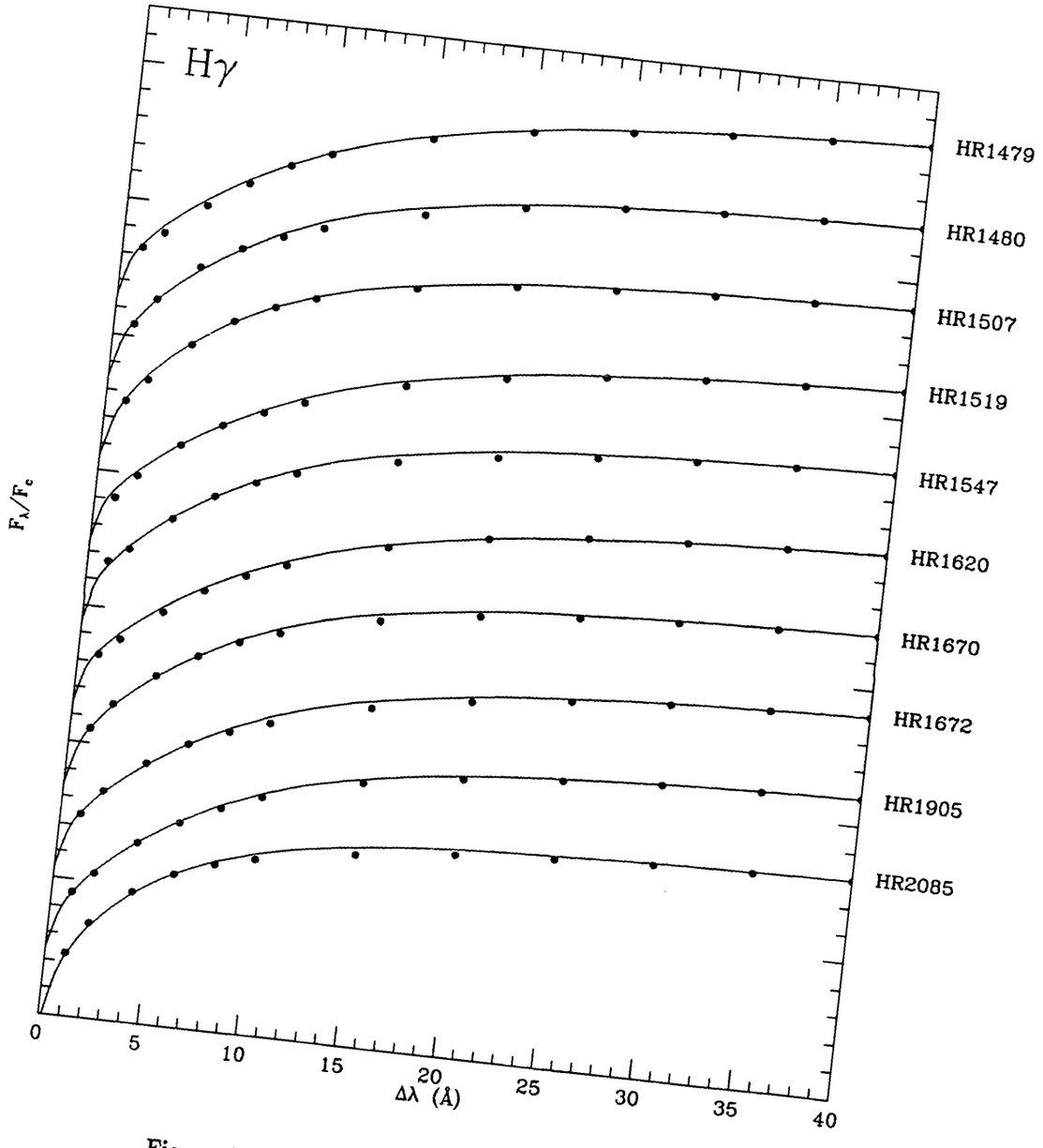

Figure C.2: *[M/H] = 0.0 fits to Hγ profiles (continued)*

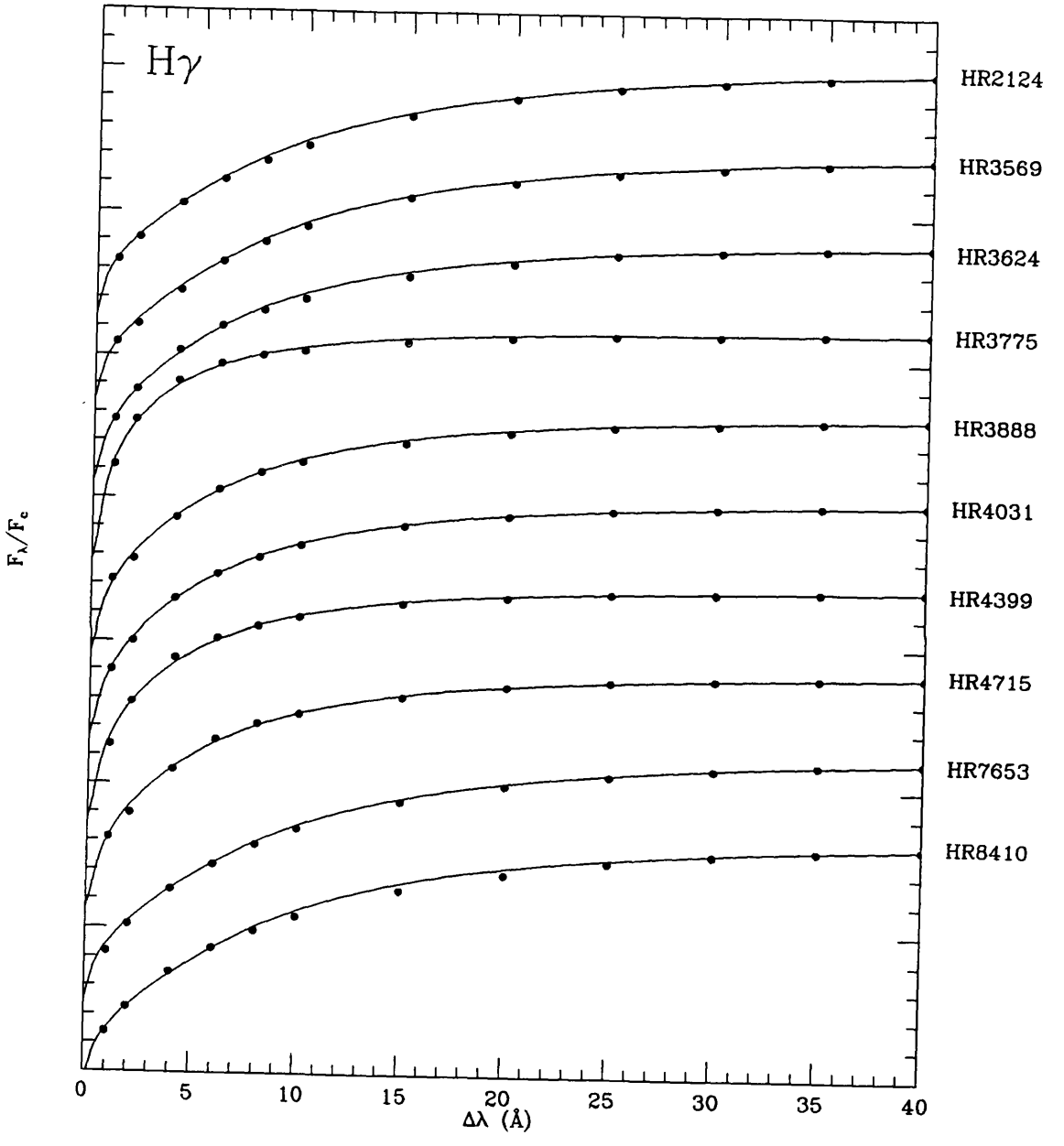

Figure C.2: *[M/H] = 0.0 fits to Hγ profiles (continued)*

Appendix D

Temperature-gravity diagrams for the JKT programme stars

The following pages contain temperature-gravity diagrams for the JKT programme stars. The symbols are defined as follows:

- • Moon & Dworetsky (1985) (β, c_0) grid
- △ Lester, Gray & Kurucz (1986) (β, c_0) grid
- × Relyea & Kurucz (1978) $((b-y), c_0)$ grid
- ▲ Lester, Gray & Kurucz (1986) $((b-y), c_0)$ grid
- o Kurucz (1991b) $((b-y), c_0)$ grid
- ■ Spectrophotometric flux fitting

The various lines have the following meanings:

——— mass-luminosity relationship

·—·—· Infra-Red Flux Method

– – – Hβ line

—— —— Hγ line

····· Fit to new synthetic β grid

Several of the $T_{\rm eff}$-log g diagrams include the effects of companion stars and use [M/H] = +0.5 models. See Chapter 8 for details.

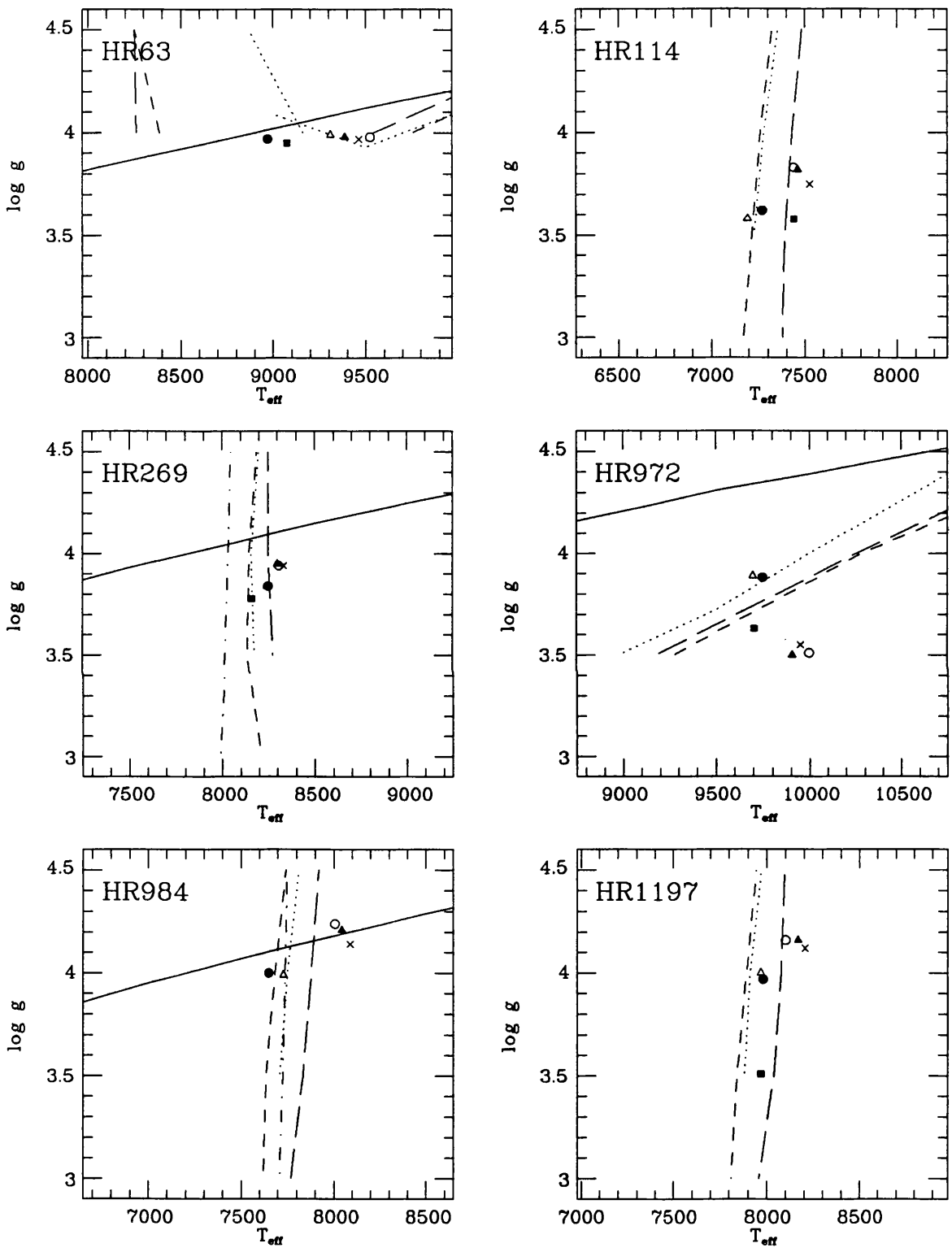

Figure D.1: *Temperature-gravity diagrams*

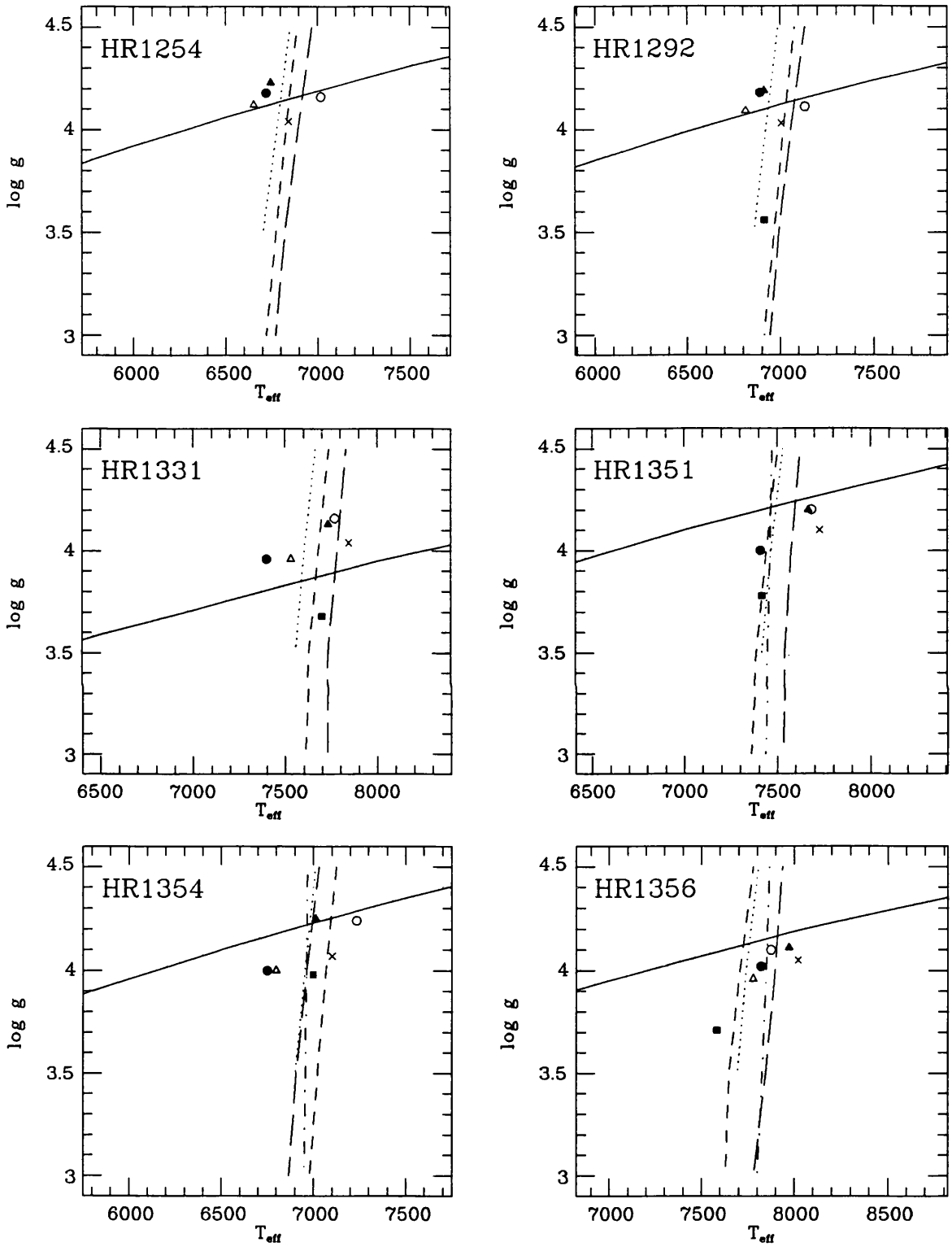

Figure D.1: *Temperature-gravity diagrams (continued)*

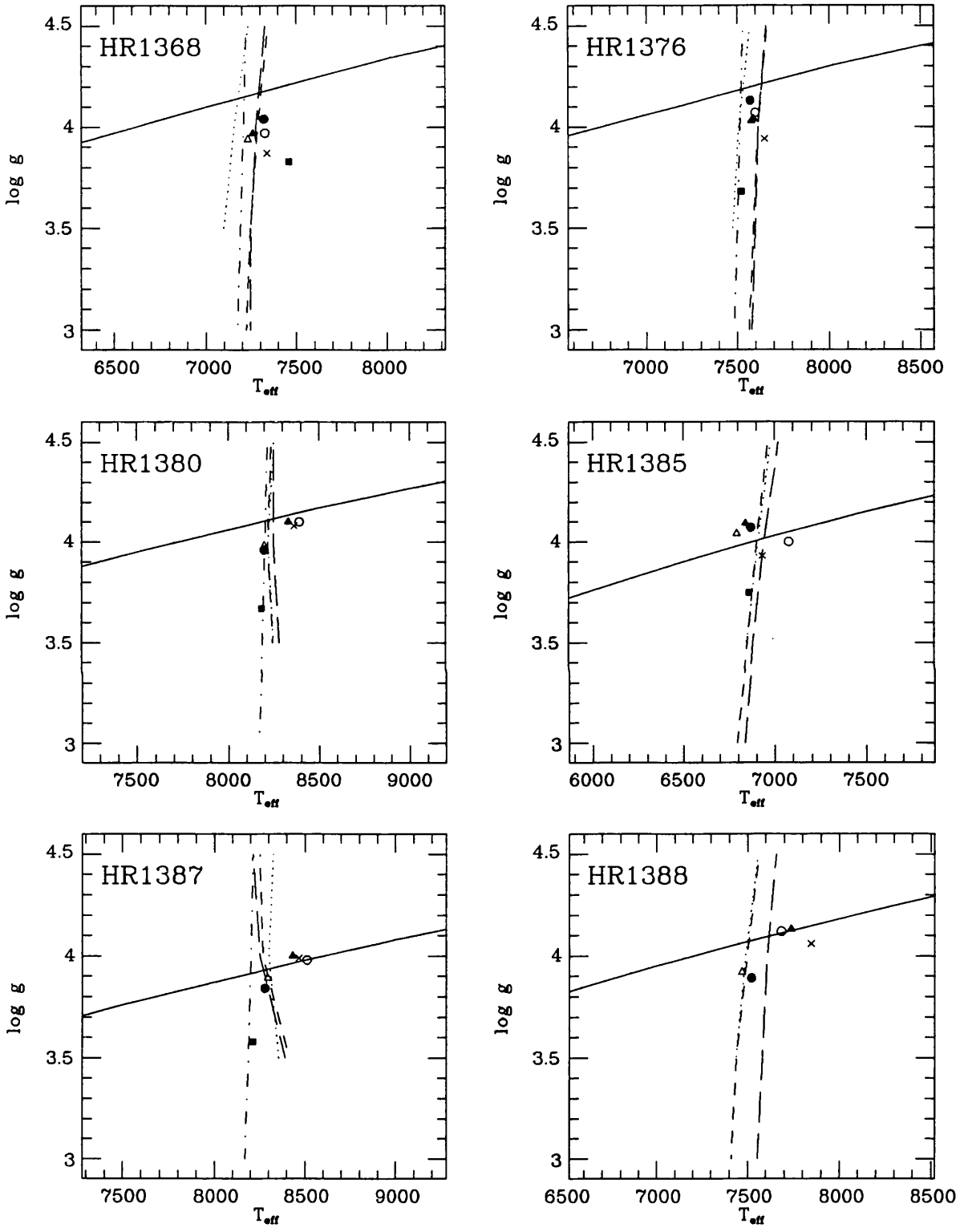

Figure D.1: *Temperature-gravity diagrams (continued)*

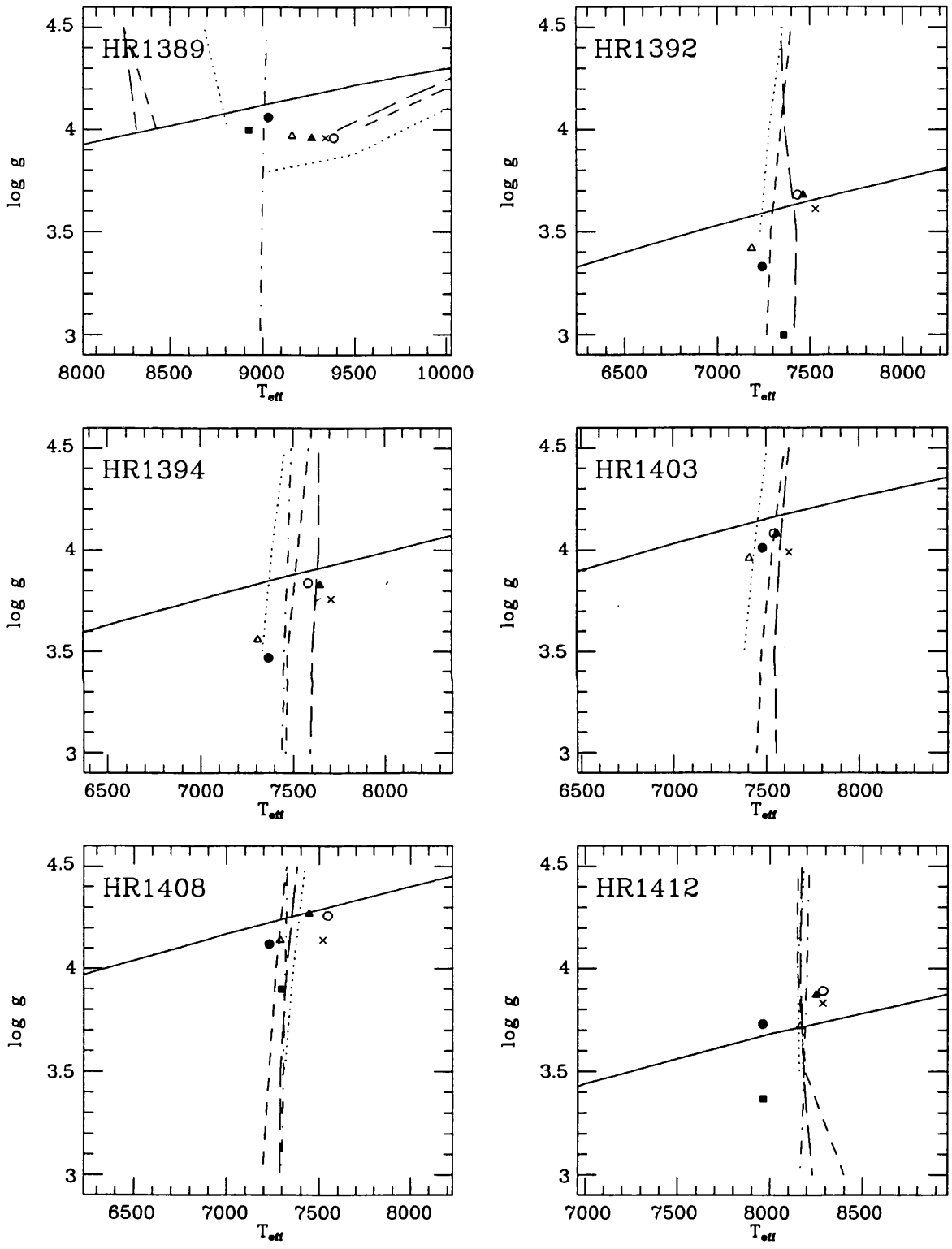

Figure D.1: *Temperature-gravity diagrams (continued)*

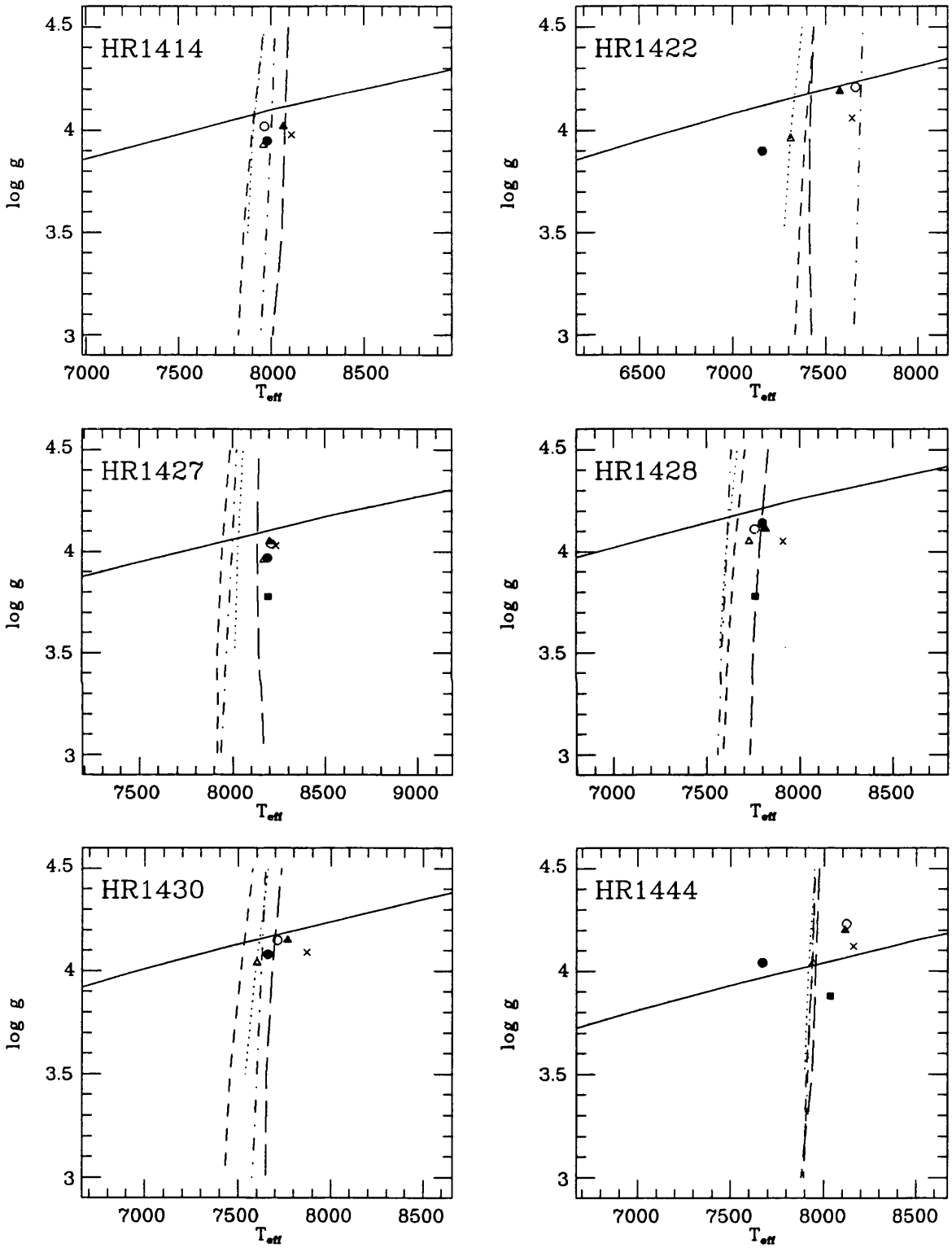

Figure D.1: *Temperature-gravity diagrams (continued)*

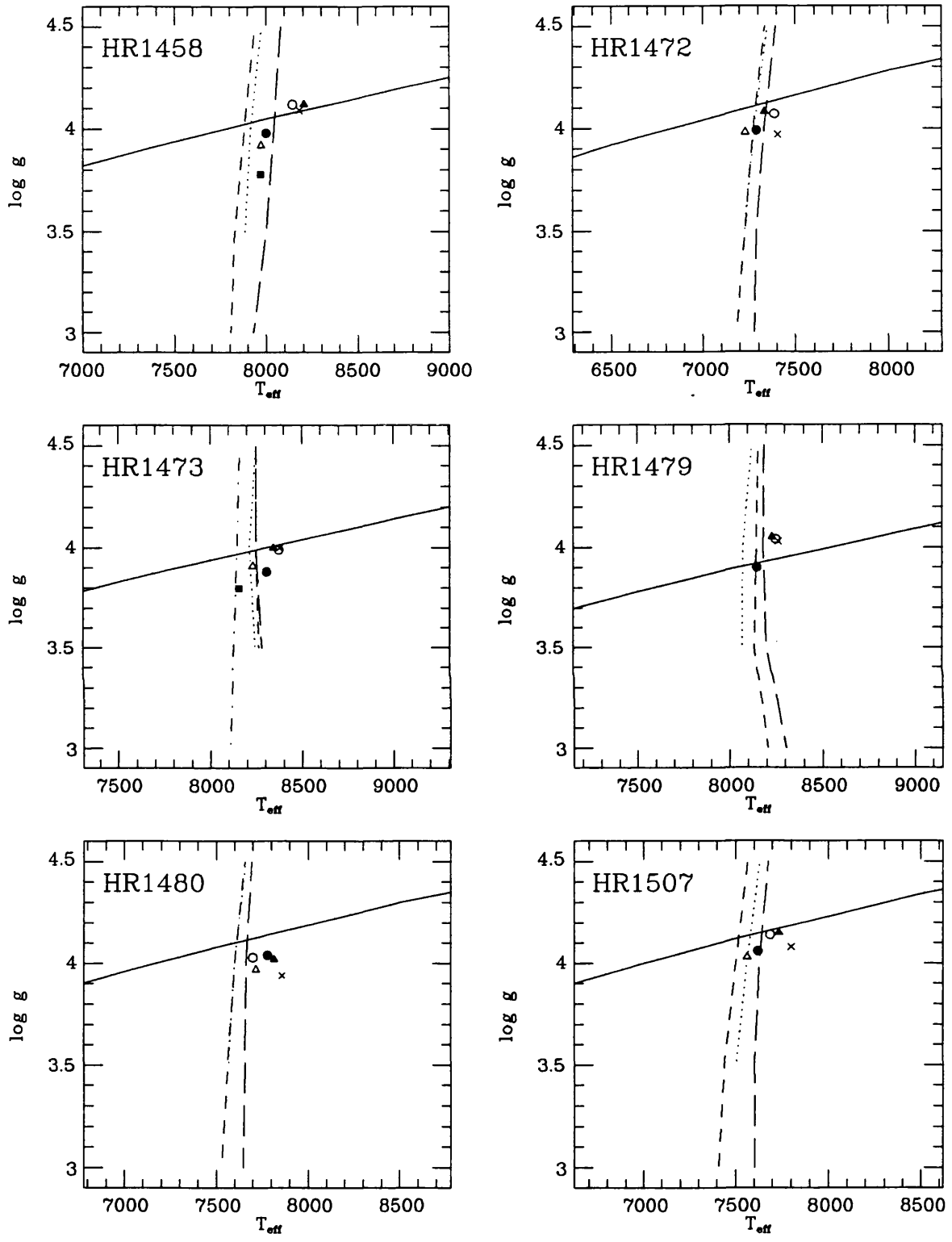

Figure D.1: *Temperature-gravity diagrams (continued)*

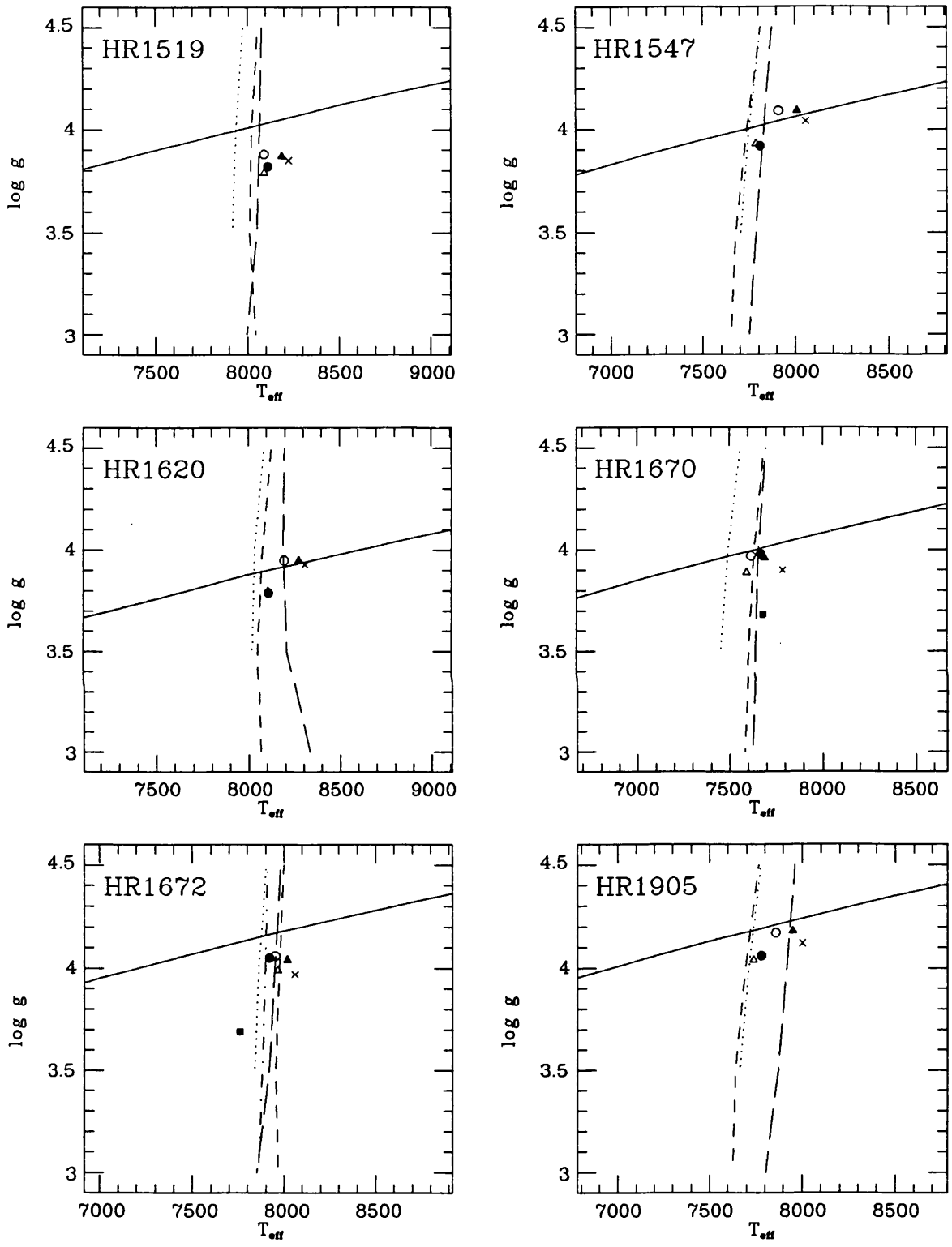

Figure D.1: *Temperature-gravity diagrams (continued)*

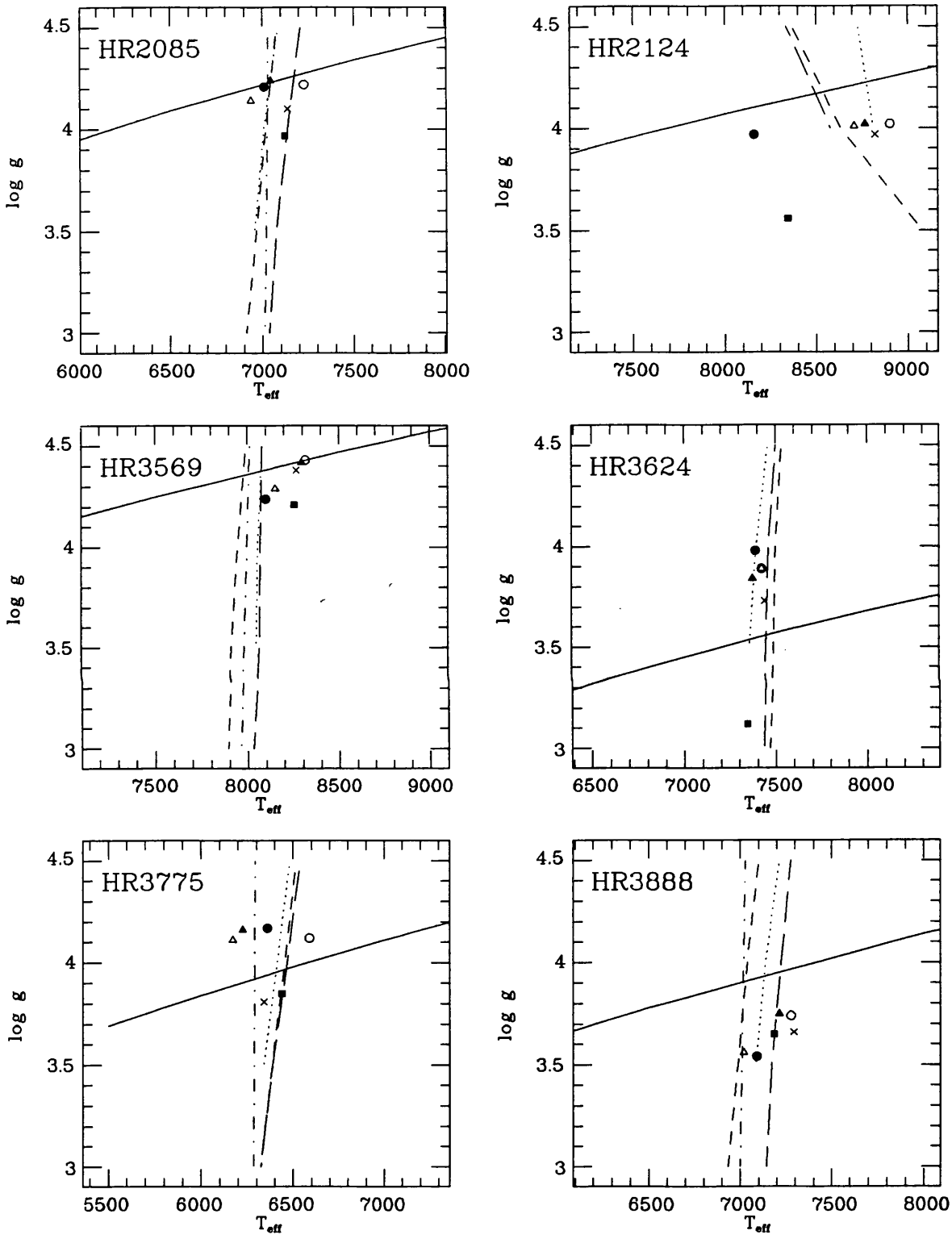

Figure D.1: *Temperature-gravity diagrams (continued)*

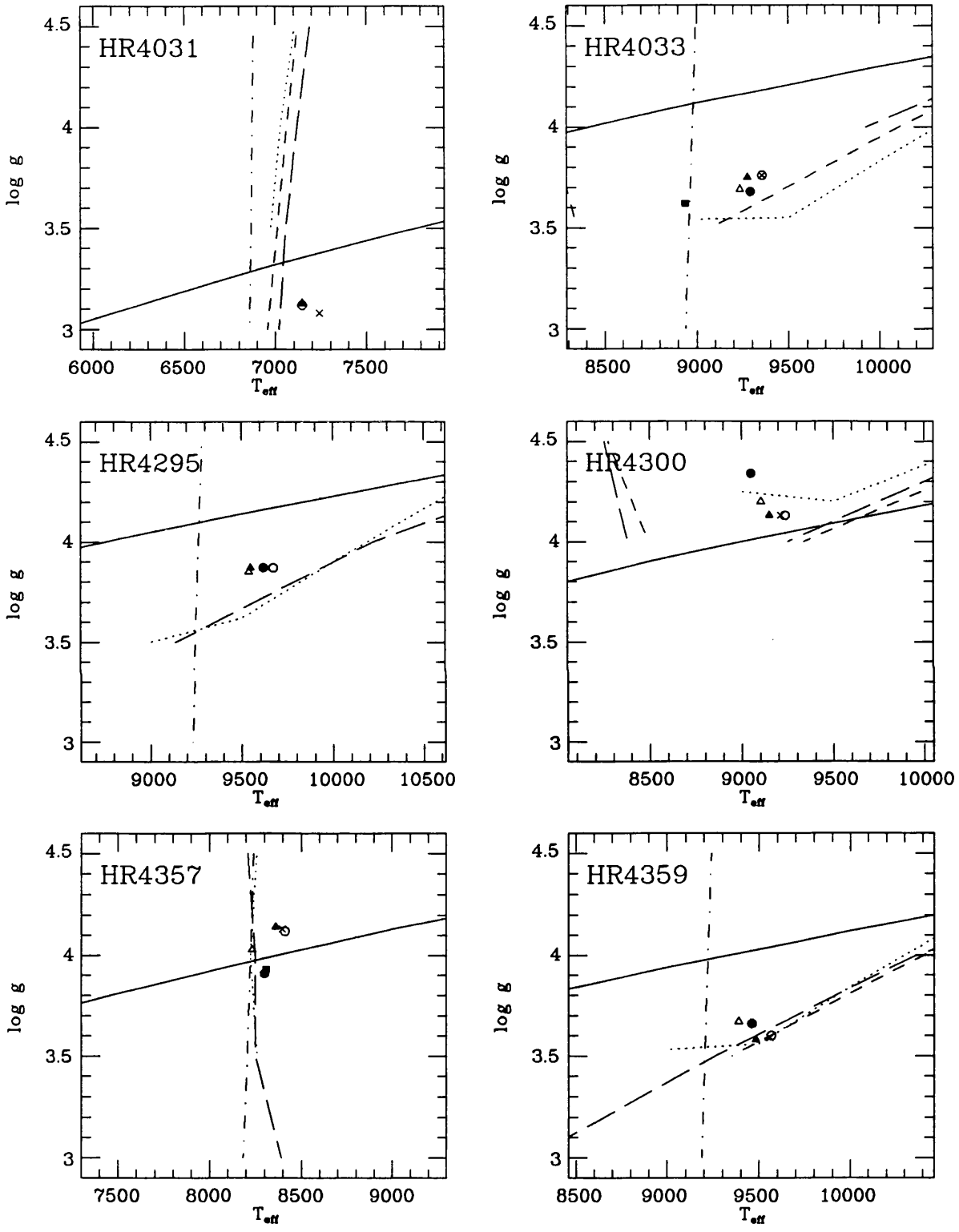

Figure D.1: *Temperature-gravity diagrams (continued)*

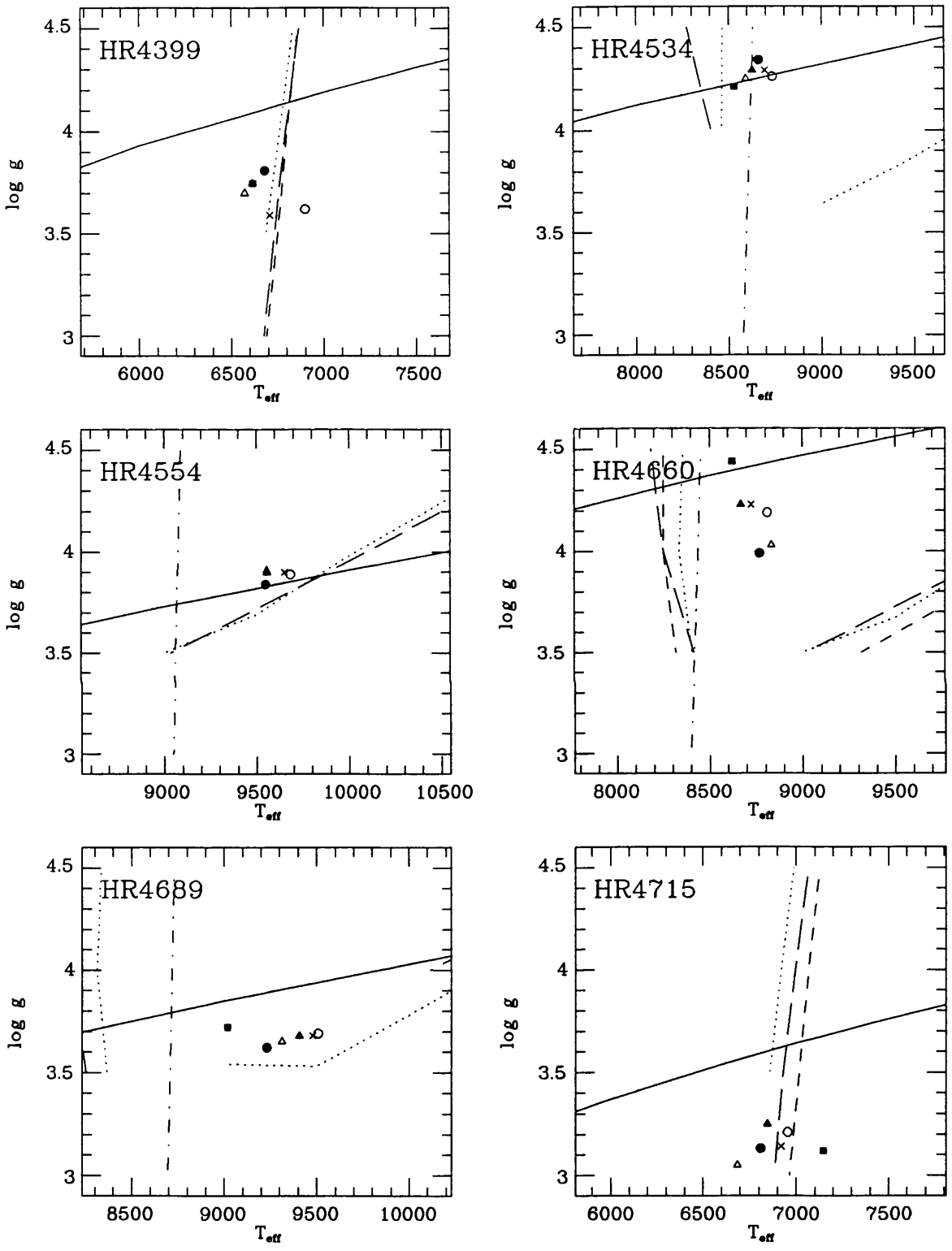

Figure D.1: *Temperature-gravity diagrams (continued)*

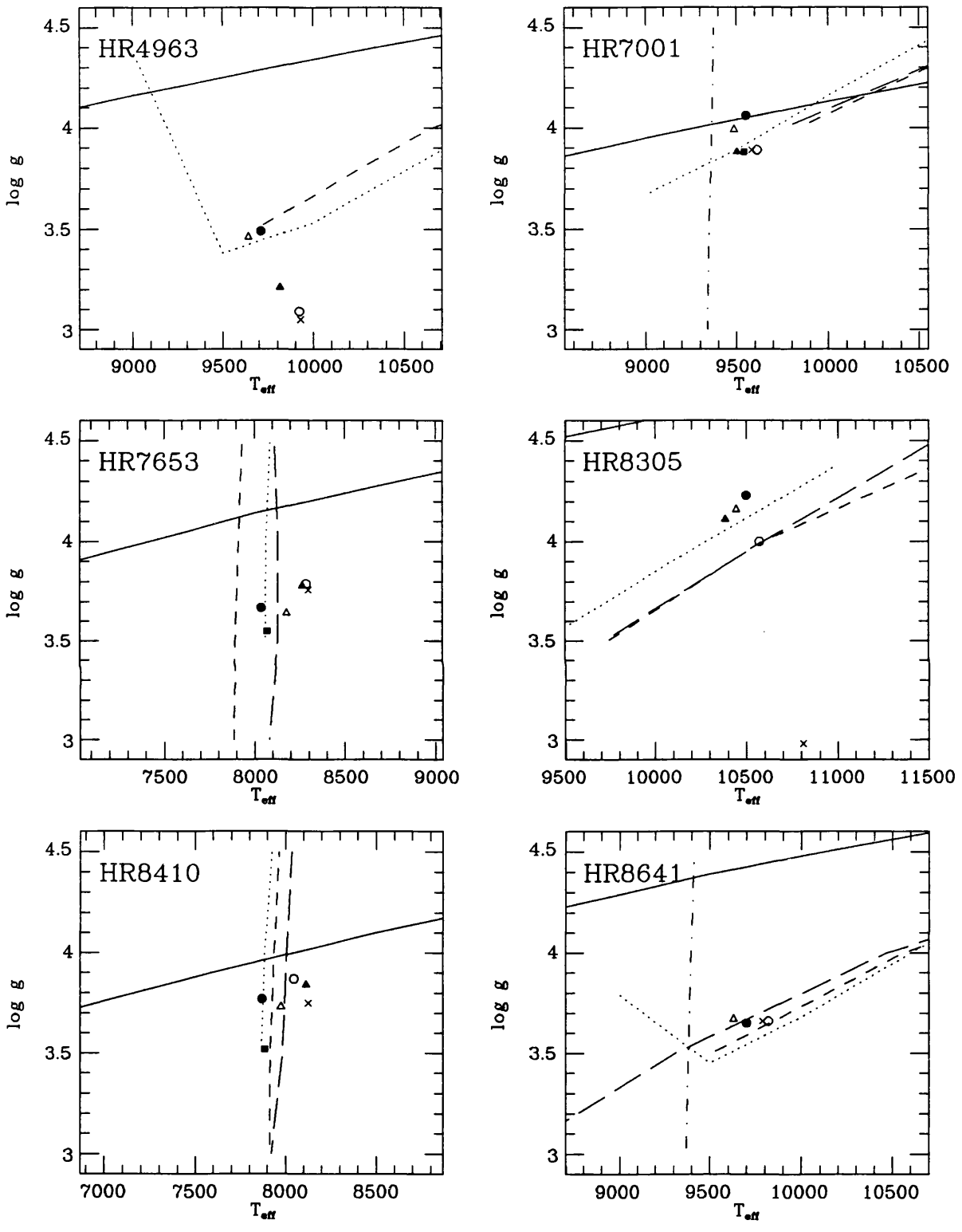

Figure D.1: *Temperature-gravity diagrams (continued)*